Liquid chromatographic analysis of weakly- and non-chromophore compounds focusing on Charged Aerosol Detection

Dissertation zur Erlangung des naturwissenschaftlichen
Doktorgrades der Julius-Maximilians-Universität Würzburg

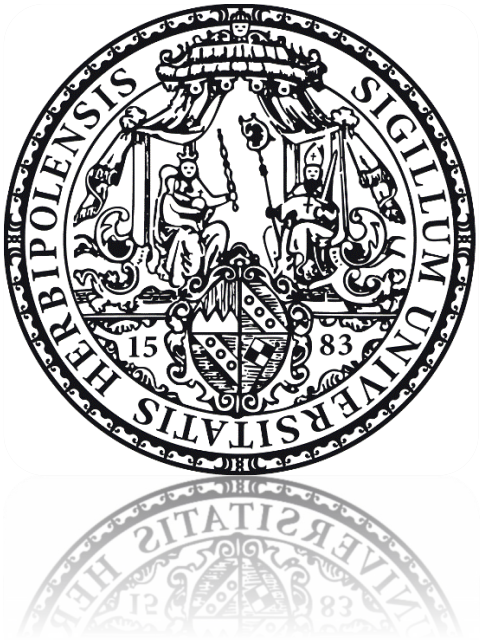

vorgelegt von
Klaus Jussi Schilling
aus
Bad Arolsen

Würzburg 2020

Liquid chromatographic analysis of weakly- and non-chromophore compounds focusing on Charged Aerosol Detection

Dissertation zur Erlangung des naturwissenschaftlichen
Doktorgrades der Julius-Maximilians-Universität Würzburg

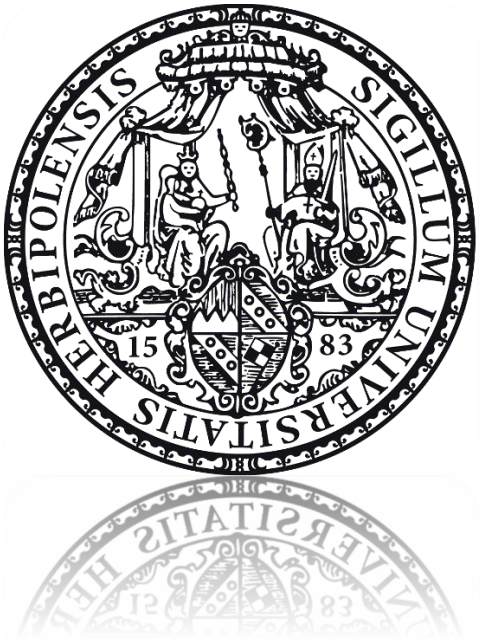

vorgelegt von
Klaus Jussi Schilling
aus
Bad Arolsen

Würzburg 2020

Eingereicht bei der Fakultät für Chemie und Pharmazie am

_____

Gutachter der schriftlichen Arbeit

1. Gutachter: _____

2. Gutachter: _____

Prüfer des öffentlichen Promotionskolloquiums

1. Prüfer: _____

2. Prüfer: _____

3. Prüfer: _____

Datum des öffentlichen Promotionskolloquiums

_____

Doktorurkunde ausgehändigt am

_____

“Deserving is not a thing in competition. You earn it, or you don’t.”

– Wehsing “SingSing” Yuen –

– Meiner Familie –

Danksagung

Die hier vorliegende Arbeit entstand
am Institut für Pharmazie und Lebensmittelchemie
der Bayerischen Julius-Maximilians-Universität Würzburg
auf Anregung und unter Anleitung von

Frau Prof. Dr. Ulrike Holzgrabe

Ihr bin ich zu besonderem Dank für die freundliche Aufnahme in ihren Arbeitskreis,
die spannenden Projekte, das stets in mich gesetzte Vertrauen
und Ihre Unterstützung und Hilfe in jeder Phase der Promotion verpflichtet.

Weiterer Dank gilt allen Kolleginnen und Kollegen
- ehemaligen sowie aktuellen -
des AK Holzgrabe, die diese Zeit so angenehm gestaltet haben:

Adrian, Alex, Anja, Anna, Antonio, Christiane, Christine E., Christine H., Daniela, David, Flo G., Flo S., Jan, Jens, Jogi, Jonas U., Jonas W., Joshi, Laura, Lina, Lu, Lukas, Markus, Michi, Miri, Mohamed, Nelson, Niclas, Nicolas, Nils, Nina, Olli, Patrick, Paul, Rasmus, Regina, Ruben, Sebastian S., Sylvia, Theresa L., Thomas sowie auch Frau Ebner, Frau Möhler und Frau Weidinger; Christoph, Karl, Matthias und Herr Walter.

Bedanken möchte ich mich auch bei Frau Prof. Dr. Högger für das Anvertrauen der Aufgaben im Rahmen des Studentenpraktikums und den anderen Kolleginnen und Kollegen der klinischen Pharmazie für die schöne Zeit:

Bettina, Sebastian Z., Simon, Charlotte, Flo L., Linda, Maike, Stoyan, Max, Theresa H., Jasmin und Arthur.

Danke an alle weiteren universitären und nicht-universitären Kooperationspartner außerhalb unseres Arbeitskreises:

Prof. Dr. Dr. Lorenz Meinel, Dr. Johannes Wiest, Dr. Maria Cecilia Amstalden, Dr. Juliane Adelmann, Dr. Paul Gamache, Dr. Frank Steiner, Dr. Katherine Lovejoy, Dr. Tibor Müllner, Dr. Benjamin Eggart und vor allem auch an Prof. Dr. Oliver Scherf-Clavel, der stets für Probleme und Diskussionen als Ansprechpartner zur Verfügung stand.

“Hvala!” an die serbischen Kolleginnen in Belgrad:

Ana, Biljana, Jelena, Jovana, Marija und Nevena.

Table of Contents

List of abbreviations

AA	amino acid
AAA	amino acid analyzer
ANN	artificial neural network
API	active pharmaceutical ingredient
CAD	charged aerosol detector
CF	correction factor
CNLSD	condensation nucleation light-scattering detector
EDQM	European Directorate for the Quality of Medicines & HealthCare
ELSD	evaporative light-scattering detector
EP	European Pharmacopoeia
FIA	flow-injection analysis
FDA	food and drug administration
FMOC	9-fluorenylmethyl chloroformate
GC	gas chromatography
HILIC	hydrophilic interaction chromatography
HPLC	high performance liquid chromatography
HPTLC	high performance thin layer chromatography
ICH	International Conference on Harmonisation of Technical Requirements for Registration of Pharmaceuticals for Human Use
i.d.	internal diameter
Imp.	impurity
LC	liquid chromatography
LoD	limit of detection
LoQ	limit of quantification
m/z	mass-to-charge ratio
MTBE	tert.-butyl methyl ether
MS	mass spectrometry

NMR	nuclear magnetic resonance
ODS	octadecylsilyl
PFPA	pentafluoropropionic acid
PEG	polyethylene glycol
Ph. Eur.	European Pharmacopoeia
PFV	Power Function Value
PS	polysorbate
QSPR	quantitative structure-property relationship
R^2	coefficient of determination
RI	refractive index
RMSE	root mean square error
RPIP	reversed phase ion-pairing
RP	reversed phase
rpm	rounds per minute
RRF	relative response factors
RRT	relative retention time
rsd	relative standard deviation
S/N-ratio	signal-to-noise ratio
SD	standard deviation
TFA	trifluoroacetic acid
TLC	thin layer chromatography
UHPLC	ultra high performance liquid chromatography
USP	United States Pharmacopeia
UV	ultra violet
UV/Vis	ultra violet/visible

1 Introduction

When taking a look at the application of different methods of analysis utilized in the pharmaceutical environment, high performance liquid chromatographic (HPLC) applications stand out as the technique of choice in the pharmaceutical industry and within many compendial methods [1]. While assay methods in the European Pharmacopoeia (Ph.Eur.) are still dominated by titration procedures, this method is almost on even numbers with HPLC in the bulk assays of the United States Pharmacopoeia (USP) [2, 3]. With regard to impurity profiling and determination of related compounds, HPLC is the most widespread method due to its high robustness, simple and cost-efficient application as well as high precision and sensitivity [4]. During method development, an HPLC procedure can be tailored towards almost all special needs of the compounds, e.g. required limits of detection and quantitation (LOD and LOQ) and separating the drug from its impurities. Nowadays, the majority of APIs usually is produced either by chemical synthesis, fermentation or extraction procedures. In order to find the optimal method for the purity analysis of an active pharmaceutical ingredient (API) or an excipient and their potential contaminants, respectively, the production pathway governs their impurity profile [5-10]. Then, one usually aims for the cheapest and most simple method achieving the desired results. Hence, most liquid chromatographic procedures for quality control utilize the principle of UV/Vis detection due to its low costs, simple operation, broad applicability, a large dynamic range and satisfying sensitivity [11-14].

However, UV/Vis detection has some serious limitations, which are highly relevant for a huge number of assay and purity determinations by means of HPLC. Not only the API, but also all of the impurities to be analysed need to possess a suitable chromophore visible at the narrow detection range of about 190 to 400 nm. Ideally, all compounds can be properly measured at the same detection wavelength. If all compounds have a suitable chromophore but exhibit strongly differing absorption maxima, either a correction factor or a diode array detector (DAD) can be used [15-19]. For many compounds such as amino acids, sugar molecules and their derivatives, certain active pharmaceutical ingredients (APIs), or fatty acid- and macrogol-based excipients, this represents a significant challenge.

1.1 Coping with the inability to use HPLC-UV/Vis

Various solutions exist to this issue. For example, derivatization procedures such as the ninhydrin-derivatization of amino acids as it is applied with the amino acid analyser (AAA) enable their detection, but this technique is still blind to e.g. related organic acids [20, 21]. This could be compensated by the introduction of a second liquid chromatographic method into the pharmacopoeial monograph (e.g. aspartic acid or glycine [22, 23]), resulting in the need to perform two steps in order to determine a substance's impurity profile. When dealing with amino acids, the second method often times is a low wavelength HPLC-UV method tailored towards the remaining related substances with very different chromatographic parameters compared to the one for related amino acids.

Instead of suggesting two separate methods, the UV absorbing properties at 210 nm of carboxylic acids can be used in order to enable detection of the amino acids and the organic acids in one run simultaneously [6, 20]. For this, a proper method that is capable of separating not only organic acids, but also amino acids and other related impurities needs to be developed. A suitable option to obtain such a method is the application of ion-pair chromatography or mixed-mode HPLC. These procedures are further discussed in chapter 1.4 and 4.1. When working with these low-wavelength UV detection methods, just like for any chromatographic method, it is necessary to use a mobile phase, which does not absorb at the very low detection wavelength. Thus, when using an organic modifier, its UV cutoff has to be considered because below that wavelength UV detection is impossible [24-27]. In the same manner, all additives and buffer substances which are present in the mobile phase must not have a higher cutoff either. Otherwise, the sensitivity will be impaired significantly [28, 29]. The UV cutoff values for common organic modifiers, mobile phase buffers and ion-pairing additives are shown in Tables 1 - 3.

This can be a challenging factor, e.g. when distinct pH values or certain ion-pairing reagents would be of interest for the method. If applicable, in order to comply with the thresholds set by the International Council for Harmonisation of Technical Requirements for Pharmaceuticals for Human Use (ICH) guidelines or pharmacopoeias, the inherently rather low sensitivity of this procedure can be overcome with a high sample load, but only if the API is sufficiently soluble and an appropriate resolution is maintained [21]. Of note, the required reporting, identification,

and qualification thresholds of an impurity are based on the daily intake of the drug substance. These are defined in the guidelines on impurities in new drug substances Q3A(R2) and on impurities in new drug products Q3B(R2) published by the International Council for Harmonisation of Technical Requirements for Pharmaceuticals for Human Use (ICH) [30, 31].

Table 1: UV cut-off and other properties of common mobile phase solvents applied in HPLC [32-35]

Solvent	UV cutoff [nm]	Viscosity [cP]	Solvent strength on silica [ε]	Volatile
Acetone	330	0.36	0.53	Yes
Acetonitrile	190	0.38	0.52	Yes
Isopropanol	205	2.40	0.60	Yes
Methanol	205	0.55	0.70	Yes
Tetrahydrofuran	212	0.55	0.53	Yes
Toluene	284	0.59	0.22	Yes
Water	190	1.00	n.a. [a]	Yes

[a] not applicable

Table 2: UV cut-offs and properties of common mobile phase buffers and additives in HPLC [35, 36]

Additive	UV cutoff [nm]	pH range	pK_a value	Volatile
Ammonia	200 at 10 mM	8.2 - 10.2	9.2	Yes
Acetic acid	210	n.a. [a]	4.8	Yes
Acetate	210 at 10 mM	3.8 - 5.8	4.8	Yes
Bicarbonate	200 at 10 mM	5.4 - 7.4 9.3 - 11.3	6.4 10.3	Yes
Citrate	230 at 10 mM	2.1 - 4.1 3.7 - 5.7 4.4 - 6.4	3.1 4.7 5.4	No
Formic acid	210	n.a. [a]	3.8	Yes
Formate	210 at 10 mM	2.8 - 4.8	3.8	Yes
Phosphate	200	1.1 - 3.1 6.2 - 8.2 11.3 - 13.3	2.1 7.2 12.3	No
TFA	210 at 0.1%	n.a. [a]	0.3	Yes
TRIS	205 at 10 mM	7.3 - 9.3	8.3	No

[a] not applicable

Table 3: UV cut-offs and properties of common ion-pairing reagents in HPLC [32, 37, 38]

Additive	UV cutoff	basic/acidic	pK_a value	Volatile
Alkylsulfonates	≈200 nm	acidic	Usually <1, slightly depending on chemical modification	No
Perflluorinated carboxylic acids	≈210 nm	acidic	Usually <1, slightly depending on chemical modification	Yes
Trialkylamines	≈235 nm	basic	Usually ≈10, slightly depending on chemical modification	Yes
Tetraalkyl ammonium salts	≈200 nm	basic	Permanently positively charged	No

Another coping strategy involves the use of other compensating analytical systems than HPLC, e.g. thin layer chromatography (TLC). In general, TLC procedures suffer from several drawbacks, such as poor reproducibility, low resolution, very time consuming experiments, and a comparably challenging automation [39-41]. While modern HPTLC procedures achieve a good resolution, the aspect of time consumption still represents a major drawback especially for compounds that cannot be assessed with a distinct spraying reagent. Either very unspecific protocols or very long exposure times are described in the major pharmacopoeias. For example, the monographs of ampicillin, fosfomycin, or metoprolol detect the substance spot after very long exposure to iodine vapour (up to 15 h) [42-45]. Additionally, when used for impurity profiling, TLC represents a rather semi-quantitative method. Reference solutions are applied alongside the test solution(s) and a subsequent size comparison of the spots is performed [46-48]. Depending on the size and shape of the TLC spots, and the analyst performing the method, this can lead to vague results. Furthermore, it can only be said whether an impurity substance is present above or below a certain threshold, instead of reporting a proper quantitative result as it is possible with other procedures such as liquid chromatography. Sensitivity is also an issue for this technique. With TLC, achievable LOQs can be as low as 0.5%.

For volatile analytes, solvent residues, certain plant extracts or excipients, gas chromatography (GC) can be used as the method of choice. However, not all compounds can be assessed with this procedure, it is rather costly, requires a complex instrumentation and consumables, and derivatization steps can be necessary. An example are fatty acids, which are often times analysed after derivatization to the respective fatty acid methyl esters (FAME) [49-52].

Another possibility is the use of capillary electrophoresis (CE). However, a major drawback of this instrumentation is that it lacks a high robustness and sensitivity, leading to a very rare use in routine analysis and pharmacopoeial monographs. Nevertheless, for the separation of enantiomers, CE can prove to be superior to HPLC where the application of chiral selectors or chiral stationary phases is expensive and challenging [53-56].

1.2 Non-UV HPLC detectors

Coupling HPLC procedures to different detectors than UV/Vis is the most recent and most versatile alternative strategy for detecting weakly-absorbing or non-chromophore compounds. Besides the aforementioned reaction with ninhydrin, different derivatization procedures with reagents that introduce or create a fluorophore into the molecule are possible and allow for subsequent use of a fluorescence detector. An example can be found in the determination of amino acids by using o-phthalaldehyde (OPA) [57-59]. Although this technique possesses a great sensitivity, derivatization procedures can be tedious, prone to errors, or lead to either incomplete or unwanted side reactions. Hence, they often are avoided in routine quality control methods [21].

Instead of having to use derivatization procedures, there are several options that allow the assessment of non-chromophore molecules amongst the so-called “universal detectors”. One of them is the refractive index detector (RI): It measures the refractive index of the mobile phase which changes when a particular analyte is present. One major drawback is the incompatibility with gradient elution mode because changes in the composition of mobile phase lead to a different refractive index, therefore long equilibration times are required before the isocratic runs in order to obtain an acceptable baseline. Unstable operating temperatures can lead to severe noise generation. In general, the sensitivity of this detection method is inferior to other techniques [60]. Nevertheless, the RI is commonly used for the analysis of many sugars and some non-chromophore APIs in compendial applications (e.g. bisphosphonates, lauromacrogol 400, glucose [61-63]).

Another universal detection method is the evaporative light scattering detector (ELSD). It was invented and had its beginning in the 1960s and was commercially introduced in the 1980s [64, 65]. Belonging to the group of aerosol-based detectors, the column effluent is nebulized with the help of nitrogen gas and the resulting aerosol is then used

for the detection. Big droplets are led to the waste and only the smaller ones enter an evaporation tube. After evaporation, the particles pass a light beam and the scattered light is measured eventually. Hence, any non-volatile substance present in the aerosol will result in a signal. Therefore, with ELSD and any other aerosol-based techniques, mobile phases need to be made up of volatile components exclusively in order to keep the baseline noise as low as possible [60]. Although this detector has found its way into compendial methods as well (e.g. in the Ph.Eur. monograph of sucrose stearate [66]), several studies have pointed out major disadvantages of this detector compared to its main competitor the charged aerosol detector (CAD). The ELSD was shown to be less sensitive, to possess an inferior linear range, to be more complicated to optimize with regard to method and instrument parameters, and likely to generate random “spike peaks” when a high sample load is used [60, 67-72]. Although modern versions of this detector have overcome the problem of a low dynamic range by introducing a new function for automated adjustment of the detector’s “gain” setting (Sedere® SAGA technology), the randomly occuring “spike peaks” can make the proper interpretation of the chromatograms challenging or even impossible as presented in chapter 4.4.

Based on the previously mentioned aerosol principle, the condensation nucleation light scattering detector (CNLSD) was developed in 1993 [65, 73]. Unlike the ELSD, this detector leads the aerosol into a condensation chamber in which a supersaturated *n*-butanol or water vapour is present. Through condensation onto the particles they increase in size making formerly too small particles detectable. Analogously to the ELSD, light scattering is used as the detection principle. Due to the condensation process, the sensitivity is improved compared to the ELSD [74]. Nevertheless, the CNLSD has never found its way into routine applications because it is not easy to use, more expensive than the ELSD, affected more severely by mobile phase contaminations, and its reproducibility is inferior to the CAD [60, 65, 72, 75].

The most recent development in the field of the aerosol-based detectors is the charged aerosol detector (CAD) that was introduced by Dixon and Peterson in 2002 and made commercially available by Gamache et al. in 2005 [60, 65, 76]. The first steps of the detection principle are identical to the other two presented aerosol detectors. However, the CAD does not rely on light scattering in order to detect the analytes. Alongside the nebulization and evaporation process that leads to the formation of dry particles from the aerosol, a secondary nitrogen gas stream passes a corona discharge needle and

then bares positive charge. The dried particles are led into a mixing chamber where they meet the secondary nitrogen stream. The positive charge is transferred to them and afterwards measured by means of an electrometer after the removal of excess charge via an ion trap. Accordingly, the CAD is also limited to non-volatile molecules and is restricted to the use of volatile mobile phase components. The resulting signal is dependent on the analyte mass and can be considered as quasi-universal when applied under constant conditions [77-79].

One of the most sophisticated and comprehensive methods is represented by mass spectrometry (MS). This procedure yields the highest amount of information since it not only can provide quantitative information but also a structural enlightenment. It can also serve as a supplementary separation technique, because molecules with different mass-to-charge (m/z) ratios can be determined simultaneously, even when they would co-elute in HPLC. The analytes are ionized during the process by means of an ion source, e.g. electrospray ionization, atmospheric pressure chemical ionization or matrix assisted laser desorption ionization. Subsequently, the ions are separated based on their m/z ratio in an electric field. Structural information is gathered during this process. Of note, the molecules can be fragmented during these steps by applying suitable instrument parameters. Special fragmentation patterns can reveal even more information about the chemical properties and substructures of the molecule. The mobile phase requirements are analogous to all other aerosol-based detectors, hence any method developed for an ELSD, a CNLSD, or a CAD can be directly transferred to MS. A major drawback of the routine use of MS is represented by its limitation to ionisable molecules, complex operating steps and a very expensive initial price and maintenance. Additionally, the quantification is not as universal as it is achievable with the CAD and unambiguous elucidation of a structure usually requires supplementary experiments with other techniques such as NMR or X-ray crystallography [60, 80-82].

Of course, these methods can also be used in combination, but as aerosol-based detectors and mass spectrometry are destructive detection methods, they need to be the last instrument if coupled in-line. An exemplary highly capable setup would comprise of an UV/Vis detector and a CAD coupled to the outlet of the UV detector. If CAD and MS detection are intended to be used in the same system, one can utilize a flow-splitting device which diverts a fixed percentage of the system effluent to each detector. These setups can be applied complementarily and make use of the benefits of each detector for the analysis; thus, the certainty of quantification results or the

range of possible analytes available for detection in one run can be improved significantly. Further information on and discussion of this aspect can be found in chapter 3 of this work.

1.3 Charged aerosol detection

As presented in previous sections of this work, the initial steps of the detection mechanism of the CAD do not differ from the other aerosol-based detectors. The nebulization of the effluent with the help of nitrogen gas and the removal of big droplets and subsequent evaporation of the droplets to dried particles occur analogously. However, the final principle for signal generation, i.e. using an electrometer to measure charge imposed to particles instead of a light beam assisted detection, represents a very different approach to ELSD and CNLSD [77, 83]. A schematic layout of the CAD is depicted in Figure 2.

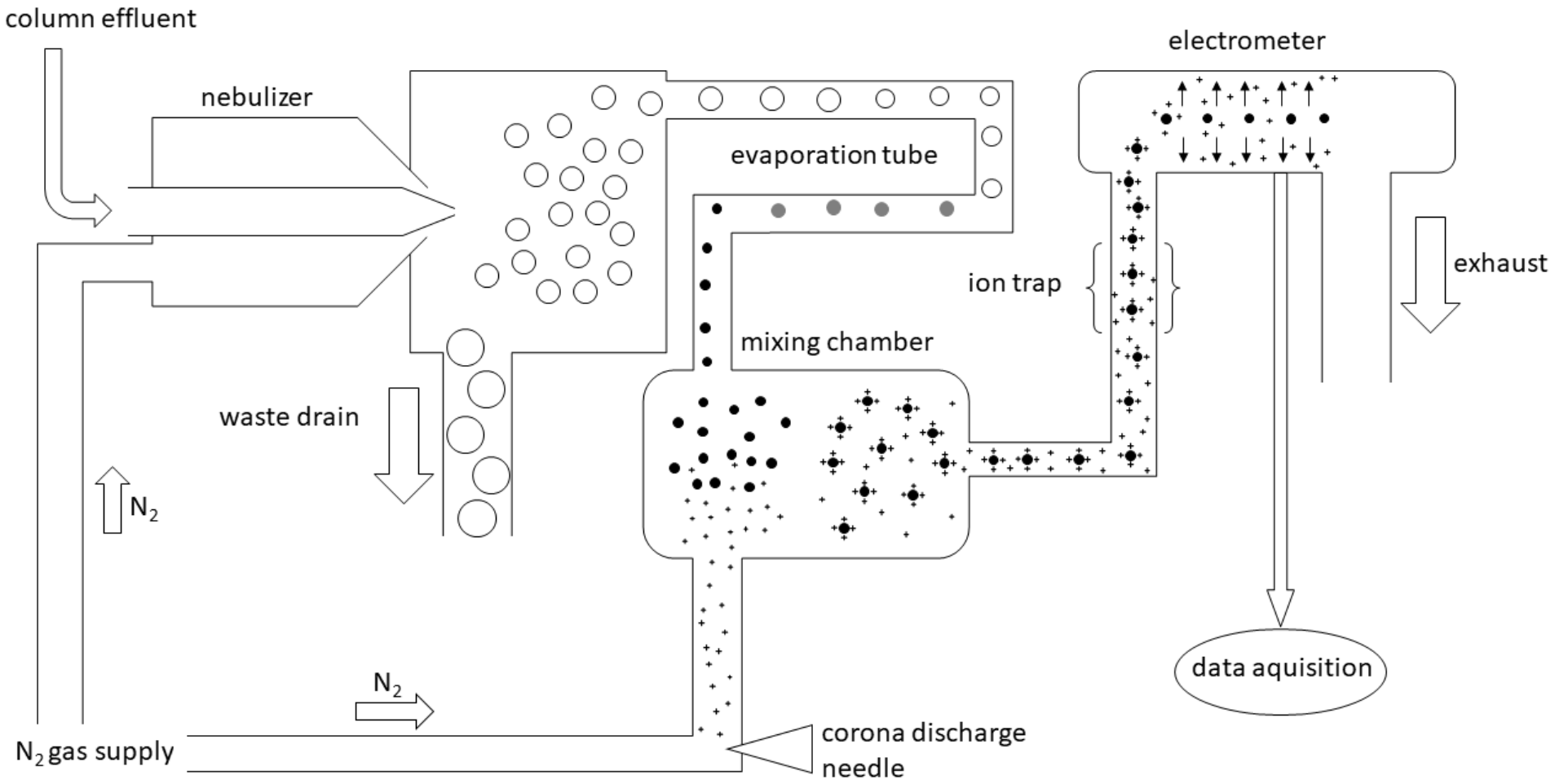

Figure 2: Schematic operating principle of the CAD [77]

Like all other aerosol-based detectors, the CAD generally generates a non-linear response, which however can be linear over a small concentration range. The signal follows a relationship that is described by the power law function

$$signal = a \times m^b \qquad \text{Eq. (I)}$$

where *a* and *b* are factors that depend on the experimental conditions and *m* is the injected mass of analyte [77]. For $b = 1.0$, the response is linear while it becomes sublinear for $b < 1$ or supralinear for $b > 1$. A common tool for signal linearization is the double logarithmic transformation [77, 79], leading to a relationship described by the equation

$$\log signal = \log a + b \times \log m \qquad \text{Eq. (II)}$$

One of the CAD's big advantages over the ELSD originates from the dependency of the aerosol-based detection methods on the particle diameter. In general, the diameter of the resulting particle can be described by two equations. The initial droplet diameter d_d after the nebulization process is described by the *Nukiyama-Tanasawa* [83, 84] equation

$$d_d = \frac{585}{(v_g - v_l)} \times \left(\frac{\sigma}{\rho}\right)^{0.5} + 597 \times \left(\frac{\mu}{\sqrt{\rho \times \sigma}}\right)^{0.45} \times \left(\frac{1000 \times Q_l}{Q_g}\right)^{1.5} \qquad \text{Eq. (III)}$$

where ρ represents the density, μ the viscosity and σ the surface tension of the eluent. The velocity of the gas and liquid streams inside the nebulizer are described by v_g and v_l, while the volume flow rate of the eluent and the scavenger gas are reflected in Q_g and Q_l. According to this equation, a low viscous, highly volatile eluent will lead to smaller particles. As it is depicted in Figure 2 and described in the introductory section about the operating principle of aerosol-based detectors, big droplets get eliminated before the evaporation process. Hence, because a certain amount of analyte is lost when big droplets are eliminated, the aerosol-based detectors perform more sensitive when a low viscosity and highly volatile mobile phase - and the concomitant formation of smaller droplets - is used [85]. This explains the general tendency of a higher sensitivity with increasing amounts of organic modifier as pointed out more in detail in later sections.

For the evaporation process, the formation of the particles from the initial droplets and their diameter d_p, respectively, is described by

$$d_p = d_d \left(\frac{c}{\rho_p} \right)^{1/3} \qquad \text{Eq. (III)}$$

where ρ_p describes the density and c the concentration of the analyte [79, 86]. Subsequently, these resulting particles are exposed to the unipolar diffusion charging process. Hence, the linearity and intensity of the signal highly depends on the particle size and number of particles [83].

For the ELSD and its light scattering principle, the proportionality between the signal and the particle size is expressed by power law exponents between 2 and 6, while the exponents describing the unipolar diffusion charging that takes place in the CAD also depend on the particle size but have a smaller range from about 2.25 to about 1.133 [87]. Because the formation of particles always underlies a size distribution, they are never of universal size [69, 83]. Therefore, the process of unipolar diffusion charging inherently yields a more linear correlation due to the smaller difference in the exponent for varying particle sizes. Power law exponents as a function of particle size for light scattering and unipolar diffusion charging are presented in Figure 3.This results in a wider quasi-linear range of the CAD's signal in comparison to its light scattering competitors. Figure 4 presents a visualization of the quasi-linear range of the CAD's signal relationship.

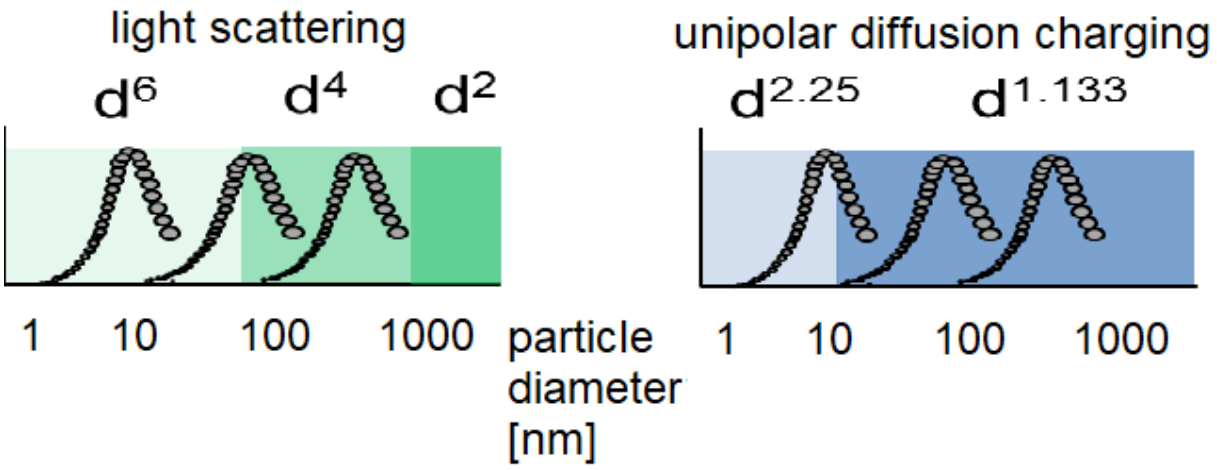

Figure 3: Proportionality between particle diameter and response for the detection principle of ELSD (light scattering) and CAD (diffusion charging). Reprinted modified with permission from [87].

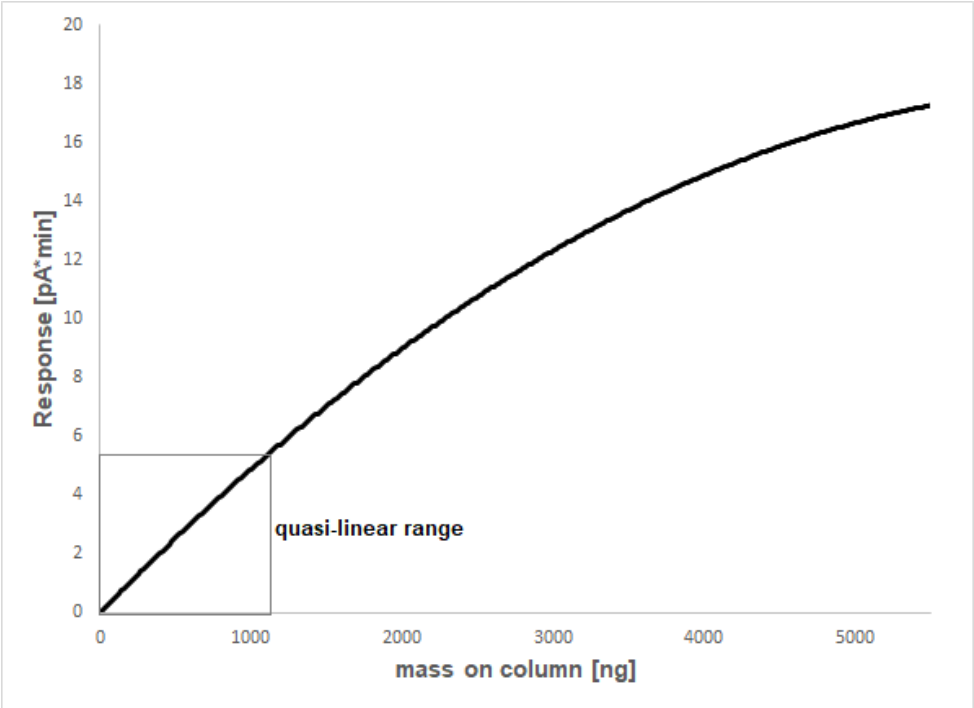

Figure 4: typical calibration curve of the CAD and demonstration of its quasi-linear range [88]

The newer models of the CADs have more adjustable parameters than the older versions. With regard to the linearity of signal, the so-called “power function value” represents a mathematical transformation tool that can linearize the signal and even increase the sensitivity and resolution of the chromatographic method [89-94]. Furthermore, the possibility of increasing the evaporation temperature can smoothen the baseline and improve the sensitivity as long as the analyte is sufficiently non-volatile. A more detailed view on these two topics is presented in chapters 3 and 4.2 of this work. Both of these parameters can be seen as a great opportunity to apply the CAD to more complex problems and in the pharmacopoeial environment. However, the major drawback preventing widespread acceptance of the CAD remains: only one manufacturer of this type of detector exists which would make compendial analysis impossible if the company would stop its production or any other problems concerning its availability occur. Implementing the detector in compendial tests would therefore also support a monopoly status which is a highly relevant argument for the regulatory authorities to be hesitant with its implementation.

1.4 Chromatographic solutions for polar analytes

As presented in the precedent sections, the analysis of polar analytes with structurally diverse impurities can prove to be complex. Since classical RP-HPLC procedures are usually not applicable, and derivatization procedures are often times undesirable, three main techniques are available as alternatives:

- Hydrophilic interaction liquid chromatography (HILIC)
- Ion-pairing chromatography
- Mixed-mode chromatography.

The principle of HILIC makes use of polar stationary phases and apolar mobile phase components. In contrast to common normal phase (NP) chromatography where usually purely hydrophobic organic phases are used, a hydrated surface is proclaimed to be built on the stationary phase in HILIC. This is achieved by a high percentage of organic solvent combined with a low percentage of water [95]. Accordingly, similar to NP chromatography, the stationary phases of choice comprise of amino phases, cyano phases, silanol groups, alcohols, and other polar functionalities [96]. Due to the fact that this technique is rather young (only being used in the last two decades) and the wide variety of stationary phases, method development in HILIC tends to be more of a “trial and error” approach instead of being done as systematically as in RP-HPLC [97, 98]. Nevertheless, nowadays certain guidelines for sensible method development exist and are communicated especially by the column manufacturers [99]. It should be mentioned that when combined with aerosol-based detection methods such as the CAD, HILIC methods proved to obtain an excellent sensitivity. Both, particle formation and signal generation benefit from the high amounts of organic modifier (usually acetonitrile) and the concomitant decreased viscosity of the mobile phase according to the deliberations shown in chapter 1.3 [65, 69, 77, 83, 100-102]. Some further thoughts on this topic are reflected in chapter 3.

Moreover, ion-pairing chromatography represents a possibility to separate polar compounds and their impurities on classical RP columns (RPIP). Ion-pairing reagents need to be amphiphilic, containing two important chemical properties: on the one hand, they have to be charged, while on the other hand a lipophilic molecular part is required. Some commonly used ion-pairing reagents have already been listed in Table 3 in chapter 1.1. Non-volatile additives such as e.g. alkylsulfonates and quarternary

alkylamines cannot be used with aerosol-based detectors. Multiple retention mechanisms contribute to a separation in RPIP-HPLC [103, 104]. Firstly, the ion-pairing reagents strongly interact with the stationary phase, modifying the surface of the column. Since this process is often described to be either fully irreversible or only partly reversible, a column that has been used in an ion-pairing application should remain dedicated to this mobile phase for its lifespan. In accordance with this mechanism, equilibration times for the stationary phases tend to be very high [105, 106]. This behavior gives ion-exchange properties to the RP column as well. Another process, which takes place, is the formation of ion-pairs between analyte molecules and the mobile phase additive itself. Hence, charged analytes become neutralized by a counterion and their retention is increased by reversed phase mechanisms as well [106-109]. As a consequence of this behavior, the response of these ion-pairs in CAD is also increased, due to the particle not only consisting of the sole analyte but of the entire ion-pair [110]. Although this can be considered beneficial for certain applications, this behavior leads to further restrictions when considering the composition of the mobile phase. For example, the ion-pair of ammonia and TFA is nonvolatile, hence these two additives which are CAD suitable individually must not be combined. Ion-pairing reagents are part of the chapters 4.1 and 4.3 of this work and the signal generation under the presence of ion-pairing effects is elaborated in chapters 3 and 4.3.

The third chromatographic solution for challenging analytes is found in mixed-mode chromatography. This terminology describes the use of stationary phases that combine multiple column chemistries in one single product [111]. There are various suppliers and types of columns such as RP columns with either anion exchange (AX) or cation exchange (CX) properties, HILIC phases with ionic exchange properties, or even ternary mixed-mode columns that combine three retention mechanisms. Another differentiation between these column chemistries is based on the pK_a values of the ionisable group, resulting in either weak or strong anion/cation exchange properties in dependency of the pH of the mobile phase. Due to the complexity of these phases, their relatively new introduction and the lack of standardization, columns from two different manufacturers cannot be simply replaced by each other even if the column chemistry has the same declared specification. The difference and complexity of these phases also makes mixed-mode method development a “trial and error” approach, especially because the prediction of their behavior under different chromatographic

parameters is convoluted. When changing the eluent system, it is not certain whether one retention mechanism will be influenced more or less than another. Additionally, mixed-mode phases were found to degrade faster than regular RP-HPLC columns, and the presence of multiple retention mechanisms can lead to irregular peak shapes or induce unpredictable tailing and fronting. Nevertheless, they have a justifiable place in modern chromatography. Because the stationary phase is already equipped with more than one retention mechanism, no ion-pairing mobile phase additives have to be used. Hence, the background noise of such a method can be improved significantly compared to a similar RPIP method and the use of expensive and toxic ion-pairing reagents such as alkylamines or perfluorinated carboxylic acids can be avoided. Especially with regard to the CAD and to MS, this can be advantageous in order to decrease the contamination of the system and the noise. However, this is limited to columns that show no or very little column bleeding only [106, 111-113].

Another factor that needs to be considered is that strong ionic interactions between the column and the analyte can affect results and column properties. In order to obtain reproducible results and reach the required sensitivity, a saturation of the column can become necessary. Ionic forces can be strong enough so that a compound permanently sticks to the column. Chapter 4.4. of this work presents experiments and considerations with regard to this phenomenon. According to this behaviour, mixed-mode and its strong ionic interactions can be a blessing and a curse at the same time and therefore require thorough effort during method development and validation phase.

During the elaboration of this thesis, mixed-mode chromatography has been used for the analysis of bisphosphonates.

1.5 References

1. Davani B. Common Methods in Pharmaceutical Analysis. Pharmaceutical Analysis for Small Molecules. John Wiley & Sons, Hoboken; 2017.

2. Siddiqui MR, AlOthman ZA, Rahman N. Analytical techniques in pharmaceutical analysis: A review. Arab J Chem. 2017;10:S1409-S21.

3. Görög S. The sacred cow: the questionable role of assay methods in characterising the quality of bulk pharmaceuticals. J Pharm Biomed Anal. 2005;36:931-7.

4. Council of Europe. General Presentation on the Role and Place of the Certification Procedure in the European Regulatory System. 2018. Available from: https://www.edqm.eu/sites/default/files/presentation-pheur-training-ppr_general_presentation_on_cep-may2018.pdf. Accessed: November 12th 2019.

5. Beyer T, Diehl B, Holzgrabe U. Quantitative NMR spectroscopy of biologically active substances and excipients. Bioanalytical Reviews. 2010;2:1-22.

6. Schilling K, Amstalden MC, Meinel L, Holzgrabe U. Impurity profiling of L-asparagine monohydrate by ion pair chromatography applying low wavelength UV detection. J Pharm Biomed Anal. 2016;131:202-7.

7. Hoppe B, Martens J. Aminosäuren–Herstellung und Gewinnung. Chemie in unserer Zeit. 1984;18:73-86.

8. Görög S. The importance and the challenges of impurity profiling in modern pharmaceutical analysis. TrAC. 2006; 25:755-757.

9. Remberg B, Stead A. Drug characterization/impurity profiling, with special focus on methamphetamine: recent work of the United Nations International Drug Control Programme. Bull Narcotics LI. 1999:97-117.

10. Kopec S, Holzgrabe U. Impurity profile of amino acids? Pharmeuropa Scientific Notes. 2005:39-45.

11. Zhang S-W, Xing J, Cai L-S, Wu C-Y. Molecularly imprinted monolith in-tube solid-phase microextraction coupled with HPLC/UV detection for determination of 8-hydroxy-2'-deoxyguanosine in urine. Anal Bioanal Chem. 2009;395:479-87.

12. Odriozola-Serrano I, Hernández-Jover T, Martín-Belloso O. Comparative evaluation of UV-HPLC methods and reducing agents to determine vitamin C in fruits. Food Chemistry. 2007;105(3):1151-8.

13. Arshad HM, Gauhar S, Bano R, Muhammad IN. Development of HPLC-UV method for analysis of cefixime in raw materials and in capsule. Jordan J Pharm Sci. 2009;2:53-65.

14. Morgan NY, Smith PD. HPLC detectors. Handbook of HPLC. chapter 7:207-31. Taylor & Francis Group, Milton Park, 2010.

15. Fejős I, Neumajer G, Béni S, Jankovics P. Qualitative and quantitative analysis of PDE-5 inhibitors in counterfeit medicines and dietary supplements by HPLC–UV using sildenafil as a sole reference. J Pharm Biomed Anal. 2014;98:327-33.

16. Mwalwisi YH, Höllein L, Kaale E, Holzgrabe U. Development of a Simple, Rapid, and Robust Isocratic Liquid Chromatographic Method for the Determination of Pyrimethamine and its Synthetic Impurities in Bulk Drugs and Pharmaceutical Formulations. Chromatographia. 2017;80:1343-52.

17. EDQM, Strasbourg, France. Chapter 2.2.46 - Chromatographic Separation Techniques. European Pharmacopoeia Online 9.8, 2019. Available from: http://online6.edqm.eu/ep908/. Accessed: November 12th 2019

18. Wang T, Guo S, Zhang S, Yue W, Ho C-T, Bai N. Identification and quantification of seven sesquiterpene lactones in Inula britannica by HPLC-DAD-MS. Anal Methods. 2019;11:1822-33.

19. Chen S, Sun G, Ma D, Yang L, Zhang J. Quantitative fingerprinting based on the limited-ratio quantified fingerprint method for an overall quality consistency assessment and antioxidant activity determination of Lianqiao Baidu pills using HPLC with a diode array detector combined with chemometric methods. Journal of separation science. 2018;41:548-59.

20. Kühnreich R, Holzgrabe U. Impurity profiling of l-methionine by HPLC on a mixed mode column. J Pharm Biomed Anal. 2016;122:118-25.

21. Wahl O, Holzgrabe U. Amino acid analysis for pharmacopoeial purposes. Talanta. 2016;154:150-63.

22. EDQM, Strasbourg, France. Monograph No. 0797 - Aspartic acid. European Pharmacopoeia Online 9.8, 2019. Available from: http://online6.edqm.eu/ep908/. Accessed: November 12th 2019

23. EDQM, Strasbourg, France. Monograph No. 0614 - Glycine. European Pharmacopoeia Online 9.8, 2019. Available from: http://online6.edqm.eu/ep908/. Accessed: November 12th 201923.

24. Li Y, Piao D, Zhang H, Kim T, Lee S-H, Chang HW et al. Quality evaluation of Carthami Flos by HPLC–UV. Arch Pharm Res. 2015;38:776-84.

25. Khandani SK, Mehrabani M, Sharififar F, Pardakhty A, Pournamdari M, Pakravanan M. Development and Validation of an RP-HPLC Method for Determination of Solasodine, a Steroidal Alkaloid. J Young Pharm. 2019;11.

26. Talele G, Porwal P. Development of validated bioanalytical HPLC-UV method for simultaneous estimation of amlodipine and atorvastatin in rat plasma. Indian J Pharm Sci. 2015;77:742.

27. Nestola M, Thellmann A. Determination of vitamins D 2 and D 3 in selected food matrices by online high-performance liquid chromatography–gas chromatography–mass spectrometry (HPLC-GC-MS). Anal Bioanal Chem. 2015;407:297-308.

28. Vinkovic K, Galic N, Schmid MG. Micro-HPLC–UV analysis of cocaine and its adulterants in illicit cocaine samples seized by Austrian police from 2012 to 2017. J Liq Chromatogr Relat Technol. 2018;41:6-13.

29. Wu X, Zeng X, Wang L, Hang T, Song M. Identification of related substances in tofacitinib citrate by LC-MS techniques for synthetic process optimization. J Pharm Biomed Anal. 2017;143:17-25.

30. International Council for Harmonization, Guideline Q3A (R2) Impurities in new drug substances.2006.

31. International Council for Harmonization Guideline Q3B (R2) Impurities in new drug products.2006.

32. Snyder LR, Kirkland JJ, Dolan JW. Introduction to modern liquid chromatography. John Wiley & Sons, Hoboken; 2011.

33. Ahuja S. Chromatography and separation science. Elsevier, Amsterdam; 2003.

34. Horváth C. High-performance liquid chromatography: advances and perspectives. Elsevier, Amsterdam; 2013.

35. McMaster MC. LC/MS: a practical user's guide. John Wiley & Sons, Hoboken; 2005.

36. HiChrom Limited UK. LC Column information - Buffer Selection. https://www.hichrom.com/assets/HichromCat9-pdfs/LC_Column_Information-Buffer_Selection_p28.pdf. Accessed: November 12th 2019.

37. Hansen SH, Pedersen-Bjergaard S, Rasmussen K. Introduction to pharmaceutical chemical analysis. John Wiley & Sons, Hoboken; 2011.

38. Winkler G, Briza P, Kunz C. Spectral properties of some ion-pairing reagents commonly used in reversed-phase high-performance liquid chromatography of proteins and peptides in acetonitrile gradient systems. J Chromatogr A. 1986;361:191-8.

39. Berezkin V, Kormishkina E. Study of a new version of classical thin-layer chromatography with a closed adsorbent layer. J Planar Chromatogr. 2006;19:81-5.

40. Zarzycki P, Bartoszuk M, Radziwon A. Optimization of TLC detection by phosphomolybdic acid staining for robust quantification of cholesterol and bile acids. J Planar Chromatogr. 2006;19:52-7.

41. Crane NA. Development of Novel Analytical Methods with the Aim of Forensic Analyte Detection using Ultra-Thin Layer Chromatography, Surface Enhanced Raman Spectroscopy, and Magneto-Elastic Wire Sensing. PhD thesis.University of Tennessee - Knoxville, 2016. Available from: https://trace.tennessee.edu/utk_graddiss/3688/

42. EDQM, Strasbourg, France. Monograph No. 0167 - Ampicillin. European Pharmacopoeia Online 9.8; 2019. Available from: http://online6.edqm.eu/ep908/. Accessed: November 12th 2019

43. EDQM, Strasbourg, France. Monograph No. 1329 - Fosfomycin sodium. European Pharmacopoeia Online 9.8, 2019. Available from: http://online6.edqm.eu/ep908/. Accessed: November 12th 2019

44. EDQM, Strasbourg, France. Monograph No. 1028 - Metoprolol tartrate. European Pharmacopoeia Online 9.8; 2019. Available from: http://online6.edqm.eu/ep908/. Accessed: November 12th 2019

45. EDQM, Strasbourg, France. Monograph No. 1980 - Heptaminol hydrochloride. European Pharmacopoeia Online 9.8; 2019. Available from: http://online6.edqm.eu/ep908/. Accessed: November 12th 2019

46. Höllein L, Kaale E, Mwalwisi YH, Schulze MH, Holzgrabe U. Routine quality control of medicines in developing countries: analytical challenges, regulatory infrastructures and the prevalence of counterfeit medicines in Tanzania. TrAC. 2016;76:60-70.

47. Roth L, Biggs KB, Bempong DK. Substandard and falsified medicine screening technologies. AAPS Open. 2019;5:2.

48. Paul P, Sänger-van de Griend C, Adams E, Van Schepdael A. Recent advances in the capillary electrophoresis analysis of antibiotics with capacitively coupled contactless conductivity detection. J Pharm Biomed Anal. 2018;158:405-15.

49. Chen TK, Phillips JG, Durr W. Analysis of residual solvents by fast gas chromatography. J Chromatogr A. 1998;811:145-50.

50. Slover H, Lanza E. Quantitative analysis of food fatty acids by capillary gas chromatography. J Am Oil Chem Soc. 1979;56:933.

51. Lisec J, Schauer N, Kopka J, Willmitzer L, Fernie AR. Gas chromatography mass spectrometry–based metabolite profiling in plants. Nat Protoc. 2006;1:387.

52. Theiss C, Holzgrabe U. Characterization of polydisperse macrogols and macrogol-based excipients via HPLC and charged aerosol detection. J Pharm Biomed Anal. 2018;160:212-21.

53. Haginaka J. Enantiomer separation of drugs by capillary electrophoresis using proteins as chiral selectors. J Chromatogr A. 2000;875:235-54.

54. Fillet M, Bechet I, Chiap P, Hubert P, Crommen J. Enantiomeric purity determination of propranolol by cyclodextrin-modified capillary electrophoresis. J Chromatogr A. 1995;717:203-9.

55. Nishi H, Nakamura K, Nakai H, Sato T. Separation of enantiomers and isomers of amino compounds by capillary electrophoresis and high-performance liquid chromatography utilizing crown ethers. J Chromatogr A. 1997;757:225-35.

56. Abushoffa AM, Clark BJ. Resolution of the enantiomers of oxamniquine by capillary electrophoresis and high-performance liquid chromatography with cyclodextrins and heparin as chiral selectors. J Chromatogr A. 1995;700:51-8.

57. Roth M. Fluorescence reaction for amino acids. Anal Chem. 1971;43:880-2.

58. Mangge H, Zelzer S, Prüller F, Schnedl WJ, Weghuber D, Enko D, Bergsten P, Haybaeck J, Meinitzer A. Branched-chain amino acids are associated with cardiometabolic risk profiles found already in lean, overweight and obese young. J Nutr Biochem. 2016;32:123-7.

59. Fonseca BM, Cristóvão AC, Alves G. An easy-to-use liquid chromatography method with fluorescence detection for the simultaneous determination of five neuroactive amino acids in different regions of rat brain. J Pharmacol Tox Met. 2018;91:72-9.

60. Zhang K, Kurita K, Venkatramani C, Russell D. Seeking universal detectors for analytical characterizations. J Pharm Biomed Anal. 2018.

61. EDQM, Strasbourg, France. Monograph No. 1564 - Sodium alendronate trihydrate. European Pharmacopoeia Online 9.8; 2019. Available from: http://online6.edqm.eu/ep908/. Accessed: November 12th 2019.

62. EDQM, Strasbourg, France. Monograph No. 2046 - Lauromacrogol 400. European Pharmacopoeia Online 9.8; 2019. Available from: http://online6.edqm.eu/ep908/. Accessed: November 12th 2019.

63. EDQM, Strasbourg, France. Monograph No. 0177 - Glucose. European Pharmacopoeia Online 9.8; 2019. Available from: http://online6.edqm.eu/ep908/. Accessed: November 12th 2019.

64. Ford D, Kennard W. Vaporization analyzer. J Oil Colour Chem Assoc. 1966;49:299-313.

65. Magnusson L-E, Risley DS, Koropchak JA. Aerosol-based detectors for liquid chromatography. J Chromatogr A. 2015;1421:68-81.

66. EDQM, Strasbourg, France. Monograph No. 2318 - Sucrose stearate. European Pharmacopoeia Online 9.8; 2019. Available from: http://online6.edqm.eu/ep908/. Accessed: November 12th 2019.

67. Bai C-C, Han S-Y, Chai X-Y, Jiang Y, Li P, Tu P-F. Sensitive determination of saponins in Radix et Rhizoma Notoginseng by charged aerosol detector coupled with HPLC. J Liq Chromatogr Relat Technol. 2008;32(2):242-60.

68. Lippold S, Koshari SH, Kopf R, Schuller R, Buckel T, Zarraga IE, Koehn H. Impact of mono-and poly-ester fractions on polysorbate quantitation using mixed-mode HPLC-CAD/ELSD and the fluorescence micelle assay. J Pharm Biomed Anal. 2017;132:24-34.

69. Almeling S, Ilko D, Holzgrabe U. Charged aerosol detection in pharmaceutical analysis. J Pharm Biomed Anal. 2012;69:50-63.

70. Holzgrabe U, Nap CJ, Beyer T, Almeling S. Alternatives to amino acid analysis for the purity control of pharmaceutical grade L-alanine. J Sep Sci. 2010;33:2402-10.

71. Almeling S, Holzgrabe U. Use of evaporative light scattering detection for the quality control of drug substances: Influence of different liquid chromatographic and evaporative light scattering detector parameters on the appearance of spike peaks. J Chromatogr A. 2010;1217:2163-70.

72. Hutchinson JP, Li J, Farrell W, Groeber E, Szucs R, Dicinoski G , Haddad PR. Comparison of the response of four aerosol detectors used with ultra high pressure liquid chromatography. J Chromatogr A. 2011;1218:1646-55.

73. Allen LB, Koropchak JA. Condensation nucleation light scattering: a new approach to development of high-sensitivity, universal detectors for separations. Anal Chem. 1993;65:841-4.

74. Cintrón JM, Risley DS. Hydrophilic interaction chromatography with aerosol-based detectors (ELSD, CAD, NQAD) for polar compounds lacking a UV chromophore in an intravenous formulation. J Pharm Biomed Anal. 2013;78:14-8.

75. Cohen RD, Liu Y, Gong X. Analysis of volatile bases by high performance liquid chromatography with aerosol-based detection. J Chromatogr A. 2012;1229:172-9.

76. Dixon RW, Peterson DS. Development and testing of a detection method for liquid chromatography based on aerosol charging. Anal Chem. 2002;74:2930-7.

77. Vehovec T, Obreza A. Review of operating principle and applications of the charged aerosol detector. J Chromatogr A. 2010;1217:1549-56.

78. Gorecki T, Lynen F, Szucs R, Sandra P. Universal response in liquid chromatography using charged aerosol detection. Anal Chem. 2006;78:3186-92.

79. Hutchinson JP, Li J, Farrell W, Groeber E, Szucs R, Dicinoski G et al. Universal response model for a corona charged aerosol detector. J Chromatogr A. 2010;1217:7418-27.

80. Awad H, Khamis MM, El-Aneed A. Mass spectrometry, review of the basics: ionization. Appl Spectrosc Rev. 2015;50:158-75.

81. El-Aneed A, Cohen A, Banoub J. Mass spectrometry, review of the basics: electrospray, MALDI, and commonly used mass analyzers. Appl Spectrosc Rev. 2009;44:210-30.

82. Boiteau R, Hoyt D, Nicora C, Kinmonth-Schultz H, Ward J, Bingol K. Structure elucidation of unknown metabolites in metabolomics by combined NMR and MS/MS prediction. Metabolites. 2018;8:8.

83. Gamache PH. Charged aerosol detection for liquid chromatography and related separation techniques. John Wiley & Sons, Hoboken; 2017.

84. Nukiyama S, Tanasawa Y. Experiment on atomization of liquid by means of air stream. Trans Soc Mech Eng. 1938;4(14):128-35.

85. Megoulas NC, Koupparis MA. Enhancement of evaporative light scattering detection in high-performance liquid chromatographic determination of neomycin based on highly volatile mobile phase, high-molecular-mass ion-pairing reagents and controlled peak shape. J Chromatogr A. 2004;1057:125-31.

86. Sadain S, Yang X, Anisimov MP. Fundamental aspects of aerosol-based light-scattering detectors for separations. Adv Chromatogr. 2000;40:1275.

87. Gamache PH. Key Factors Affecting the Performance of Evaporative Aerosol Detectors. 28th Pharmaceutical and Biomedical Analysis Conference (PBA 2017); Madrid 2017.

88. Bailey B. Expanding Your High Performance Liquid Chromatography and Ultra High Performance Liquid Chromatography Capabilities with Universal Detection: Shedding Light on Compounds That Lack a Chromophore. Pittcon Conference & Expo 2014.

89. Dasgupta PK, Chen Y, Serrano CA, Guiochon G, Liu H, Fairchild JN et al. Black box linearization for greater linear dynamic range: the effect of power transforms on the representation of data. Anal Chem. 2010;82:10143-50.

90. Shalliker RA, Stevenson PG, Shock D, Mnatsakanyan M, Dasgupta PK, Guiochon G. Application of power functions to chromatographic data for the enhancement of signal to noise ratios and separation resolution. J Chromatogr A. 2010;1217:5693-9.

91. Plante M, Bailey B, Acworth IN, Crafts C. A Single Method for the Direct Determination of Total Glycerols in All Biodiesels Using Liquid Chromatography and Charged Aerosol Detection. 2012. Available from: https://assets.thermofisher.com/TFS-Assets/CMD/Application-Notes/AN-1049-LC-Glycerols-Biodiesels-AN70159-EN.pdf. Accessed: November 12th 2019

92. Tam J, Ahmad IAH, Blasko A. A four parameter optimization and troubleshooting of a RPLC–charged aerosol detection stability indicating method for determination of S-lysophosphatidylcholines in a phospholipid formulation. J Pharm Biomed Anal. 2018;155:288-97.

93. Zhang Q, Bailey B, Thomas D, Plante M, Acworth I. Determination of Polymerized Triglycerides by High Pressure Liquid Chromatography and Corona Veo Charged Aerosol Detector. 2015. Available from: https://www.researchgate.net/publication/325857533_Determination_of_Polymerized_Triglycerides_by_High_Pressure_Liquid_Chromatography_and_Corona_Veo_Charged_Aerosol_Detector. Accessed: November 12th 2019

94. Schilling K, Pawellek R, Lovejoy K, Muellner T, Holzgrabe U. Influence of charged aerosol detector instrument settings on the ultra-high-performance liquid chromatography analysis of fatty acids in polysorbate 80. J Chromatogr A. 2018;1576:58-66.

95. Callahan DL, Souza DD, Bacic A, Roessner U. Profiling of polar metabolites in biological extracts using diamond hydride-based aqueous normal phase chromatography. Journal of separation science. 2009;32:2273-80.

96. Buszewski B, Noga S. Hydrophilic interaction liquid chromatography (HILIC)—a powerful separation technique. Anal Bioanal Chem. 2012;402:231-47.

97. Niihori Y, Shima D, Yoshida K, Hamada K, Nair LV, Hossain S et al. High-performance liquid chromatography mass spectrometry of gold and alloy clusters protected by hydrophilic thiolates. Nanoscale. 2018;10:1641-9.

98. Fekete S, Molnár I. Software-Assisted Method Development in High Performance Liquid Chromatography. World Scientific, London; 2019.

99. McKeown AP. A Simple, Generally Applicable HILIC Method Development Platform Based Upon Selectivity. Chromatography Today, 2015.

100. Wahl O, Holzgrabe U. Impurity profiling of ibandronate sodium by HPLC–CAD. J Pharm Biomed Anal. 2015;114:254-64.

101. Russell JJ, Heaton JC, Underwood T, Boughtflower R, McCalley DV. Performance of charged aerosol detection with hydrophilic interaction chromatography. J Chromatogr A. 2015;1405:72-84.

102. Bailey B, Plante M, Thomas D, Crafts C, Gamache PH. Practical Use of CAD: Achieving Optimal Performance. Charged Aerosol Detection for Liquid Chromatography and Related Separation Techniques. John Wiley & Sons, Hoboken, 2017.

103. Gennaro M, Giacosa D, Abrigo C. The role of pH of the mobile-phase in ion-interaction RP-HPLC. J Liq Chromatogr Relat Technol. 1994;17:4365-80.

104. Balinova A. Ion-pairing mechanism in the solid-phase extraction and reversed-phase high-performance liquid chromatographic determination of acidic herbicides in water. J Chromatogr A. 1996;728:319-24.

105. Walseth TF, Graff G, Moos Jr MC, Goldberg ND. Separation of 5′-ribonucleoside monophosphates by ion-pair reverse-phase high-performance liquid chromatography. Anal Biochem. 1980;107:240-5.

106. Lamotte S, Kromidas S, Steiner F. Comparison and selection of modern HPLC columns. The HPLC Expert: Possibilities and Limitations of Modern High Performance Liquid Chromatography. John Wiley & Sons, Hoboken; 2016.

107. Cecchi T. Ion pairing chromatography. Crit Rev Anal Chem. 2008;38:161-213.

108. Cecchi T. Theoretical models of ion pair chromatography: a close up of recent literature production. J Liq Chromatogr Relat Technol. 2015;38:404-14.

109. Haney WG, Wittmer DP. Ion-pairing chromatography. Google Patents; 1977.

110. Robinson MW, Hill AP, Readshaw SA, Hollerton JC, Upton RJ, Lynn SM et al. Use of calculated physicochemical properties to enhance quantitative response when using charged aerosol detection. Anal Chem. 2017;89:1772-7.

111. Zhang K, Liu X. Mixed-mode chromatography in pharmaceutical and biopharmaceutical applications. J Pharm Biomed Anal. 2016;128:73-88.

112. Zhang L, Dai Q, Qiao X, Yu C, Qin X, Yan H. Mixed-mode chromatographic stationary phases: Recent advancements and its applications for high-performance liquid chromatography. TrAC. 2016;82:143-63.

113. Botero-Coy AM, Ibáñez M, Sancho J, Hernández F. Direct liquid chromatography–tandem mass spectrometry determination of underivatized glyphosate in rice, maize and soybean. J Chromatogr A. 2013;1313:157-65.

2 Aim of the thesis

Different solutions to overcome two challenges in pharmaceutical analysis are studied in this doctoral thesis. The first challenge is of chromatographic nature and represented by polar molecules which are not suitable for classical RP-HPLC analysis. For these molecules and a possibility for compendial quality control, different chromatographic solutions have to be found, developed and validated in order to enable their reliable analysis. Techniques used for this usually comprise of mixed-mode HPLC and ion-pairing chromatography.

The second challenge is a question of detection methods and is represented by weakly detectable and non-chromophore molecules, which either do not allow for the use of UV/Vis at all or only under special considerations. For these compounds, several universal detector solutions are presented in the introductory section. Amongst these, the CAD has been shown to outperform the ELSD and the CNLSD in the literature. Further studies on the CAD and its capabilities should contribute to the usage of its full potential and understanding.

A study performed in order to elaborate on a chromatographically challenging compound with low wavelength UV detection was the impurity profiling of the amino acid L-asparagine.

The isolated analysis of the CAD's characteristics and the method transfer to newer systems was performed with the method transfer and fatty acid analysis of polysorbate 80.

A combination of these aims was delved into with:

- The analysis of bisphosphonate drugs with mixed-mode HPLC-CAD
- A chemometric evaluation of the CAD signal behavior under RPIP conditions for sugars and the sugar-derived antibiotics streptomycin and kanamycin

3 Recent applications of the CAD

Recent applications of the Charged Aerosol Detector for liquid chromatography in drug quality control

Klaus Schilling, Ulrike Holzgrabe

Accepted Manuscript at Journal of Chromatography A,

Elsevier, Amsterdam, 2020

Abstract

High performance liquid chromatography (HPLC) methods with UV/Vis detection are the most widespread analytical procedures in modern pharmaceutical applications, but reach their limitations when it comes to non chromophore molecules. Hence, instead of using tiresome derivatization procedures, many liquid chromatography methods make use of the so-called aerosol-based universal detectors, namely the evaporative light scattering detector (ELSD), the condensation nucleation light scattering detector (CNLSD) and the charged aerosol detector (CAD). Amongst these, the CAD, being the youngest (introduced in 2005) of these three options, is often described as the most easy-to-use detector and is stated to exhibit sufficient sensitivity and good linearity of signal in a dedicated range of concentration. Therefore, this review sets its focus on the recent applications of the CAD for active pharmaceutical ingredients, excipient analysis as well as botanical applications. Alongside the post column addition techniques, the new CAD's ability to adjust the evaporation temperature and the possibility to use an integrated power function for signal linearization are reviewed as previously unavailable, new parameters for optimization.

1. Introduction

High-performance liquid chromatography (HPLC) has become the most commonly used technique in pharmaceutical analysis ever since its introduction in the early 20th century, now covering over one third of all industrial and pharmacopoeial methods [1, 2]. In order to properly benefit from the robustness and simplicity of HPLC methods, it is necessary to have an appropriate detection method for the analyte of interest. Non-chromophoric compounds can be analyzed by tedious derivatization procedures or by sensitivity-impairing low-UV-wavelength methods; this should be avoided, since these kinds of analytical procedures can be blind to certain impurities, e.g. the amino acid analyzer (AAA) being blind to ninhydrin-negative analytes, and method development and validation can be long-winded [3].

Amongst the so-called aerosol-based universal detectors, solutions to this issue are found in the evaporative light scattering detector (ELSD), the condensation nucleation light scattering detector (CNLSD) and the charged aerosol detector (CAD). As reviewed by Magnusson et al. in 2015 [4], all three detectors have their benefits and drawbacks. Zhang et al. summarized universal detection methods in 2019 [5] and showed that the CNLSD is the least used of those three. Several publications have highlighted sensitivity and linearity advantages of the CAD over the ELSD and the latter was also found to show irreproducible spikes during chromatographic runs with high sample load [6-13]. Although there are other various universal detection principles, such as measurements of the refractive index (RI), or of the conductivity, mass spectrometry (MS), or nuclear magnetic resonance spectroscopy (NMR), they all have certain drawbacks with regard to compendial quality control. In case of the RI and conductivity detector, they lack sensitivity and robustness, respectively. While MS is nowadays a routine application in the industry and research and development because it is not only capable of quantification but also capable of identification procedures, it is still scarcely found in the major pharmacopoeias' monographs. This is mainly due to the increased initial price and maintenance alongside the greater amount of work necessary to establish easily transferrable and robustly validated methods. High sample load, as it is common in pharmaceutical purity control, can also be a risk of contamination for such sophisticated systems. Furthermore, in the field of compendial quality control, the advantage of MS to be able to identify peaks within the chromatogram often times turns obsolete for a monographed pharmaceutical with a

known impurity profile but is beneficial in case a nre impurity occurs. NMR has its very high price, costly maintenance and complex operation that often requires manual adjustments of e.g. the baseline and phasing as major drawbacks [5].

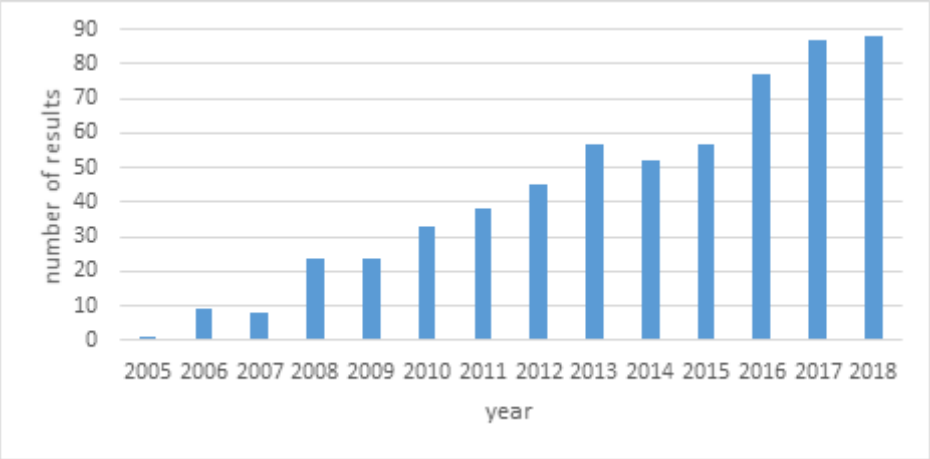

Figure 1: number of search results for the search term “charged aerosol detector” OR “charged aerosol detection” on www.sciencedirect.com

Hence, ever since its introduction in 2005 by ESA biosciences, the CAD has received growing interest and a yearly increasing number of papers have been published on this topic (Figure 1). The general measuring principle of the charged aerosol detector has already been described in depth elsewhere [4, 8, 14-17] and is herein only described shortly and illustrated in Figure 2. In brief, the column effluent is converted into small droplets with the help of a nitrogen gas stream. Next, the evaporation tube produces dried particles from these droplets. A secondary nitrogen gas stream which gets positively charged by passing a corona discharge needle then transfers its charge onto these dried particles in the mixing chamber. Subsequently, the imposed charge on the particles is measured by a highly sensitive electrometer after removal of excess charge via an ion trap. Hence, the signal output is entirely dependent on the created particles and a nearly universal response depending on the analyte mass is often described [18-22]. According to this operating principle, all substances that behave as semi- and non-volatiles can be assessed with this method. The mobile phase is required to consist of volatile components only, which allows for direct transfer of CAD methods to mass spectrometry (MS) for more detailed information on e.g. impurities and degradation products [23-25]. The older generation CADs have very few parameters to optimize (filter setting, signal output range, data collection rate), while the more recent releases allow for adjustments of the evaporation temperature and the use of an integrated power function for signal linearization without the common log-log

transformation [26-29]. For further reading on the CAD's theory and detailed explanations, the 2017 book by P. Gamache is recommended [17].

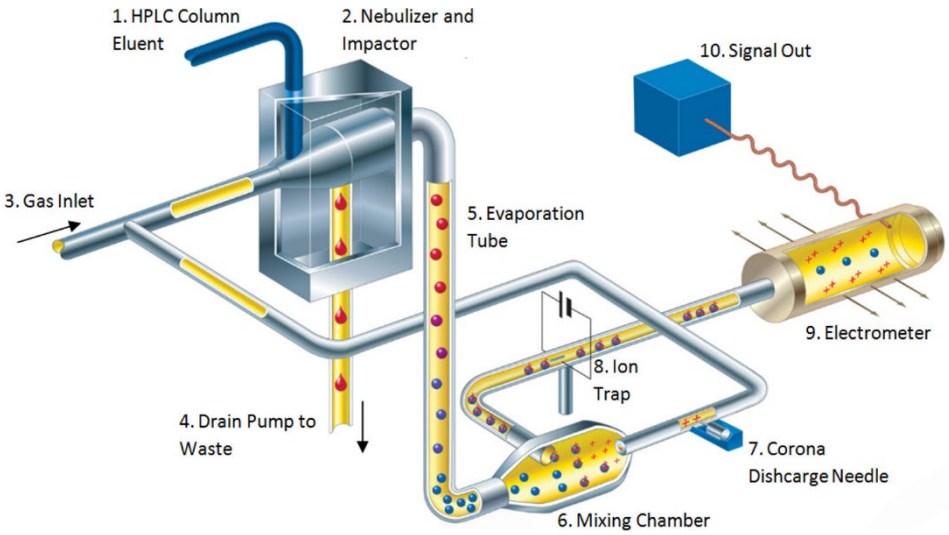

Figure 2: Schematic operating principle of the CAD. Reprinted with permission from [30].

As of now, despite having only one manufacturer, which is an issue in terms of compendial analysis, the CAD is already implemented into two of the major pharmacopoeias, and is to be implemented into the Chinese Pharmacopoeia as presented in Table 1. Moreover, new applications are in the pipeline.

Table 1: Phamacopoeial implementation of the Charged Aerosol Detector

Pharmacopoeia	**Type of implementation**	
European Pharmacopoeia (Ph.Eur.)	Monograph on gadobutrol	[31]
	Listed in the general chapter on liquid chromatography	
United States Pharmacopoeia (USP)	Monograph on deoxycholic acid	[32]
Chinese Pharmacopoeia (CP)	New introduction in the general chapter	[33]

The aerosol-based detectors all share the inability to assess volatile molecules. As a parameter to estimate the suitability of aerosol-based detection, the vapor pressure was found to be a suitable physicochemical property [34]. When it comes to the

comparison of CAD and ELSD, multiple studies have displayed advantages of the CAD over the latter. Some of these are a better reproducibility of the detector response of about 5 %, compared to 11 % for the ELSD [35], less variation of the signal for different compounds, resulting in a more universal response [4] and a two to six times superior sensitivity [36]. The CAD shows a nearly uniform response to different analytes, which can be beneficial to the (semi-) quantitative assessment of substances when no reference standards are available [37]. The range of response factors for different substances is narrow for physicochemically related nonvolatile substances, however, this does not hold true for substances that undergo salt formation (leading to an increased signal) or behave as semivolatiles (leading to a decreased signal). The response of a variety of substances, illustrating the near uniformity as well as the limitations, is shown in Figure 3 and is elaborated more detailed in chapter 2.5.

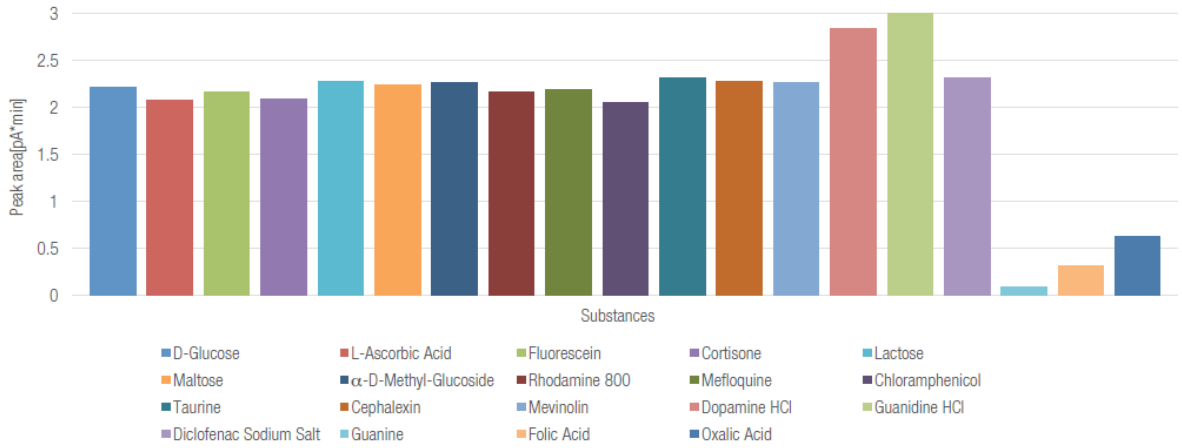

Figure 3: CAD response of identical amounts of various substances presented to the detector by means of flow injection analysis under identical conditions. Dopamine HCl, Guanidine HCl and Diclofenac Sodium show increased values due to salt formation. Guanine, Folic Acid and Oxalic Acid show decreased values due to their high volatility. Reprinted with permission from [37].

This review aims to focus on recent applications of the CAD alongside an overview of the current state of the elaboration of the new adjustable parameters and quantitation approaches.

2. Case studies and applications of the CAD

2.1. Active pharmaceutical ingredients (APIs)

The impurity profiling of many APIs proves to be a challenging task since a detector's sensitivity needs to be optimal in order to achieve the necessary limits of detection (LOD) and limits of quantification (LOQ). Impurity contents as low as 0.03% (when the daily dose exceeds 2 grams of substance) are requested by the ICH guideline Q3A(R2) and the major pharmacopoeias, and need to be determined while the concentration of the API usually is very high, leading to large and tailing main peaks [38-40].

Even if the API contains a chromophore, it is not mandatory for impurities to possess a chromophore as well. Xu et al. published a method capable of analyzing the non-chromophore impurities of metoprolol in 2016 [41]. Here, a hydrophilic interaction chromatography (HILIC) method with a high percentage of organic modifier is established after a thorough column screening. In comparison to an ELSD in this study, the CAD shows an about 10-20 fold better sensitivity than the ELSD. The Ph. Eur. currently describes a thin-layer chromatography (TLC) test for metoprolol's impurities M, N and O [42]. According to the Ph. Eur., the TLC needs to develop for at least 1 h, then dry for at least 3 h and detection is performed with iodine vapor for at least 15 h. Hence, the Ph. Eur. procedure takes over 19 h and only yields a TLC to compare the spots' intensities. Xu et al. successfully anticipated the suitability of aerosol detection by simply evaluating the impurities' vapor pressures at 25 °C and developed a method for the assessment of impurity M and N in less than 8 minutes.

Topiramate's impurity profile was analyzed by Ilko et al. [43] and by Pinto et al. [44]. Ilko et al. utilized a pentafluorophenyl column with a gradient elution using ammonium acetate and acetonitrile. An enormous ninefold increase in sensitivity could be achieved by a post-column addition of acetonitrile. The authors also compared the CAD to an ELSD and found the CAD to outperform the ELSD with regard to sensitivity and repeatability. The sensitivity was 3 to 9 times better with the CAD and the RSD of consecutive measurements was below 3%, whereas the ELSD had deviations of up to 18.3%. Furthermore, the hereinbefore mentioned "spike-" or "ghost-" peaks once again occurred upon using the ELSD [7, 43], which is a problem that still occurs in the modern versions of the detector with high sample load. The problem of impurity A (2,3:4,5-bis-O-(1-methylethylidene)-β-D-fructopyranose) of topiramate being rather volatile, which was solved by usage of TLC and HPTLC by Ilko et al., was overcome

with a C18 column HPLC method by Pinto et al. using an elevated column and system temperature of 50 °C in order to obtain improved particle formation. Instead of a pentafluorophenyl column, Pinto et al. utilized a ternary mixed mode column with reversed-phase, cation exchange and anion-exchange properties for topiramate itself. This is an immense improvement over the USP method, which requires four HPLC methods and the use of a refractive index and a conductivity detector [32, 44]. The topiramate method developed by Ilko et al. is prospectively to be introduced into the Ph. Eur [45] establishing the CAD in another monograph of one of the major pharmacopoeias.

Further HPLC-CAD method examples for the impurity profiling of APIs and their respective benefits are listed in Table 2.

Another type of analysis, which the CAD has been used for is the assay of compounds. One publication dealing with the assay of amikacin by Soliven et al. [27] showed the capabilities of the optimization of the power function value and evaporation temperature. Optimization of these parameters led to increased signal-to-noise ratios, and hence improved LODs and LOQs. Furthermore, an optimized linear dynamic range resulted from an appropriate adjustment of these parameters alongside an improved precision showing RSD values of only about 1%. Further information on the use of the instrument parameters for optimization follows in section 2.5.

Table 2: Further examples of HPLC-CAD applications in impurity profiling

Analyte	**Method characteristics**	**Results and benefits of the method**	
Ibandronate	Mixed-mode CAD	Validated stability indicating method; Direct transfer of the CAD method to MS possible	[25]
Alendronate	Zwitterionic HILIC-CAD	Validated stability indicating method for ions that are inaccessible with UV; low LOQs due to high organic modifier in HILIC	[46]
Gabapentin	RPLC-CAD	Validated stability indicating method; Direct transfer of the CAD method to MS allowed identification/proposal of degradation products; 2 mg/mL instead of 15 mg/mL sample solution when low wavelength UV is used, protecting the system from high sample load;	[47]
Lincomycin and spectinomycin	RPLC-CAD	Identification of peaks and impurities due to parallel detection by means of flow-splitting between CAD and MS; quantification of impurities of which no reference standard was available; CAD was shown to have better robustness and reproducibility than MS and ELSD	[48]
Apramycin	HILIC-CAD	Impurity profiling with CAD was compared to the compendial analysis in the Chinese Pharmacopoeia (SCX-UV with post-column derivatization) and could detect more than twice the number of impurities; identification of impurities possible due to the direct transfer to LC-MS	[49]

Dietary supplements are not monitored as strictly as pharmaceutical products, hence their analytic can be of high interest. Therefore, studies on the content determination of substances and their formulations in the non-pharmacopoeial field have been performed with the CAD as well. For example, Asthana et al. analyzed dietary supplements containing glucosamine, which are used against osteoarthiritis, without the need of derivatization procedures [50]. The authors could show that several Indian products differed more than 10% from the labeled claim of glucosamine content. Furthermore, the dependency of the CAD signal, which is not only increasing upon higher percentage of organic modifier, but also increasing when salt formation between analyte and mobile phase buffer occur, is presented. This behavior of the CAD is discussed more in-depth in section 2.5.

Various comparative studies using UV and CAD detection have been published. Carlos et al. analyzed lisdexamfetamine capsules using both techniques and found the UV detection to be slightly superior in terms of sensitivity but evaluated both techniques as interchangeable and valid, showing recovery rates of 100.39% ± 0.39 for UV and 100.50% ± 0.93 for the CAD and an absolute difference of less than 0.3% in the assay method [51]. Bertol et al. analyzed alogliptin tablets using both techniques and found the CAD to have slightly better LODs and LOQs, but again the detectors were both deemed to be suitable and interchangeable showing an absolute difference of less than 0.2% in the performed assay of alogliptin, with both detectors' RSDs below 1% for 15 consecutive measurements [52]. Brondi and colleagues analyzed amlodipine besylate and olmesartan medoxomil using both detectors and found the UV measurements to be slightly more sensitive than the CAD, having LOQs of 4 and 10 µg/mL for amlodipine and olmesartan, respectively, compared to LOQs of 10 and 15 µg/mL for the CAD. Nevertheless, the CAD was deemed to be suitable in the range of interest, proving to be a robust tool of analysis with inter- and intraday precision experiments yielding RSD values below 1% [53].

Viinamäki and Ojanperä had a very interesting approach with the use of tandem HPLC-UV/CAD and the evaluation of the response ratios of the analytes between UV/CAD [54]. The authors analyzed 161 various basic APIs with this method. The obtained response ratios of UV to CAD enabled an improved identification of the analytes. Hence, this ratio is selective enough to use this approach as a screening method without the need for the use of MS.

Studies reporting the comparison between analytical methods involving derivatization procedures and direct determinations by means of CAD have been performed numerously. Pereira et al. assessed cocaine and its metabolites by means of tandem HPLC-UV/CAD [55]. As this is usually performed by means of GC and derivatization, this approach offers a much simpler solution to this important analysis. A HILIC method was developed by the authors and the results of low wavelength UV detection and CAD were found to be interchangeable for four analytes. While the CAD was blind to one of the volatile compounds, this could be compensated with UV. On the other hand, the CAD could analyze another metabolite, which could not be detected by UV because of insufficient sensitivity. Hereby, the authors showed that a tandem UV/CAD setup can easily fill the gaps of each detector. Dong et al. analyzed 3-aminopiperidine, which is an important precursor for the synthesis of DPP-4 inhibitors, underivatized with a ternary mixed-mode column and CAD [56]. The special column was chosen due to low column bleed and the possibility to use low amounts of buffer salts, which is favorable for maintaining low levels of noise with the CAD. The author's comparison of the new proposal to the well-established precolumn derivatization UV method which has a LOQ equal to 0.06% of the sample concentration showed the CAD to be slightly superior with a LOQ of 0.05%. Additionally, the inter- and intraday precision of the CAD (measured as RSD of n = 6 injections) were both below 1.05%, whereas they were 1.34% and 2.28% for the UV method, respectively. The linear range was also extended by more than one order of magnitude with the CAD, while also decreasing the costs, having a shorter required time for the analysis and a lowered amount of organic waste produced, which is another important factor with regard to the ecological footprint of a method. The benefits of mixed-mode chromatography and its applications have been comprehensively reviewed by Zhang and Liu in 2016 and the compatibility of mixed-mode and aerosol detection together with various applications was presented as well [57].

2.2. Amino acids

Especially amino acids have received special attention with regard to the use of aerosol detectors. As previously reviewed by Wahl and Holzgrabe in 2016, the old-fashioned TLC procedures are nowadays mainly replaced by automatic derivatization procedures such as the AAA, which was originally developed for the determination of the composition of a peptide and not for impurity profiling. Despite being an improvement

in comparison to the TLC methods, these procedures are tedious and can be blind to e.g. ninhydrin-negative impurities such as organic acids. Hence, direct determination of amino acids by means of HPLC-CAD has been applied frequently and with various approaches [3].

Furota et al. utilized an ion-pairing approach with the volatile ion-pairing agent nonafluoropentanoic acid (NFPA) on a porous graphitic carbon column [58]. The method developed could successfully separate 19 underivatized amino acids. In this experiment, the CAD exhibited similar response factors for compounds eluting under similar conditions within the gradient. Ginésy et al. also developed a reversed-phase ion-pairing (RPIP) method for the analysis of amino acids [59], more specifically for arginine. 13 underivatized amino acids were unambiguously resolved with a gradient composed of heptafluorobutyric acid (HFBA) and acetonitrile. Ginésy et al. also evaluated the suitability of reusing washed vials or storing vials in comparison to the usage of fresh HPLC vials, revealing possible interference peaks when using washed vials instead of fresh ones. This showed that the materials in contact with samples and the time of exposure of solutions to certain materials need to be considered when working with CAD due to its high sensitivity and signal generation for all non-volatiles [59]. Socia and Foley used an approach different from the aforementioned ones: a HILIC method with a dual gradient setup was used to separate underivatized amino acids and applied to hydrolyzed proteins [60].

2.3. Botanical extracts and substances

Numerous plants, plant extracts and their secondary metabolites can be challenging from a chromatographic perspective and a detection perspective. Complex matrices and non-chromophore analytes limit the usability of UV methods. Often there are no reference standards of all derivatives available, hence the nearly universal response of the CAD for similar molecules under similar eluent conditions becomes a valuable tool for quantification purposes [36]. Furthermore, by applying statistical tools, the analysis methods can be used for the determination of batches and regional origins when the results are evaluated by means of principal component analysis (PCA) or cluster analysis (CA).

Some example applications of CAD in the field of botanical extracts are listed in Table 3.

Table 3: selection of CAD applications analyzing botanical extracts and substances

Investigated botanical	**Method of analysis**	**Results**	
Astragali Radix	Tandem LC-UV/CAD combined with PCA and CA	Determination of the regional origin of the product, based on the detection of astragalosides and flavonoids	[61]
Toosendan Fructus	HPLC-CAD combined with CA	Determination of the regional origin and quality control of the product based on the chromatographic fingerprint	[62]
Avocado varieties	HPLC-CAD combined with PCA and CA	Classification tree for botanical varieties of avocados based on RP and NP chromatography	[63]
Leonurus sibiricus	HPLC-CAD with internal standard	Quantification of the product's ingredients. Identification of unknown compounds by direct transfer to LC-MS	[64]
Fritillaria thunbergii	Non-derivative HPLC-CAD and HPLC-ELSD	Quantitative analysis of the contained isosteroidal alkaloids Comparison of ELSD and CAD	[65]
Psoraleae Fructus	HPLC-CAD and HPLC-DAD with external standard	Quantification of the major compounds of the product Comparison of CAD and UV	[66]
Ginkgo biloba	HPLC-UV/CAD/MS	Risk assessment of the extracts: quantification by means of CAD, identification by means of UV/HRMS	[67]

Amongst these studies, three of them should be highlighted. The experiments of Long et al. [65], who analyzed isosteroidal alkaloids in *Fritillaria thunbergii* by means of CAD, performed a comparison to the ELSD during the method development. The CAD was found to have an over 30-fold higher sensitivity and was capable of detecting impurities that were not visible for the ELSD. It was further shown, that the CAD possesses a dynamic range of nearly four orders of magnitude and its reproducibility and precision was shown with experimental peak area RSD values below 3%. The APIs peimine and peiminine could be quantified with the final method.

In a comparative study between UV and CAD by Zhang et al. for compounds found in *Psoraleae Fructus*, an about 2-fold increased sensitivity of the CAD over UV was found. Nevertheless, the use of CAD was limited due to not being able to detect two rather volatile molecules, so both detectors should be used simultaneously and complementarily for this purpose [66]. This study serves as an example for aerosol-based detection not being a solution to every detection issue and analytical problem, because it does not achieve the formation of dried particles for molecules that behave as volatiles. As further discussed in section 2.5, one solution to this problem can be the addition of ion-pair forming agents to the mobile phase in order to obtain an analyte ion-pair (i.e. a volatile base pairing with TFA or a volatile acid pairing with ammonia) that behaves as a non-volatile [68].

Baker and Regg's 2018 study of *Ginkgo biloba* extracts with regard to their toxicological risk [67] applied a multi-detector approach by means of flow-splitting between a high resolution mass spectrometer (HRMS) and a CAD. Before this splitting, the analytes were detected by means of a PDA and then an inverse gradient pump delivered a compensating eluent, in order to keep the mobile phase conditions arriving at the CAD and HRMS continuous throughout the measurements. Keeping the eluent conditions constant leads to the CAD responding fairly universally to similar compounds, whereas the individual intensity difference between injections at 100% aqueous and 100% organic solvent varied by a factor of 6. Hence, with the inverse gradient the CAD signal could be used as a semi-quantitative method with individual response factors not differing worse than factor 2, which was found to be sufficient for the risk assessment of the extracts. Structural information needed for the characterization of the molecules was obtained by means of the UV spectra and the HRMS measurements, while being able to work (semi-) quantitative by means of CAD. The CAD was also again pointed out to be more sensitive than the ELSD [67].

2.4. Excipients

2.4.1. Lipids, polyethylenglycols and fatty acid based excipients

Polyethylenglycols, which are also known as macrogols or PEGs, and all excipients esterified or etherified with them, are polydisperse mixtures, whose quality and properties depend on the chain length of the polymer. The pharmacopoeial characterization of these substances is either performed via conventional protocols such as the peroxide value or the hydroxyl value or by means of derivatization procedures prior to spectrophotometric measurements, since they lack chromophores. These analytical methods are very time-consuming and provide bulk parameters rather than full information about the excipient's polydispersity, composition and quality [24, 69]. Of note, when it comes to the fatty acids, the aerosol-based detectors quickly reach their limitations with regard to the volatility of the analytes when dealing with short chain length molecules. Fatty acids of chain lengths below C12 are too volatile for a proper analysis by means of CAD or ELSD, and thereby present one major drawback of these aerosol-based detectors. This shows a field of analysis in which additional techniques such as the use of gas chromatography and derivatization or the use of MS are mandatory [24, 26, 69-71].

Smith et al. [72] analyzed gold nanoparticles functionalized with PEG. Other detection methods such as UV, dynamic light scattering (DLS) or zeta potential measurements are rather used in a qualitative manner in this context. With the presented RPLC-CAD method, the authors enable the nanomedicine field to quantitatively assess the PEGs, which is important because their orientation and chemistry strongly influence the aggregation behavior. Alternative UV-derivatization procedures lack robustness and are hard to handle. A wide range of PEGs ranging from a molecular weight of 2,000 to 20,000 Da can be identified and quantified in one run.

Theiss and Holzgrabe developed a HPLC-CAD method, that was capable of characterizing fatty acids and fatty acid alcohols, the composition of various different macrogols and evaluate their polydispersity as well as analyze the respective excipients in one single run [69]. Successful fatty acid analysis was limited to molecules with more than 12 carbon atoms. The application proved to gain significantly more information, most importantly on the polydispersity, about the excipients than the pharmacopoeial bulk parameter approach, while also being less tedious and time-consuming for the analyst. Due to the possibility of directly transferring LC-CAD

methods to MS systems, LC-MS analyses were used to prove the method's capability of separating single PEG oligomers ranging from n = 3 to n = 54. Furthermore, the applicability of the method to macrogol-based excipients such as Brij®, Myrj® and Tween® was shown and is depicted in Figure 4.

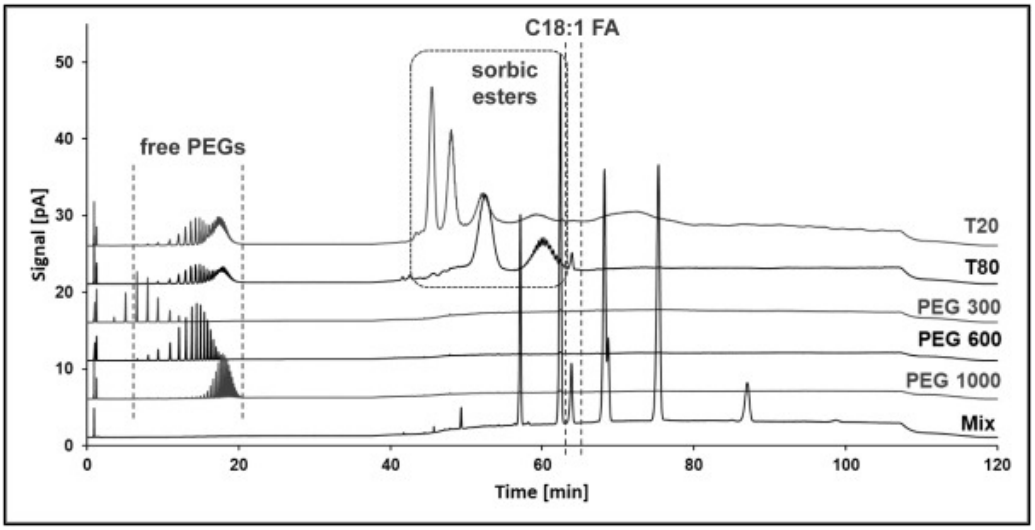

Figure 4: Analysis of free macrogols as well as polysorbate 20 and 80 by HPLC CAD, "Mix" sample contains a mix of fatty acids of the chain lengths C12, C16, C17, C18, C18:1, C18:2 and fatty alcohols of the chain lengths C16 and C18. Reprinted with permission from [69].

A specific study of polysorbate 80 (Tween® 80) was performed by Ilko et al. in 2015 [24], in which the direct transfer of the developed method to mass spectrometry was utilized to identify previously unknown fatty acids occurring in this excipient and several batches were assessed with regard to their conformity with the pharmacopoeial regulations. This method was later transferred to UHPLC and the newest generation CAD by Schilling et al. [26] while setting a strong focus on the most recent adjustable CAD parameters and the limits of its use for rather volatile molecules such as short chain length fatty acids, which is further discussed in section 2.5.

Polysorbates were also of interest for He et al. [73] and Lippold et al. [74]. The former used a 2D-chromatographic approach with a hydrophobic interaction chromatography (HIC) column and a RP column coupled to CAD and MS detection and used this method for the observation of degradation profiles of pharmaceutical protein formulations. The latter used a fluorescence micelle assay (FMA) and a mixed-mode CAD and ELSD method in order to determine poly- and mono-esters of polysorbate. Here, the application of CAD yielded more uniform results than the FMA approach and was beneficial for the determination of polysorbate's chemical hydrolysis.

Additional examples of applications revolving around lipids and counterions are shown in Table 4.

Table 4: selection of CAD applications analyzing excipients and counterions

Analyte	Method of analysis	Results	
Lipids of medium polarity	NP-HPLC	Generic method for the analysis of lipid classes. CAD outperformed ELSD in terms of range and linearity	[75]
Phospholipids in food products	Two-dimensional NP and RP CAD/ESI-MS	Comprehensive analysis of food phospholipids. Identification of peaks through coupling of CAD and MS	[76]
Nucleoside lipids	RP-UPLC with tandem UV/CAD	CAD response depending on pH modifiers, but nearly universal under isocratic conditions. Possible assessment of a compound lacking a chromophore by means of CAD	[77]
Potassium aspartate and magnesium aspartate (PAMA) injections	Mixed-mode HPLC-CAD	Cation analysis in the injections possible. Optimization of the method by means of response surface methodology	[78]
Dissolved boron and silicon in water	Electrodialytic ion isolation and ion-exclusion chromatography	Eco-friendly method using an only aqueous eluent. Superior sensitivity of CAD over conductivity measurements was shown.	[79]

2.4.2 Sugar molecules and sugar derivatives

Boßmann and coworkers [80] used the CAD to determine the chain length of non-chromophore polysialic acid chains produced from *E. coli*. The method was found to be able to assess different chain sizes resulting from hydrolysation procedures and the CAD enabled the researchers to avoid time-consuming derivatization procedures, resulting in time savings of about 24 h when compared to the standard derivatization and fluorescence detection approach for characterization. The CAD method was then optimized and found to correlate highly with quantification results from an orthogonal method, while saving about 18 h in comparison to the common thiobarbituric acid

assay Hetrick, Kramer and Risley [81] developed a HILIC design space using CAD and ELSD detection in which sugars and sugar alcohols can be analyzed. Various stationary phases were evaluated based on a design space and the capability of quantification from complex matrices is shown. The established method shows an LOQ of well below 0.009% (w/w) for the analysis of glucose in trehalose samples. Yan and coworkers [82] established a HILIC-CAD method that was used for the analysis of monosaccharides while also separating possible impurities such as sodium or chloride from the sugar molecules. In this study, eight sugars could simultaneously be quantified directly with LOQs ranging from 50 to 150 ng on column. Although GC-MS methods can obtain superior sensitivity, the developed HILIC-CAD method was adequate for the purpose of determining the monosaccharide composition.

Saokham and Loftsson [83] were able to quantify gamma-cyclodextrin (γ-CD) and its aggregation behavior alongside the critical aggregation concentration by means of RPLC-CAD. An application of this approach is presented for the determination of γ-CD in phase-solubility and permeation studies. The method validation revealed a good linear relationship over the range from 0.005% to 1% (w/v), while the LOQ was calculated to be 0.0002% (w/v) and a high precision with RSDs below 1% for multiple determinations of the recovery rates was demonstrated. Schilling et al. [84] developed a quantitative structure-property relationship (QSPR) model based on sugars and sugar derived antibiotics, which related the physicochemical properties of the analytes to the generated CAD signal. Other aspects from this paper are presented in section 2.5. alongside the utilized parameters and molecular descriptors.

2.4.3 Counterions and other molecules

Due to its functioning principle, the CAD is capable of detecting ions in chromatographic runs. This has already been applied e.g. to the 20 most common pharmaceutical counterions by Zhang et al. in 2010 [85]. New approaches such as the work from Wu and coworkers [86] in 2019 quantify ions in various matrices. Here, the authors assess the ions in liposomal formulations, demonstrating a short analysis time of about 20 min per run and LOQs in the nanomolar range for ammonium and sulphate, outperforming other ion quantitation techniques.

This ability of the CAD inspired Gilmore et al. [87] to use this detector for the quality assessment of water and the total dissolved solids in it. Unlike the usual electrochemical or gravimetric methods used for the characterization of water quality,

the presented CAD method applying a flow injection analysis instead of a chromatographic separation also detects non-conductive impurities alongside all non- or semi-volatile compounds and thereby offers a broader range of compounds covered.

Perfluorinated carboxylic acids (PFCAs), which can be utilized as sufficiently volatile anionic ion-pairing reagents for RPIP-CAD methods [58, 68, 88-91], can also be assessed by means of CAD, when appropriate conditions are chosen. Zhou and colleagues [92] described an isocratic method employing ammonium acetate and methanol on a C8 column. A wide linear range from LOQs between 5 and 14.8 µg/mL up to 1000 µg/mL was found for perfluorinated carboxylic acids between a chain length of C_4 and C_8. The LODs could be improved further by means of a solid phase extraction preconcentration step, leading to 0.075-0.22 µg/mL and a sensitivity nearly on par with ESI-MS/MS. The method was validated with regard to its precision, linearity and accuracy and was applied to wastewater samples. The addition of ammonium acetate as a buffer substance in order to create non-volatile ion pairs between the PFCAs and the ammonium was mandatory for the CAD signal generation. The assessment of the purity of the PFCAs can prove to be important, since different purities of the ion-pairing reagent can result in changing chromatographic behavior for a given RPIP method.

Matsuyama et al. [93] used the CAD for the analysis of brominated flame retardants and made relevant observations with regard to the general functioning principle of the CAD. Although the response for compounds of non-differing volatility was fairly similar, a correlation between a decreasing density and a stronger response was found. Hence, because the surface area of a particle is dependent on the density of the particle, a particle of the same mass can exhibit very different surface areas and very different signal intensities based on the charge imposed to the particle. Therefore, the CAD signal is not only governed by the mass of a particle, but rather by the surface area created during the particle formation. This is in accordance with the particle size d_p having dependency on the density of the analyte. The particle diameter is described as $d_p = d_D \left(\frac{c}{\rho_p}\right)^{\frac{1}{3}}$ with d_D being the droplet diameter, ρ_p being the density of the particle and c is the analyte concentration [16, 17]. Some further findings and studies on the influence of the surface area and particle size follow in section 2.5.

2.5. Modern techniques and parameters to circumvent drawbacks

As mentioned in the previous sections, one of the CAD's advantages aside from the ability to directly transfer developed methods to MS and its ability to detect non-chromophore substances, is the near universality of the CAD signal. Under appropriate conditions and for molecules of comparable physicochemical properties, the CAD response is fairly similar and universal. Thus, it can be used for quantitation purposes when no reference standards of a substance are available [36, 47, 48, 53, 54, 58, 64, 77]. However, this universality is limited by two factors.

The first limitation are difficulties with gradient elution and the resulting mobile phase conditions. The CAD signal is not robust to changes in the mobile phase, as it increases upon augmenting amounts of organic modifier due to an increased transport efficiency, a higher volatility and a lower viscosity in comparison to aqueous eluents. Hence, the usually as a benefit presented quasi-universal response does not hold true for gradient elution. The augmentation of the response under the influence of increasing percentage of the organic modifier does not follow a linear trend. Especially for an organic modifier content greater than 80% the effect can be very unpredictable for different analytes. This behavior is well-known in the literature and has often been described [4, 8, 14, 20, 25, 94-96]. Accordingly, in modern applications, the CAD is also described to perform with better sensitivity in HILIC methods, which utilize higher percentages of organic modifier in comparison to RPLC. This knowledge led to the technique of post-column addition of organic modifier in order to improve signals and signal-to-noise ratios as performed by several authors [8, 43, 95, 97-99]. Since the signal intensities are significantly increased as presented in Figure 5, it can be a helpful tool for improving the LOQs and the LODs of a method.

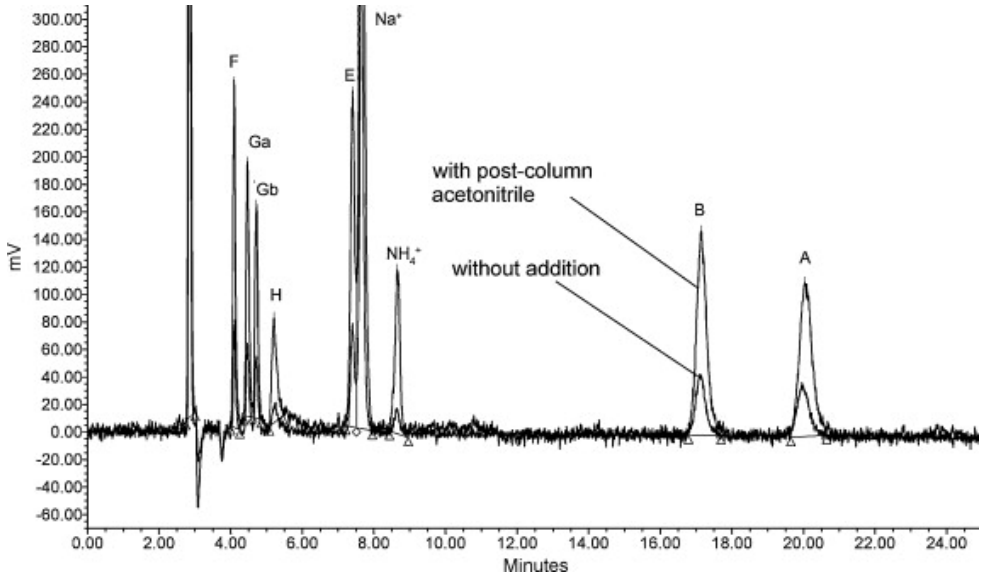

Figure 5: The effect of post-column addition of acetonitrile on the analysis of carbocisteine. Reprinted with permission from [95].

In order to obtain a more universal response even when using gradient elution mode, the concept of the post-column addition of eluent was taken one step further. The so-called “inverse gradient compensation” delivers a post-column gradient directly inverse to the gradient of the chromatographic system. Hence, the eluent composition arriving at the detector is kept constant during the entire chromatographic run, and the response results to be more universal. Some very early studies with inverse gradient compensation were already performed in 2006, just one year after the commercial introduction of the CAD, by Gorecki et al. [100]. More recent studies [18, 22, 67, 101-103] have shown, that the inverse gradient compensation is a valuable tool for generating a rather universal response even in gradient elution mode and hence for quantitation purposes when reference standards are lacking. Furthermore, a drifting baseline due to mobile phase changes can be avoided and stabilized, leading to less noise in the chromatogram, thereby also being beneficial for obtaining better sensitivity.

The second factor is the analyte molecule itself and its physicochemical properties. As pointed out by Matsuyama and coworkers [93], the surface area of the particle is relevant for the signal generation. This is in accordance with the functioning principle of the CAD, which detects the positive charge on the particles. Hence, a larger surface area can bare more charge and will lead to a higher signal. The authors found the surface area to be depending on the density of brominated flame retardants. The according equation is presented in section 2.4.3. of this work. These findings are

supported by the study of Schilling et al. [84], who developed a QSPR model for sugar molecules. After calculation of their physicochemical properties and characteristics encoded in the topological and geometrical molecular descriptors by means of the *Dragon* software, these were linked to the generated CAD signal under different chromatographic conditions. After demonstrating the predictive capabilities of the QSPR model built by means of artificial neural networks (ANN) and external validation with a previously unseen substance, the authors correlated the molecular descriptors to the signal output. A very high importance of the molecular descriptor SpMin1_Bh(v) emphasized the surface area dependency of the CAD. However, this field requires further research incorporating physicochemically diverse substances. However, the influence of other factors than the vapor pressure, which is often used as the primary parameter to estimate detectability with aerosol-based techniques, was shown [34, 41]. An in-depth look into this topic was taken by Robinson et al. in 2017, who related the physicochemical properties of 50 different neutral and basic compounds to the CAD signal [30]. A highly improved linearity and universality of the signal was achieved by the authors, when taking the surface area into account, rather than the mass presented to the detector. The calculated surface area of the particles using physicochemical data, namely the density and pK_a values, and a mathematic algorithm incorporated the ion-pairing effect of basic molecules with TFA present in the mobile phase. The relationship between the relative surface area and the CAD response was more linear than the correlation to the mass concentration. This is presented in Figure 6. Furthermore, the quantification results differed less from the orthogonally used ^{1}H NMR results when using the surface area approach. These studies emphasize that the CAD should also be regarded as a surface area dependent detector rather than just a mass dependent detector. Further research on the detailed behavior of non-ion-pairing and non-volatile molecules based on their molecular descriptors could be considered necessary [84]. Calculations to accommodate for surface area changes e.g. by ion-pairing effects can be performed as shown by Robinson et al. [30] as briefly described above.

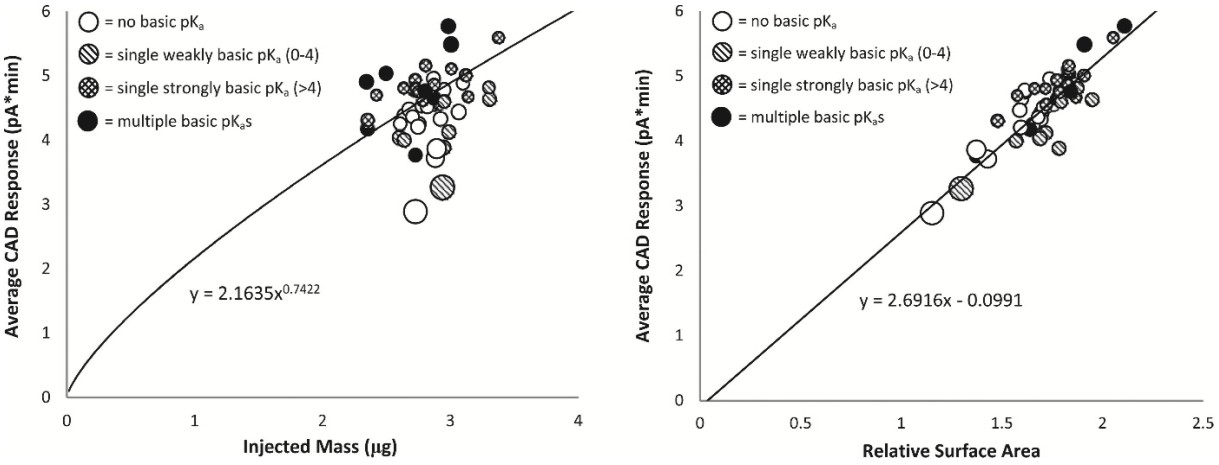

Figure 6: Comparison of the correlation between injected mass and CAD response as well as the correlation between relative surface area and CAD response. Reprinted with permission from [30].

As mentioned in the introductory section, the nowadays CADs allow for an adjustment of the integrated power function value (PFV) and of the evaporation temperature. The evaporation temperature affects the selectivity of the detector's response, by e.g. reducing the noise created from mobile phase additives and is highly dependent on the volatility of the molecules. The PFV is mathematically related to the signal output and can influence the intensity and linearity of the response.

Hence, the PFV allows for an optimization of the sensitivity and accordingly the signal-to-noise ratio as well as especially optimizing the linearity of the signal as shown in various studies [26-28, 104] and applications of the producer [105-108]. All these manage to eliminate the non-linear characteristic of the CAD signal and thereby allow for calibration curves without the application of the usually applied double logarithmic transformation procedures. This can be a solution for linearization purposes especially in GMP regulated laboratories, where data transformations must be validated as well [28]. Three factors should be noted: firstly, the R^2 of a calibration is not necessarily the only informative parameter, because a good R^2 can be misleading and represent a calibration with non-optimal residuals. Secondly, changing the PFV will also affect the resolution of the peaks in question. This needs to be considered especially for critical separations [109]. The studies present that an optimal PFV cannot be established before an analysis; finding the best conditions and the best value does require some work and experiments. This is either done by means of establishment of a predictive model and subsequent measurement of a series of samples at the default PFV, or by measurements at different PFVs [26-28]. For different compounds or compound classes, one will find different optimal PFVs based on e.g. their volatility [26, 110], but

the newer detectors allow for changing this value even during a chromatographic run based on a time scheme saved within the method. Lastly, data transformation such as applying a logarithmic transformation or the utilization of the software's PFV function need to underlie special considerations with regard to the variances of the measurements. As pointed out by Ebel [111] the transformation of the data is not only restricted to the data itself, but also to error margins and variances of the experiments. Therefore, such linearization procedures are potentially faulty over wide ranges and should only be applied if the errors are represented by a normal distribution. Error propagation can lead to an incorrect representation of the actual quality of calibration procedures. As mentioned above, the quality of a regression is usually reported by means of the coefficient of determination of the regression line, however, the residuals of a regression can be more conclusive [26]. Because the CAD's response can be linear over a small concentration range and pharmaceutical quality control often takes place covering only 1 or 2 orders of magnitude, these considerations find limited application in this environment, but should nevertheless not be neglected. An example of signal linearization by means of PFV is shown in Figure 7, whereas the signal linearization by means of double logarithmic transformation is presented in Figure 8.

The background noise in CAD mainly originates from additives and impurities in solvents, hence LC-MS grade solvents are beneficial to the sensitivity. Increasing the evaporation temperature can improve the signal-to-noise ratios by decreasing the noise created by mobile phase additives such as TFA, ammonium acetate or other (semi-) volatile buffer salts. The optimal compromise between decreasing the noise and maintaining sufficient analyte signal is necessary for achieving the best possible LOQs and LODs [26, 29, 112]. Figure 9a depicts the change of the response for homologous fatty acids with decreasing volatility for higher chain lengths when increasing the evaporation temperature. As expected, the signal decreases more severely for volatile molecules and hence, this optimization parameter needs to be evaluated and adjusted carefully. An optimal sensitivity is not achieved when the analyte signal is the highest, but rather as presented in Figure 9b and stated hereinbefore, when the compromise between the reduction of baseline noise and the generated signal is optimal. Hence, the volatility of the analyte molecules needs to be considered.

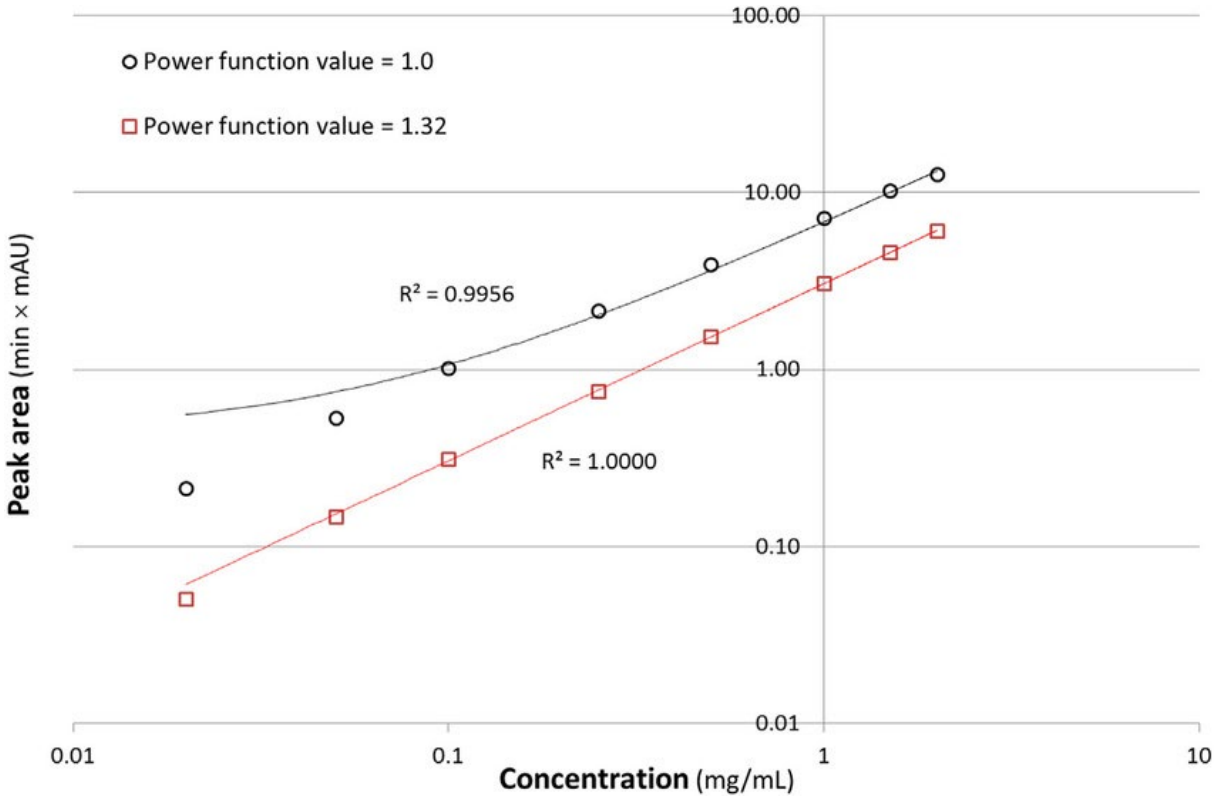

Figure 7: Plot of peak area as a function of concentration for PFV 1.0 and PFV 1.32. Reprinted with permission from [27].

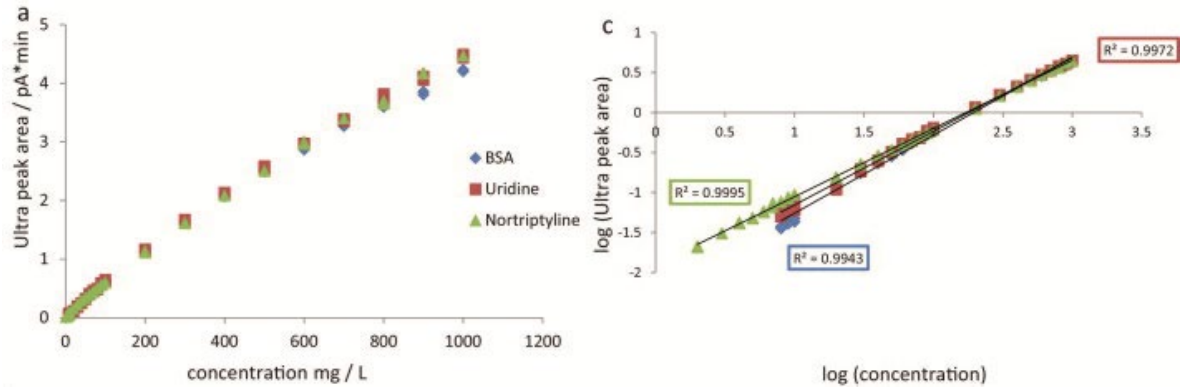

Figure 8: Peak area vs. concentration plots for CAD on a linear scale and a double logarithmic scale. Modified after and reprinted with permission from [16].

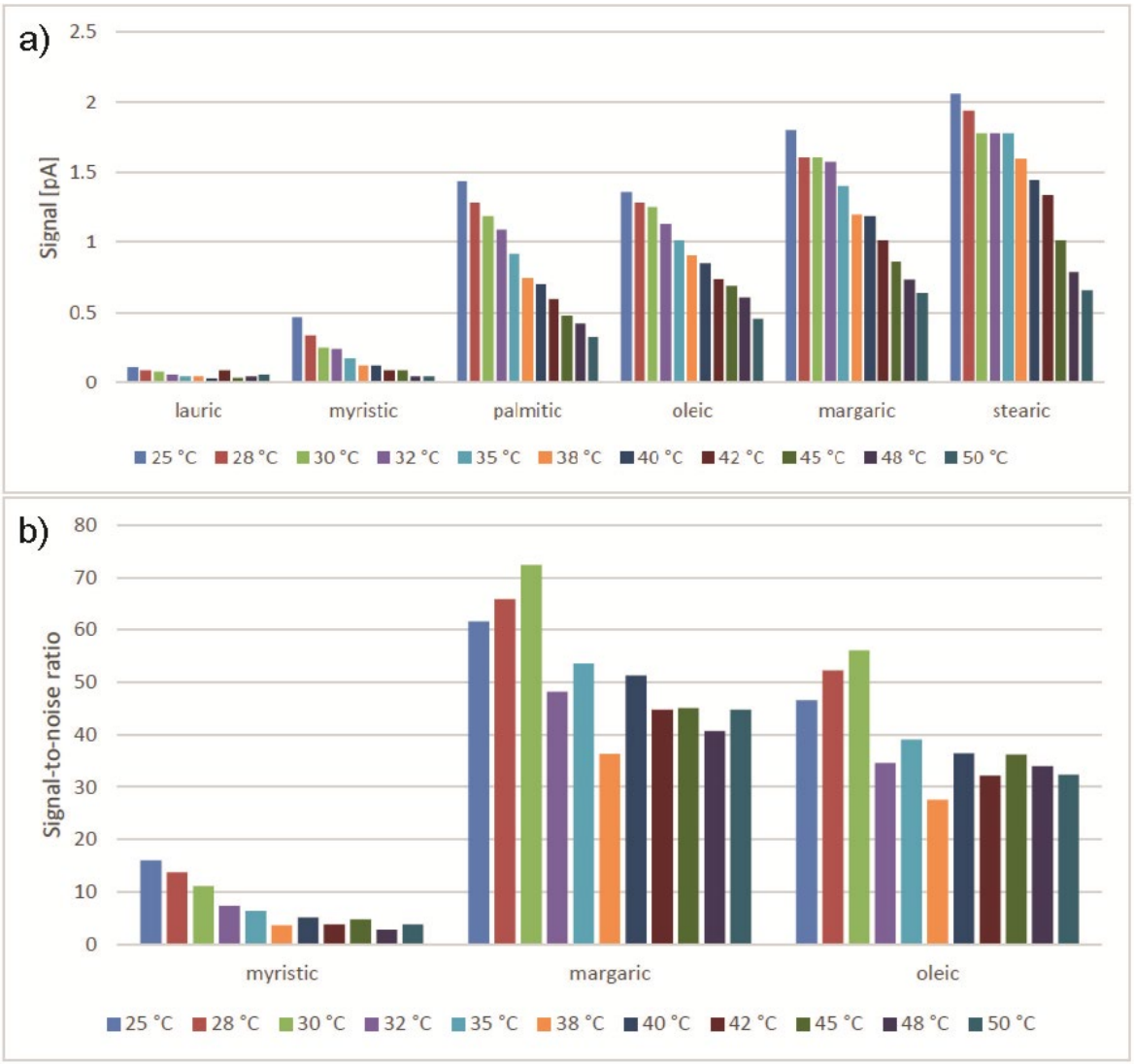

Figure 9: a) CAD signal, expressed as peak height, generated by a series of fatty acids of different chain lengths for different evaporation temperatures. **b)** signal-to-noise ratios achieved for three different fatty acids at various evaporation temperatures. Reprinted with permission from [26].

3. Conclusions

HPLC procedures coupled to UV/Vis detection are limited to chromophoric molecules only. Amongst the aerosol based universal detectors, according to most of the applications reported in the literature, the CAD is more widespread than the CNLSD and more sensitive than the ELSD, and thus a great option of these three detectors. Nevertheless, its application in the compendial field is not widespread because there is only one manufacturer of these systems. If any adverse events regarding the products availability occur, the compendial analyses would be impossible.

Furthermore, the compendial authorities try to avoid the establishment of a procedure that is controlled by a monopoly.

As presented in this review, the CAD can be a valuable tool in the purity analytics of APIs of various compound classes. Even chromophore pharmaceutical drugs often times can contain non-chromophore side products, starting materials or impurities. However, the CAD cannot be used for every type of analyte because volatile molecules are not accessible, therefore hyphenated techniques, such as in-line coupling of UV and CAD or flow-splitting between a CAD and MS detector, can be considered an even more universal choice of detection.

Especially HILIC and mixed-mode HPLC-CAD methods can be found in several recent publications. In HILIC, the aerosol-based detector benefits from improved sensitivity under highly organic conditions. For mixed-mode HPLC-CAD, optimal S/N ratios can be achieved due to the absence of ion-pairing reagents, which would be necessary in RPIP chromatography in order to obtain similar selectivity. The use of ion-pairing reagents can lead to elevated background noise and reduce the sensitivity drastically, if no compensatory adjustments of e.g. the evaporation temperature can be used.

Recent advances in the CAD research have elaborated more detailed on the methodology of inverse gradient compensation in order to optimize the universality of the CAD signal even in gradient elution mode for purposes of quantification when no reference standards are available. It has to be noted, that a few recent studies have shown that the signal behavior and signal intensity of the CAD is dependent on the analyte's density, its tendency to form ion-pairs with the mobile phase and surface area characteristics - not only the injected mass concentration. Therefore, the near universality of the CAD response is restricted to physicochemically related molecules under isocratic conditions that generate similar relative surface areas during the particle formation. The inherent non-linearity of the CAD signal can nowadays be overcome with an optimization of the PFV, while the log-log transformation of the calibration curves can still be sufficient, it can be undesirable in a GMP environment, where every change to the raw data needs to happen in validated procedures [28]. With regard to this, one should keep the possible error propagation due to signal transformation in mind when wide calibration ranges are necessary [111]. New developments and changes in e.g. the detector's nebulization principle or the possibility to adjust certain instrument parameters from one system generation to

another one can make method transfer procedures more challenging when non-identical setups are used. This is in contrast to linear detectors such as classical UV systems. For the GMP environment, this results is greater effort for validation, system suitability testing and revalidation of methods. During method development and the validation procedure it should ideally be checked, whether the sensitivity or resolution depends on the model of CAD being used and whether the transferability of the method is guaranteed. However, since most quality control methods tend to operate in small concentration ranges of 1 or 2 orders of magnitude, and the majority of the currently available publications focuses on the use within research applications instead of usage in the GMP environment, these theoretical drawbacks need to be considered, but the relevance in a practical GMP setting can currently only be estimated.

With the most recent instruments, an increase of the evaporation temperature can improve the signal-to-noise ratios and thereby the CAD's sensitivity through the elimination of background noise while maintaining the analyte's signal. These adjustments should be made with special care, since the analyte needs to be sufficiently non-volatile and the optimal compromise has to be elaborated experimentally. This rather new feature allows for a more sensitive detection of non-volatiles at elevated evaporation temperatures, while a decrease below the default temperature of 35 °C could even make compounds behaving as (semi-) volatiles better accessible if the background noise is kept at an acceptable level.

Due to having similar requirements for the mobile phase as MS, all CAD methods can be directly transferred to MS for identification purposes or a multidetector setup with flow-splitting can be used. The benefits of MS can be used complimentarily to the CAD. While the CAD is capable of achieving a nearly universal response without requiring reference standards, the lack of the specificity can be compensated by the information given with the m/z values. The main argument for the use of aerosol-based detectors instead of MS is that they are economically more attractive. Unless the characterization aspect, that is exclusive to MS or NMR, is necessary, the CAD can be seen as a cost-effective substitute for routine analysis of substances with known impurity profiles because similar or even superior sensitivity is possible with a cheaper instrumentation [113].

Conflict of interest statement

The authors are in a cooperative relationship with Thermo Fisher Scientific® and also were generously provided with a Sedere® ELSD by ERC® GmbH for trial experiments.

References

1. B Davani. Common Methods in Pharmaceutical Analysis. Pharmaceutical Analysis for Small Molecules. John Wiley & Sons, Hoboken, 2017.

2. MR Siddiqui, ZA AlOthman, N Rahman. Analytical techniques in pharmaceutical analysis: A review. Arab J Chem. 2017;10:S1409-S21.

3. O Wahl, U Holzgrabe. Amino acid analysis for pharmacopoeial purposes. Talanta. 2016;154:150-63.

4. L-E Magnusson, DS Risley, JA Koropchak. Aerosol-based detectors for liquid chromatography. J Chromatogr A. 2015;1421:68-81.

5. K Zhang, K Kurita, C Venkatramani, D Russell. Seeking universal detectors for analytical characterizations. J Pharm Biomed Anal. 2018.

6. U Holzgrabe, CJ Nap, T Beyer, S Almeling. Alternatives to amino acid analysis for the purity control of pharmaceutical grade L-alanine. J Sep Sci. 2010;33:2402-10.

7. S Almeling, U Holzgrabe. Use of evaporative light scattering detection for the quality control of drug substances: Influence of different liquid chromatographic and evaporative light scattering detector parameters on the appearance of spike peaks. J Chromatogr A. 2010;1217:2163-70.

8. S Almeling, D Ilko, U Holzgrabe. Charged aerosol detection in pharmaceutical analysis. J Pharm Biomed Anal. 2012;69:50-63.

9. N Vervoort, D Daemen, G Török. Performance evaluation of evaporative light scattering detection and charged aerosol detection in reversed phase liquid chromatography. J Chromatogr A. 2008;1189:92-100.

10. RG Ramos, D Libong, M Rakotomanga, K Gaudin, P Loiseau, P Chaminade. Comparison between charged aerosol detection and light scattering detection for the analysis of Leishmania membrane phospholipids. J Chromatogr A. 2008;1209:88-94.

11. A Hazotte, D Libong, M Matoga, P Chaminade. Comparison of universal detectors for high-temperature micro liquid chromatography. J Chromatogr A. 2007;1170:52-61.

12. K Takahashi, S Kinugasa, M Senda, K Kimizuka, K Fukushima, T Matsumoto et al. Quantitative comparison of a corona-charged aerosol detector and an evaporative light-scattering detector for the analysis of a synthetic polymer by supercritical fluid chromatography. J Chromatogr A. 2008;1193:151-5.

13. S Jia, JH Park, J Lee, SW Kwon. Comparison of two aerosol-based detectors for the analysis of gabapentin in pharmaceutical formulations by hydrophilic interaction chromatography. Talanta. 2011;85:2301-6.

14. T Vehovec, A Obreza. Review of operating principle and applications of the charged aerosol detector. J Chromatogr A. 2010;1217:1549-56.

15. PH Gamache, RS McCarthy, SM Freeto, DJ Asa, MJ Woodcock, K Laws et al. HPLC analysis of nonvolatile analytes using charged aerosol detection. LC GC Europe. 2005;18:345.

16. JJ Russell, JC Heaton, T Underwood, R Boughtflower, DV McCalley. Performance of charged aerosol detection with hydrophilic interaction chromatography. J Chromatogr A. 2015;1405:72-84.

17. PH Gamache. Charged aerosol detection for liquid chromatography and related separation techniques. John Wiley & Sons; Hoboken, 2017.

18. M Eckardt, M Kubicova, TJ Simat. Universal response quantification approach using a Corona Charged Aerosol Detector (CAD)–Application on linear and cyclic oligomers extractable from polycondensate plastics polyesters, polyamides and polyarylsulfones. J Chromatogr A. 2018;1572:187-202.

19. JP Hutchinson, J Li, W Farrell, E Groeber, R Szucs, G Dicinoski et al. Universal response model for a corona charged aerosol detector. J Chromatogr A. 2010;1217:7418-27.

20. M Poplawska, A Blazewicz, K Bukowinska, Z Fijalek. Application of high-performance liquid chromatography with charged aerosol detection for universal quantitation of undeclared phosphodiesterase-5 inhibitors in herbal dietary supplements. J Pharm Biomed Anal. 2013;84:232-43.

21. S Schiesel, M Lämmerhofer, W Lindner. Comprehensive impurity profiling of nutritional infusion solutions by multidimensional off-line reversed-phase liquid chromatography× hydrophilic interaction chromatography–ion trap mass-spectrometry and charged aerosol detection with universal calibration. J Chromatogr A. 2012;1259:100-10.

22. B Behrens, M Baune, J Jungkeit, T Tiso, LM Blank, H Hayen. High performance liquid chromatography-charged aerosol detection applying an inverse gradient for quantification of rhamnolipid biosurfactants. J Chromatogr A. 2016;1455:125-32.

23. K Zhang, Y Li, M Tsang, NP Chetwyn. Analysis of pharmaceutical impurities using multi-heartcutting 2D LC coupled with UV- charged aerosol MS detection. J Sep Sci. 2013;36:2986-92.

24. D Ilko, A Braun, O Germershaus, L Meinel, U Holzgrabe. Fatty acid composition analysis in polysorbate 80 with high performance liquid chromatography coupled to charged aerosol detection. Eur J Pharm Biopharm. 2015;94:569-74.

25. O Wahl, U Holzgrabe. Impurity profiling of ibandronate sodium by HPLC–CAD. J Pharm Biomed Anal. 2015;114:254-64.

26. K Schilling, R Pawellek, K Lovejoy, T Muellner, U Holzgrabe. Influence of charged aerosol detector instrument settings on the ultra-high-performance liquid chromatography analysis of fatty acids in polysorbate 80. J Chromatogr A. 2018;1576:58-66.

27. A Soliven, IAH Ahmad, J Tam, N Kadrichu, P Challoner, R Markovich et al. A simplified guide for charged aerosol detection of non-chromophoric compounds—Analytical method development and validation for the HPLC assay of aerosol particle size distribution for amikacin. J Pharm Biomed Anal. 2017;143:68-76.

28. IAH Ahmad, A Blasko, J Tam, N Variankaval, HM Halsey, R Hartman et al. Revealing the inner workings of the power function algorithm in Charged Aerosol Detection: A simple and effective approach to optimizing power function value for quantitative analysis. J Chromatogr A. 2019.

29. H Takeda, M Takahashi, T Hara, Y Izumi, T Bamba. Improved quantitation of lipid classes using supercritical fluid chromatography with charged aerosol detector. J Lipid Res. 2019:jlr. D094516.

30. MW Robinson, AP Hill, SA Readshaw, JC Hollerton, RJ Upton, SM Lynn et al. Use of calculated physicochemical properties to enhance quantitative response when using charged aerosol detection. Anal Chem. 2017;89:1772-7.

31. Council of Europe, European Pharmacopoeia Online 9.8, 2019, EDQM, Strasbourg, France. Monograph No. 2735. Available from: http://online6.edqm.eu/ep908/. Accessed: September 18th 2019

32. The United States Pharmacopoeia and National Formulary. USP 42 - NF 37, The United States Pharmacopoeia and National Formulary: United Stats Pharmacopoeial Convention Inc.; 2019.

33. K Lovejoy, I Acworth, P Gamache. Charged Aerosol Detection and Method Transfer of Compendial, including USP, Methods. 2019. Available from: https://assets.thermofisher.com/TFS-Assets/CMD/posters/po-72934-cad-method-transfer-usp-pittcon2019-po72934-en.pdf. Accessed: September 5th 2019

34. M Swartz, M Emanuele, A Awad, A Grenier, D Hartley. An Overview of Corona Charged Aerosol Detection in Pharmaceutical Analysis. Synomics Pharma, 2009. Available from: http://citeseerx.ist.psu.edu/viewdoc/download?doi=10.1.1.453.2169&rep=rep1&type=pdf . Accessed: November 14th 2019.

35. JP Hutchinson, J Li, W Farrell, E Groeber, R Szucs, G Dicinoski et al. Comparison of the response of four aerosol detectors used with ultra high pressure liquid chromatography. J Chromatogr A. 2011;1218:1646-55.

36. HY Eom, S-Y Park, MK Kim, JH Suh, H Yeom, JW Min et al. Comparison between evaporative light scattering detection and charged aerosol detection for the analysis of saikosaponins. J Chromatogr A. 2010;1217:4347-54.

37. M Menz, B Eggart, K Lovejoy, I Acworth, PH Gamache, F Steiner. Charged aerosol detection - factors affecting uniform analyte response. 2018. Available from: https://assets.thermofisher.com/TFS-Assets/CMD/Technical-Notes/tn-72806-uhplc-charged-aerosol-detection-tn72806-en.pdf, Accessed: January 10th 2020.

38. S Görög. The importance and the challenges of impurity profiling in modern pharmaceutical analysis. TrAC. 2006;25:755-757.

39. D Jain, PK Basniwal. Forced degradation and impurity profiling: recent trends in analytical perspectives. J Pharm Biomed Anal. 2013;86:11-35.

40. International Council for Harmonization, Guideline Q3A(R2). Impurities in new drug substances. 2006.

41. Q Xu, S Tan, K Petrova. Development and validation of a hydrophilic interaction chromatography method coupled with a charged aerosol detector for quantitative analysis of nonchromophoric α–hydroxyamines, organic impurities of metoprolol. J Pharm Biomed Anal. 2016;118:242-50.

42. Council of Europe, European Pharmacopoeia Online 9.8, 2019, EDQM, Strasbourg, France. Monograph No. 1028. Available from: http://online6.edqm.eu/ep908/. Accessed: September 18th 2019

43. D Ilko, RC Neugebauer, S Brossard, S Almeling, M Türck, U Holzgrabe. Impurity Control in Topiramate with High Performance Liquid Chromatography: Validation and Comparison of the Performance of Evaporative Light Scattering Detection and Charged Aerosol Detection. Charged Aerosol Detection for Liquid Chromatography and Related Separation Techniques. John Wiley & Sons, Hoboken, 2017:379-92.

44. EC Pinto, MdS Gonçalves, LM Cabral, DW Armstrong, VP de Sousa. Development and validation of a stability-indicating HPLC method for topiramate using a mixed-mode column and charged aerosol detector. J Sep Sci. 2018;41:1716-25.

45. Council of Europe, EDQM, Strasbourg, France. Outcome of the 162nd Session of the European Pharmacopoeia Commission. Press Release of the EDQM. 2018.

46. SPK Raju, M Narayanam, BK Kumar, S Tejaswee, S Singh. Validated stability-indicating method for alendronate sodium employing zwitterionic hydrophilic interaction chromatography coupled with charged aerosol detection. Chromatographia. 2015;78:1245-50.

47. PK Ragham, KB Chandrasekhar. Development and validation of a stability-indicating RP-HPL C-CAD method for gabapentin and its related impurities in presence of degradation products. J Pharm Biomed Anal. 2016;125:122-9.

48. K Stypulkowska, A Blazewicz, A Brudzikowska, M Warowna–Grzeskiewicz, K Sarna, Z Fijalek. Development of high performance liquid chromatography methods with charged aerosol detection for the determination of lincomycin, spectinomycin and its impurities in pharmaceutical products. J Pharm Biomed Anal. 2015;112:8-14.

49. Z Long, Z Guo, X Liu, Q Zhang, X Liu, Y Jin et al. A sensitive non-derivatization method for apramycin and impurities analysis using hydrophilic interaction liquid chromatography and charged aerosol detection. Talanta. 2016;146:423-9.

50. C Asthana, GM Peterson, M Shastri, RP Patel. Development and validation of a novel high performance liquid chromatography-coupled with Corona charged aerosol detector method for quantification of glucosamine in dietary supplements. PloS one. 2019;14:e0216039.

51. G Carlos, E Comiran, MH de Oliveira, RP Limberger, AM Bergold, PE Fröehlich. Development, validation and comparison of two stability-indicating RP-LC methods using charged aerosol and UV detectors for analysis of lisdexamfetamine dimesylate in capsules. Arab J Chem. 2016;9:S1905-S14.

52. CD Bertol, MT Friedrich, G Carlos, PE Froehlich. Analytical Stability-Indicating Methods for Alogliptin in Tablets by LC–CAD and LC–UV. J AOAC Int. 2017;100:400-5.

53. AM Brondi, JS Garcia, MG Trevisan. Development and Validation of a Chromatography Method Using Tandem UV/Charged Aerosol Detector for Simultaneous Determination of Amlodipine Besylate and Olmesartan Medoxomil: Application to Drug-Excipient Compatibility Study. J Anal Methods Chem. 2017;2017.

54. J Viinamäki, I Ojanperä. Photodiode array to charged aerosol detector response ratio enables comprehensive quantitative monitoring of basic drugs in blood by ultra-high performance liquid chromatography. Anal Chim Acta. 2015;865:1-7.

55. AG Pereira, FB D'Avila, PCL Ferreira, MG Holler, RP Limberguer, PE Froehlich. Method Development and Validation for Determination of Cocaine, its Main Metabolites and Pyrolytic Products by HPLC–UV–CAD. Chromatographia. 2016;79:179-87.

56. S Dong, Z Yan, H Yang, Z Long. Fast and Simple Determination of 3-Aminopiperidine without Derivatization Using High Performance Liquid Chromatography–Charged Aerosol Detector with an Ion-Exchange/Reversed-Phase Mixed-mode Column. Anal Sci. 2017;33:293-8.

57. K Zhang, X Liu. Mixed-mode chromatography in pharmaceutical and biopharmaceutical applications. J Pharm Biomed Anal. 2016;128:73-88.

58. S Furota, NO Ogawa, Y Takano, T Yoshimura, N Ohkouchi. Quantitative analysis of underivatized amino acids in the sub-to several-nanomolar range by ion-pair HPLC using a corona-charged aerosol detector (HPLC–CAD). J Chromatogr B. 2018;1095:191-7.

59. M Ginésy, J Enman, D Rusanova-Naydenova, U Rova. Simultaneous Quantification of L-Arginine and Monosaccharides during Fermentation: An Advanced Chromatography Approach. Molecules. 2019;24:802.

60. A Socia, JP Foley. Direct determination of amino acids by hydrophilic interaction liquid chromatography with charged aerosol detection. J Chromatogr A. 2016;1446:41-9.

61. C-E Zhang, L-J Liang, X-H Yu, H Wu, P-f Tu, Z-J Ma et al. Quality assessment of Astragali Radix from different production areas by simultaneous determination of thirteen major compounds using tandem UV/charged aerosol detector. J Pharm Biomed Anal. 2019;165:233-41.

62. C Zhang, Y Wang, X Sun, Y Zhao, W Zheng, W Li et al. Chromatographic fingerprint analysis of Toosendan Fructus by HPLC-CAD coupled with chemometrics methods. Acta Pharm Sinic. 2017;52:456-61.

63. S Martín-Torres, AM Jiménez-Carvelo, A González-Casado, L Cuadros-Rodríguez. Differentiation of avocados according to their botanical variety using liquid chromatographic fingerprinting and multivariate classification tree. J Sci Food Agr. 2019;99:4932-41.

64. A Pitschmann, M Zehl, E Heiss, S Purevsuren, E Urban, VM Dirsch et al. Quantitation of phenylpropanoids and iridoids in insulin-sensitising extracts of Leonurus sibiricus L.(Lamiaceae). Phytochem Anal. 2016;27:23-31.

65. Z Long, Z Guo, IN Acworth, X Liu, Y Jin, X Liu et al. A non-derivative method for the quantitative analysis of isosteroidal alkaloids from Fritillaria by high performance liquid chromatography combined with charged aerosol detection. Talanta. 2016;151:239-44.

66. Y Zhang, Z Chen, X Xu, Q Zhou, X Liu, L Liao et al. Rapid separation and simultaneous quantitative determination of 13 constituents in Psoraleae Fructus by a single marker using high-performance liquid chromatography with diode array detection. J Sep Sci. 2017;40:4191-202.

67. TR Baker, BT Regg. A multi-detector chromatographic approach for characterization and quantitation of botanical constituents to enable in silico safety assessments. Anal Bioanal Chem. 2018;410:5143-54.

68. RD Cohen, Y Liu, X Gong. Analysis of volatile bases by high performance liquid chromatography with aerosol-based detection. J Chromatogr A. 2012;1229:172-9.

69. C Theiss, U Holzgrabe. Characterization of polydisperse macrogols and macrogol-based excipients via HPLC and charged aerosol detection. J Pharm Biomed Anal. 2018;160:212-21.

70. CD Cappa, ER Lovejoy, A Ravishankara. Evaporation Rates and Vapor Pressures of the Even-Numbered C8− C18 Monocarboxylic Acids. J Phys Chem A. 2008;112:3959-64.

71. A Banel, B Zygmunt. Application of gas chromatography-mass spectrometry preceded by solvent extraction to determine volatile fatty acids in wastewater of municipal, animal farm and landfill originA. Banel and B. ZygmuntSolvent extraction and GC-MS to determine volatile fatty acids in wastewater. W Sci Technol. 2011;63:590-7.

72. MC Smith, RM Crist, JD Clogston, SE McNeil. Quantitative analysis of PEG-functionalized colloidal gold nanoparticles using charged aerosol detection. Anal Bioanal Chem. 2015;407:3705-16.

73. Y He, P Brown, MRB Piatchek, JA Carroll, MT Jones. On-line coupling of hydrophobic interaction column with reverse phase column-charged aerosol detector/mass spectrometer to characterize polysorbates in therapeutic protein formulations. J Chromatogr A. 2019;1586:72-81.

74. S Lippold, SH Koshari, R Kopf, R Schuller, T Buckel, IE Zarraga et al. Impact of mono-and poly-ester fractions on polysorbate quantitation using mixed-mode HPLC-CAD/ELSD and the fluorescence micelle assay. J Pharm Biomed Anal. 2017;132:24-34.

75. S Abreu, A Solgadi, P Chaminade. Optimization of normal phase chromatographic conditions for lipid analysis and comparison of associated detection techniques. J Chromatogr A. 2017;1514:54-71.

76. R Takahashi, M Nakaya, M Kotaniguchi, A Shojo, S Kitamura. Analysis of phosphatidylethanolamine, phosphatidylcholine, and plasmalogen molecular species in food lipids using an improved 2D high-performance liquid chromatography system. J Chromatogr B. 2018;1077:35-43.

77. L Ferey, SA Slabi, C-E Roy, P Barthelemy, K Gaudin. Chromatographic study of nucleoside-lipids by RP-UHPLC-DAD/CAD. Anal Bioanal Chem. 2018;410:7711-21.

78. P Li, W Sun, L Zuo, Z Zhu, T Zhao, R Wang et al. Fast simultaneous determination of main components and impurity sodium ion in PAMA injection by mixed-mode chromatography. J Pharm Biomed Anal. 2018;161:407-13.

79. M Mori, K Sagara, K Arai, N Nakatani, S-i Ohira, K Toda et al. Simultaneous analysis of silicon and boron dissolved in water by combination of electrodialytic salt removal and ion-exclusion chromatography with corona charged aerosol detection. J Chromatogr A. 2016;1431:131-7.

80. D Boßmann, B Bartling, I de Vries, J Winkler, H Neumann, F Lammers et al. Charged aerosol detector HPLC as a characterization and quantification application of biopharmaceutically relevant polysialic acid from E. coli K1. J Chromatogr A. 2019, 1599:85-94.

81. EM Hetrick, TT Kramer, DS Risley. Evaluation of a hydrophilic interaction liquid chromatography design space for sugars and sugar alcohols. J Chromatogr A. 2017;1489:65-74.

82. J Yan, S Shi, H Wang, R Liu, N Li, Y Chen et al. Neutral monosaccharide composition analysis of plant-derived oligo-and polysaccharides by high performance liquid chromatography. Carbohyd polym. 2016;136:1273-80.

83. P Saokham, T Loftsson. A new approach for quantitative determination of γ-cyclodextrin in aqueous solutions: application in aggregate determinations and solubility in hydrocortisone/γ-cyclodextrin inclusion complex. J Pharm Sci. 2015;104:3925-33.

84. K Schilling, J Krmar, N Maljurić, R Pawellek, A Protić, U Holzgrabe. Quantitative structure-property relationship modeling of polar analytes lacking UV chromophores to charged aerosol detector response. Anal Bioanal Chem. 2019;411:2945-59.

85. K Zhang, L Dai, NP Chetwyn. Simultaneous determination of positive and negative pharmaceutical counterions using mixed-mode chromatography coupled with charged aerosol detector. J Chromatogr A. 2010;1217:5776-84.

86. J Wu, RM Crist, SE McNeil, JD Clogston. Ion quantification in liposomal drug products using high performance liquid chromatography. J Pharm Biomed Anal. 2019;165:41-6.

87. KR Gilmore, HV Luong. Improved Method for Measuring Total Dissolved Solids. Anal Lett. 2016;49:1772-82.

88. L Rystov, R Chadwick, K Krock, T Wang. Simultaneous determination of Maillard reaction impurities in memantine tablets using HPLC with charged aerosol detector. J Pharm Biomed Anal. 2011;56:887-94.

89. A Joseph, A Rustum. Development and validation of a RP-HPLC method for the determination of gentamicin sulfate and its related substances in a pharmaceutical cream using a short pentafluorophenyl column and a charged aerosol detector. J Pharm Biomed Anal. 2010;51:521-31.

90. A Soman, M Jerfy, F Swanek. Validated HPLC method for the quantitative analysis of a 4-methanesulfonyl-piperidine hydrochloride salt. J Liq Chromatogr Relat Technol. 2009;32:1000-9.

91. P Chaimbault, K Petritis, C Elfakir, M Dreux. Ion-pair chromatography on a porous graphitic carbon stationary phase for the analysis of twenty underivatized protein amino acids. J Chromatogr A. 2000;870:245-54.

92. Q Zhou, M Chen, L Zhu, H Tang. Determination of perfluorinated carboxylic acids in water using liquid chromatography coupled to a corona-charged aerosol detector. Talanta. 2015;136:35-41.

93. S Matsuyama, Y Orihara, S Kinugasa, H Ohtani. Effects of densities of brominated flame retardants on the detection response for HPLC analysis with a corona-charged aerosol detector. Anal Sci. 2015;31:61-5.

94. G Kiełbowicz, D Smuga, W Gładkowski, A Chojnacka, C Wawrzeńczyk. An LC method for the analysis of phosphatidylcholine hydrolysis products and its application to the monitoring of the acyl migration process. Talanta. 2012;94:22-9.

95. O Wahl, U Holzgrabe. Impurity profiling of carbocisteine by HPLC-CAD, qNMR and UV/vis spectroscopy. J Pharm Biomed Anal. 2014;95:1-10.

96. X Bu, EL Regalado, J Cuff, W Schafer, X Gong. Chiral analysis of poor UV absorbing pharmaceuticals by supercritical fluid chromatography-charged aerosol detection. J Supercrit Fluid. 2016;116:20-5.

97. MM Khandagale, EF Hilder, RA Shellie, PR Haddad. Assessment of the complementarity of temperature and flow-rate for response normalisation of aerosol-based detectors. J Chromatogr A. 2014;1356:180-7.

98. B Bailey, M Plante, D Thomas, C Crafts, PH Gamache. Practical Use of CAD: Achieving Optimal Performance. Charged Aerosol Detection for Liquid Chromatography and Related Separation Techniques. John Wiley & Sons, Hoboken, 2017:163-89.

99. M Khandagale. Investigation of the analytical performance of aerosol-based detectors in liquid chromatography. Doctoral thesis at the University of Tasmania; 2015.

100. T Gorecki, F Lynen, R Szucs, P Sandra. Universal response in liquid chromatography using charged aerosol detection. Anal Chem. 2006;78(9):3186-92.

101. P Lucci, S Moret, F Buchini, G Ferlat, L Conte. Improved analysis of olive oils triacylglycerols by UHPLC-charged aerosol detection. J Food Compos Anal. 2018;66:230-6.

102. G Yang, X Zhao, J Wen, T Zhou, G Fan. Simultaneous fingerprint, quantitative analysis and anti-oxidative based screening of components in Rhizoma Smilacis Glabrae using liquid chromatography coupled with Charged Aerosol and Coulometric array Detection. J Chromatogr B. 2017;1049:41-50.

103. ME Fridén, F Jumaah, C Gustavsson, M Enmark, T Fornstedt, C Turner et al. Evaluation and analysis of environmentally sustainable methodologies for extraction of betulin from birch bark with a focus on industrial feasibility. Green Chem. 2016;18:516-23.

104. J Tam, IAH Ahmad, A Blasko. A four parameter optimization and troubleshooting of a RPLC–charged aerosol detection stability indicating method for determination of S-lysophosphatidylcholines in a phospholipid formulation. J Pharm Biomed Anal. 2018;155:288-97.

105. Q Zhang, B Bailey, D Thomas, M Plante, I Acworth. Determination of Polymerized Triglycerides by High Pressure Liquid Chromatography and Corona Veo Charged Aerosol Detector. doi: 10.13140/RG.2.2.25216.53769.; Poster at Pittcon, 2015.

106. M Plante, B Bailey, IN Acworth, C Crafts. A Single Method for the Direct Determination of Total Glycerols in All Biodiesels Using Liquid Chromatography and Charged Aerosol Detection. 2012. Available from: https://assets.thermofisher.com/TFS-Assets/CMD/posters/PN-70995-AOAC2014-Emulsifiers-Food-PN70995-EN.pdf; Accessed: November 14th 2019

107. M Plante, B Bailey, IN Acworth. Analysis of Emulsifiers in Foods by High Pressure Liquid Chromatography and Corona Charged Aerosol Detection. Available from: https://assets.thermofisher.com/TFS-Assets/CMD/posters/PN-70995-AOAC2014-Emulsifiers-Food-PN70995-EN.pdf; Accessed: November 14th 2019

108. M Plante, B Bailey, IN Acworth. Determination of Olive Oil Adulteration by Principal Component Analysis with HPLC–Charged Aerosol Detector Data. Thermo Fisher Scientific. 2013. Available from: https://assets.thermofisher.com/TFS-Assets/CMD/Application-Notes/an-73174-lc-ms-triacylglycerols-olive-oil-an731374-en.pdf; Accessed: September 6th 2019.

109. C Crafts, M Plante, B Bailey, I Acworth. Enhancement of Linearity and Response in Charged Aerosol Detection. 2016. Available from: https://assets.thermofisher.com/TFS-Assets/CMD/posters/PN-70003-Enhancement-Linearity-Response-CAD-PN70003-EN.pdf. Accessed: September 4th 2019

110. B Bailey, P Gamache, I Acworth. Guidelines for method transfer and optimization - from earlier model Corona detectors to Corona Veo and Vanquish charged aerosol detectors 2017. Available from: https://assets.thermofisher.com/TFS-Assets/CMD/Technical-Notes/tn-71290-cad-method-transfer-tn71290-en.pdf. Accessed: September 4th 2019

111. S Ebel. Evaluation and calibration in quantitative thin-layer chromatography. Anal Chem Progress. Springer, Heidelberg; 1984. p. 71-94.

112. D Thomas, I Acworth, B Bailey, M Plante, Q Zhang. Label-Free Analysis by UHPLC with Charged Aerosol Detection of Glycans Separated by Charge, Size and Isomeric Structure. 2015. Available from: https://assets.thermofisher.com/TFS-Assets/CMD/Application-Notes/AN-1127-LC-CAD-Label-Free-Glycans-AN71656-EN.pdf. Accessed September 4th 2019.

113. M Pistorino, BA Pfeifer. Polyketide analysis using mass spectrometry, evaporative light scattering, and charged aerosol detector systems. Anal Bioanal Chem. 2008;390:1189-93.

4 Results

4.1 Impurity profiling of L-asparagine monohydrate by Ion Pair Chromatography applying low wavelength UV detection

Klaus Schilling, Maria Cecilia Amstalden, Lorenz Meinel, Ulrike Holzgrabe

Reprinted with permission from J Pharm Biomed Anal 2016, 131, 202-207.

Abstract

L-Asparagine is a non-essential amino acid being used for a variety of pharmaceutical applications. The compound may be produced following synthetic or fermentative pathways leading to the formation of distinct impurities such as organic acids, other amino acids, dipeptides, or cyclic amino acid derivatives. Analysis of the respective analytes is challenging due to the lack of a chromophore, thus the monograph of the European pharmacopoeia describes a thin layer chromatographic test for detection of other amino acids. Thus, a sensitive and robust liquid chromatographic method was developed and validated applying a detection at 210 nm for determining the related substances. Separation and quantification of the analytes was achieved on a reversed phase C18 column using a mobile phase composed of a mixture of a phosphate buffer, sodium octanesulfonate, and acetonitrile in an isocratic elution mode. In contrast to the currently used thin layer chromatographic test, the method is capable of separating and quantitatively assessing expected ninhydrin-positive and -negative impurities from synthetic and enzymatic production pathways.

1. Introduction

Amino acids (AAs) such as L-asparagine play an important role in pharmaceutical applications as nutritive supplements and drugs. L-asparagine is a non-essential AA which is a significant factor during the development of the brain [1] and for regulating the ammonia levels of the human body [2]. Being a polar, ionisable, and structurally similar analyte in comparison to other AAs it is challenging to develop good analytical procedures for evaluating the impurities in L-asparagine.

Currently the Ph. Eur. describes a thin layer chromatographic test using ninhydrin as spraying reagent for impurity profiling. Though this procedure is able to detect other AAs, it can be considered obsolete because it is blind for ninhydrin-negative impurities and not only lacks sensitivity but also resolving power [3]. Nowadays the Amino Acid Analyzer, as described in chapter 2.2.56 of the Ph. Eur. [4], is applied. It makes use of cation exchange resins using lithium or sodium buffers applying a pre- or post-column derivatization with ninhydrin or fluorescent reagents, respectively [4]. Even though it is being considered more sensitive it cannot detect other impurities than AAs, too. In addition, it is a rather expensive method as it needs special instrumentation. Derivatization methods producing fluorescent compounds through reaction with 9 fluorenylmethyl chloroformate (FMOC) [5] or o-phthalaldehyde [6] are selective for primary amines; however, organic acids which might be present as impurities cannot be detected. Since most AAs lack typical UV/Vis chromophores, one needs to benefit from the absorbing properties of the carboxylic acid moiety at 210 nm when detecting them without preceding derivatization [3, 7-9]. Of note, the poor sensitivity in low wavelength detection may be compensated by highly concentrated sample preparations for impurity profiling [3].

The synthetic pathway of L-asparagine has to be considered for impurity profiling (see Figure 1). L-asparagine (8) can be produced through the reaction of L-aspartic acid beta methylester (4) with ammonia [10, 11]. Alternatively, an excessive fermentative approach using recombinant microorganisms and disabled negative feedback mechanisms and degradation processes [12] can be applied: The ATP dependent enzyme asparagine synthetase catalyzes the transfer of ammonia from L-glutamine (5) to L-aspartic acid (2) and thereby produces L-glutamic acid (6) and L-asparagine (8) [13]. However, all production pathways use L-aspartic acid (2) as a precursor: it is

therefore inevitable to have an analytical procedure capable of analyzing ninhydrin negative organic acids which might be present in L-aspartic acid (2).

The most common approach involves fermentation and enzymatic reaction starting from fumaric acid (1) as a substrate of the enzyme aspartase [14-17]. Besides, the enzyme fumarase may convert fumaric acid (1) which is produced from maleic acid (7) to malic acid (3) [18], representing additional possible ninhydrin negative impurities (see Fig. 1). Furthermore, dimerization products like dipeptides consisting of L-asparagine and L-aspartic acid and the cyclic dipeptide diketoasparagine can be expected (see Fig. 2).

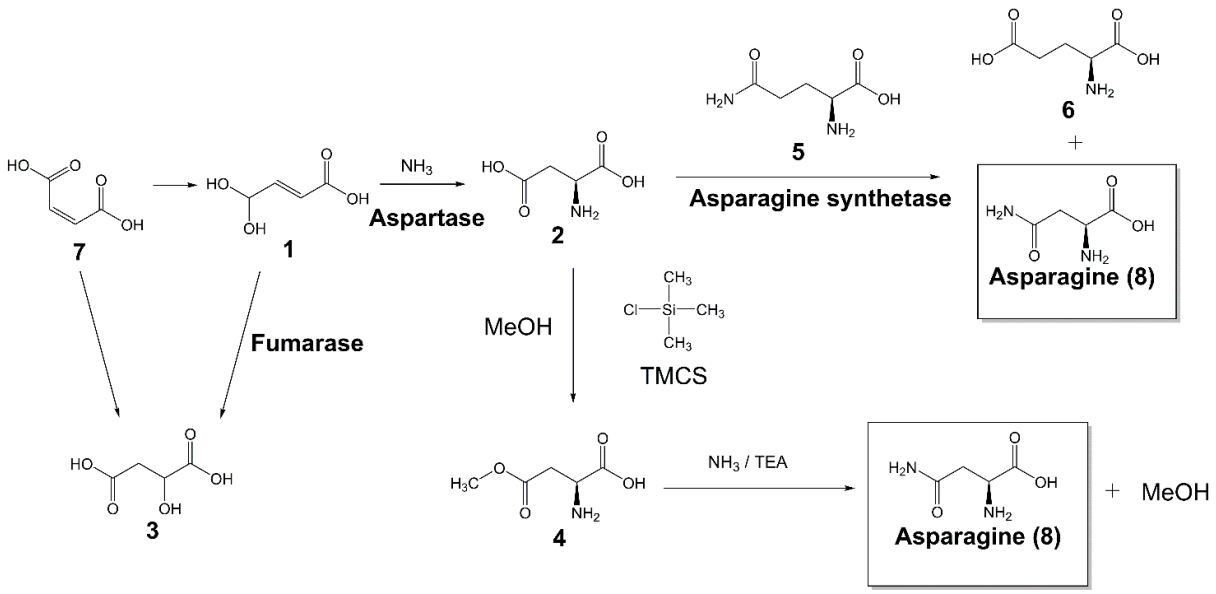

Fig. 1. Production pathway of L-asparagine (8) from L-aspartic acid (2) showing its potential organic acid impurities 1, 3, and 7 [13–17] as well as L-glutamine (5) and L-glutamic acid (6) as impurities from the enzymatic approach [12]; TMCS = Trimethylchlorosilane.

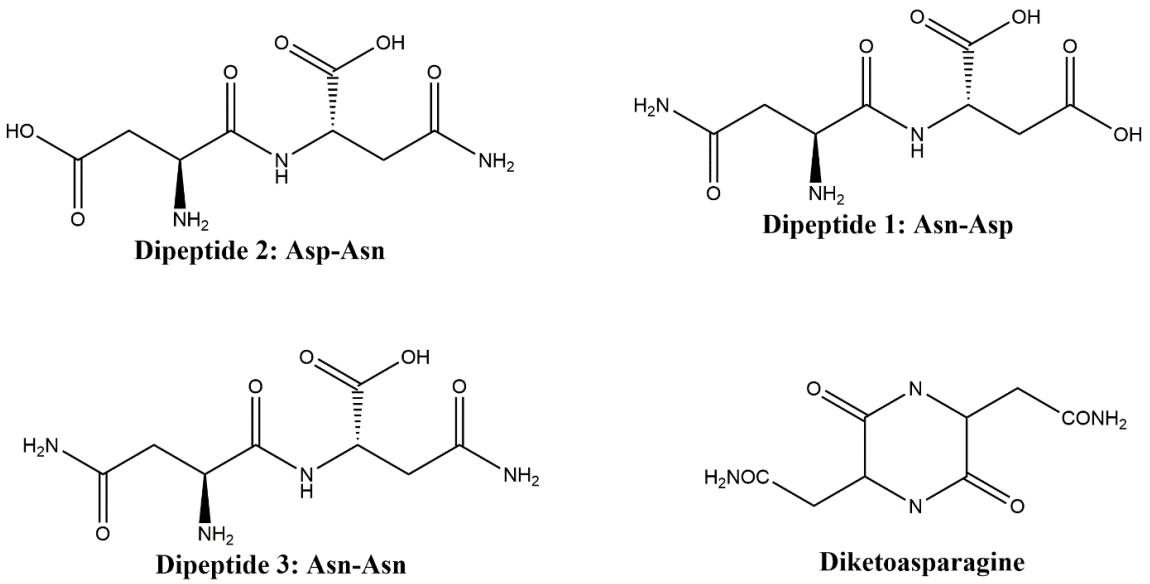

Fig. 2. Structures of the dipeptides Asn-Asp, Asp-Asn, Asn-Asn, and the cyclic dipeptide diketoasparagine

Instead of using expensive ion exchange resins [19] and/or complicated derivatization methods [5, 6] in HPLC analysis, it was aimed to analyze these polar and ionisable impurities non-derivatized on an ordinary reversed phase (RP) column. This can be achieved by using ion pairing reagents such as perfluorinated carboxylic acids [20] or alkylsulfonates [21] at a low detection wavelength of 210 nm to address the carboxylic acid moieties of the organic acids as well as the amino acids [3].

2. Experimental

2.1. Chemicals and reagents

L-Asparagine monohydrate, L-aspartic acid and diketoasparagine were obtained from the European Directorate for the Quality of Medicines & HealthCare (EDQM; Strasbourg, France). L-glutamine, L-glutamic acid, potassium dihydrogenphosphate (KH2PO4), phosphoric acid, dichloromethane, diethyl ether, FMOC-amino acids, diisopropylethylamine, 1,2-ethanedithiol, methanol, thioanisole, anisole and acetonitrile (HPLC gradient grade) were purchased from Sigma-Aldrich Chemie GmbH (Steinheim, Germany), sodium 1 octanesulfonate from Alfa-Aesar GmbH & Co. KG (Karlsruhe, Germany), dimethyl formamide (DMF) from Fisher Scientific (Schwerte, Germany), and 2-chlorotrityl chloride resin (CTC) from Chem-Impex Wood (Dale, IL, USA). All chemicals used for quantification were of analytical grade or even better.

Ultrapure water was produced by a water purification system from Merck Millipore (Schwalbach, Germany). All solutions were filtered through 0.45 µm cellulose acetate filters supplied by Macherey-Nagel GmbH & Co. KG (Düren, Germany) prior to use.

2.2. Apparatus

The HPLC-UV experiments were performed on an Agilent 1100 modular liquid chromatographic system consisting of an online vacuum degasser, a binary pump, an auto sampler, and a variable wavelength detector (Agilent Technologies, Waldbronn, Germany). A column oven from Beckman Coulter GmbH (Krefeld, Germany) was additionally used. Chromatograms were recorded and integrated using the Agilent ChemStation® software (Rev B.03.02). A Sigma 3K12 centrifuge (Sigma Laborzentrifugen GmbH, Osterode am Harz, Germany), an ultrasonic bath from Bandelin electronic GmbH & Co. KG (Berlin, Germany), and an analytical balance from Mettler Toledo (Gießen, Germany) were used.

2.3. Chromatographic procedure

An octadecylsilyl (C18) Microsorb®-MV column (250 x 4.6 mm, 5 µm particle size, 100 Å pore size, Agilent Technologies, Santa Clara, CA, USA) was used as the stationary phase. The chromatographic system was operated using an isocratic elution at 25 °C and a flow rate of 0.7 mL/min. The mobile phase was a 100 mM potassium dihydrogenphosphate buffer solution containing 10 mM sodium 1-octanesulfonate and 5 mL acetonitrile per liter. The pH of the solution was adjusted to 2.2 using phosphoric acid (85%) prior to the addition of acetonitrile. UV detection was carried out at a wavelength of 210 nm, and a sample of 20 µL of the respective solution was injected into the chromatographic system.

2.3.1. Preparation of solutions

A test solution containing 10 mg/mL of L-asparagine monohydrate was prepared dissolved in water. The solutions of the dipeptides for peak identification were prepared in the mobile phase and had an approximate concentration of 0.58 mg/mL. For the test solutions for linearity a solution containing 0.25 mg/mL of L-aspartic acid was diluted to 2.5, 5, 10, 20, 30, 40, 50, 60, 70, 80 µg/mL. The reference solution for quantification and system suitability contained 0.025 mg/mL of L-aspartic acid, diketoasparagine, and L-asparagine monohydrate (calculated to correspond to anhydrous L-asparagine). All solutions were prepared immediately before use or thawed from storage at -20 °C before use. All solutions were sonicated to achieve complete dissolution.

2.4 Synthesis of the dipeptides

Dipeptides were synthesized using the fluorenylmethyloxycarbonyl (FMOC) amino acid coupling strategy (solid phase peptide synthesis – SPPS) [22]. In brief, the first FMOC-protected amino acid was added to the CTC resin in a 5-molar excess in comparison to its loading capacity with 0.2 M diisopropylethylamine (0.2 M solution in dichloromethane), and incubated under agitation at RT for 1 h. Eventually remaining unreacted binding sites of the resin were deactivated by adding 80 µL methanol and incubating for 15 min. The resin was subsequently washed three times using dichloromethane and methanol, respectively. The FMOC group was removed by treatment with a 40% solution of piperidine in DMF for 3 min and a solution of 20% of piperidine in DMF for additional 10 min. The second amino acid was coupled using a solution of 2-(1H-benzotriazol-1-yl)-1,1,3,3-tetramethyluronium-hexafluorophosphat (0.2 M, HBTU) and 250 µL of diisopropylethylamine, incubating under agitation at room temperature for at least 1 h. Dipeptides were cleaved from the resin using a solution being composed of 90% of TFA and 10% of a scavenger mixture (thioanisole, ethanedithiol, anisole 5:3:2 v/v) for 3 h and precipitated with diethyl ether at -20 °C. The suspension was centrifuged for 5 min (5,500 min^{-1}); the supernatant was discarded and washed twice using diethyl ether. The identity of the dipeptides was confirmed by analysis with an ion trap mass spectrometer in positive mode (Agilent 1100 Series LC/MSD Trap SL, model: G2445D).

3. Results and discussion

3.1. HPLC method development

3.1.1. Chromatographic procedure

Since it was aimed to quantify organic acids as potential impurities, the classical amino acid derivatization was not applied. Thus, a detection at 210 nm is necessary and the low sensitivity will be compensated by a high sample concentration [3]. Nevertheless, components absorbing at 210 nm should be avoided within the mobile phase. As it was intended to develop an ion-pair chromatographic method, alkylsulfonates such as sodium octanesulfonate were used because the corresponding perfluorinated carboxylic acids would further decrease the sensitivity.

The choice of the pH is critical because deprotonated carboxylic acid groups have to be avoided. Due to the pKA of about 2.1 for the carboxylic acid moiety, low pH values and high buffer salt concentrations are necessary; otherwise the peak of L-asparagine

will be split. [23]. According to Hearn [24] no major experimental problems are to be expected when working at pH 2.2 and alkylsulfonates at or below 25 mM when using a detection wavelength of 210 nm. Hence, pH 2.2 was chosen. Variation of the ion pair reagent concentration between 10 and 20 mM resulted in 10 mM being the best.

In order to decrease the analysis time a shorter core shell column was applied and the flow rate was increased up to 1.5 mL/min, however, in all cases the separation got worse. Eventually a 250 x 4.6 column with 5 µm particles and a flow rate of 0.7 mL/min gave the best separation of all compounds. Experiments assessing a temperature range within 25 and 45 °C resulted in an optimal outcome for room temperature (i.e., 25 °C).

Taken together the best separation was achieved using a flow rate of 0.7 mL/min, a 250 x 4.6 mm C18 column with 5 µm particles, a column temperature of 25 °C, and a mobile phase being a 100 mM KH_2PO_4 buffer with 10 mM of sodium 1-octanesulfonate, and 5 mL of acetonitrile per liter. The pH of the buffer solution was adjusted to 2.2 using phosphoric acid before acetonitrile was added.

As can be seen from Fig. 3, the method is able to separate the main peak of L-asparagine (8) from the impurities. However, a baseline separation between L-asparagine (8) and L-glutamine (5) as well as L-aspartic acid (2) could not be achieved (Fig. 3 and 4) because the amino acids are structurally very similar. Fumarate is considered the most relevant impurity, thus the separation of maleate (7) and malate (3) was not further studied nor optimized. However, the compounds are supposed to elute after diketoasparagine and before asparagine.

Table 1. Investigated impurities and their approximate relative retention times (RRTs) referring to L-asparagine (t_r approx. 6.6 min).

Substance	RRT	Substance	RRT
Diketoasparagine	0.59	Dipeptide 2: Asp-Asn	1.12 and 1.28
Fumaric Acid	0.89	Glutamic Acid	1.48
Glutamine	1.10	Dipeptide 3: Asn-Asn	1.29 and 1.54
Aspartic Acid	1.20	Dipeptide 1: Asn-Asp	1.71

Peak identification was performed by spiking the reference solution with the impurities to obtain the retention times (see Table 1 for relative retention times (RRTs)). The dipeptides were synthesized by means of solid phase peptide synthesis (SPPS). The dipeptides were identified by evaluating their mass spectrometric data. For dipeptide 1 (Asn Asp) and dipeptide 2 (Asp Asn) a m/z of 248.1 was measured, corresponding to the molecular weight of the molecules bearing a positively charged amine. For dipeptide 3 (Asn Asn) a m/z of 247.1 was found, again corresponding to the molecular weight of the molecule having a positively charged amine. For every dipeptide a mass loss of 18 in relation to their theoretical/calculated mass was found indicating the formation of their respective cyclic dipeptides. The cyclic dipeptides are clearly separated from the other peaks once they elute at the beginning of the chromatogram and therefore do not interfere with peaks due to dipeptides or other impurities. The dipeptides were coarsely purified in order to determine their retention times which are RRT = 1.71 for Asn-Asp; RRT = 1.12 and 1.28 for Asp-Asn, and RRT = 1.29 and 1.54 for Asn-Asn (see Table 1). Thus, they are clearly separated from the other peaks. In the case of Asn-Asp and Asp-Asn, respectively, the formation of two peaks was observed, very likely representing two molecule species which might be due an incomplete ionization of the carboxylic acid moieties at pH = 2.2.

Furthermore the method is capable of selectively analyzing diketoasparagine (RRT = 0.59) which is not detectable applying the thin layer chromatography and ninhydrin method [25].

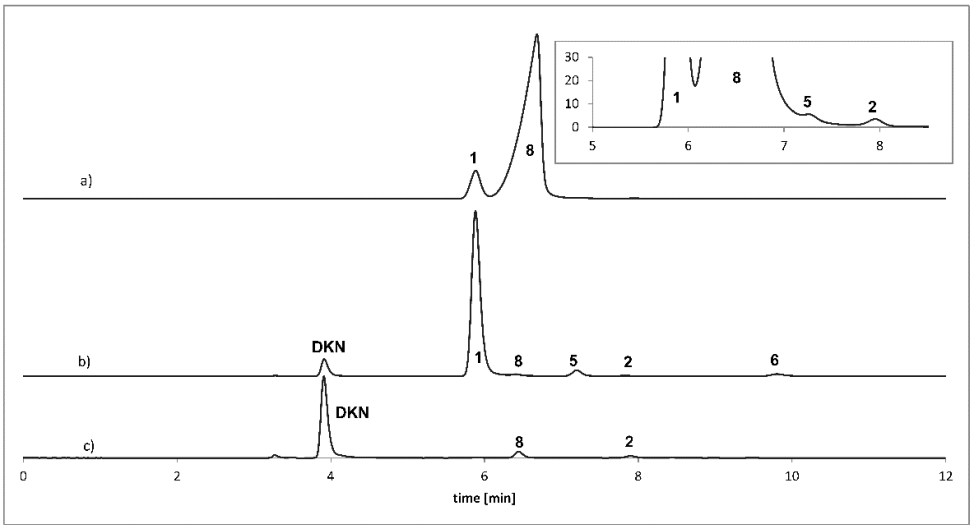

Fig. 3. Example chromatograms of: a) sample solution of L-asparagine (8) spiked with 0.1% fumaric acid (1) and 0.1% L-glutamine (5); b) reference solution spiked with fumaric acid (1), L-glutamine (5), and L-glutamic acid (6); c) reference solution as in 2.3.1 containing diketoasparagine, L-aspartic acid (2), and L-asparagine (8) at 0.025 mg/mL each; chromatographic conditions see Section 2.3.

3.1.2. Sample preparation

Since L-asparagine monohydrate is soluble in water up to 29.4 mg/mL [26], a highly concentrated aqueous sample solution (10 mg/mL) was prepared allowing for compensation of the low sensitivity of the detection method and assuring low detection and quantification limits. Sample preparation in water avoided additional peaks belonging to phosphate and octanesulfonate. The sample solution was considered not stable since an additional peak between L-aspartic acid and L-glutamic acid occurred when the solution was kept at room temperature for 24 h (not further investigated). Preparing the solutions freshly or thawing them from -20 °C was found to be suitable to avoid the instability problems.

3.2. Sensitivity

The method was validated for impurity profiling of L-asparagine with regards to the following parameters: specificity, linearity, range, precision, accuracy, LOQ and robustness, following the International Council for Harmonisation (ICH) guideline Q2(R1) [27]. Since the drug substance is being administered in doses below 2 g per day, a reporting threshold of 0.05% has to be applied according to the ICH guideline

Q3A(R2) [28]. The validation parameters considering quantitation were performed for L-aspartic acid only as it was found to be the main impurity.

Specificity of the method was proven by comparing spiked samples with a blank solution. Not every impurity was baseline separated from the main peak but the method was found to be able to selectively identify impurities present in the batches and to deliver an acceptable quantification of the analytes.

The linearity and range for L-aspartic acid were determined by constructing a calibration curve from 2.5 to 80 µg/mL (equal to 0.025-0.80%) in aqueous solution. The regression coefficient of the determination was R^2 = 0.99993.

The LOQ for L-aspartic acid was calculated using the signal to noise ratio which was determined based on the peak to peak method for determining the baseline noise as described in the ICH guideline Q2(R1) [26]. The LOQ experiments showed a S/N ratio of about 50 at 0.025% (i.e., 2.5 µg/mL).

Accuracy was assessed on spiked sample solutions. The recovery rate was calculated at 0.05, 0.40, and 0.80%; the recovery rates were found to be between 93 and 111% (n = 3; RSD = 0.97–7.03%) for each level. The quantification was performed by the one point external standard method using the respective peak areas of the reference solution.

Repeatability and precision were determined on a real sample that contained L-aspartic acid as an impurity. The impurity content was measured in sextuple on two different days and was approximately 0.07%. The RSD intra day was 3.3 and 4.1%; the difference in content determined on two consecutive days was about 13 per cent.

The sample solutions were found to be instable since an additional peak was noticed when the sample solutions were stored at ambient temperature for 24 h.

For checking the robustness, the chromatographic parameters were varied: temperature (20 and 30 °C), flow rate (0.6 and 0.8 mL/min), pH of the mobile phase (2.1 and 2.3), phosphate buffer concentration (90 and 110 mM), ion pairing reagent concentration (9 and 11 mM), and acetonitrile content of mobile phase (4.5 and 5.5 mL/L). A spiked sample solution containing the already present L aspartic acid plus 0.50% and a solution solely containing L-aspartic acid at the concentration of the reporting threshold (5 µg/mL) were analyzed. The quantitation results were within

89-104% of the initial value and the LOQ, being defined as S/N ≥ 10, was exceeded at the reporting threshold for all changes except for the decrease of acetonitrile.

For the establishment of a system suitability test, the resolution between L-aspartic acid and L-asparagine in the reference solution was monitored. A resolution of minimum 5 was found to be suitable.

3.3. Batch results

Three batches of manufacturer A (I to III), three batches of a second supplier B (IV to VI), and two batches of a third manufacturer C (VII to VIII) were screened using the new method (see Table 2 for results). Two additional impurities which could not be assigned to any of the investigated ones were found in one batch; since they were only present in very low amounts, this was not further investigated.

Table 2. Results of batch testing using the newly developed HPLC method. Substances not listed were not detected in any batch; n.d. = not detected.

Manufacturer	A			B			C	
Batch	**1**	**2**	**3**	**1**	**2**	**3**	**1**	**2**
Diketoasparagine	n.d.	n.d.	n.d.	0.114%	0.091%	0.091%	<0.05%	n.d.
Aspartic Acid	0.238%	0.249%	0.242%	0.089%	0.080%	0.070%	0.058%	0.049%
Unspecified impurity at RRT 0.71	n.d.	n.d.	n.d.	n.d.	n.d.	n.d.	<0.05%	n.d.
Unspecified impurity at RRT 1.44	n.d.	n.d.	n.d.	n.d.	n.d.	n.d.	<0.05%	n.d.
Total	0.238%	0.249%	0.242%	0.203%	0.171%	0.161%	0.058%	0.049%

L-Aspartic acid (2) was found to be the most relevant impurity for L-asparagine (8) since it was present in every batch. Manufacturers B and C use a process capable of delivering low amounts of L-aspartic acid as impurity (≤ 0.09%), whereas manufacturer A produces L-asparagine containing higher amounts (about 0.24%) of L-aspartic acid as the main impurity. Diketoasparagine occurred in the batches of supplier B in amounts higher than the reporting threshold (about 0.09%). The synthetic approach most likely produces more diketoasparagine in comparison to the fermentative approach. In all tested batches no possible organic acid impurities or other AAs than L-aspartic acid, nor the respective dipeptides were found (see Fig. 1 and 2 as well as Table 2).

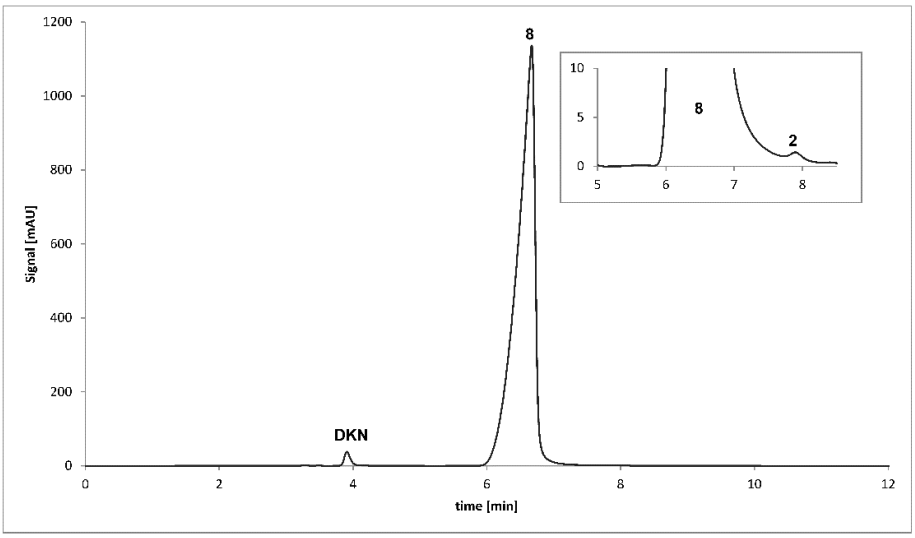

Fig. 4. Example chromatogram of a 10 mg/mL solution of L-asparagine monohydrate (8) of manufacturer B batch 3 containing 0.091% diketoasparagine, and 0.070% L-aspartic acid (2); chromatographic conditions see under 2.3.

4. Conclusion

A new and robust method for the determination of the related compounds in L-asparagine monohydrate was developed and validated. The method is capable of detecting ninhydrin-negative substances such as diketoasparagine, and a possible procedure of detecting diketoasparagine, fumaric acid, and the respective dipeptides was developed.

Conflict of interest statement

None of the authors of this paper does have a financial or personal relationship with other people or organizations that could inappropriately influence or bias the content of the paper.

Acknowledgements

Thanks are due to the German Federal Institute of Drugs and Medical Devices (Bonn, Germany) for financial support, the European Directorate for the Quality of Medicines & HealthCare (Strasbourg, France) for the sample and reference substance supply, the Science without Borders Program (CAPES Foundation, Ministry of Education of Brazil, Brasilia) for supporting Maria Cecilia Amstalden, and to Oliver Wahl (University of Würzburg) for valuable discussions and support throughout the project.

References

[1] E. K. Ruzzo, J. M. Capo-Chichi, B. Ben-Zeev, D. Chitayat, H. Mao, A. L. Pappas, Y. Hitomi, Y. F. Lu, X. Yao, F. F. Hamdan, K. Pelak, H. Reznik-Wolf, I. Bar-Joseph, D. Oz-Levi, D. Lev, T. Lerman-Sagie, E. Leshinsky-Silver, Y. Anikster, E. Ben-Asher, T. Olender, L. Colleaux, J. C. Decarie, S. Blaser, B. Banwell, R. B. Joshi, X. P. He, L. Patry, R. J. Silver, S. Dobrzeniecka, M. S. Islam, A. Hasnat, M. E. Samuels, D. K. Aryal, R. M. Rodriguiz, Y. H. Jiang, W. C. Wetsel, J. O. McNamara, G. A. Rouleau, D. L. Silver, D. Lancet, E. Pras, G. A. Mitchell, J. L. Michaud, D. B. Goldstein, Deficiency of asparagine synthetase causes congenital microcephaly and a progressive form of encephalopathy, Neuron 80 (2013), 429-41.

[2] L. L. Madison, D. W. Seldin, Ammonia Excretion and Renal Enzymatic Adaptation in Human Subjects, as Disclosed by Administration of Precursor Amino Acids, J Clin Invest 37 (1958), 1615-1627.

[3] O. Wahl, U. Holzgrabe, Amino acid analysis for pharmacopoeial purposes, Talanta 154 (2016), 150-63.

[4] Council of Europe, European Pharmacopoeia 8th edition, EDQM, Strasbourg, France, 2016.

[5] S. Einarsson, B. Josefsson, S. Lagerkvist, Determination of Amino-Acids with 9-Fluorenylmethyl Chloroformate and Reversed-Phase High-Performance Liquid-Chromatography, J Chromatogr 282 (1983), 609-618.

[6] M. Roth, Fluorescence reaction for amino acids, Anal Chem 43 (1971), 880-2.

[7] R. Schuster, Determination of free amino acids by high performance liquid chromatography, Anal Chem 52 (1980), 617-20.

[8] Y. Yokoyama, S. Tsuji, H. Sato, Simultaneous determination of creatinine, creatine, and UV-absorbing amino acids using dual-mode gradient low-capacity cation-exchange chromatography, J Chromatogr A 1085 (2005), 110-116.

[9] A. Fialaire, E. Postaire, R. Prognon, D. Pradeau, Bioavailability Prediction of Amino-Acids and Peptides in Nutritive Mixtures by Separation on Nonpolar Stationary Phases by High-Performance Liquid-Chromatography and Direct Uv Detection at 210 Nm, J Liq Chromatogr 16 (1993), 3003-3015.

[10] L. Jian, Z. Jiahua, W. Yu, Improved technology for chemical synthesizing L-asparagine, CN1082044 C; 1997.

[11] P. Hirsbrunner, R. Bertholet, Preparation of an asparagine or a glutamine, US3979449 A; 1976.

[12] Mihashi S., N. T., Method for producing L-asparagine, JP2013106588A; 2011.

[13] N. G. Richards, S. M. Schuster, Mechanistic issues in asparagine synthetase catalysis, Adv Enzymol Ramb 72 (1998), 145-98.

[14] M. Kisumi, Y. Ashikaga, I. Chibata, Studies on the Fermentative Preparation of L-Aspartic Acid from Fumaric Acid, B Agr Chem Soc Japan 24 (1960), 296-305.

[15] T. Tosa, T. Sato, T. Mori, Y. Matuo, I. Chibata, Continuous Production of L-Aspartic Acid by Immobilized Aspartase, Biotechnol Bioeng 15 (1973), 69-84.

[16] K. Kitahara, S. Fukui, M. Misawa, Preparation of L-Aspartic Acid by bacterial aspartase, J. Gen. Appl. Microbiol. 5 (1959), 74-77.

[17] S. Takamatsu, T. Tosa, I. Chibata, Industrial-Production of L-Alanine from Ammonium Fumarate Using Immobilized Microbial-Cells of 2 Kinds, J Chem Eng Jpn 19 (1986), 31-36.

[18] M. C. Fusee, W. E. Swann, G. J. Calton, Immobilization of Escherichia coli Cells Containing Aspartase Activity with Polyurethane and Its Application for L-Aspartic Acid Production, Appl. Environ. Microbiol. 42 (1981), 672-6.

[19] C. Murren, D. Stelling, G. Felstead, Improved Buffer System for Use in Single-Column Gradient-Elution Ion-Exchange Chromatography of Amino-Acids, J Chromatogr 115 (1975), 236-239.

[20] K. N. Petritis, P. Chaimbault, C. Elfakir, M. Dreux, Ion-pair reversed-phase liquid chromatography for determination of polar underivatized amino acids using perfluorinated carboxylic acids as ion pairing agent, J Chromatogr A 833 (1999), 147-155.

[21] J. Saurina, S. Hernandezcassou, Determination of Amino-Acids by Ion-Pair Liquid-Chromatography with Postcolumn Derivatization Using 1,2-Naphthoquinone-4-Sulfonate, J Chromatogr A 676 (1994), 311-319.

[22] F. Albericio, Developments in peptide and amide synthesis, Curr Opin Chem Biol 8 (2004), 211-21.

[23] E. Tomlinson, T. M. Jefferies, C. M. Riley, Ion-Pair High-Performance Liquid-Chromatography, J Chromatogr 159 (1978), 315-358.

[24] M. T. W. Hearn, Ion-pair chromatography: theory and biological and pharmaceutical applications, M. Dekker, New York, USA, 1985.

[25] V. J. Harding, R. M. MacLean, The ninhydrin reaction with amines and amides, J Biol Chem 25 (1916), 337-350.

[26] S. H. Yalkowsky, R. M. Dannenfelser, The Aquasol Database of Aqueous Solubility, Fifth Edition, College of Pharmacy, University of Arizona, Tucson, AZ (1992),

[27] International Council for Harmonization, Guideline Q2(R1): Validation of Analytical Procedures: Text and Methodology, 2005.

[28] International Council for Harmonization, Guideline Q3A(R2): Impurities in new drug substances, 2006.

4.2 Influence of charged aerosol detector instrument settings on the ultra-high-performance liquid chromatography analysis of fatty acids in polysorbate 80

Klaus Schilling[1], Ruben Pawellek[1], Katherine Lovejoy, Tibor Muellner, Ulrike Holzgrabe

[1] These authors contributed equally to this work.

Reprinted with permission from J Chromatogr A 2018, 1576, 58-66.

Abstract

The analysis of polysorbate 80 is a challenge because all components lack a chromophore. Here, an ultra-high-performance liquid chromatography system equipped with a charged aerosol detector (UHPLC-CAD) was used to study the effect of systematic variation of the CAD settings, namely evaporation temperature, filter constant and power function value (PFV), on the detector response of fatty acid standards and manufacturing batches of polysorbate. Evaporation temperature and filter constant strongly affect the detection limits described by signal to noise (S/N) ratios. Although evaporation temperature can be increased to improve signal to noise ratios, analyte volatility at higher temperatures is an important limiting factor. The PFV was found to be a strong tool for optimizing response linearity, but the optimal PFV differed depending on analyte volatility. Because PFV optimization required some additional measurement time and because double-logarithmic transformation at the default PFV of 1.0 yielded satisfying universal results with less measurement time over a range of two orders of magnitude for every homologue fatty acid from C14 to C18, use of the log-log transformation is the favored linearization strategy. Possible optimization procedures for semi volatile substances are presented. Overall, this new UHPLC method method offers improved detection limits, as well as time savings of over 75% and eluent savings of more than 40% compared to the previously published HPLC-CAD method for polysorbate analysis.

1 Introduction

Fatty acids play an important role in the pharmaceutical and cosmetic field as excipients [1]. They are present in various diverse substance classes as emulsifiers [2]. Polysorbates are esterified with a sorbitan backbone together with polyethylene glycols (PEGs) [3]. Furthermore, esters of fatty acids with fatty alcohols yield waxes and esters of fatty acids with glycerin form triglycerides which, as well as the free fatty acids themselves, are commonly used in dermatological formulations [4].

An in-depth comparison of currently applied methods for the analysis of fatty acids was given by Wu et al. [5], elaborating on advantages and disadvantages of the respective methods. Due to their physicochemical properties, fatty acids are mainly assessed by means of gas chromatography (GC) after derivatization with methanol to fatty acid methyl esters (FAMEs) [6, 7] as also described in the Ph. Eur. [8]. The most common approach involves a flame ionization detector (FID), whereas GC-mass-spectrometry (MS) can be used for more selective and sensitive analysis [9]. Analytical methods such as capillary electrophoresis (CE) with indirect UV detection [10] or tedious pre-column derivatization with e.g. naphthoyl chloride and coupling to HPLC [11] have been described but rarely used. More recently, near infrared spectroscopy [12] and NMR [13-15] as non destructive methods of analysis have been reported; however, model establishment for NIR is tedious and both methods lack sensitivity [5]. HPLC-MS methods are accessible without derivatization procedures [16], yet are very costly [5].

Furthermore, aerosol-based detection methods utilizing either evaporative light scattering detection (ELSD) or charged aerosol detection (CAD) combined with HPLC have been reported [5, 17-20]. They are rather easy to use, cheap in comparison to MS analytics and not dependent on chromophores. The aerosol-based detection of CAD and ELSD relies on nebulization of the effluent which, by evaporation of the solvent, forms particles [21]. These particles are then detected by measuring electrical charge that was transferred to the particles by a nitrogen stream passing a corona needle in case of the CAD. Alternatively, in case of the ELSD, the particles pass a light beam and the combined angular light scattering in the detection flow path is analyzed. Thus, analytes do not need to possess a chromophore - as it is the case for fatty acids - but only need to be sufficiently non volatile in order to ensure acceptable signals [21]. The ELSD is known to be inferior when it comes to dynamic range, sensitivity and

signal irregularities when highly concentrated samples have to be used [22] as is the case for impurity profiling. This leaves the CAD as the more reliable and more suitable of the two quasi universal aerosol detectors because it possesses a greater linear and dynamic range [23, 24]. Ilko et al. [25] presented a HPLC-CAD method for the analysis of free fatty acids in polysorbate 80 batches after liquid liquid extraction and for the fatty acid composition after hydrolysis and liquid liquid extraction.

To the best of our knowledge, no UHPLC CAD method benefiting from the time and eluent saving and the capabilities of modern CAD detection for fatty acids has been established. Interestingly, although the semi-volatile character of the fatty acids significantly affects the detector signal, no systematic study of the settings of CAD parameters and their impact on the signal intensity of these homologues has been undertaken. The UHPLC method development is described shortly and a focus on the systematic evaluation of CAD settings is presented in this article

2 Experimental

2.1 Chemicals and reagents

Octanoic acid, decanoic acid, lauric acid, myristic acid, palmitic acid, petroselinic acid, oleic acid, linoleic acid, alpha linolenic acid, stearic acid, HPLC grade acetonitrile, potassium hydroxide, tert. butyl methyl ether (MTBE), HPLC grade methanol, HPLC grade 50% formic acid and 100% formic acid were purchased from Sigma Aldrich Chemie GmbH (Steinheim, Germany). Margaric acid was purchased from VWR international (Darmstadt, Germany). All chemicals used were of analytical grade unless otherwise stated. Ultrapure water was produced by a water purification system from Merck Millipore (Schwalbach, Germany) specified at a resistivity of 18.2 MΩ cm.

The polysorbate batches were from NOF (Tokyo, Japan), Kolb (Hedingen, Switzerland), Merck (Darmstadt, Germany) and Croda (East Yorkshire, UK). The batch coding does not necessarily match with the presented manufacturer order.

2.2 Apparatus

The UHPLC-CAD experiments were performed on a Thermo Scientific™ Vanquish™ Flex modular chromatographic system consisting of a binary flex pump with online degasser, a thermostatted split sampler, a thermostatted column compartment with integrated pre heater, a variable wavelength detector and a Vanquish Horizon charged aerosol detector (Thermo Fisher Scientific, Germering, Germany). The charged

aerosol detector was supplied with nitrogen gas from an ESA nitrogen generator (Thermo Fisher Scientific, Germering, Germany) connected to the in house compressed air system. The instrument was controlled and runs were processed using the Chromeleon® Data System Version 7.2.6 software program (Thermo Fisher Scientific).

2.3 Chromatographic procedure

A core shell octadecylsilyl (C18) Kinetex column (100 x 2.1 mm i.d., with a particle size of 2.6 µm and pore size of 100 Å) (Phenomenex, Aschaffenburg, Germany) was used as stationary phase. The chromatographic system was operated using gradient elution at a column compartment temperature of 25 °C ran in still air mode. Mobile phase A consisted of an aqueous 0.05% (v/v) formic acid solution, whereas mobile phase B was acetonitrile with addition of 0.05% (v/v) formic acid.

The final gradient runs at a flow rate of 1.5 mL/min and utilizes 75% B from 0 to 0.8 min, linearly increases to 85% B within 1.7 min and holds at 85% B for 0.5 min, followed by a re-equilibration with a gradient to 75% B within 0.5 min and a 1 min hold, resulting in a total run time of 4.5 min. The injection volume was 10 µL.

Detection was performed by means of the Vanquish® CAD with the evaporation temperature set to 30 °C, a power function value of 1.0, a filter constant of 1 s, a data collection rate of 10 Hz and a gas inlet pressure of 56.4 psi unless specified otherwise.

2.4 Prepatation of solutions

The stock solutions for the respective fatty acids were prepared by exactly weighing 10.0 mg of the fatty acid and dissolving in 10.0 mL of methanol. These stock solutions were stored in a freezer at -20 °C and diluted with a mixture of acetonitrile 75% and water 25% (v/v) to the appropriate concentration on a daily basis. The procedures for the preparation of the sample solutions were adopted from Ilko et al. [25] who modified a saponification process from Hu et al. [26] and a liquid liquid extraction from Matyash et al. [27].

2.4.1. Preparation of the sample solutions for the determination of the fatty acid composition in batches of polysorbate 80

15.0 mg of the polysorbate was exactly weighed and dissolved in 1 M potassium hydroxide solution containing 10% (v/v) methanol and made up to 10.0 mL. Saponification was achieved after incubation at 40 °C for a minimum of 6 hours.

50 µL of 100% formic acid was added to 250 µL of the solution after saponification in a glass centrifuge tube (VWR International, Darmstadt, Germany). After addition of 500 µL of MTBE the mixture was vortexed and centrifuged at 2700 rpm (EBA 20 centrifuge, Hettich, Tuttlingen, Germany) for 5 min. The entire organic phase was collected in a vial, dried under a gentle nitrogen gas stream and the residue reconstituted in 1000 µL of a mixture of acetonitrile 75%/water 25% (v/v).

Quantitative analysis of the fatty acid composition was performed using external standards and double logarithmic calibration curves for each individual fatty acid.

2.4.2. Preparation of the sample and reference solutions for the determination of the free fatty acids in batches of polysorbate 80

100.0 mg of the polysorbate was exactly weighed in a 10.0 mL volumetric flask. After addition of 500 µL of the 1 mg/mL methanolic margaric acid stock solution as internal standard, the analyte was dissolved and made up to 10.0 mL with water. The internal standard is added in a concentration of about 0.5% (m/m). The exact concentration of the internal standard needs to be calculated referring to the sample weight.

100 µL of 100% formic acid was added to 1000 µL of the polysorbate and internal standard solution in a glass centrifuge tube. After addition of 1000 µL of MTBE the mixture was vortexed and centrifuged at 2700 rpm for 45 min. 500 µL of the organic phase was collected, dried under a gentle nitrogen gas stream and the residue reconstituted in 500 µL of a mixture of acetonitrile 75%/water 25% (v/v).

The reference solution consisted of margaric acid and oleic acid at a concentration of 50 µg/mL each. It was obtained by diluting the respective stock solutions with a mixture of acetonitrile 75%/water 25% (v/v). For the evaluation of the free fatty acids, the peak area ratio of this reference solution was determined and used in the batch analysis with the internal standard.

3 Results and discussion

3.1 UHPLC method optimization

The initial LC method employing a conventional HPLC instrument reported by Ilko et al. [25] used a core shell octadecylsilyl (C18) Kinetex (Phenomenex, Aschaffenburg, Germany) column in the dimensions 100 x 3.0 mm with 2.6 µm particles. The mobile phase flow rate was set at 0.6 mL/min and a gradient method with a run time of 15 min consisting of an initial hold at 75% B for 5 min and a linear 10 min gradient step to 85% B was applied. Mobile phase A was aqueous 0.05% (v/v) formic acid, while mobile phase B consisted of acetonitrile with addition of 0.05% (v/v) formic acid.

To keep the column's selectivity and chemistry as close as possible to the original method, a Kinetex C18 column, was chosen for the method optimization to UHPLC as well. The standard Kinetex columns (i.d. 3.0 mm) are stable up to a backpressure of 600 bar, whereas the columns with an internal diameter of 2.1 mm are stable up to a backpressure of 1000 bar and thus suitable for UHPLC applications. Hence, a 100 x 2.1 mm column of the same chemistry and particle size was chosen.

Since the smaller diameter column and the UHPLC system are capable of withstanding higher backpressure, it was the ultimate goal to save time and eluent consumption after the optimization. Because all column parameters aside from the i.d. are the same for both columns, their correlation in column volume can be narrowed down to the formula shown in equation 1 [8].

$$Ratio_{V_c} = \left(\frac{ID_1}{ID_2}\right)^2 \quad (1)$$

V_C : column volume; ID : internal diameter

Using the resulting factor of 2, the mobile phases and percentage gradient levels were initially used according to Ilko et al. [25] as mentioned at the beginning of this section. In order to evaluate which flow rate would be the most appropriate, flow rates between 0.6 and 1.5 mL/min were screened. A mixture of the main fatty acid, namely oleic acid, and the internal standard, namely margaric acid, was used. Additionally, a batch of polysorbate 80 was analyzed for its free fatty acids. The initial method screening was performed with the default CAD settings of 35 °C evaporation temperature, a power function value (PFV) of 1.0 and a filter constant of 1 s.

Upon method development, variations in the gradient steps and levels were examined as well. Since a decrease of mobile phase B to 70% resulted in a slightly better

separation but inferior signal intensities, increased analysis time and increased backpressure, a gradient of initial 75% of mobile phase B up to 85% was considered more appropriate.

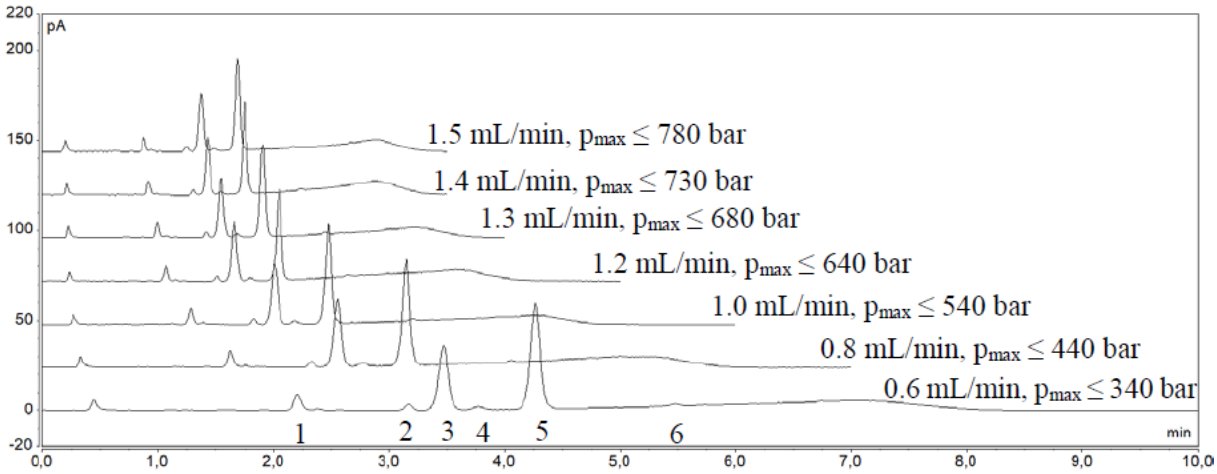

Fig. S1. Chromatograms and resulting maximum backpressure for variation of flow rate while adjusting hold and gradient time by the ratio of flow rates; 10 µL injection of a 50 µg/mL oleic acid (65-88% purity) and margaric acid solution; elution order: 1: linoleic acid, 2: palmitic acid, 3: oleic acid, 4: petroselinic acid, 5: margaric acid, 6: stearic acid

Figure S1 illustrates the chromatograms of the reference solution containing 50 µg/mL of oleic acid (65-88% purity) and margaric acid in addition to the impurities of linoleic acid, palmitic acid, petroselinic acid and stearic acid at different flow rates. The injection volume was maintained to be 10 µL since no indicators of overloading of the column occurred.

The final optimized method utilized a flow rate of 1.5 mL/min with an initial hold at 75% B for 0.8 min and a linear gradient to 85% B within 1.7 min. Resulting in a separation time lower than 3 minutes, with no backpressure problems. Reequilibration starting with 85% B for 0.5 min, back to 75% B in 0.5 min, followed by 1 min of 75% B was found to be sufficient, resulting in a total run time of 4.5 min compared to the 19 min of the HPLC method when reequilibration is also considered. The time reduction of over 75% and an eluent consumption reduction of more than 40% compared to the HPLC method of Ilko et al. [25] underlines the superiority of the UHPLC method.

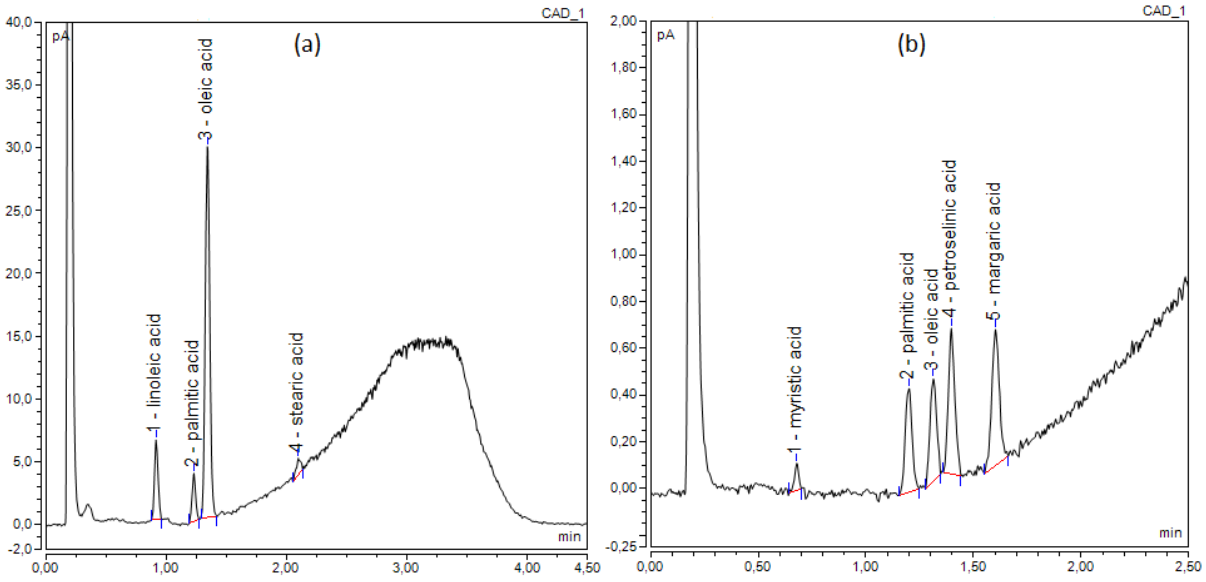

Fig. 1. (a) Chromatogram of the fatty acid composition of batch D1. Linoleic acid, palmitic and stearic acid are present besides the main component oleic acid. Percentage contents (% m/m) are listed in Table 3, for chromatographic conditions: see section 2.3.;

(b) Chromatogram of 5 ng on column of myristic acid, palmitic acid, oleic acid, petroselinic acid and margaric acid for LOQ determination. Linoleic acid and stearic acid were injected separately (chromatograms not shown), for chromatographic conditions: see section 2.3.

The optimized CAD parameters used in batch analysis were: 30 °C evaporation temperature, a power function value of 1.0, a gas inlet pressure of 56.4 psi, a filter constant of 1 s and a data collection rate of 10 Hz. Double logarithmic transformation was applied to the calibration curves of the fatty acids. The optimization of the CAD instrument settings is presented in detail in section 3.2. Example chromatograms of a batch analysis with regard to its fatty acid composition and of injections near the LOQ are presented in Figure 1.

3.2 Evaluation of CAD parameters for the detection of fatty acids

Since CAD detection is based on the formation of analyte particles, non-volatility is crucial for the response of a substance [29]. Fatty acids show different volatilities depending on the chain length. The main fatty acid present in polysorbate 80 is oleic acid (C18:1) together with others ranging from C14 (myristic acid) to C18 (stearic acid). To include a broader range of fatty acids and to evaluate the CADs limits in this mobile phase composition, a selection of shorter chain length fatty acids was added. The fatty

acids from C8 to C18 were chosen in an initial screening at the default CAD settings of 35 °C evaporation temperature, a PFV of 1.0 and a filter constant of 1 s at a concentration of 50 µg/mL. No peaks due to caprylic acid and capric acid could be detected using these conditions. Only fatty acids of C12 or longer are sufficiently non-volatile to give a measurable detector response at lower concentration levels. Additionally, fatty acids shorter than C12 are not well retained. Because of these two factors, this method is most applicable for analysis of C12 (lauric acid) and longer fatty acids.

3.2.1. Evaluation of evaporation temperature based on sensitivity

The evaporation temperature setting controls the temperature of the thermostatted evaporation tube in which, ideally, the mobile phase is quickly and completely evaporated. After eluent evaporation, the condensed phase analyte particles that remain undergo unipolar diffusion charging and produce a signal in the form of a current. The evaporation temperature setting controls the relative solute partitioning between gas and condensed phases and is therefore of utmost importance for detection selectivity [30]. Whereas the evaporation tube temperature of the 2005 ESA Corona CAD cannot vary from ambient temperature, the evaporation tube temperature of the CAD used here can set anywhere between ambient temperature and 100 °C.

Since particle formation is based on the volatility, a higher temperature generally leads to a decrease of the signal intensity for semivolatile substances [31]. Figure 2 shows the correlation of peak height and the variation of evaporation temperature settings exemplarily for the series of saturated fatty acids and for the non saturated C18:1 oleic acid for evaporation temperature settings between 25 °C and 50 °C. As expected, the signals decrease substantially upon raising the evaporation temperature. Temperatures higher than 50 °C do not give analyzable results, especially for the more volatile shorter chain length fatty acids.

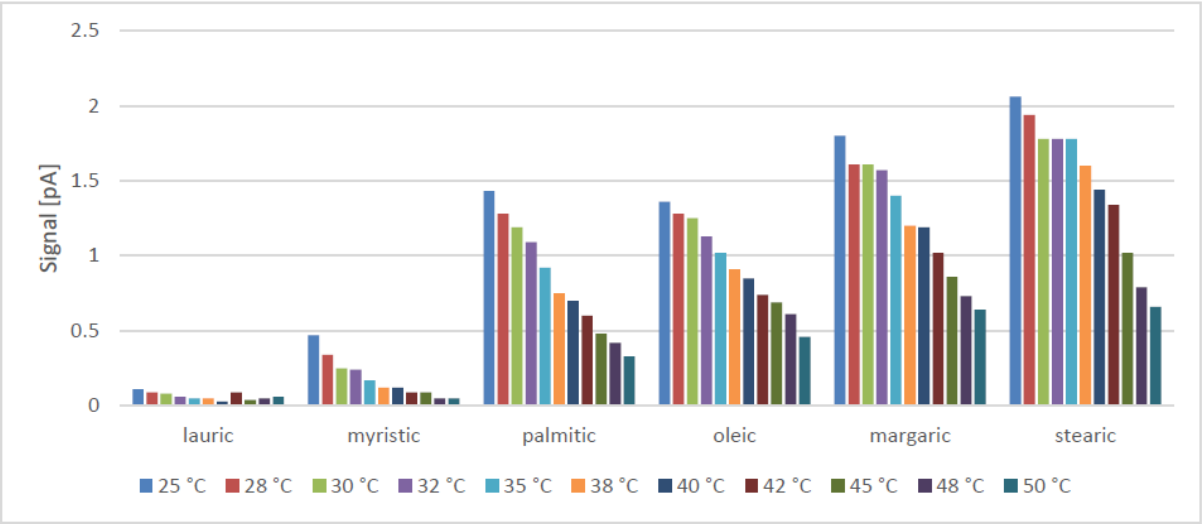

Fig. 2. Peak height at different evaporation temperatures of injections of 10 ng on column of the respective fatty acid; for chromatographic parameters see section 2.3

For non-volatile analytes, the signal is depending on the size distribution of the dried aerosols. While this size distribution does vary with the cube root of the particle density, this effect is only minor in nature. In conjunction with the unipolar charging process which is virtually independent from the analytes` physicochemical properties the charged aerosol detector shows a highly similar response for all analytes. This behavior is often referred to as uniformity of response [29]. This is in contrast to ELSD, where a significant influence on the materials' properties, like density, refractive index, absorption and fluorescence have been suggested and verified by experiments [32]. The mobile phase composition on the other hand has been found to have a severe impact on the generated aerosol, thus the uniformity of response can only be observed when the mobile phase composition entering the detector is constant, i.e. during isocratic elution or by utilizing an inverse gradient setup. With the non-compensated gradient elution described here, we expect an increased signal for later eluting peaks, as the signal intensity increases with higher acetonitrile content in acetonitrile-water mixtures. Even with this consideration, the significantly reduced signal intensity for the shorter chain length lauric and myristic acid is more than would be expected due to the varying acetonitrile content and confirms that they possess a significantly higher volatility than the longer fatty acids.

One may suggest that increasing the evaporation temperature does not bring any positive effects, but the opposite is the case. Sensitivity can be improved drastically by optimization. Detection limits as per definition of the ICH guidelines [28] are usually assessed through the S/N approach. The baseline noise mainly depends on the mass

concentration of nonvolatile and semivolatile impurities in the effluent, which can be minimized by using ultra pure solvents and additives, but cannot be completely eliminated. If the impurities have a higher volatility than the analytes of interest, a modest increase in temperature can shift the ratio of analyte amount vs. impurities in the condensed phase and thus improve the observed S/N ratios. Lowest detection limits are therefore obtained at the best compromise between decreasing baseline noise and maintaining sufficient analyte signal.

Figure 3 shows the correlation of the S/N ratios for the same data shown in Figure 2 representatively for myristic acid as a saturated short fatty acid (C14), margaric acid as a saturated long fatty acid (C17) and oleic acid as an unsaturated long fatty acid (C18:1).

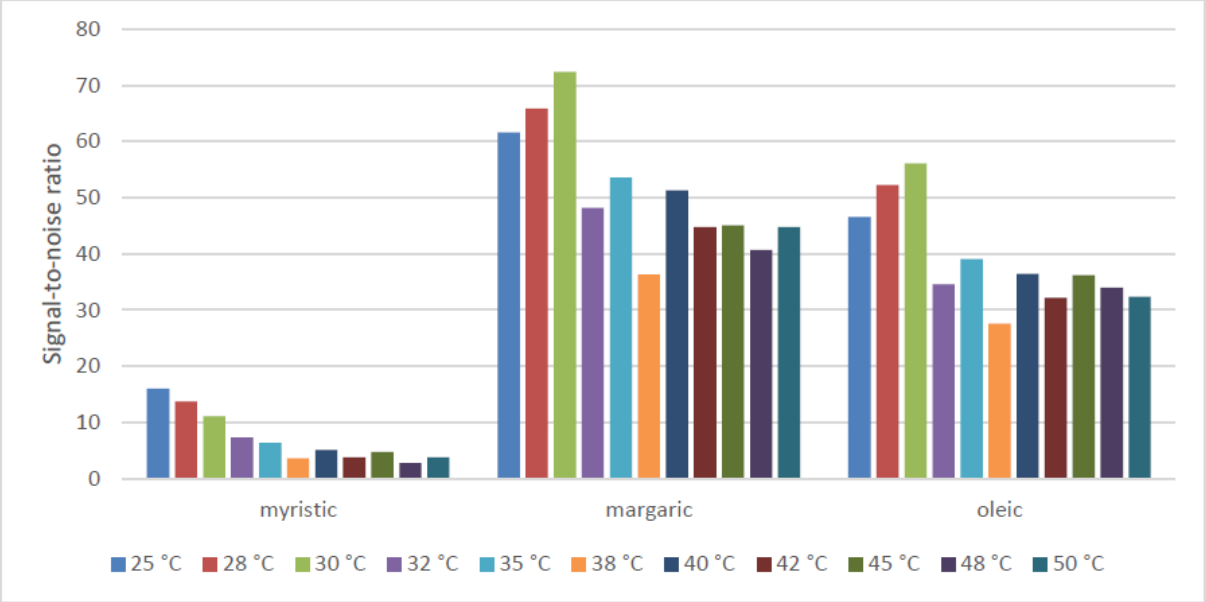

Fig. 3. S/N ratios at different evaporation temperatures of injections of 10 ng on column of the respective fatty acid; for chromatographic parameters see section 2.3.

A maximum of S/N ratio could be identified at 30 °C for most of the analytes when injected at low level concentrations that are slightly above the LOQs of the original method.

The experimental LOQs were determined using the S/N approach according to the ICH guideline [28] and injecting 1 ng, 5 ng and 10 ng on column. Table 1 displays the comparison of the LOQs obtained with the original HPLC method coupled to the “older” CAD [25] with the UHPLC method. The superiority of detection for every analyte with the exception of the most volatile, myristic acid, using the CAD parameter optimized UHPLC method can be clearly seen. RSD values calculated for 5 ng on column

injections (n = 4) ranged from 0.84 to 1.82%, except for myristic acid (9.17%) where 5 ng on column is below its LOQ. The superiority of the LOQ for myristic acid in the previous method can be traced down to the ambient evaporation temperature of the older CAD used. Myristic acid showed improved S/N ratios at lower temperatures in our measurements as well (see Figure 3).

Table 1 LOQs of the transferred UHPLC-CAD method with optimized evaporation temperature at 30 °C compared to the HPLC method with the old CAD of Ilko et al. [25]

Analyte	LOQ [ng on column] of Ilko et al [25] using HPLC-CAD	LOQ [ng on column] of optimized UHPLC-CAD
Myristic acid ($C_{14}H_{28}O_2$)	6.1	8.1
Palmitic acid ($C_{16}H_{32}O_2$)	4.0	2.2
Stearic acid ($C_{18}H_{36}O_2$)	3.4	1.3
Linoleic acid ($C_{18}H_{32}O_2$)	3.0	1.8
Oleic acid ($C_{18}H_{34}O_2$)	3.9	2.1
Petroselinic acid ($C_{18}H_{34}O_2$)	3.2	1.4

3.2.2. Evaluation of sensitivity in dependence on filter constant setting

The filter constant has significant impact on the baseline noise and thus on the detection limits of a method. It is applied to the output current of the detector and affects the collection of the raw data and the data collection rate. Generally, a higher filter constant results in smoothed baseline, whereas a lower filter constant does not remove a lot or any baseline noise at all [33].

This was confirmed by examining injections of 10 ng on column of a mixture of myristic acid, palmitic acid, oleic acid, petroselinic acid and margaric acid at different filter constant settings of 0.1 seconds (s), 1 s, 3.6 s, 5 s and 10 s with an evaporation temperature of 30, 35 and 40 °C. An evaluation of the S/N ratios for an evaporation temperature of 30 °C is shown in Figure 4. The trend was also analogous for the other evaporation temperatures (data not shown).

Although these plain data show a significant baseline smoothing resulting from an increased filter constant and a tremendous gain in S/N ratio obtained, it was no option to choose this filter setting from chromatographic point of view due to the loss of resolution by peak broadening effects. This makes the enormous S/N ratio obtained with the higher filter constants less appealing when the separation efficiency is taken

into consideration. Thus, a filter constant of 1 s was chosen because best resolution was achieved.

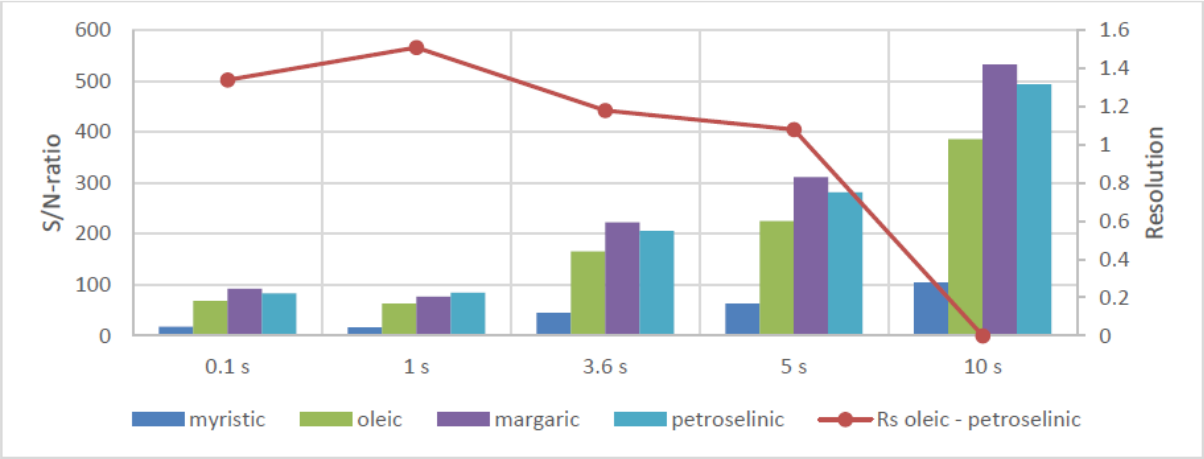

Fig. 4. S/N ratios and resolution of the critical peak pair oleic acid - petroselinic acid, 10 ng on column of the mixture of the fatty acids at varied filter settings; for chromatographic parameters see section 2.3.

3.2.2. Evaluation of sensitivity in dependence on filter constant setting

Similar to all aerosol-based detectors, the CAD is a non linear detector and response can be described by a power law function equation [34] as shown in equation 2:

$$A = a(m_{inj})^b \quad (2)$$

A linear response can be observed when b equals 1.0 and the sensitivity coefficient a then is the slope of the ratio of peak area/mass injected. With b > 1, the shape of the response curve is supralinear. Sublinear response is indicated by b < 1. Although CAD response is typically quasi-linear over about two orders of magnitude [34], it is advisable to have a closer look at the curve fit, especially for the lower calibration levels. By itself, a coefficient of determination close to 1 does not necessarily indicate good linearity over the whole range investigated [35]. In order to extend the quasi-linear dynamic range of the detector, newer CAD instruments allow for an alteration of the power function value in the range of 0.7-2.0, which affects signal output.

To evaluate the optimal power function value for each analyte, calibration curves were established covering concentration levels of 1 µg/mL, 25 µg/mL, 50 µg/mL, 75 µg/mL and 100 µg/mL at power function values ranging from 0.8 to 1.6. All measurements were performed at 30 °C, 35 °C and 40 °C evaporation temperature. The R^2-values

were established by means of linear regression (Table 2, values for evaporation temperature of 30 °C). Double logarithmic transformation was performed at the default PFV of 1.0.

Table 2 Coefficients of determination obtained at 30 °C evaporation temperature; PFV 1.0 with lg-lg transformation was used for batch testing

Analyte/ PFV	myristic acid	palmitic acid	margaric acid	stearic acid	oleic acid	petrosel-inic acid	linoleic acid	alpha-linolenic acid
0.8	0.9999	0.9909	0.9891	0.9994	0.9876	0.9836	0.9994	0.9994
0.9	0.9605	0.9935	0.9897	0.9883	0.9891	0.9861	0.9873	0.9955
1.0	0.9981	0.9972	0.9947	0.9914	0.9937	0.9922	0.9929	0.9988
1.1	0.997	0.999	0.9977	0.9979	0.9996	0.9973	0.9978	0.9975
1.2	0.9938	0.9983	0.9994	0.9993	0.9993	0.9991	0.9994	0.9985
1.3	0.9902	0.9983	0.9994	0.9996	0.9992	0.9999	0.9997	0.9942
1.4	0.9804	0.995	0.9976	0.9979	0.9981	0.9994	0.9985	0.9936
1.5	0.9782	0.9928	0.9947	0.9921	0.9953	0.9976	0.9949	0.9876
1.6	0.9664	0.9878	0.9921	0.9906	0.9914	0.9949	0.9919	0.9843
1.0 lg-lg	0.9998	0.9998	0.9995	0.9993	0.9994	0.9993	0.9995	0.9995

For a better estimation of linearity, the response factor (peak area/mass injected) was plotted against the respective concentration level (Fig. 5, shown for the example of palmitic acid). Response linearity is represented by the slope of the resulting regression line. The optimal power function value would then have a slope of zero [36]. The obtained regression lines either show a negative slope indicating sublinear response, or a positive slope indicating supralinear response.

The optimal power function value of the examined levels was determined by comparing the relative standard deviation of the response factors of each analyte for every power function as shown in Figure 6. The lowest RSD indicates the best linearity of response [36].

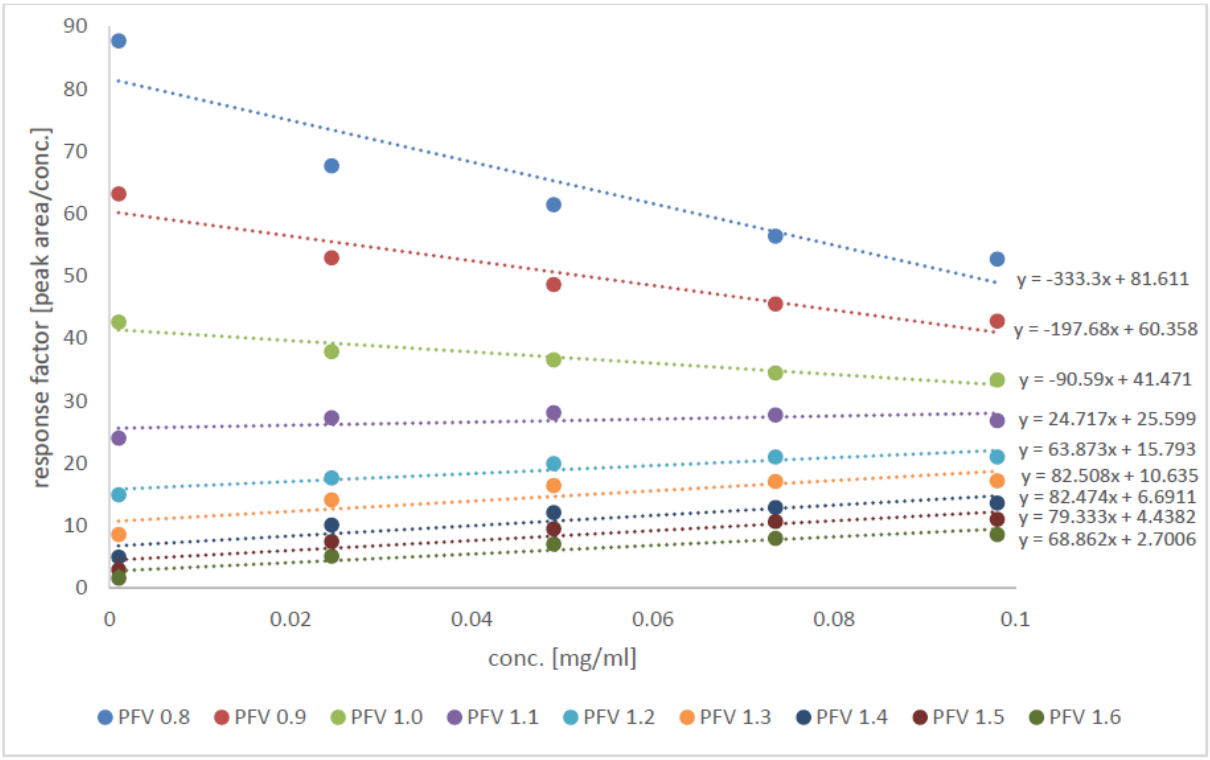

Fig. 5. Response factor versus analyte concentration plot for palmitic acid exemplarily at 30 °C evaporation temperature for power function values 0.8-1.6

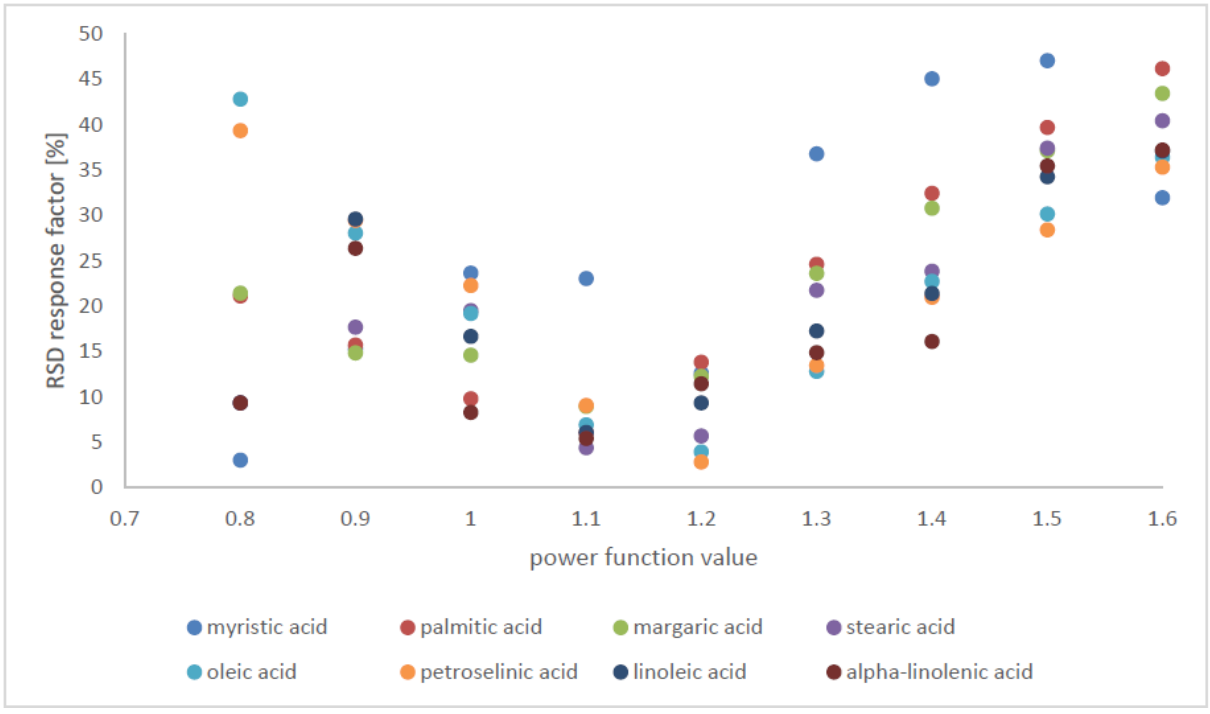

Fig. 6. RSD of the response factors [%] at evaporation temperature 30 °C (n = 5)

The same experiments were performed at evaporation temperatures of 35 and 40 °C and used to assess power function values ranging from 0.8 to 1.6 in steps of 0.1 units (Supplementary material: Fig S2). The optimal power function value was then determined for each analyte as described above.

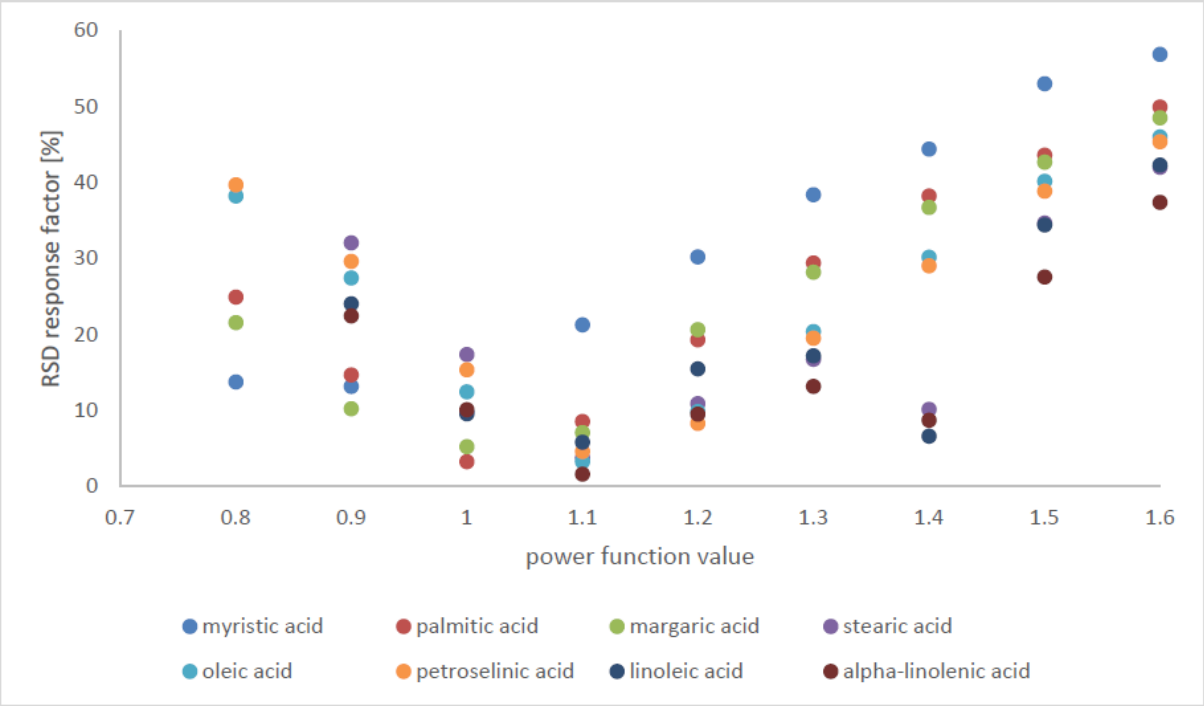

Fig. S2. RSD of the response factors [%] for PFV 0.8 to 1.6 at evaporation temperature 35 °C (n = 5)

After identifying a suitable power function value, different evaporation temperatures were evaluated. The evaluation was equivalent to the determination of the optimal power function value. Response factor versus concentration plots were obtained for evaporation temperatures of 30 °C, 35 °C and 40 °C at the same PFV. The optimal evaporation temperature for a given PFV was determined by comparison of the slopes of the regression lines as well as of the relative standard deviations of the corresponding response factors (Figure 7, restricted to five analytes for better readability). With exception of myristic acid, all fatty acids followed the same trend.

Although the optimal power function value slightly differed for each analyte, a PFV of 1.1 turned out to be beneficial in terms of linearity of response and coefficient of determination compared to the standard value of 1.0 (see Fig. 6).

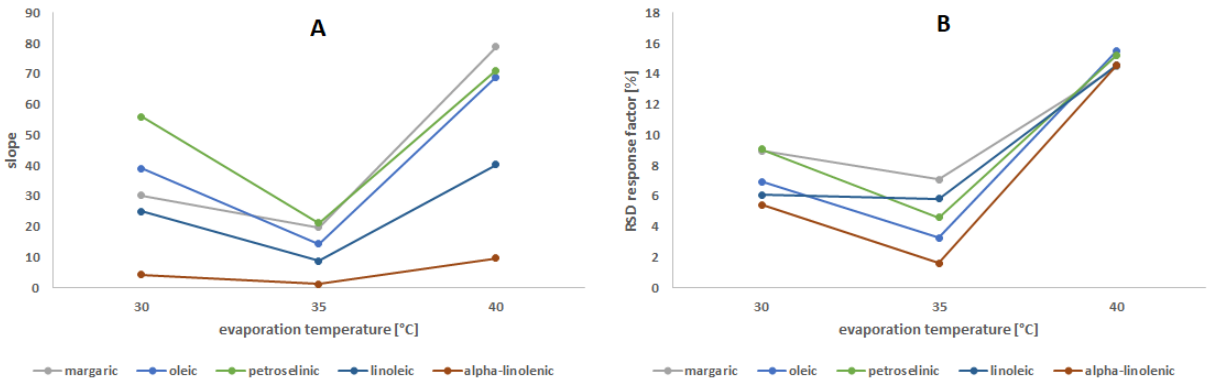

Fig. 7. **A:** Slope of the response factors versus evaporation temperature plot for PFV 1.1;

B: RSD of the response factors versus evaporation temperature plot for PFV 1.1 (n = 5)

Of note, myristic acid, the most volatile fatty acid, did not follow that trend. Being a rather volatile compound, the best results are expected at a PFV <1.0 [37]. In accordance with this, optimal results for this analyte were found at a PFV of 0.8.

For all fatty acids, response linearity at 30 °C and 35 °C was similar when maintaining a PFV of 1.1 (median RSD 5.21% to 6.50%), whereas response linearity at 40 °C and a PFV of 1.1 was not optimal (median RSD 15.37%). For partially volatile analytes such as the fatty acids, it can therefore be concluded that an optimal PFV determined at a given temperature is no longer valid when evaporation temperature is changed (Figure 7).

An alternative to using the power function value is a double logarithmic transformation of the calibration curve. The quality of the linear fit for every analyte, expressed as the coefficient of determination achieved by the double logarithmic transformation, was $R^2 > 0.999$. Furthermore the obtained residuals for the calibration levels showed very satisfying results, even at low concentrations (Supplementary material: Fig S3), whereas residuals, especially at the lowest concentrations, varied drastically with changes in PFV.

This shows that, for a multiple analyte mixture, it can be sufficient to use the default PFV of 1.0 and log log transformation to achieve a linear fit of the response, rather than to apply a more complex fitting model.

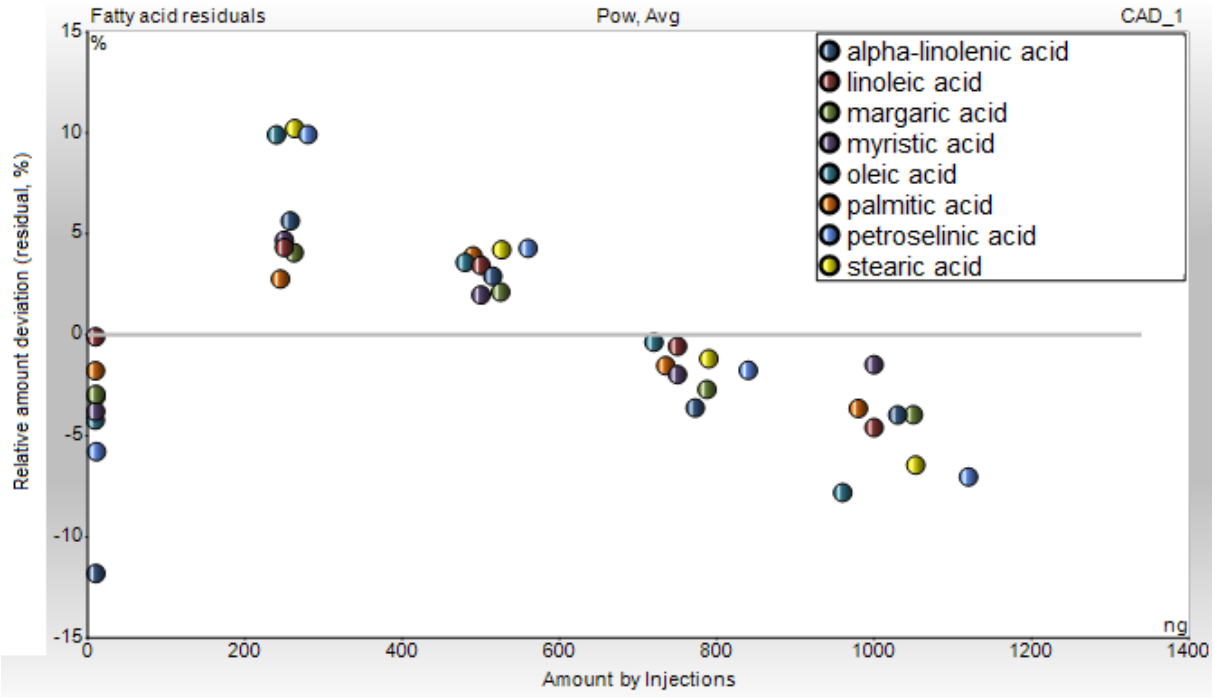

Fig. S3. Residual plot of the relative amount deviation for each calibration level for lg-lg transformation at 30 °C evaporation temperature and a PFV of 1.0 (n = 5)

In many cases the application's goal is to obtain satisfactory and low LOQs. Thus, for partially volatile analytes, it seems most appropriate to evaluate the optimal evaporation temperature before determining the best power function value to receive an appropriate fit. This conclusion arises from the facts that evaporation temperature strongly affects sensitivity (Fig. 3) and that the ideal PFV changes when altering evaporation temperature (Fig. 7). This is in contrast to the common approach of determining PFV before evaporation temperature for non volatiles [34].

3.3 Validation and application of the optimized method

3.3.1 Method validation

The method was validated with regard to ICH guideline Q2(R1) [28]. Hereby, specificity, linearity and range, accuracy, precision, limit of quantitation (LOQ) and robustness were assessed.

Specificity could be demonstrated by individual analysis and analysis of mixtures of reference standards of all possible sample compounds. Separation of the fatty acids

from each other was achieved and the extraction procedure did not interfere with any peaks needed for quantitation as confirmed with the analysis of blank extractions.

Linearity was shown by establishing calibration curves over a range of two orders of magnitude at concentration levels of 1, 25, 50, 75 and 100 µg/ml covering the estimated analyte amount of the sample. Application of linear regression after double logarithmic transformation of concentration and peak area resulted in coefficients of determination (R^2) higher than 0.999 for each analyte over the investigated range (Table 2).

For demonstration of *accuracy*, recovery rates were calculated at 1, 25 and 100 µg/mL concentration levels for each fatty acid standard (n = 3) using calibration curves. Quantification was done by linear regression after double logarithmic transformation of concentration and peak area. The mean recoveries were satisfactory with values ranging from 94.3 to 107.1%.

Precision was assessed by injections of fatty acid standards in triplicate at concentration levels of 1, 25 and 100 µg/mL. RSD values ranging from 0.07 to 2.52% were obtained indicating good precision with exception of the 1 µg/ml level of myristic acid showing an increased RSD of 6.61%. Since myristic acid was not present in the current investigation and the method was still capable of meeting the requirements set by the Ph. Eur. (limit of 5%), this was accepted.

LOQs of the fatty acids were determined with respect to the S/N approach according to ICH guideline Q2(R1) [28]. A S/N ratio of 10, derived from analyte signal compared to a blank, was hereby defined as the LOQ. For linear extrapolation, standard solutions at 0.1, 0.5 and 1.0 µg/mL concentration level were used. Ranging from 1.3 to 8.1 ng on column (Table 1), the LOQs were significantly affected by the chain length of the fatty acid as further elaborated in section 3.2.

Robustness in terms of CAD parameter settings could be evaluated with regard to the systematic variations of the method optimization procedure and is elaborated in depth in section 3.2., here especially evaporation temperature was found to be critical. Chromatographic robustness in general was evaluated for the following variations: column temperature ± 2.5 °C, initial percentage of mobile phase B ± 1%, final percentage of mobile phase B ± 1% and flow rate ± 0.06 mL/min. Robustness is sufficient with recovery rates ranging from 96 to 102% for all substances with exception of myristic acid having recovery rates between 103 and 110% (Supplementary

material: Table S1) which was acceptable due to its absence within the current batch analysis (Table 3). Separation was maintained for all examined variations.

Table S1. Robustness of the UHPLC method. Percentage recovery rates of a 100 µg/mL solution for different chromatographic variations

	No variation	Temperature (°C)		Flow rate (ml/min)		% Mobile Phase B at start		% Mobile Phase B at end	
		22.5	27.5	1.44	1.56	74	76	84	86
% Recovery									
Alpha-linolenic	100	99	99	101	96	98	98	100	98
Myristic	100	108	109	110	103	104	105	107	110
Linoleic	100	100	101	102	98	102	98	99	100
Palmitic	100	99	97	102	96	98	97	96	96
Oleic	100	99	96	98	96	100	98	99	99
Petroselinic	100	101	97	99	96	96	96	98	98
Stearic	100	100	99	98	97	99	100	97	97

3.2.2 Polysorbate 80 batch analysis

16 batches of polysorbate 80 analyzed by Ilko et al. [25] were subjected to analysis applying the optimized UHPLC method. The findings indicate sufficient stability of polysorbate 80 when stored at room temperature for four years with only rare exposure to light (Table 3).

Of note, the analysis of the fatty acid composition revealed an increase in linoleic acid for all batches except for the ones of manufacturer B and batch E3. Since linoleic acid is a double unsaturated fatty acid that can originate from oxidation of oleic acid, oxidative degradation during storage can be suggested because the increase in linoleic acid occurred upon a decrease of oleic acid content only. Batch E3 was stored in a brown glass bottle, which should prevent photo oxidation. Consequently, no formation of linoleic acid was observed in this batch, supporting the suggested degradation pathway.

Only three batches, namely A2, A3 and D3, were no longer within the specifications of the European Pharmacopoeia (Ph. Eur.) due to an excessive content of linoleic acid greater than 18% (m/m).

Table 3. Percentage (% m/m) content of fatty acids in polysorbate 80 batches, average of n=2 extractions shown with standard error; n/a= error not available because only n=1 was evaluated.

Values in brackets indicate the percentage change after four years of storage

	Alpha-linolenic acid	Myristic acid	Palmitoleic acid	Linoleic acid	Palmitic acid	Oleic acid	Petroselinic acid	Stearic acid	Free fatty acids
A1	-	-	- (-0.8)	16.5±0.25 (+9.9)	4.9±0.16 (-0.5)	75.8±0.74 (-9.4)	1.5±0.02 (+0.7)	1.4±0.35 (+0.2)	0.7±0.02 (+0.1)
A2	-	-	- (-0.8)	19.2±0.06 (+9.6)	4.8±0.09 (-0.6)	72.7±0.33 (-9.2)	1.8±0.00 (+0.6)	1.6±0.30 (+0.2)	0.8±0.07 (+0.2)
A3	-	-	- (-0.8)	18.7±0.54 (+8.6)	4.4±0.08 (-1.4)	74.4±0.77 (-6.2)	1.7±0.09 (+0.7)	0.9±0.05 (-0.8)	0.8 n/a (-0.4)
A4	-	-	- (-0.8)	14.9±0.81 (+8.1)	4.2±0.12 (-1.6)	78.4±0.58 (-5.7)	1.7±0.05 (+0.5)	0.8±0.07 (-0.8)	1.1 n/a (+0.5)
B1	-	-	-	-	- (-0.8)	100±0.00 (+3.3)	-	- (-0.4)	0.3±0.00 (+0.3)
B2	-	-	-	-	- (-1.0)	100±0.00 (+3.6)	-	- (-0.5)	0.2±0.00 (+0.2)
B3	-	-	- (-0.6)	-	- (-0.7)	100±0.00 (+4.7)	-	- (-0.4)	0.1±0.03 (+0.1)
C1	-	-	- (-0.5)	15.7±0.02 (+6.3)	9.4±0.12 (-2.8)	72.7±0.11 (-1.3)	1.0±0.21 (-)	1.1±0.04 (-1.6)	0.4±0.00 (-0.3)
C2	-	-	- (-0.7)	15.2±0.26 (+8.1)	9.5±0.23 (-1.1)	72.3±0.41 (-5.7)	1.0±0.01 (+0.1)	2.0±0.06 (-0.9)	0.4±0.01 (-)
C3	-	-	-	16.0±0.19 (+5.3)	11.4± 0.07 (-3.2)	67.2±0.14 (-0.6)	3.3±0.06 (+0.7)	2.0±0.03 (-1.6)	0.3 n/a (-)
D1	-	- (-0.2)	-	17.4±0.88 (+6.1)	6.5±0.31 (-1.8)	75.1±0.73 (-2.6)	- (-0.3)	1.0±0.46 (1.0)	0.5±0.06 (+0.1)
D2	-	- (-0.1)	-	16.9±0.22 (+5.3)	6.2±0.37 (-1.3)	75.5±0.49 (-2.7)	- (-0.3)	1.4±0.10 (-0.5)	0.4±0.00 (+0.1)
D3	-	-	-	18.5±0.07 (+6.7)	6.0±0.02 (-1.4)	74.4±0.10 (-3.7)	- (-0.3)	1.1±0.04 (-0.9)	0.4±0.01 (+0.1)
E1	-	-	-	10.0±0.15 (+8.9)	1.6±0.01 (-0.9)	85.4±0.03 (-7.0)	1.6±0.08 (+0.4)	1.4±0.19 (-1.3)	0.1±0.01 (+0.1)
E2	-	-	-	8.5±0.13 (+8.5)	2.1±0.10 (-0.9)	86.1±0.12 (-6.1)	1.6±0.18 (+0.6)	1.6±0.10 (-1.5)	0.1±0.00 (+0.1)
E3	-	-	-	-	3.4±0.05 (-1.0)	93.9±0.25 (+1.6)	0.8±0.25 (-0.2)	1.9±0.23 (-0.9)	0.8±0.05 (+0.8)

4 Conclusion

An UHPLC method for the analysis of polysorbate 80 was successfully optimized for use with the newest generation CAD resulting in time savings of over 75% and eluent consumption savings of more than 40%, respectively, while achieving superior LOQs when compared to a former method run on a conventional HPLC-CAD system. Moreover, the dependence of detector response on CAD settings was assessed in a systematic approach for a series of homologous fatty acids ranging from C14 to C18. It could be verified that the evaporation temperature of the detector has a significant impact on sensitivity. Furthermore, S/N ratios can be optimized by the choice of an appropriate evaporation temperature. Modern CAD detectors allow for the use of an integrated power function value which was evaluated here. Use of the power function value can drastically improve linearity of response, especially at the lower levels of the

calibration curve. However, a double-logarithmic transformation proved to be superior and less time consuming for the investigated two order concentration range of rather volatile analytes. It was shown that linearity of response and limit of quantification vary greatly with different PFV and evaporation temperature settings. Thus, these two parameters should be chosen and optimized based on an application's individual goal and depending on volatility of the analytes.

Conflict of interest statement

The Thermo Fisher Scientific Vanquish™ UHPLC System was generously provided by Thermo Fisher Scientific for this cooperation.

Acknowledgement

Special thanks are due to Christiane Theiss and her assistance with her expert knowledge of fatty acids and their properties as well as Oliver Wahl (both University of Wuerzburg) for insightful discussions and advices, as well as Paul Gamache (Thermo Fisher Scientific, Chelmsford, Massachusetts, USA) and Frank Steiner (Thermo Fisher Scientific, Germering, Germany) for project coordination and crucial ideas, reviews and discussions.

References

1. A.C. Rustan, C.A. Drevon, Fatty acids: structures and properties. Encyclopedia of Life Sciences, 2005: John Wiley & Sons.

2. A. Tomlinson, B.l. Demeule, B. Lin, S. Yadav, Polysorbate 20 degradation in biopharmaceutical formulations: quantification of free fatty acids, characterization of particulates, and insights into the degradation mechanism. Mol pharm, 2015. 12: p. 3805-3815.

3. S. Fekete, K. Ganzler,J. Fekete, Fast and sensitive determination of Polysorbate 80 in solutions containing proteins. J. Pharm. Biomed. Anal., 2010. 52: p. 672-679.

4. G. Eccleston, Functions of mixed emulsifiers and emulsifying waxes in dermatological lotions and creams. Colloid Surface A, 1997. 123: p. 169-182.

5. Z. Wu, Q. Zhang, N. Li, Y. Pu, B. Wang, T. Zhang, Comparison of critical methods developed for fatty acid analysis: a review. J. Sep. Sci., 2017. 40: p. 288-298.

6. M. Collomb, U. Bütikofer, R. Sieber, B. Jeangros, J.O. Bosset, Composition of fatty acids in cow's milk fat produced in the lowlands, mountains and highlands of Switzerland using high-resolution gas chromatography. Int Dairy J, 2002. 12: p. 649-659.

7. T. Seppänen-Laakso, I. Laakso, R. Hiltunen, Analysis of fatty acids by gas chromatography, and its relevance to research on health and nutrition. Anal. Chim. Acta, 2002. 465: p. 39-62.

8. European Directorate for the Quality of Medicine and Healthcare, European Pharmacopoeia Online 9.5, Monograph No. 01848. 2018. Available from: http://online6.edqm.eu/ep905/, Access Date: April 3rd 2018

9. D. Kloos, H. Lingeman, O. Mayboroda, A. Deelder, W.M.A. Niessen, M. Giera, Analysis of biologically-active, endogenous carboxylic acids based on chromatography-mass spectrometry. TrAC, Trends Anal. Chem., 2014. 61: p. 17-28.

10. E. Drange,E. Lundanes, Determination of long-chained fatty acids using non-aqueous capillary electrophoresis and indirect UV detection. J. Chromatogr. A, 1997. 771: p. 301-309.

11. S.-H. Chen,Y.-J. Chuang, Analysis of fatty acids by column liquid chromatography. Anal. Chim. Acta, 2002. 465: p. 145-155.

12. W. Liu, Z.-Z. Wang, J.-P. Qing, H.-J. Li, W. Xiao, Classification and quantification analysis of peach kernel from different origins with near-infrared diffuse reflection spectroscopy. Pharmacogn. mag., 2014. 10: p. 441.

13. G. Knothe, J.A. Kenar, Determination of the fatty acid profile by 1H-NMR spectroscopy. Eur. J. Lipid Sci. Technol., 2004. 106: p. 88-96.

14. C. Skiera, P. Steliopoulos, T. Kuballa, B. Diehl, et al., Determination of free fatty acids in pharmaceutical lipids by 1H NMR and comparison with the classical acid value. J. Pharm. Biomed. Anal., 2014. 93: p. 43-50.

15. C. Skiera, P. Steliopoulos, T. Kuballa, U. Holzgrabe, B. Diehl, Determination of free fatty acids in edible oils by 1H NMR spectroscopy. Lipid Technol., 2012. 24: p. 279-281.

16. D. Perret, A. Gentili, S. Marchese, M. Sergi, et al., Determination of free fatty acids in chocolate by liquid chromatography with tandem mass spectrometry. Rapid Commun. Mass Spectrom., 2004. 18: p. 1989-1994.

17. J. Zhao, S. Li, F. Yang, P. Li, Y.T. Wang, Simultaneous determination of saponins and fatty acids in Ziziphus jujuba (Suanzaoren) by high performance liquid chromatography-evaporative light scattering detection and pressurized liquid extraction. J. Chromatogr. A, 2006. 1108: p. 188-194.

18. L.M. Nair, J.O. Werling, Aerosol based detectors for the investigation of phospholipid hydrolysis in a pharmaceutical suspension formulation. J. Pharm. Biomed. Anal., 2009. 49: p. 95-99.

19. M. Plante, B. Bailey, I. Acworth, The use of charged aerosol detection with HPLC for the measurement of lipids, in Lipidomics. 2009, Springer. p. 469-482.

20. E. Bravi, G. Perretti, L. Montanari, Fatty acids by high-performance liquid chromatography and evaporative light-scattering detector. J. Chromatogr. A, 2006. 1134: p. 210-214.

21. N. Vervoort, D. Daemen, G. Török, Performance evaluation of evaporative light scattering detection and charged aerosol detection in reversed phase liquid chromatography. J. Chromatogr. A, 2008. 1189: p. 92-100.

22. S. Almeling, U. Holzgrabe, Use of evaporative light scattering detection for the quality control of drug substances: Influence of different liquid chromatographic and evaporative light scattering detector parameters on the appearance of spike peaks. J. Chromatogr. A, 2010. 1217: p. 2163-2170.

23. S. Almeling, D. Ilko, U. Holzgrabe, Charged aerosol detection in pharmaceutical analysis. J. Pharm. Biomed. Anal., 2012. 69: p. 50-63.

24. T. Vehovec,A. Obreza, Review of operating principle and applications of the charged aerosol detector. J. Chromatogr. A, 2010. 1217: p. 1549-1556.

25. D. Ilko, A. Braun, O. Germershaus, L. Meinel, U. Holzgrabe, Fatty acid composition analysis in polysorbate 80 with high performance liquid chromatography coupled to charged aerosol detection. Eur J Pharm Biopharm, 2015. 94: p. 569-574.

26. M. Hu, M. Niculescu, X. Zhang, A. Hui, High-performance liquid chromatographic determination of polysorbate 80 in pharmaceutical suspensions. J. Chromatogr. A, 2003. 984: p. 233-236.

27. V. Matyash, G. Liebisch, T.V. Kurzchalia, A. Shevchenko, D. Schwudke, Lipid extraction by methyl-tert-butyl ether for high-throughput lipidomics. J. Lipid Res., 2008. 49: p. 1137-1146.

28. International Conference on Harmonisation of Technical Requirements for Registration of Pharmaceuticals for Human Use, Validation of analytical procedures: text and methodology Q2(R1)2005.Available from: https://www.ich.org/fileadmin/Public_Web_Site/ICH_Products/Guidelines/Quality/Q2_R1/Step4/Q2_R1__Guideline.pdf, Access Date: April 3rd 2018

29. T. Gorecki, F. Lynen, R. Szucs, P. Sandra, Universal response in liquid chromatography using charged aerosol detection. Anal. Chem., 2006. 78: p. 3186-3192.

30. J.P. Hutchinson, J. Li, W. Farrell, E. Groeber, R. Stucs, G. Dicinoski, P.R. Haddad, Comparison of the response of four aerosol detectors used with ultra high pressure liquid chromatography. J. Chromatogr. A, 2011. 1218: p. 1646-1655.

31. A.G. Osborn, D.R. Douslin, Vapor-pressure relations for 15 hydrocarbons. J. Chem. Eng. Data, 1974. 19: p. 114-117.

32. S. Lane, B. Boughtflower, I. Mutton, C. Paterson, D. Farrant, N. Taylor, Z. Blaxill, C. Carmody, P. Borman, Toward single-calibrant quantification in HPLC. A comparison of three detection strategies: evaporative light scattering, chemiluminescent nitrogen, and proton NMR. Analytical chemistry, 2005. 77: p. 4354-4365.

33. M. Plante, B. Bailey, P. Gamache, I. Acworth, Guidelines for Method Transfer and Optimizaion of the Corona Veo Charged Aerosol Detector. 2016. Available from: https://assets.thermofisher.com/TFS-Assets/CMD/posters/PN-64690-CAD-Method-Transfer-Guidelines-Corona-Veo-Pittcon2016-PN64690-EN.pdf, Access Date: April 3rd 2018

34. P.H. Gamache, Charged aerosol detection for liquid chromatography and related separation techniques. John Wiley & Sons, Hoboken, 2017.

35. M.M. Kiser, J.W. Dolan, Selecting the best curve fit. LC GC NORTH AMERICA, 2004. 22: p. 112-117.

36. A. Soliven, I.A.H. Ahmad, J. Tam, N. Kadrichu, P. Challoner, R. Markovich, A. Blasko, A simplified guide for charged aerosol detection of non-chromophoric compounds—Analytical method development and validation for the HPLC assay of aerosol particle size distribution for amikacin. J. Pharm. Biomed. Anal., 2017. 143: p. 68-76.

37. B. Bailey, P. Gamache, I. Acworth, Guidelines for method transfer and optimization—from earlier model Corona detectors to Corona Veo and Vanquish charged aerosol detectors. 2017. Available from: https://assets.thermofisher.com/TFS-Assets/CMD/Technical-Notes/tn-71290-cad-method-transfer-tn71290-en.pdf, Access Date: April 3rd 2018

4.3 Quantitative Structure – Property Relationship modeling of polar analytes lacking UV chromophores to Charged Aerosol Detector Response

Klaus Schilling[1], Jovana Krmar[1], Nevena Maljuric, Ruben Pawellek, Ana Protic, Ulrike Holzgrabe

[1]These authors contributed equally to this work.

Reprinted with permission from Anal Bioanal Chem 2019, 411:2945-2959.

Abstract

In this study, a QSPR model was built in order to link molecular descriptors and chromatographic parameters as inputs towards CAD responsiveness. Aminoglycoside antibiotics, sugars and acetylated amino-sugars, which all lack a UV/Vis chromophore, were selected as model substances due to their polar nature that represents a challenge in generating a CAD response. Acetone, PFPA, flow rate, data rate, filter constant, SM5_B(s), ATS7s, SpMin1_Bh(v), Mor09e, Mor22e, E1u, R7v+ and VP as the most influential inputs were correlated with the CAD response by virtue of ANN applying a backpropagation learning rule. External validation on previously unseen substances showed that the developed 13-6-3-1 ANN model could be used for CAD response prediction across the examined experimental domain reliably (R^2: 0.989 and RMSE: 0.036).

The obtained network was used to reveal CAD response correlations. The impact of organic modifier content and flow rate was in accordance with the theory of the detector's functioning. Additionally, the significance of SpMin1_Bh(v) aided in emphasizing the often neglected surface-dependent CAD character, while the importance of Mor22e as a molecular descriptor accentuated its dependency on the number of electronegative atoms taking part in charging the formed particles. The significance of PFPA demonstrated the possibility of using evaporative chaotropic reagents in CAD response improvement when dealing with highly polar substances that act as kosmotropes. The network was also used in identifying possible interactions

between the most significant inputs. A joint effect of PFPA and acetone was shown, representing a good starting point for further investigation with different and, especially, eco-friendly organic solvents and chaotropic agents in the routine application of CAD.

1. Introduction

Compounds lacking suitable chromophores for classical HPLC-UV analysis represent a challenge in the analytical field. They are often analyzed by means of derivatization procedures, either pre- or post-column, which are tedious, prone to errors and can be complicated for automation. There are several so-called “universal detectors” offering a solution to this issue, among which the Charged Aerosol Detector (CAD) stands out favorably as an easy-to-use and highly sensitive mass dependent detector, giving a fairly universal response over a broad dynamic range regardless of the analyte’s structure [1, 2]. The CAD is a suitable choice for aminoglycoside antibiotics (streptomycin and kanamycin), sugars (glucose, fructose, mannose, sucrose, maltose and raffinose) and acetylated amino-sugars (*N*-acetyl-D-mannosamine and *N*-acetyl-D-glucosamine), due to their lack of chromophores. Yet, these compounds represent a challenge in CAD detection since the lower amount of organic solvent in the mobile phase, necessary for the RP-HPLC analysis of those polar substances, is not beneficial for the CAD response [3]. Hence, they were chosen as model analytes (Figure 1).

In CAD, the effluent is nebulized with the help of a nitrogen gas stream and particles are formed after an evaporation process and removal of large droplets. A secondary nitrogen gas stream that has previously passed a corona needle transfers positive charge onto the particles in a diffuse manner, which is then detected by a highly sensitive electrometer. Thus, for each non-volatile or semi-volatile substance, acceptable CAD responsiveness can be expected [1, 3-5].

The employed principle of functioning, concisely described above, indicates experimental parameters that influence the CAD’s response intensity. This includes the mobile phase composition as well as instrumental conditions. The influence of the mobile phase properties is mostly associated with the type and content of organic modifier used, with a special attention to additives that manipulate the mobile phase viscosity and volatility. Higher content of organic solvent in the mobile phase enhances the CAD’s response by producing smaller droplets via low viscosity and providing a high rate of evaporation. Variations in the response due to different instrumental settings are most prominent when changing the flow rate of the mobile phase and the evaporation temperature. To illustrate, a decreased mobile phase flow rate contributes to an enhanced response by producing smaller initial droplets, similar to HPLC-MS.

Smaller initial droplets, in comparison to the larger ones, experience faster and more efficient evaporation, yielding a higher response [1, 3-5]

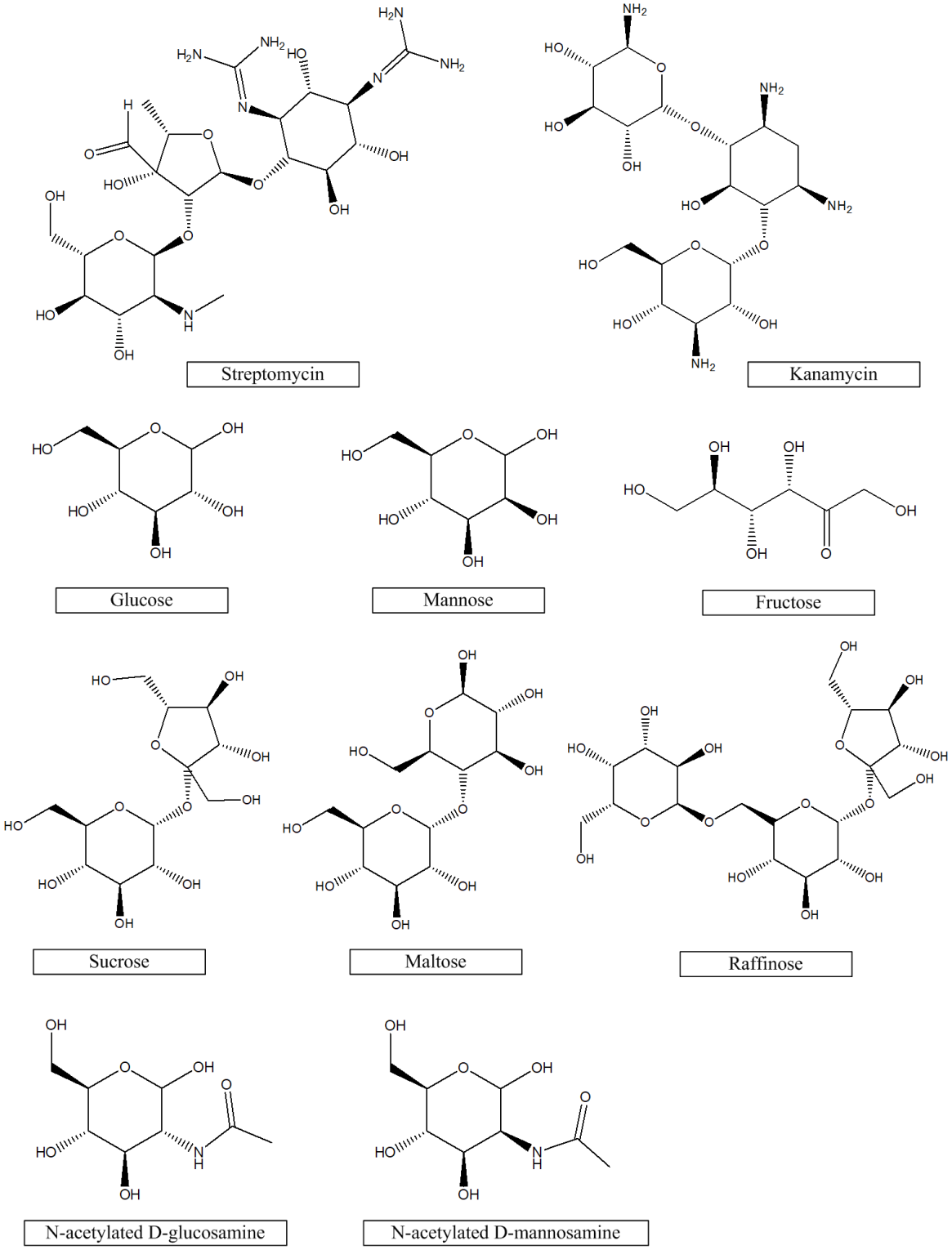

Figure 1 - Chemical structures of the investigated analytes

In light of the presented facts, it is believed that under stable conditions CAD, as a particle detector, always produces an equal signal if the same mass quantity of substance is entering the detector. Inconsistently with this theory, the intensity of the CAD response can significantly vary among different compounds of the same injected mass concentration, analyzed under constant experimental settings [3]. Thus, empirical observations indicate that the complete understanding of the underlying mechanisms is still missing and that the CAD response behavior is dependent on the analyte's structure, as well. In order to elaborate this, Quantitative Structure-Property Relationships (QSPRs) as methods of mathematical modeling that quantify the dependency on the physicochemical properties of the analytes according to their structural characteristics (molecular descriptors), were employed. Considering the fact that the CAD response largely depends on experimental parameters, there was a need to incorporate them into the QSPR modeling. Although the classical QSPR approach solely links molecular descriptors to the observed response, performing analysis under only one defined set of conditions significantly constrains the practical applicability of the developed model and its future usage is confined to the concrete factors' values [6], increasing interest in so-called "mixed modeling" that incorporates both, experimental parameters and molecular descriptors as independent variables into a single model has been observed [7]. Including all influential factors towards the examined response increases the rate of explained variance and, hence, improves the predictive performance of the model and allows for the investigation of interactions among the influential parameters. Artificial neural networks (ANN) as a machine learning algorithm capable of finding solutions for complex modeling problems was used for building of the QSPR model [7].

To the best of our knowledge, until now most papers have only dealt with the examination of the CAD response behavior under varying working conditions [8, 9] or physicochemical parameters of the observed analytes [10]. Therefore, the aim of this work was to allow for quantification of structure-property relationships in HPLC-CAD and prediction of CAD responsiveness upon different experimental parameters for new, previously unseen substances. Also, this study should contribute to the understanding of factors influencing the generated response of polar substances and provide a more detailed understanding of the CAD's functioning principle, based on the physicochemical meaning of the utilized molecular descriptors and diverse mobile phase additives.

2. Experimental

2.1. Chemicals and reagents

D-(+)-Glucose [>99.5%], D-(-)-fructose [>99.5%], D-(+)-mannose [>99.5%], sucrose [>99.5%] D-(+)-maltose monohydrate [>99%], D-(+)-raffinose pentahydrate [>99%], *N*-acetyl-D-glucosamine [>99%] and *N*-acetyl-D-mannosamine [>98%] as well as HPLC plus grade acetone and pentafluoropropionic acid (PFPA) [97%] were purchased from Sigma Aldrich Chemie GmbH (Steinheim, Germany). Streptomycin sulfate CRS was purchased from the EDQM (Strasbourg, France). Kanamycin sulfate monohydrate was obtained from the BfArM (Bonn, Germany). Ultrapure water was produced by a water purification system from Merck Millipore (Schwalbach, Germany) specified at a resistivity of 18.2 MΩ cm.

2.2. Apparatus

The HPLC-CAD experiments were performed on an Agilent 1100 modular chromatographic system equipped with an online vacuum degasser, a binary pump, an autosampler and a thermostatted column compartment (Agilent, Waldbronn, Germany). Detection was performed using the ESA Corona charged aerosol detector (Thermo Fisher Scientific, Germering, Germany), which was connected directly to the column compartment with PEEK capillaries and a 0.5 µm inlet filter. The CAD was supplied with nitrogen gas from an ESA nitrogen generator (Thermo Fisher Scientific, Germering, Germany) connected to the in house compressed air system. The inlet pressure was 35.0 psi. Agilent ChemStation® Rev. B03.02 software was used for data processing.

2.3. Chromatographic procedure

2.3.1 Experiments on column

An octadecylsilyl (C18) Knauer Eurospher II H column (250 x 4.6 mm; particle size 3 µm; pore size 100 Å) (Knauer, Berlin, Germany) was used as stationary phase. The chromatographic system was operated in isocratic elution mode at a column compartment temperature of 40 °C. The mobile phase consisted of acetone, PFPA and ultrapure water in different compositions according to the Box-Behnken Design (BBD) of experiments presented in Table 1. The flow-rates were 0.5, 0.8 and 1.1 mL min^{-1},

respectively. Necessary run times were estimated by preliminary experiments and ranged from 20 to 80 min, depending on acetone and PFPA content as well as flow rate. The injection volume was 10 µL. Column equilibration was obtained with a minimum of 20 column volumes after every change to the eluent system.

Detection of the analytes was performed by means of the ESA Corona CAD with different settings of filter constant (none – low – high) and sampling rate (2 Hz - 30 Hz – 60 Hz), varied according to the employed experimental design

2.3.1 Flow-injection experiments

An octadecylsilyl (C18) Security Guard Cartridge (4 x 3 mm) (Phenomenex, Aschaffenburg, Germany) was used to generate sufficient backpressure for operation. The chromatographic system and detection operated as in section 2.3.1., utilizing the parameters according to Table 1. Run time was 3 min. Equilibration of detector baseline and the system was ensured by having eluent flow at the upcoming conditions for a minimum of 20 minutes after every change to the eluent system. Injection consisted of the following steps: draw 10 µL from sample, draw 40 µL from the excessively concentrated mobile phase vial (see 2.4. and 3.1.), draw 10 µL air, mix five times and injection

2.4 Preparation of solutions

10.0 mg of the aminoglycoside antibiotic, exactly weighed, was dissolved in 10.0 mL of ultrapure water. The solutions were stored at 2 °C and an aliquot of about 500 µL was used freshly on a day to day basis after letting the solution adapt to room temperature and thorough mixing. 10.0 mg of the respective sugar, exactly weighed, was dissolved in 10.0 mL of ultrapure water. The sample weighing of the two hydrated sugars, namely maltose monohydrate and raffinose pentahydrate, was increased to account for 10.0 mg of the anhydrous substance. Both N acetylated amino-sugars were dissolved at 10.0 mg/mL and diluted to yield a 1 mg/mL sample solution.

All sugar solutions were stored in aliquots of 500 µL at -20 °C and one aliquot was unfrozen at room temperature and protected from light and transferred to a brown glass vial on a daily basis.

The excessively concentrated mobile phase was prepared with an acetone and PFPA content equal to 125% of the current mobile phase composition in a 10.0 mL volumetric

flask. This was necessary to yield the appropriate mobile phase concentration after mixing in the injector program as described in section 3.1.

2.5 Selection of experimental design levels

Acetone percentage, PFPA content, flow rate, filter settings and data collection rate were varied using an experimental design methodology in order to properly define the experimental domain, i.e. to facilitate ANN process of learning of underlying patterns conserved in the data. These parameters and their levels were selected according to preliminary experiments and instrumental constraints (Section 3.1) [11]. The Box-Behnken experimental scheme was obtained by the Design-Expert 7.0.0. software (Stat-Ease, Inc., Minneapolis, USA) and included the plan of experiments and corresponding CAD responses (Table 1). The experiments were carried out in random order.

2.6 Computation of molecular descriptors

In order to preserve every possibly influential information computation of molecular descriptors started with a large group of descriptors, also including those with known linkage to response. Dragon 6.0.7. software (Talete srl, Milano, Italy) was used for calculation of 4885 molecular descriptors divided into 29 different blocks. The number of descriptors was reduced as only one, among highly correlated molecular descriptors encoding the same chemical information, was kept for further evaluation, and then further reduced to those that significantly correlated with the output.

Additionally, vapor pressure (VP), solvent–excluded volume (SEV), Connolly solvent accessible area (SAS) and Connolly molecular area (MS) were calculated in Chem 3D Ultra 7.0.0 software (CambridgeSoft Corporation, Surrey, UK). For all aforementioned calculations, structures subjected to the energy minimization by the MOPAC/AM1 method of Chem 3D Ultra 7.0.0 were used. The final selection of descriptors to be included in the ANN model was done by employing enter Multi Linear Regression (MLR) in PASW Statistics 18 (SPSS Inc., Hong Kong, PRC).

2.6.1 Artificial neural networks

ANNs were used as a machine learning tool for QSPR model building. The network type and topology, training algorithm and function parameters were firstly defined. Multi-layer feed-forward networks are most commonly used for their clear topology and

simple algorithm that usually fits the best. During the training process, the weights (adaptive coefficients that characterize connections between layers) and biases were randomly initialized at values between -1 and +1. The learning of the network consisted of minimizing the prediction error, particularly, Root Mean Square Error, RMSE. The RMSE is calculated to account for the error between the mean of the experimentally obtained values and those predicted by the network according to the formula (1). An increase in RMSE in the verification data set indicates an overfitting of the network and initiates the end of the training as a stopping criterion.

$$RMSE = \sqrt{\frac{\sum_{i=1}^{n}(y_i - \hat{y}_i)^2}{n}} \quad (1)$$

The quality of the modeling in terms of predictiveness is explained by the RMSE accompanied with the squared correlation coefficient (R^2), determining how well the model fits the data calculated according to the formula (2).

$$R^2 = 1 - \frac{\sum_{i=1}^{n}(y_i - \hat{y}_i)^2}{\sum_{i=1}^{n}(y_i - \acute{y})^2} \quad (2)$$

In both formulas above y_i stands for the experimentally obtained response, $\hat{y}_i$ for the model derived calculated response, $\acute{y}$ for the average of experimentally obtained response values, n for the number of samples and *i* represents the sample index. After optimization, the actual predictive performance of the trained network was evaluated using an external validation. In this study, the external validation was performed using two substances, glucose and *N*-acetyl-D-glucosamine (89 cases in total). The remaining data points were randomly split to the training and verification data contingents, so that the training data set included 277 cases, while the verification data set included 89 cases. Glucose and *N*-acetyl-D-glucosamine were chosen as test substances to cover molecular descriptor levels near the extreme values of the experimental domain, assuming that if the model predicts well for these values near the limit, it would predict even better for all other investigated compounds with descriptor values within the experimental domain.

ANN analysis was carried out using the STATISTICA Neural Networks (StatSoft Inc., USA).

3. Results and discussion

3.1. Preliminary investigation of chromatographic parameters and chromatographic procedure

Since the aminoglycoside antibiotics are multicomponent mixtures themselves and also contain a number of impurities that are not structurally unambiguously identified, but only characterized by their m/z values, their analysis was performed by means of a chromatographic separation according to the quality control method for streptomycin sulfate published by Holzgrabe et al. [12]. The evaluation was then restricted to the main substance peak of the antibiotics due to the aforementioned substance profile of the aminoglycosides. A separation of streptomycin and kanamycin from its impurities was achieved with an endcapped RP 18 column using 10.5% (v/v) of acetone and 20 mM of PFPA. In order to examine a broad range of chromatographic conditions and its influence on the generation of CAD response, the acetone content was varied from 1 to 20% (v/v) and the PFPA content from 10 to 30 mM. The suitability of these ranges was confirmed by preliminary experiments in which the separation of the main peak from the related impurities was maintained for all variations.

The sugars and acetylated amino-sugars were analyzed by means of flow injection analysis (FIA) since they were available as pure substances. A comparison of the response obtained for glucose on column and by means of FIA initially showed a decreased response for the FIA experiments. This was caused by detection in aqueously diluted media due to insufficient mixing within the short flow path and because the detector is highly dependent on the mobile phase composition [3].

Thus, an injector program to ensure proper mixing was developed. A mixture of the sample solution with a solution containing a concentration of acetone and PFPA higher than the current mobile phase was subjected to CAD. The injector program was set to mix 40 µL of the excessively concentrated mobile phase containing 25% more acetone and PFPA than the current eluent condition with 10 µL of the sample solution. Hereby, the correct mass, being the important factor in CAD response generation, was injected as if it was dissolved in the mobile phase itself. Since the peak areas obtained by this approach and by the experiments on column resulted to be highly comparable, it was confirmed that this approach was appropriate to overcome the issue of aqueous dilution of the sample. Hence, the absolute peak areas obtained by means of FIA and experiments on column were used for model building without further considerations.

The reason for utilization of constant mass concentration (mg mL^{-1}), and not molar concentration (mmol mL^{-1}) for the injections is the fundamental functioning principle of CAD. The CAD response depends on the charge transferred to the substance particles that correlate with the mass of the analyte because it is a mass dependent detector [4].

Due to its importance within the nebulization process, the flow rate was varied from 0.5 to 0.8 and 1.1 mL min^{-1}. The ESA Corona CAD has a fixed evaporation temperature and gas inlet pressure level, and could thus not be modified. In contrast, filter constant and data collection rate were expected to influence the signal behavior and thus chosen to be varied. These parameters were integrated into the BBD plan of experiments and their levels were selected to represent the minimum and maximum, as well as an intermediate value of the instrument's range.

The chromatographic conditions of both experimental approaches were identical and are reflected in the Box-Behnken design in Table 1.

Table 1 Experimental plan and obtained CAD responses

	Variables					CAD response									
	Acetone (%)	**PFPA (mM)**	**Flow rate (mL min^{-1})**	**Data rate (Hz)**	**Filter constant**	**Strepto-mycin**	**Kana-mycin**	**Glu-cose**	**Fruc-tose**	**Man-nose**	**Su-crose**	**Maltose**	**Raffi-nose**	***N*-acetyl D-glucosa-mine**	***N*-acetyl D-mannosa-mine**
1	10.5	20	1.1	30	high	1792.100	2822.5	921.60	897.63	910.93	893.86	893.800	885.73	945.100	907.700
2	10.5	20	1.1	2	low	1811.800	2866.4	888.33	874.83	887.33	868.23	861.433	857.13	912.000	888.767
3	10.5	20	1.1	30	none	1748.867	2772.8	888.36	865.70	873.50	855.93	853.000	850.80	911.100	884.667
4	10.5	20	1.1	60	low	1754.400	2747.8	872.63	838.96	859.86	839.10	840.800	834.36	893.967	662.033
5	10.5	20	0.8	30	low	1952.433	3128.7	965.80	942.40	952.73	937.53	937.700	936.66	978.200	936.733
6	10.5	20	0.8	2	none	1977.600	3146.2	909.43	887.50	892.63	874.33	878.967	879.00	944.367	912.300
7	10.5	20	0.8	60	high	1909.367	3040.4	937.10	907.93	917.16	897.13	900.767	893.46	990.400	959.567
8	10.5	20	0.8	2	high	1907.833	3049.0	966.23	914.83	923.80	903.50	901.633	901.60	988.867	960.100
9	10.5	20	0.8	60	none	1944.200	3092.8	923.30	901.93	909.33	903.40	887.067	901.26	952.567	928.600
10	10.5	20	0.8	30	low	1960.567	3114.7	932.40	904.96	914.93	897.86	898.333	897.36	958.000	928.700
11	10.5	20	0.5	60	low	2048.133	3247.8	1068.0	1045.7	1058.0	1039.7	1038.067	1038.8	1094.167	1057.800
12	10.5	20	0.5	2	low	2076.267	3298.7	1043.8	1011.2	1027.2	1004.2	1010.067	1012.6	1073.567	1038.033
13	10.5	20	0.5	30	high	2094.767	3299.8	1039.5	1010.5	1032.9	1010.6	1010.600	1009.7	1079.233	1043.500
14	10.5	20	0.5	30	none	2265.267	3606.9	1024.0	998.46	1013.7	991.40	989.633	993.26	1058.267	1021.500
15	1	20	1.1	30	low	1108.133	1762.3	335.26	328.33	330.90	322.43	318.000	319.13	345.600	334.633
16	1	20	0.8	60	low	1260.400	2035.5	342.83	334.93	340.56	336.70	329.733	332.46	360.433	348.567
17	1	20	0.8	2	low	1267.967	2022.8	352.10	343.23	344.73	338.90	334.367	338.06	368.067	354.100
18	1	20	0.8	30	none	1184.300	1912.8	350.66	344.96	348.60	340.13	337.367	338.53	368.700	354.467
19	1	20	0.8	30	high	1210.967	1971.1	355.03	345.16	348.96	341.70	340.667	341.06	369.133	358.500
20	1	20	0.5	30	low	1385.267	2234.2	381.93	372.93	376.83	370.73	365.133	365.83	393.367	376.300
21	10.5	20	0.8	30	low	2013.567	3097.3	952.83	925.53	942.46	921.20	913.767	913.06	973.100	937.367
22	20	20	1.1	30	low	2111.467	3007.9	1230.4	1192.8	1212.9	1177.2	1177.667	1174.7	1264.667	1227.133
23	20	20	0.8	2	low	2351.433	3393.7	1335.4	1305.4	1310.5	1274.6	1271.100	1273.2	1365.933	1319.433
24	20	20	0.8	60	low	2382.333	3427.2	1348.7	1325.4	1340.6	1310.5	1312.400	1314.0	1400.133	1357.933
25	20	20	0.8	30	none	2393.167	3432.0	1376.4	1348.6	1362.4	1346.0	1343.733	1347.7	1424.433	1387.500
26	20	20	0.8	30	high	2398.333	13775.	1370.4	1343.9	1360.0	1323.3	1320.000	1327.0	1430.633	1379.100
27	20	20	0.5	30	low	2647.533	3805.3	1575.7	1528.6	1539.7	1507.6	1504.733	1494.4	1603.533	1548.733
28	10.5	20	0.8	30	low	1921.900	2919.3	923.96	896.66	914.73	887.43	892.367	892.03	955.067	922.200
29	10.5	10	1.1	30	low	1193.567	1864.2	610.63	593.20	600.46	586.50	586.500	580.83	615.633	603.100
30	10.5	10	0.8	2	low	1334.500	2077.5	660.20	642.13	648.56	633.46	629.967	629.23	670.367	651.867
31	10.5	10	0.8	60	low	1358.733	2106.8	661.60	642.90	652.66	634.90	634.333	632.20	675.333	651.133

32	10.5	10	0.8	30	high	1379.300	2127.6	654.50	634.96	645.03	627.36	627.900	624.66	669.400	646.600
33	10.5	10	0.8	30	none	1385.833	2131.0	652.70	634.53	643.93	627.86	626.067	627.10	668.200	646.300
34	10.5	10	0.5	30	low	1581.967	2484.7	738.76	715.46	724.86	712.20	709.033	707.90	754.700	730.400
35	1	10	0.8	30	low	855.100	1321.3	295.73	288.90	290.16	281.46	278.967	278.63	301.067	292.133
36	20	10	0.8	30	low	1677.367	2434.8	1000.4	978.60	991.90	963.33	970.500	972.00	1035.300	995.800
37	10.5	20	0.8	30	low	1762.500	2698.2	967.66	932.76	N/A	927.20	931.100	927.53	988.367	954.800
38	10.5	30	1.1	30	low	1939.633	2937.6	1067.2	1045.0	1056.7	1021.5	1023.833	1027.2	1110.100	1072.100
39	10.5	30	0.8	30	none	2220.967	3407.3	1200.0	1175.6	1191.0	1155.8	1147.067	1136.7	1213.500	1183.433
40	10.5	30	0.8	60	low	2262.400	3470.2	1148.4	1118.0	1130.8	1091.9	1104.467	1107.0	1187.033	1144.400
41	10.5	30	0.8	30	high	2294.133	3512.5	1191.5	1162.7	1175.2	1141.7	1149.867	1150.1	1223.900	1190.467
42	10.5	30	0.8	2	low	2265.867	3467.6	1162.1	1138.0	1145.5	1114.5	1122.767	1117.0	1207.600	1176.100
43	10.5	30	0.5	30	low	2501.167	3803.3	1334.8	1298.6	1305.9	1279.8	1285.700	1281.7	1380.733	1331.633
44	20	30	0.8	30	low	2362.900	3291.7	1459.4	1418.3	1437.0	1397.1	1399.200	1405.0	1507.433	1459.433
45	1	30	0.8	30	low	1396.667	2170.8	577.53	551.43	556.60	545.66	540.200	536.43	587.167	557.200
46	10.5	20	0.8	30	low	1842.100	2741.4	936.06	912.73	928.20	902.43	907.367	903.56	960.533	929.467

N/A – not assessed due to system malfunction

Filter constant: none = 1 s; low = 3.6 s; high = 10 s

3.2. Selection of input variables

The main role of molecular descriptors, whether they are obtained experimentally or computed theoretically, is to encode the chemical structure of the observed analytes. However, not all molecular descriptors are of the same importance for a particular task of modeling. Therefore, in its initial phase, it is very important to diminish redundant and insufficiently informative ones, i.e. to come up with the rational number of descriptors while acquiring as much chemical and structural information as possible [13-15].

Since the detailed study of the structural influence of polar substances on the CAD response is lacking, Dragon software was used to calculate a large pool of theoretical descriptors. The cut off for elimination of redundant molecular descriptors was set to a coefficient of correlation value of 0.99, which led to 798 uncorrelated descriptors. These descriptors along with the chromatographic conditions and CAD parameters were then subjected to multilinear regression analysis (MLR), using an enter method to identify those with the most important contribution to the output. The selected inputs were: acetone (v/v, %), PFPA (mM), flow rate (mL min^{-1}), data rate (Hz), filter constant (s), SM5_B(s), ATS7s, SpMin1_Bh(v), Mor09e, Mor22e, E1u, R7v+ and VP. Data rate and filter constant were found to be insignificant ($p>0.05$) with respect to CAD response. But since they did not compromise the overall significance of the enter-MLR model, they were considered as ANN's inputs as well.

Molecular descriptors, finally defined as relevant to the target outputs, belonged to the groups of both topological and geometrical descriptors. SM5_B(s), ATS7s and SpMin1_Bh (v) are classified as 2D matrix-based descriptors, 2D autocorrelations and Burden eigenvalues, respectively. They contain a weighting component in terms of physicochemical property addressing the topology of the structure or its parts associated with the selected property [16]. Complementing these topological descriptors, the following geometrical descriptors were selected for further ANN

modeling: Mor09e and Mor22e from the group of 3D-MoRSE descriptors, and E1u and R7v+ belonging to WHIM and GETAWAY descriptors, respectively.

The developed mixed model was utilized to reveal and quantify the influence of the selected molecular descriptors and instrumental parameters on the targeted output.

3.3. ANN modeling

The abovementioned experimental parameters and molecular descriptors, as model inputs, were related to CAD response by means of ANN. The CAD response was transformed logarithmically, because a skewed distribution of data points initially led to a reduced predictive performance of the model. Namely, the employed ANN machine learning algorithm, based on minimizing prediction error, tends to learn to predict the data in their dense region as good as it is possible. However, adoption of such a principle causes a drastic increase in error for the prediction of the cases that do not reside in the dense region. In the observed case, due to wide variation in the instrumental and chromatographic conditions as well as the structural characteristics between the analytes, the models' output values (CAD responses) varied in a great span. Thus, the employed machine learning algorithm learned to predict the smaller values of the modeled response better, due to the greater representation in the data and consequently in the training set. On the contrary, when dealing with high values, the ANN showed poor predictive ability. Employing a logarithmic transformation of the response helped in overcoming the mentioned problem and in obtaining a network of good predictive ability by rescaling the actual measurements, i.e. by achieving homogeneous variability of the followed response [17, 18].

In order to confirm our hypothesis that a mixed model would have better predictive ability compared to the classical QSPR or to a model relating only experimental parameters towards the logarithmic values of CAD response, two independent neural networks were developed, but neither of them showed satisfactory performances.

Thus, a mixed QSPR model, including both, the relevant molecular descriptors and the experimental parameters, was developed and a multilayer Perceptron with 13-6-3-1 topology (Figure 2) showed the best performance towards logarithmic values of CAD response.

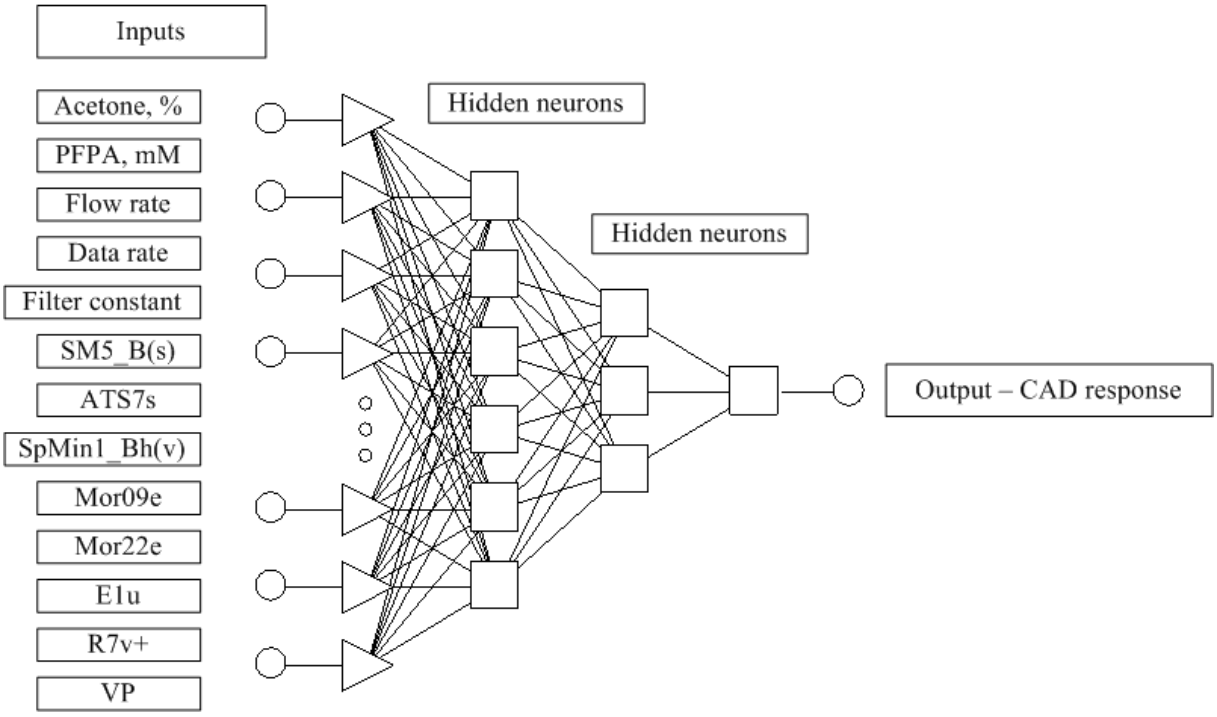

Figure 2 - Graphical presentation of the artificial neural network with 13-6-3-1 topology

A logistic activation function for the input alteration was employed in neurons of the hidden and output layers. The network was trained with a back-propagation algorithm with the learning rate set to 0.3 and the momentum set to 0.1, through 10000 epochs. High R^2 values of 0.989, 0.995 and 0.989 and low RMSE values of 0.041, 0.023 and 0.036 for training, verification and validation data set, respectively, indicated the good predictive ability and that no overfitting occurred during the training process. The results of ANN computing for training, verification and validation data set are presented in Table S1. Since the modeling was carried out with a logarithmic transformation of the output values (CAD response), the performance of the model should be confirmed with back-transformed CAD response as well. In order to prove that the model's performance is preserved with the back-transformed response, the agreement between the experimentally obtained and the predicted CAD responses is presented in Figure 3a-d for training, verification and validation data set, respectively. As evident from Figure 3a, one single case is completely out of range, so it was labeled and consequently eliminated as an outlier. The outlier appeared as a consequence of a system malfunction. After careful consideration of the other experimental results, no other outliers were noticed even when similar conditions and the same substance were

used, hence it was concluded that the disagreement was not related to the analyte's structure. Given the fact that only one case appeared to be an outlier and the sufficient number of over 450 valid values provided a highly predictive network, no remeasurement was conducted and the outlier was eliminated. After discarding the outlier, good agreement was obtained for all data sets, which is especially significant for the validation data set, as a data set of analytes previously unseen in the network (Figure 3b-d).

When evaluating the predictive ability of the model, a difference can occur in case of the low and high values of response, due to the greater representation of the lower values in the data set.

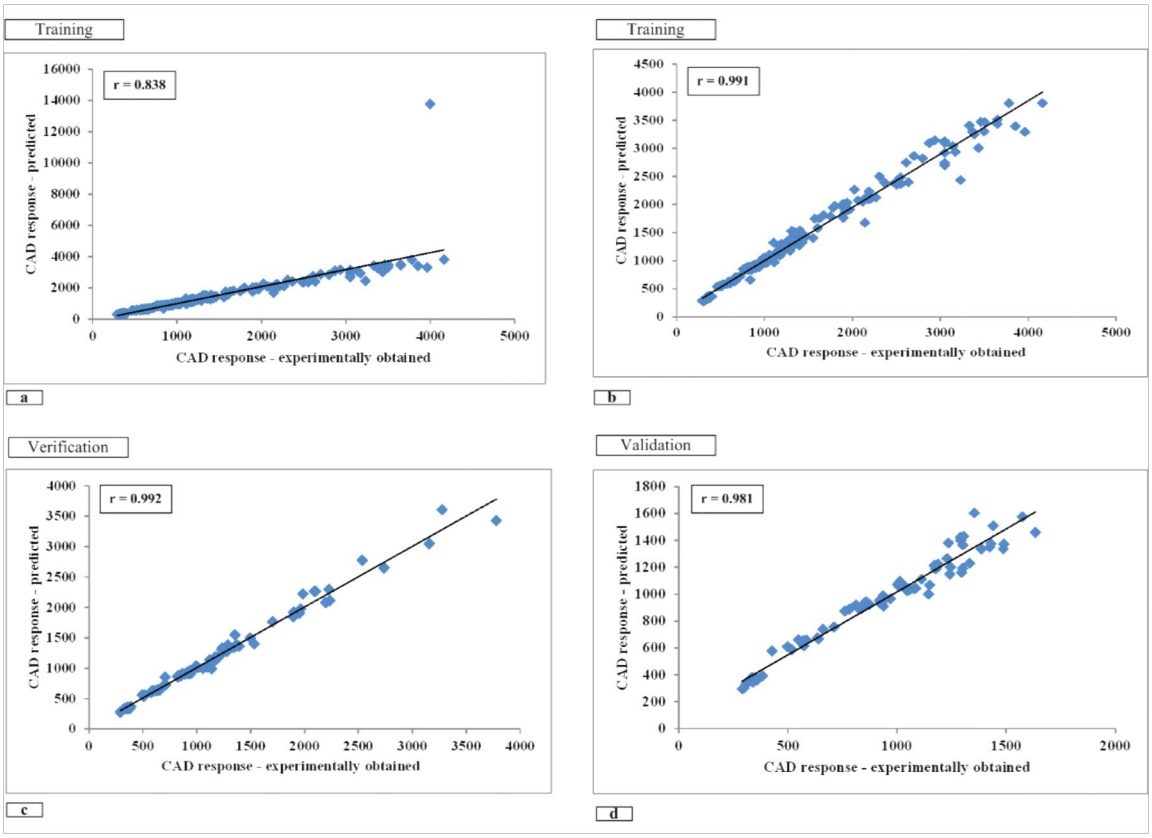

Figure 3 - Agreement between experimentally obtained CAD response and CAD response predicted by ANN

3a - Training data set ; **3b -** Training data set with excluded outlier ; **3c -** Verification data set ; **3d** - Validation data se**t**

In order to examine the predictive ability of the model for low and high values of response, the data set was divided into two groups – the group of antibiotics giving high CAD responses and the group of sugars and acetylated amino-sugars giving low

CAD responses. Since there is no defined limit above which the responses could be classified as high and vice versa, forming one group with antibiotics and the other with sugars and acetylated amino-sugars seemed to be a reasonable solution with regard to their responses. Then, the log (response) is back-transformed in response units and used in the RMSE calculation for both groups. Since the RMSE is expressed in absolute values and the unit of the data set, its value largely depends on the intensities of the response, e.g. when the response is measured in thousands it is expected that the RMSE is larger compared to the RMSE obtained from values measured in hundreds. Because of that, a higher RMSE for higher CAD intensities does not necessarily represent a larger error in prediction. Therefore, in order to compare the RMSE values obtained for different ranges of CAD intensity, the back-transformed experimentally obtained and the predicted CAD intensities were subjected to a min max normalization in the range from 0 to 100. The min-max normalization was applied since it preserves all relationships within the data, while each feature lies within the new range of values. The RMSEs calculated with normalized response values were now comparable [19]. The normalized RMSE values for the group of antibiotics were 6.05 and 5.53 for the training and verification data sets, respectively. Additionally, the RMSEs for the group of sugars and acetylated amino-sugars were 3.87, 4.70 and 5.81 for the training, verification and validation data set. Differences in RMSE values could be noticed between these two groups. Higher normalized RMSE values calculated for the group of antibiotics indicated that the prediction error is increasing with an increase of CAD response. However, the difference could not prevent the usage of the network in the evaluation of the variables towards the response intensities. Moreover, no antibiotic was used as a test substance, so the predictive ability of the network on an unseen analyte generating a rather high CAD response was not demonstrated. Accordingly, it is advisable to include more antibiotics in future studies - or more generally speaking, bigger and more homogenous group sizes of subclasses of substances - and incorporate some of them as a test substance to fully demonstrate the predictive ability of the network throughout the whole measured range of the CAD response.

The contribution of each selected variable to the performance of the proposed mixed model was evaluated by means of a sensitivity analysis. The variable sensitivity ratio (VSR), representing the model’s performance if that variable is unavailable, was calculated as a ratio of the variable sensitivity error (VSE) and the error of the model

when all variables are available. A high VSR value assigned to a certain variable indicates its influential contribution to the model's performance [20]. The VSR values: acetone (VSR = 4.57), PFPA concentration (VSR = 2.35), SpMin1_Bh (v) (VSR = 5.94) and Mor22e (VSR = 2.82) were found to have the highest impact on the model's performance. Thus, those variables are essential to be included in the QSPR model.

On the contrary, vapor pressure, which is recognized as the most relevant descriptor for CAD responsiveness in the literature [5] showed the least influence on the model performance compared to other molecular descriptors within the sensitivity analysis. This finding could be in agreement with the polar nature of the analyzed substances whose molecules experience strong inter-forces and, consequently, difficult gas-phase transitioning [21]. Furthermore, all analytes have a very low VP and can all be classified as nonvolatile, hence only a minor influence of the VP is expected. If an independent variable to which the network is less sensitive is known, it can be removed from the input selection for the purpose of obtaining a better model. Although the mixed model was not sensitive to vapor pressure as a variable, it remained included because its removal did not improve the model.

The proposed, optimal ANN was further used in constructing diagrams and response surface plots that helped in revealing the most influential inputs for CAD response generation, trends of CAD response towards inputs and interactions between the most influential parameters.

Response graphs estimating the trends of CAD response behavior towards molecular descriptors are presented in Figure 4. The influence of each molecular descriptor included in the network was investigated individually, taking into account the difference in the highest and the lowest CAD responses across the examined range of descriptor's values. Clearly, SpMin1_Bh (v) (ratio = 3.95) and Mor22e (ratio = 2.28) were determined as the most influential descriptors towards CAD response among SM5_B(s) (ratio = 1.66), ATS7s (ratio = 1.21), Mor09e (ratio = 1.13), E1u (ratio = 1.36) and R7v+ (ratio = 2.18).

One of the most influential descriptors, SpMin1_Bh (v) belongs to the group of topochemical descriptors. It is defined as eigenvalues of a modified connectivity matrix (Burden matrix), where the diagonal elements of the Burden matrix are weighted by the van der Waals volume. The basic assumption was that the lowest eigenvalues

contain contributions from all atoms, and thus reflect the topology of the whole molecule and not only its fragments. Including information on the electronic environment of the atoms in the matrix should connect the matrix eigenvalues to the electronic distribution of the whole molecule. The predominant influence of SpMin1_Bh(v) on CAD response as well as the fact that the analytes with the highest values of the descriptor (antibiotics) generate the greatest response among the observed substances strongly indicates the surface-dependent character of the CAD. Since the signal is produced by measuring the charge imposed on the outer edges of the particles, particles with larger surface area may carry more charge and, thus, generate higher responses.

On the other hand, Mor22e belongs to the group of very sophisticated 3D-MoRSe molecular descriptors. 3D-MoRSE descriptors are derived from 3D projections of the molecular structure based on electronic diffraction [22]. Although each of these descriptors carries the information about the whole molecule, short-distance atomic pairs determine its values predominantly. The applied Dragon software recognizes five classes of these descriptors weighted by different atomic properties. Mor22e represents the signal 22 weighted by atomic Sanderson electronegativity [23]. The intention of the employed weighting scheme is to increase the contribution of fluorine, oxygen and chlorine [24]. The observed increase in CAD responsiveness of the examined antibiotics due to the increase in this descriptor's value indicates the shortest distances between oxygen and hydrogen atoms as a major part of Mor22e. Hence, this means that hydroxyl groups are preferential structural fragments for a high intensity of CAD response. This finding pointed out a previously unattended aspect of the CAD detector's functioning. Namely, it seems that structures with a larger number of electronegative atoms, that take part in forming short chemical bonds, generate higher CAD response. This might be due to a more extensive transfer of positive charge to the surface of the analyte particles. Further, the 3D plot that shows the interaction between the two most influential molecular descriptors of the model substances towards the target output was constructed and given in Figure 5.

A drastic increase in CAD response along with the increase in values of both relevant descriptors, SpMin1_Bh (v) and Mor22e, pointed to the aforementioned structural characteristics being very beneficial for generating high-intensity responses under constant experimental conditions.

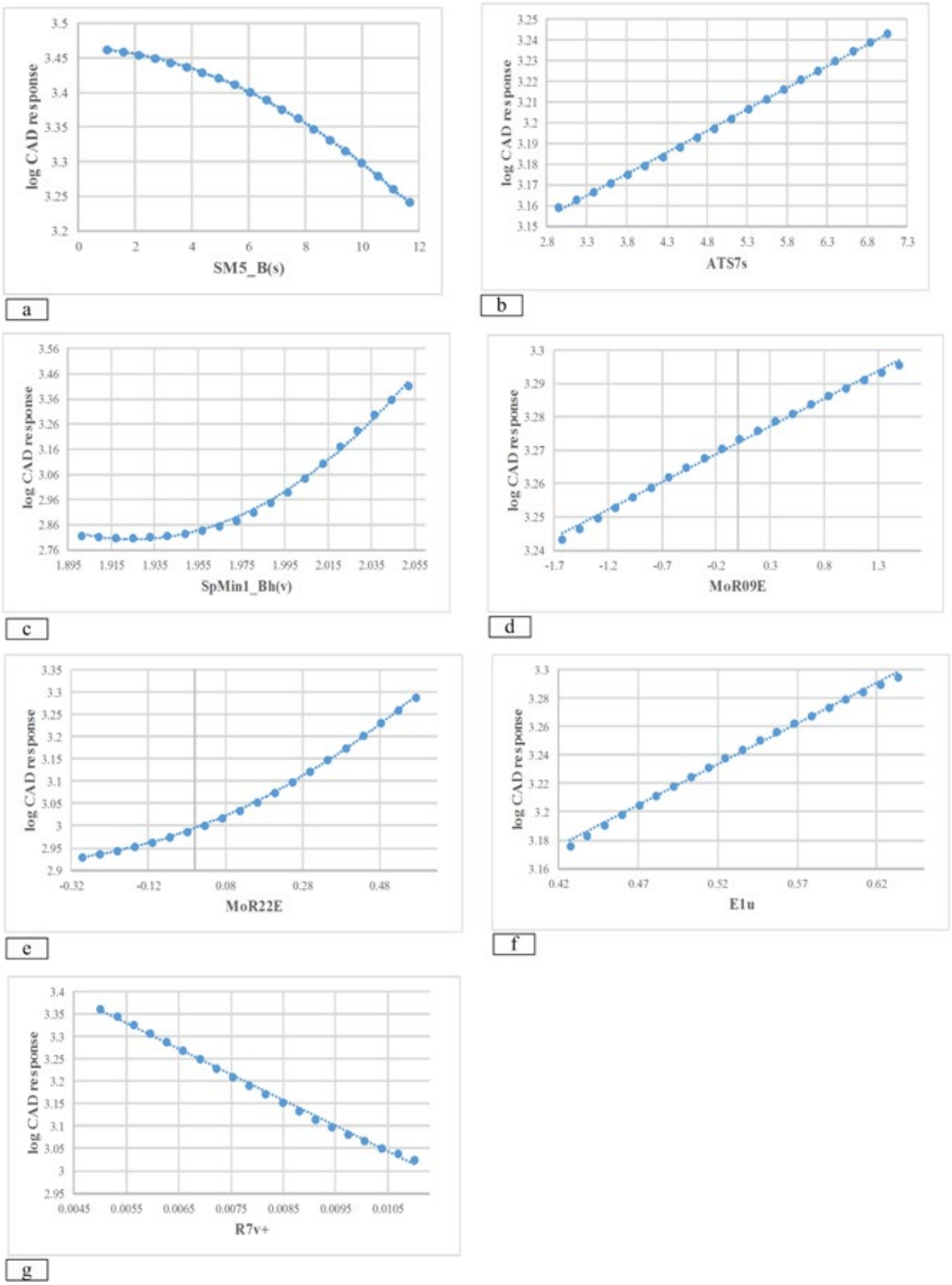

Figure 4 - Response graphs representing the influence of molecular descriptors on CAD response

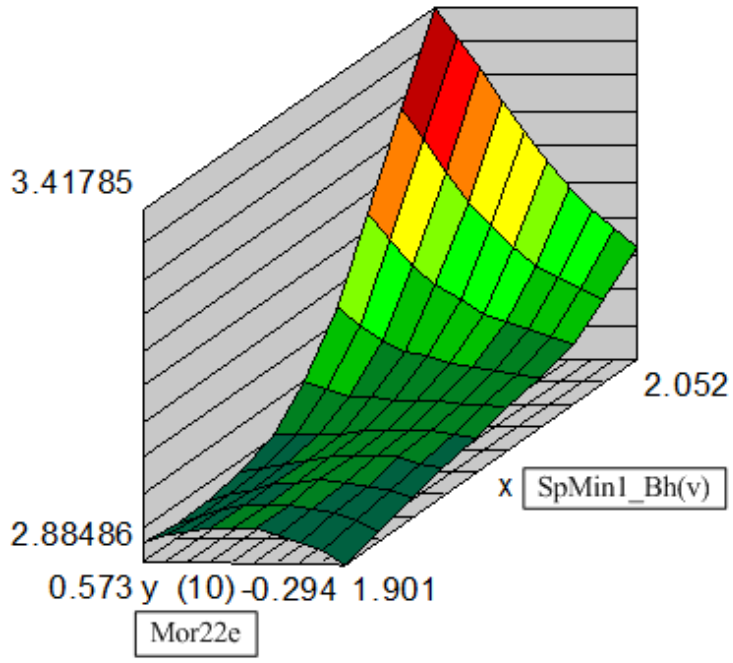

Figure 5 - Response surface plot of CAD response predicted by ANN against SpMin1_Bh (v) and Mor22e

The observed behavior of the response of each analyte linked to the most important instrumental factors is given in Figure 6. For obtaining the individual dependencies of CAD response on the acetone fraction (v/v, %), PFPA concentration (mM) and mobile phase flow rate (mL min^{-1}), each experimental parameter was varied within the defined range, while the other parameters were kept constant at their mean levels. A second-degree polynomial (quadratic) regression appeared to best illustrate the relationship between acetone content or PFPA molarity and the response, while the flow rate followed a linear trend. High R^2 values indicated a very good linear fit of the data.

The CAD response of each analyte showed a positive correlation with PFPA concentration in the mobile phase (Fig 6a). In the previous paper, PFPA played a role as an ion pairing reagent, employed for the purpose of prolonging the retention times of polar, positively charged aminoglycoside antibiotics analyzed under RP-HPLC conditions [12]. The free amino groups of the antibiotics were recognized as their site of interaction with the PFPA additive. Although ion pairing influences the retention mechanism, it was quite important to estimate how it affects CAD responsiveness when varying the PFPA molarity. The measured higher signals can be explained through the combination of the aforementioned molecular descriptors and the ion pairing process increasing the mass of the detected particles. However, an unexpected observation regarding the PFPA molarity was made. More specifically, the slope of the

curve representing the correlation between the PFPA molarity and the sugar molecules' response was steeper than that of the antibiotics (Fig. 6a). This indicated that, besides being ion pairing agent and a modifier that decreases the viscosity of mobile phase, PFPA influenced the CAD response as a chaotropic agent [25, 26]. Namely, it is known that sugars, due to the relatively large number of OH groups which form hydrogen bonds with water, act as kosmotropes and create a solvation shell around the molecule [27, 28]. Due to the chaotropic behavior, PFPA has an ability to jeopardize the generated bonds and disrupt the solvation shell. Consequently, the decreased extent of solvation and the presence of highly evaporative PFPA in the molecule's microenvironment benefit the particle formation efficiency.

Hence, the responses of all solutes increased along with the increase in PFPA molarity. This effect is greater for the sugar molecules due to their higher kosmotropic properties as small polyhydroxy compounds.

An increase of acetone content in the mobile phase correlated with the CAD response in positive manner, as it was the case with the PFPA concentration as well. This result can be explained in the context of evaporation rate and mobile phase viscosity. Namely, the higher organic content results in faster and, consequently, more efficient evaporation of the mobile phase. Moreover, the higher content of organic modifier in the mobile phase leads to the production of droplets of smaller initial diameters that need less evaporation time, compared to bigger droplets that are generated at a lower organic content [3].

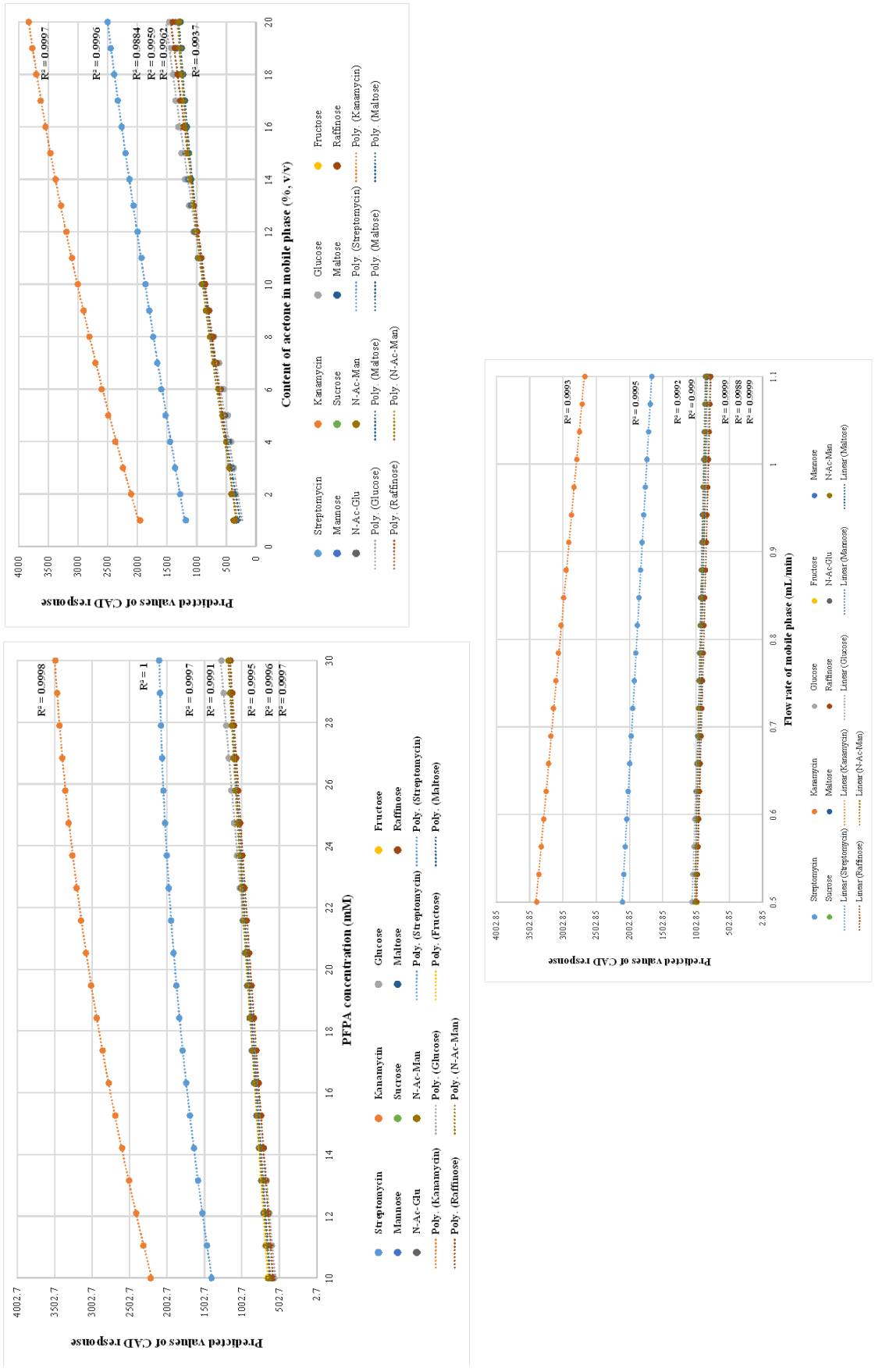

Figure 6 - Effect of chromatographic parameters on CAD response predicted by ANN

6a - Effect of PFPA concentration on CAD response ; **6b** - Effect of acetone content on CAD response ; **6c** - Effect of flow rate on CAD response

Hence, the responses of all solutes increased along with the increase in PFPA molarity. This effect is greater for the sugar molecules due to their higher kosmotropic properties as small polyhydroxy compounds.

An increase of acetone content in the mobile phase correlated with the CAD response in positive manner, as it was the case with the PFPA concentration as well. This result can be explained in the context of evaporation rate and mobile phase viscosity. Namely, the higher organic content results in faster and, consequently, more efficient evaporation of the mobile phase. Moreover, the higher content of organic modifier in the mobile phase leads to the production of droplets of smaller initial diameters that need less evaporation time, compared to bigger droplets that are generated at a lower organic content [3].

The curves constructed for the set of sugars and acetylated amino-sugars had steeper slopes in comparison to the curves of the antibiotics (Fig 6b), which implied that the change in acetone content did not influence their response behavior in the same manner. This observation followed the aforementioned explanation of PFPA's role in the generation of CAD response. A disturbed solvation shell provided more efficient interaction of the molecule with acetone and, hence, an increased response with a higher percentage of acetone. The level of the solvation shell's disturbance was higher when dealing with sugars, independent of their structure, in comparison to the aminoglycoside antibiotics. The favorable character of the PFPA-aided disruption of the primary sheath of water for smaller, more kosmotrope molecules explains their relatively higher contact with acetone and the consequent achievement of higher responses in comparison with larger molecules. For visualization of the influence of acetone content and PFPA concentration on CAD response, the ANN model was utilized to construct 3D response surfaces (Figure 7). Both, PFPA concentration and acetone content, led to an increase in response, while the greatest peak areas were obtained when both parameters were at their maximum levels of the design domain, with acetone having more impact within these ranges. This analysis of joint effects represents a very promising starting point for future investigations on the interaction and influence of different organic modifiers and agents with chaotropic properties on CAD response enhancement when dealing with polar structures.

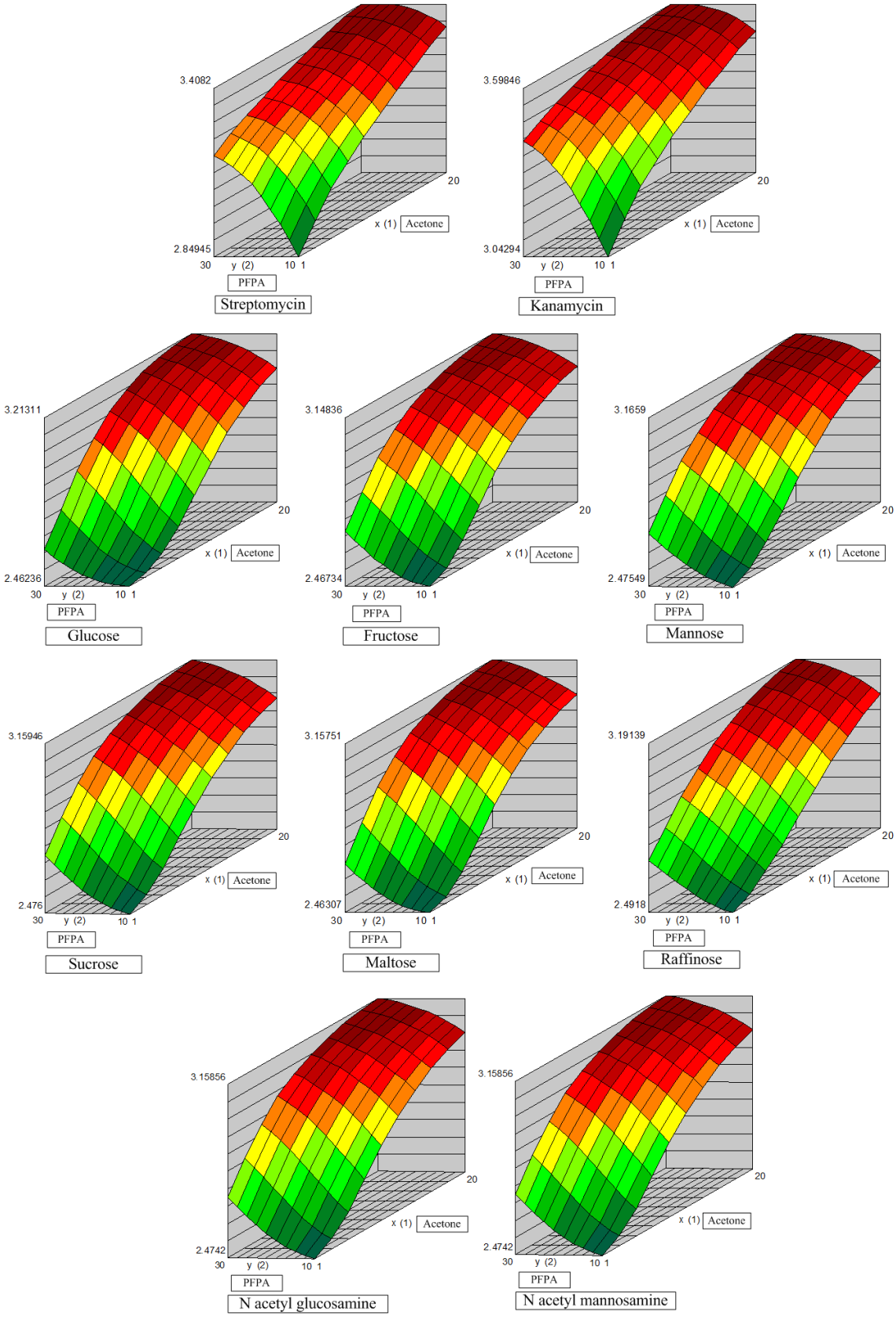

Figure 7 - Response surface plot of log CAD response predicted by ANN against PFPA concentration and acetone content in the mobile phase

Finally, in accordance with the familiar principles of the instrument's functioning, a decrease of CAD response was observed along with an increase in the mobile phase flow rate (Fig. 6c). This correlation was found to be linear within the examined range. The generation of smaller droplets at lower flow rates allows for more efficient evaporation of solvent as well as transfer of charges between gas stream and analyte particles, whereas high flow rates lead to a reduced responsiveness.

Data rate and filter constant, as non-analyte dependent parameters, were excluded from correlation analysis.

4. Conclusions

A mixed QSPR model including molecular descriptors and experimental conditions as independent variables towards CAD response has been successfully developed by means of ANN. The parameters with the most significant influence on the target output were obtained by applying the created model. Among the molecular descriptors, SpMin1_Bh (v) and Mor22e were labeled as the most significant, while slight variations in vapor pressure appeared to be the least influential when dealing with a group of polar, non-volatile analytes. Due to the physicochemical meaning of the SpMin1_Bh (v) descriptor, the surface-dependent nature of the CAD's operating principle was emphasized. In the same manner, namely due to the denotation of the Mor22e molecular descriptor, the CAD response dependency on the number of electronegative atoms that take part in forming short chemical bonds, like oxygen bound within hydroxyl groups, was achieved. The mixed model was externally validated on previously unseen test substances and its ability to predict the CAD response of two new polar compounds was confirmed. Although low RMSE and high R^2 values for the test set confirmed good predictive ability of the network, the limitation of the present study is reflected in the lack of antibiotics in the test data set.

The relationships between chromatographic parameters and CAD response observed indicated the chaotropic characteristics of PFPA to induce the CAD response enhancement along with acetone content. This hints to the exploration of potentially beneficial interactions of evaporative chaotropic reagents with different organic modifiers, especially those with an eco-friendly character, such as ethanol and dimethyl sulfoxide.

Taken together, obtained network showed the potential to predict CAD responsiveness of structurally similar compounds under varied experimental conditions. Thus, it is a helpful tool in purity analytics and analytical chemistry.

Conflict of interest statement

The authors declare that they have no conflict of interest.

Acknowledgements

This work was financially supported by the Ministry of Education and Science of the Republic of Serbia (project no. 172033) and travels were funded by the Bayerische

Forschungsallianz (Munich, Germany). Thanks are due to Oliver Wahl (University of Würzburg) and ThermoFisher Scientific/Dionex Softron (Germering, Germany) for insightful discussions.

References

1. Almeling S, Ilko D, Holzgrabe U. Charged aerosol detection in pharmaceutical analysis. J Pharmaceut Biomed. 2012;69:50-63.

2. Vervoort N, Daemen D, Török G. Performance evaluation of evaporative light scattering detection and charged aerosol detection in reversed phase liquid chromatography. J Chromatogr A. 2008;1189:92-100.

3. Ligor M, Studzińska S, Horna A, Buszewski B. Corona-charged aerosol detection: an analytical approach. Crit Rev Anal Chem. 2013;43:64-78.

4. Vehovec T, Obreza A. Review of operating principle and applications of the charged aerosol detector. J Chromatogr A. 2010;1217:1549-56.

5. Swartz M, Emanuele M, Awad A, Grenier A, Hartley D. An Overview of Corona Charged Aerosol Detection in Pharmaceutical Analysis. Synomics Pharma, White Paper, http://info synomicspharma com/CAD. 2009.

6. Čolović J, Kalinić M, Vemić A, Erić S, Malenović A. Investigation into the phenomena affecting the retention behavior of basic analytes in chaotropic chromatography: Joint effects of the most relevant chromatographic factors and analytes' molecular properties. J Chromatogr A. 2015;1425:150-7.

7. Golubović J, Birkemeyer C, Protić A, Otašević B, Zečević M. Structure–response relationship in electrospray ionization-mass spectrometry of sartans by artificial neural networks. J Chromatogr A. 2016;1438:123-32.

8. Hutchinson JP, Li J, Farrell W, Groeber E, Szucs R, Dicinoski G, et al. Comparison of the response of four aerosol detectors used with ultra high pressure liquid chromatography. J Chromatogr A. 2011;1218:1646-55.

9. Khandagale MM, Hutchinson JP, Dicinoski GW, Haddad PR. Effects of eluent temperature and elution bandwidth on detection response for aerosol-based detectors. J Chromatogr A. 2013;1308:96-103.

10. Robinson MW, Hill AP, Readshaw SA, Hollerton JC, Upton RJ, Lynn SM, et al. Use of Calculated Physicochemical Properties to Enhance Quantitative Response When Using Charged Aerosol Detection. Anal Chem. 2017;89:1772-7.

11. Ragonese R, Macka M, Hughes J, Petocz P. The use of the Box–Behnken experimental design in the optimisation and robustness testing of a capillary electrophoresis method for the analysis of ethambutol hydrochloride in a pharmaceutical formulation. J Pharmaceut Biomed. 2002;27:995-1007.

12. Holzgrabe U, Nap C-J, Kunz N, Almeling S. Identification and control of impurities in streptomycin sulfate by high-performance liquid chromatography coupled with mass detection and corona charged-aerosol detection. J Pharmaceut Biomed. 2011;56:271-9.

13. Todeschini R, Consonni V. Molecular descriptors for chemoinformatics: volume I: alphabetical listing/volume II: appendices, references: John Wiley & Sons, Hoboken; 2009.

14. Todeschini R, Consonni V. Handbook of molecular descriptors: John Wiley & Sons, Hoboken; 2008.

15. Consonni V, Todeschini R, Pavan M. Structure/response correlations and similarity/diversity analysis by GETAWAY descriptors. 1. Theory of the novel 3D molecular descriptors. J Chem Inf Comp Sci. 2002;42:682-92.

16. Singh P, Kumar R, Sharma B, Prabhakar Y. Topological descriptors in modeling malonyl coenzyme A decarboxylase inhibitory activity: N-Alkyl-N-(1, 1, 1, 3, 3, 3-hexafluoro-2-hydroxypropylphenyl) amide derivatives. J Enzym Inhib Med Ch. 2009;24:77-85.

17. Curran-Everett D. Explorations in statistics: the log transformation. Adv Physiol Educ. 2018;42:343-7.

18. Changyong F, Hongyue W, Naiji L, Tian C, Hua H, Ying L. Log-transformation and its implications for data analysis. Shanghai Arch Psychiatry. 2014;26:105.

19. Jayalakshmi T, Santhakumaran A. Statistical normalization and back propagation for classification. International Journal of Computer Theory and Engineering. 2011;3:1793-8201.

20. Lou W, Nakai S. Artificial neural network-based predictive model for bacterial growth in a simulated medium of modified-atmosphere-packed cooked meat products. J Agr Food Chem. 2001;49:1799-804.

21. Israelachvili JN. Intermolecular and surface forces: Academic press; 2011.

22. Dobričić V, Marković B, Nikolic K, Savić V, Vladimirov S, Čudina O. 17β-carboxamide steroids–in vitro prediction of human skin permeability and retention using PAMPA technique. Eur J Pharm Sci. 2014;52:95-108.

23. Mercader AG, Duchowicz PR, Fernández FM, Castro EA, Bennardi DO, Autino JC, et al. QSAR prediction of inhibition of aldose reductase for flavonoids. Bioorgan Med Chem. 2008;16:7470-6.

24. Schuur JH, Selzer P, Gasteiger J. The coding of the three-dimensional structure of molecules by molecular transforms and its application to structure-spectra correlations and studies of biological activity. J Chem Inf Comp Sci. 1996;36:334 44.

25. Schubert B, Oberacher H. Impact of solvent conditions on separation and detection of basic drugs by micro liquid chromatography–mass spectrometry under overloading conditions. J Chromatogr A. 2011;1218:3413-22.

26. Cecchi T. Theoretical models of ion pair chromatography: A close up of recent literature production. J Liq Chromatogr R T. 2015;38:404-14.

27. Magazu S, Migliardo F, Ramirez-Cuesta A. Kosmotrope character of maltose in water mixtures. J Mol Struct. 2007;830:167-70.

28. Shpigelman A, Paz Y, Ramon O, Livney YD. Isomeric sugar effects on thermal phase transition of aqueous PNIPA solutions, probed by ATR-FTIR spectroscopy; insights to protein protection by sugars. Colloid Polym Sci. 2011;289:281-90.

Table S1 - Results of ANN computing and prediction for CAD response

Drug	Acetone content	PFPA	Flow rate	Data rate	Filter constant	Data set	Log CAD response (exp.)	Log CAD response (ANN)	Residuals	Error
Streptomycin	10.5	20	1.1	30	2	Training	3.2433	3.2534	-0.0100	0.0059
Streptomycin	10.5	20	1.1	2	1	Training	3.2238	3.2581	-0.0344	0.0203
Streptomycin	10.5	20	1.1	30	0	Training	3.1969	3.2428	-0.0458	0.0270
Streptomycin	10.5	20	1.1	60	1	Validation	3.2120	3.2441	-0.0321	0.0190
Streptomycin	10.5	20	0.8	30	1	Training	3.2779	3.2906	-0.0127	0.0075
Streptomycin	10.5	20	0.8	2	0	Training	3.2554	3.2961	-0.0408	0.0241
Streptomycin	10.5	20	0.8	60	2	Training	3.2939	3.2809	0.0130	0.0077
Streptomycin	10.5	20	0.8	2	2	Training	3.2904	3.2805	0.0098	0.0058
Streptomycin	10.5	20	0.8	60	0	Validation	3.2507	3.2887	-0.0381	0.0225
Streptomycin	10.5	20	0.8	30	1	Training	3.2779	3.2924	-0.0145	0.0086
Streptomycin	10.5	20	0.5	60	1	Training	3.3254	3.3114	0.0140	0.0083
Streptomycin	10.5	20	0.5	2	1	Training	3.3153	3.3173	-0.0020	0.0012
Streptomycin	10.5	20	0.5	30	2	Training	3.3389	3.3211	0.0177	0.0105
Streptomycin	10.5	20	0.5	30	0	Training	3.3060	3.3551	-0.0491	0.0290
Streptomycin	1	20	1.1	30	1	Training	3.0237	3.0446	-0.0209	0.0124
Streptomycin	1	20	0.8	60	1	Training	3.0682	3.1005	-0.0323	0.0191
Streptomycin	1	20	0.8	2	1	Training	3.0658	3.1031	-0.0373	0.0220
Streptomycin	1	20	0.8	30	0	Validation	3.0696	3.0735	-0.0038	0.0023
Streptomycin	1	20	0.8	30	2	Training	3.0699	3.0831	-0.0132	0.0078
Streptomycin	1	20	0.5	30	1	Training	3.1102	3.1415	-0.0314	0.0185
Streptomycin	10.5	20	0.8	30	1	Training	3.2779	3.3040	-0.0261	0.0154
Streptomycin	20	20	1.1	30	1	Validation	3.3492	3.3246	0.0246	0.0146
Streptomycin	20	20	0.8	2	1	Validation	3.3982	3.3713	0.0269	0.0159
Streptomycin	20	20	0.8	60	1	Training	3.3947	3.3770	0.0177	0.0104
Streptomycin	20	20	0.8	30	0	Validation	3.3740	3.3790	-0.0050	0.0029
Streptomycin	20	20	0.8	30	2	Validation	3.4211	3.3799	0.0412	0.0243
Streptomycin	20	20	0.5	30	1	Training	3.4378	3.4228	0.0149	0.0088
Streptomycin	10.5	20	0.8	30	1	Training	3.2779	3.2837	-0.0058	0.0035
Streptomycin	10.5	10	1.1	30	1	Training	3.0827	3.0768	0.0058	0.0034

Streptomycin	10.5	10	0.8	2	1	Training	3.1421	3.1253	0.0168	0.0099
Streptomycin	10.5	10	0.8	60	1	Validation	3.1446	3.1331	0.0115	0.0068
Streptomycin	10.5	10	0.8	30	2	Training	3.1556	3.1397	0.0160	0.0094
Streptomycin	10.5	10	0.8	30	0	Training	3.1365	3.1417	-0.0052	0.0031
Streptomycin	10.5	10	0.5	30	1	Training	3.2056	3.1992	0.0064	0.0038
Streptomycin	1	10	0.8	30	1	Training	2.8494	2.9320	-0.0826	0.0487
Streptomycin	20	10	0.8	30	1	Training	3.3301	3.2246	0.1063	0.0628
Streptomycin	10.5	20	0.8	30	1	Training	3.2779	3.2461	0.0318	0.0187
Streptomycin	10.5	30	1.1	30	1	Training	3.2782	3.2877	-0.0095	0.0056
Streptomycin	10.5	30	0.8	30	0	Training	3.2980	3.3465	-0.0485	0.0286
Streptomycin	10.5	30	0.8	60	1	Training	3.3203	3.3546	-0.0342	0.0202
Streptomycin	10.5	30	0.8	30	2	Validation	3.3475	3.3606	-0.0131	0.0077
Streptomycin	10.5	30	0.8	2	1	Training	3.3227	3.3552	-0.0326	0.0192
Streptomycin	10.5	30	0.5	30	1	Training	3.3631	3.3981	-0.0349	0.0206
Streptomycin	20	30	0.8	30	1	Validation	3.4069	3.3734	0.0335	0.0198
Streptomycin	1	30	0.8	30	1	Training	3.1853	3.1451	0.0403	0.0238
Streptomycin	10.5	20	0.8	30	1	Validation	3.2779	3.2653	0.0126	0.0074
Kanamycin	10.5	20	1.1	30	2	Validation	3.4469	3.4506	-0.0037	0.0022
Kanamycin	10.5	20	1.1	2	1	Validation	3.4316	3.4573	-0.0258	0.0152
Kanamycin	10.5	20	1.1	30	0	Training	3.4041	3.4429	-0.0388	0.0229
Kanamycin	10.5	20	1.1	60	1	Training	3.4171	3.4390	-0.0219	0.0129
Kanamycin	10.5	20	0.8	30	1	Training	3.4845	3.4954	-0.0109	0.0064
Kanamycin	10.5	20	0.8	2	0	Training	3.4680	3.4978	-0.0298	0.0176
Kanamycin	10.5	20	0.8	60	2	Training	3.4973	3.4829	0.0144	0.0085
Kanamycin	10.5	20	0.8	2	2	Training	3.4993	3.4842	0.0151	0.0089
Kanamycin	10.5	20	0.8	60	0	Training	3.4584	3.4904	-0.0319	0.0189
Kanamycin	10.5	20	0.8	30	1	Training	3.4845	3.4934	-0.0089	0.0053
Kanamycin	10.5	20	0.5	60	1	Validation	3.5300	3.5116	0.0183	0.0108
Kanamycin	10.5	20	0.5	2	1	Validation	3.5273	3.5184	0.0089	0.0053
Kanamycin	10.5	20	0.5	30	2	Training	3.5440	3.5185	0.0255	0.0150
Kanamycin	10.5	20	0.5	30	0	Validation	3.5155	3.5571	-0.0416	0.0246
Kanamycin	1	20	1.1	30	1	Training	3.2314	3.2461	-0.0147	0.0087

Kanamycin	1	20	0.8	60	1	Validation	3.2875	3.3087	-0.0212	0.0125
Kanamycin	1	20	0.8	2	1	Training	3.2860	3.3060	-0.0200	0.0118
Kanamycin	1	20	0.8	30	0	Training	3.2848	3.2817	0.0031	0.0018
Kanamycin	1	20	0.8	30	2	Training	3.2931	3.2947	-0.0016	0.0009
Kanamycin	1	20	0.5	30	1	Training	3.3403	3.3491	-0.0088	0.0052
Kanamycin	10.5	20	0.8	30	1	Training	3.4845	3.4910	-0.0065	0.0038
Kanamycin	20	20	1.1	30	1	Training	3.5361	3.4783	0.0578	0.0341
Kanamycin	20	20	0.8	2	1	Training	3.5860	3.5307	0.0553	0.0327
Kanamycin	20	20	0.8	60	1	Training	3.5774	3.5349	0.0425	0.0251
Kanamycin	20	20	0.8	30	0	Training	3.5624	3.5356	0.0269	0.0159
Kanamycin	20	20	0.8	30	2	Training	3.6017	4.1391	-0.5374	0.3172
Kanamycin	20	20	0.5	30	1	Training	3.6194	3.5804	0.0390	0.0230
Kanamycin	10.5	20	0.8	30	1	Validation	3.4845	3.4653	0.0192	0.0113
Kanamycin	10.5	10	1.1	30	1	Validation	3.2821	3.2705	0.0116	0.0068
Kanamycin	10.5	10	0.8	2	1	Training	3.3416	3.3175	0.0241	0.0142
Kanamycin	10.5	10	0.8	60	1	Training	3.3443	3.3236	0.0207	0.0122
Kanamycin	10.5	10	0.8	30	2	Training	3.3559	3.3279	0.0280	0.0165
Kanamycin	10.5	10	0.8	30	0	Training	3.3338	3.3286	0.0052	0.0031
Kanamycin	10.5	10	0.5	30	1	Training	3.4060	3.3953	0.0107	0.0063
Kanamycin	1	10	0.8	30	1	Validation	3.0429	3.1210	-0.0781	0.0461
Kanamycin	20	10	0.8	30	1	Training	3.5092	3.3865	0.1227	0.0725
Kanamycin	10.5	20	0.8	30	1	Training	3.4845	3.4311	0.0534	0.0315
Kanamycin	10.5	30	1.1	30	1	Training	3.5013	3.4680	0.0333	0.0197
Kanamycin	10.5	30	0.8	30	0	Training	3.5225	3.5324	-0.0099	0.0058
Kanamycin	10.5	30	0.8	60	1	Training	3.5394	3.5404	-0.0010	0.0006
Kanamycin	10.5	30	0.8	30	2	Training	3.5622	3.5456	0.0166	0.0098
Kanamycin	10.5	30	0.8	2	1	Validation	3.5446	3.5400	0.0046	0.0027
Kanamycin	10.5	30	0.5	30	1	Validation	3.5777	3.5802	-0.0025	0.0015
Kanamycin	20	30	0.8	30	1	Training	3.5981	3.5174	0.0807	0.0476
Kanamycin	10.5	20	0.8	30	1	Training	3.4845	3.4380	0.0465	0.0275
Glucose	10.5	20	1.1	30	2	Test	2.9096	2.9645	-0.0550	0.0325
Glucose	10.5	20	1.1	2	1	Test	2.9174	2.9486	-0.0311	0.0184

Glucose	10.5	20	1.1	30	0	Test	2.8930	2.9486	-0.0556	0.0328
Glucose	10.5	20	1.1	60	1	Test	2.8813	2.9408	-0.0596	0.0352
Glucose	10.5	20	0.8	30	1	Test	2.9681	2.9849	-0.0168	0.0099
Glucose	10.5	20	0.8	2	0	Test	2.9726	2.9588	0.0139	0.0082
Glucose	10.5	20	0.8	2	2	Test	2.9869	2.9851	0.0018	0.0011
Glucose	10.5	20	0.8	60	0	Test	2.9416	2.9653	-0.0237	0.0140
Glucose	10.5	20	0.8	30	1	Test	2.9681	2.9696	-0.0015	0.0009
Glucose	10.5	20	0.5	60	1	Test	3.0124	3.0286	-0.0161	0.0095
Glucose	10.5	20	0.5	2	1	Test	3.0357	3.0186	0.0171	0.0101
Glucose	10.5	20	0.5	30	2	Test	3.0325	3.0168	0.0157	0.0093
Glucose	10.5	20	0.5	30	0	Test	3.0201	3.0103	0.0098	0.0058
Glucose	1	20	1.1	30	1	Test	2.4904	2.5254	-0.0350	0.0206
Glucose	1	20	0.8	60	1	Test	2.5007	2.5351	-0.0344	0.0203
Glucose	1	20	0.8	2	1	Test	2.5104	2.5467	-0.0363	0.0214
Glucose	1	20	0.8	30	0	Test	2.5079	2.5449	-0.0370	0.0219
Glucose	1	20	0.8	30	2	Test	2.5042	2.5503	-0.0460	0.0272
Glucose	1	20	0.5	30	1	Test	2.5261	2.5820	-0.0559	0.0330
Glucose	10.5	20	0.8	30	1	Test	2.9681	2.9790	-0.0109	0.0064
Glucose	20	20	1.1	30	1	Test	3.1248	3.0901	0.0347	0.0205
Glucose	20	20	0.8	2	1	Test	3.1723	3.1256	0.0467	0.0276
Glucose	20	20	0.8	60	1	Test	3.1540	3.1299	0.0240	0.0142
Glucose	20	20	0.8	30	0	Test	3.1556	3.1388	0.0169	0.0099
Glucose	20	20	0.8	30	2	Test	3.1733	3.1368	0.0364	0.0215
Glucose	20	20	0.5	30	1	Test	3.1971	3.1975	-0.0004	0.0002
Glucose	10.5	20	0.8	30	1	Test	2.9681	2.9657	0.0025	0.0014
Glucose	10.5	10	1.1	30	1	Test	2.6972	2.7858	-0.0886	0.0523
Glucose	10.5	10	0.8	2	1	Test	2.7676	2.8197	-0.0521	0.0308
Glucose	10.5	10	0.8	60	1	Test	2.7394	2.8206	-0.0812	0.0479
Glucose	10.5	10	0.8	30	2	Test	2.7567	2.8159	-0.0592	0.0350
Glucose	10.5	10	0.8	30	0	Test	2.7542	2.8147	-0.0605	0.0357
Glucose	10.5	10	0.5	30	1	Test	2.8201	2.8685	-0.0484	0.0286
Glucose	1	10	0.8	30	1	Test	2.4624	2.4709	-0.0085	0.0050

Glucose	20	10	0.8	30	1	Test	3.0587	3.0002	0.0585	0.0345
Glucose	10.5	20	0.8	30	1	Test	2.9681	2.9857	-0.0176	0.0104
Glucose	10.5	30	1.1	30	1	Test	3.0604	3.0283	0.0322	0.0190
Glucose	10.5	30	0.8	30	0	Test	3.0954	3.0792	0.0162	0.0096
Glucose	10.5	30	0.8	60	1	Test	3.0940	3.0601	0.0339	0.0200
Glucose	10.5	30	0.8	30	2	Test	3.1140	3.0761	0.0378	0.0223
Glucose	10.5	30	0.8	2	1	Test	3.1126	3.0653	0.0473	0.0280
Glucose	10.5	30	0.5	30	1	Test	3.1420	3.1254	0.0165	0.0098
Glucose	20	30	0.8	30	1	Test	3.2131	3.1642	0.0489	0.0289
Glucose	1	30	0.8	30	1	Test	2.6305	2.7616	-0.1311	0.0774
Glucose	10.5	20	0.8	30	1	Test	2.9681	2.9713	-0.0032	0.0019
Fructose	10.5	20	1.1	30	2	Validation	2.9367	2.9531	-0.0164	0.0097
Fructose	10.5	20	1.1	2	1	Training	2.9394	2.9419	-0.0026	0.0015
Fructose	10.5	20	1.1	30	0	Training	2.9360	2.9374	-0.0014	0.0008
Fructose	10.5	20	1.1	60	1	Validation	2.9317	2.9237	0.0079	0.0047
Fructose	10.5	20	0.8	30	1	Validation	2.9684	2.9742	-0.0058	0.0034
Fructose	10.5	20	0.8	2	0	Training	2.9699	2.9482	0.0218	0.0129
Fructose	10.5	20	0.8	60	2	Training	2.9638	2.9581	0.0058	0.0034
Fructose	10.5	20	0.8	2	2	Training	2.9654	2.9613	0.0040	0.0024
Fructose	10.5	20	0.8	60	0	Training	2.9656	2.9552	0.0104	0.0061
Fructose	10.5	20	0.8	30	1	Training	2.9684	2.9566	0.0118	0.0070
Fructose	10.5	20	0.5	60	1	Training	2.9926	3.0194	-0.0268	0.0158
Fructose	10.5	20	0.5	30	2	Validation	2.9891	3.0046	-0.0155	0.0091
Fructose	10.5	20	0.5	2	1	Validation	2.9903	3.0048	-0.0146	0.0086
Fructose	10.5	20	0.5	30	0	Training	2.9957	2.9993	-0.0036	0.0021
Fructose	1	20	1.1	30	1	Training	2.5180	2.5163	0.0017	0.0010
Fructose	1	20	0.8	60	1	Training	2.5382	2.5250	0.0132	0.0078
Fructose	1	20	0.8	2	1	Training	2.5402	2.5356	0.0046	0.0027
Fructose	1	20	0.8	30	0	Training	2.5430	2.5378	0.0052	0.0031
Fructose	1	20	0.8	30	2	Training	2.5367	2.5380	-0.0014	0.0008
Fructose	1	20	0.5	30	1	Training	2.5644	2.5716	-0.0072	0.0043
Fructose	10.5	20	0.8	30	1	Training	2.9684	2.9664	0.0020	0.0012

Fructose	20	20	1.1	30	1	Training	3.0830	3.0766	0.0064	0.0038
Fructose	20	20	0.8	2	1	Training	3.1040	3.1158	-0.0118	0.0070
Fructose	20	20	0.8	60	1	Training	3.0999	3.1224	-0.0224	0.0132
Fructose	20	20	0.8	30	0	Training	3.1026	3.1300	-0.0274	0.0162
Fructose	20	20	0.8	30	2	Training	3.1026	3.1284	-0.0257	0.0152
Fructose	20	20	0.5	30	1	Validation	3.1174	3.1843	-0.0669	0.0395
Fructose	10.5	20	0.8	30	1	Training	2.9684	2.9526	0.0158	0.0093
Fructose	10.5	10	1.1	30	1	Validation	2.7831	2.7732	0.0099	0.0059
Fructose	10.5	10	0.8	2	1	Training	2.8204	2.8076	0.0128	0.0076
Fructose	10.5	10	0.8	60	1	Validation	2.8164	2.8081	0.0083	0.0049
Fructose	10.5	10	0.8	30	2	Training	2.8154	2.8028	0.0127	0.0075
Fructose	10.5	10	0.8	30	0	Training	2.8235	2.8025	0.0210	0.0124
Fructose	10.5	10	0.5	30	1	Validation	2.8544	2.8546	-0.0002	0.0001
Fructose	1	10	0.8	30	1	Training	2.4673	2.4607	0.0066	0.0039
Fructose	20	10	0.8	30	1	Training	3.0171	2.9906	0.0265	0.0156
Fructose	10.5	20	0.8	30	1	Training	2.9684	2.9698	-0.0013	0.0008
Fructose	10.5	30	1.1	30	1	Validation	3.0445	3.0191	0.0253	0.0150
Fructose	10.5	30	0.8	30	0	Training	3.0629	3.0703	-0.0073	0.0043
Fructose	10.5	30	0.8	60	1	Validation	3.0616	3.0484	0.0132	0.0078
Fructose	10.5	30	0.8	30	2	Training	3.0617	3.0655	-0.0038	0.0023
Fructose	10.5	30	0.8	2	1	Training	3.0620	3.0561	0.0058	0.0034
Fructose	10.5	30	0.5	30	1	Training	3.0761	3.1135	-0.0374	0.0221
Fructose	20	30	0.8	30	1	Validation	3.1484	3.1518	-0.0034	0.0020
Fructose	1	30	0.8	30	1	Validation	2.6891	2.7415	-0.0524	0.0309
Fructose	10.5	20	0.8	30	1	Training	2.9684	2.9603	0.0081	0.0048
Mannose	10.5	20	1.1	30	2	Training	2.9379	2.9595	-0.0216	0.0127
Mannose	10.5	20	1.1	2	1	Validation	2.9401	2.9481	-0.0080	0.0047
Mannose	10.5	20	1.1	30	0	Training	2.9296	2.9413	-0.0116	0.0069
Mannose	10.5	20	1.1	60	1	Training	2.9251	2.9344	-0.0094	0.0055
Mannose	10.5	20	0.8	30	1	Training	2.9758	2.9790	-0.0032	0.0019
Mannose	10.5	20	0.8	2	0	Training	2.9758	2.9507	0.0251	0.0148
Mannose	10.5	20	0.8	60	2	Training	2.9702	2.9624	0.0077	0.0046

Mannose	10.5	20	0.8	2	2	Validation	2.9802	2.9656	0.0146	0.0086
Mannose	10.5	20	0.8	60	0	Validation	2.9655	2.9590	0.0065	0.0038
Mannose	10.5	20	0.8	30	1	Training	2.9758	2.9614	0.0144	0.0085
Mannose	10.5	20	0.5	60	1	Training	3.0047	3.0245	-0.0198	0.0117
Mannose	10.5	20	0.5	2	1	Training	3.0098	3.0117	-0.0019	0.0011
Mannose	10.5	20	0.5	30	2	Training	3.0092	3.0141	-0.0049	0.0029
Mannose	10.5	20	0.5	30	0	Validation	3.0078	3.0059	0.0019	0.0011
Mannose	1	20	1.1	30	1	Training	2.5304	2.5197	0.0107	0.0063
Mannose	1	20	0.8	60	1	Training	2.5459	2.5322	0.0137	0.0081
Mannose	1	20	0.8	2	1	Training	2.5558	2.5375	0.0184	0.0108
Mannose	1	20	0.8	30	0	Training	2.5562	2.5423	0.0138	0.0082
Mannose	1	20	0.8	30	2	Validation	2.5474	2.5428	0.0046	0.0027
Mannose	1	20	0.5	30	1	Training	2.5760	2.5761	-0.0001	0.0001
Mannose	10.5	20	0.8	30	1	Training	2.9758	2.9743	0.0015	0.0009
Mannose	20	20	1.1	30	1	Training	3.1107	3.0838	0.0268	0.0158
Mannose	20	20	0.8	2	1	Training	3.1332	3.1175	0.0158	0.0093
Mannose	20	20	0.8	60	1	Validation	3.1278	3.1273	0.0005	0.0003
Mannose	20	20	0.8	30	0	Training	3.1285	3.1343	-0.0058	0.0034
Mannose	20	20	0.8	30	2	Validation	3.1339	3.1335	0.0003	0.0002
Mannose	20	20	0.5	30	1	Validation	3.1471	3.1874	-0.0404	0.0238
Mannose	10.5	20	0.8	30	1	Training	2.9758	2.9613	0.0145	0.0086
Mannose	10.5	10	1.1	30	1	Training	2.7606	2.7785	-0.0179	0.0105
Mannose	10.5	10	0.8	2	1	Training	2.8179	2.8120	0.0059	0.0035
Mannose	10.5	10	0.8	60	1	Validation	2.8009	2.8147	-0.0137	0.0081
Mannose	10.5	10	0.8	30	2	Validation	2.8097	2.8096	0.0001	0.0001
Mannose	10.5	10	0.8	30	0	Training	2.8126	2.8088	0.0037	0.0022
Mannose	10.5	10	0.5	30	1	Training	2.8596	2.8603	-0.0006	0.0004
Mannose	1	10	0.8	30	1	Validation	2.4755	2.4626	0.0129	0.0076
Mannose	20	10	0.8	30	1	Training	3.0560	2.9965	0.0596	0.0352
Mannose	10.5	30	1.1	30	1	Training	3.0452	3.0240	0.0213	0.0126
Mannose	10.5	30	0.8	30	0	Training	3.0666	3.0759	-0.0093	0.0055
Mannose	10.5	30	0.8	60	1	Training	3.0676	3.0534	0.0142	0.0084

Mannose	10.5	30	0.8	30	2	Training	3.0739	3.0701	0.0038	0.0022
Mannose	10.5	30	0.8	2	1	Training	3.0717	3.0590	0.0127	0.0075
Mannose	10.5	30	0.5	30	1	Training	3.0912	3.1159	-0.0247	0.0146
Mannose	20	30	0.8	30	1	Training	3.1659	3.1575	0.0084	0.0050
Mannose	1	30	0.8	30	1	Training	2.6951	2.7455	-0.0505	0.0298
Mannose	10.5	20	0.8	30	1	Validation	2.9758	2.9676	0.0081	0.0048
Sucrose	10.5	20	1.1	30	2	Validation	2.9199	2.9513	-0.0314	0.0185
Sucrose	10.5	20	1.1	2	1	Training	2.9140	2.9386	-0.0246	0.0145
Sucrose	10.5	20	1.1	30	0	Validation	2.9028	2.9324	-0.0297	0.0175
Sucrose	10.5	20	1.1	60	1	Training	2.9064	2.9238	-0.0174	0.0103
Sucrose	10.5	20	0.8	30	1	Validation	2.9615	2.9720	-0.0105	0.0062
Sucrose	10.5	20	0.8	2	0	Training	2.9548	2.9417	0.0132	0.0078
Sucrose	10.5	20	0.8	60	2	Training	2.9656	2.9529	0.0127	0.0075
Sucrose	10.5	20	0.8	2	2	Training	2.9660	2.9559	0.0101	0.0060
Sucrose	10.5	20	0.8	60	0	Training	2.9500	2.9559	-0.0059	0.0035
Sucrose	10.5	20	0.8	30	1	Training	2.9615	2.9532	0.0083	0.0049
Sucrose	10.5	20	0.5	60	1	Training	3.0037	3.0169	-0.0133	0.0078
Sucrose	10.5	20	0.5	2	1	Validation	3.0001	3.0018	-0.0018	0.0010
Sucrose	10.5	20	0.5	30	2	Training	3.0080	3.0046	0.0034	0.0020
Sucrose	10.5	20	0.5	30	0	Training	2.9984	2.9962	0.0021	0.0013
Sucrose	1	20	1.1	30	1	Training	2.5286	2.5084	0.0201	0.0119
Sucrose	1	20	0.8	60	1	Training	2.5553	2.5272	0.0280	0.0166
Sucrose	1	20	0.8	2	1	Training	2.5537	2.5301	0.0236	0.0140
Sucrose	1	20	0.8	30	0	Training	2.5549	2.5316	0.0232	0.0137
Sucrose	1	20	0.8	30	2	Training	2.5558	2.5336	0.0221	0.0131
Sucrose	1	20	0.5	30	1	Training	2.5878	2.5691	0.0187	0.0111
Sucrose	10.5	20	0.8	30	1	Training	2.9615	2.9644	-0.0029	0.0017
Sucrose	20	20	1.1	30	1	Training	3.0734	3.0709	0.0025	0.0015
Sucrose	20	20	0.8	2	1	Training	3.1068	3.1054	0.0014	0.0008
Sucrose	20	20	0.8	60	1	Training	3.1005	3.1174	-0.0169	0.0100
Sucrose	20	20	0.8	30	0	Training	3.0998	3.1291	-0.0293	0.0173
Sucrose	20	20	0.8	30	2	Training	3.1093	3.1217	-0.0124	0.0073

Sucrose	20	20	0.5	30	1	Validation	3.1295	3.1783	-0.0488	0.0288
Sucrose	10.5	20	0.8	30	1	Validation	2.9615	2.9481	0.0134	0.0079
Sucrose	10.5	10	1.1	30	1	Training	2.7479	2.7683	-0.0204	0.0120
Sucrose	10.5	10	0.8	2	1	Training	2.7938	2.8017	-0.0080	0.0047
Sucrose	10.5	10	0.8	60	1	Training	2.7957	2.8027	-0.0070	0.0042
Sucrose	10.5	10	0.8	30	2	Validation	2.8002	2.7975	0.0026	0.0016
Sucrose	10.5	10	0.8	30	0	Training	2.7919	2.7979	-0.0060	0.0035
Sucrose	10.5	10	0.5	30	1	Training	2.8461	2.8526	-0.0065	0.0039
Sucrose	1	10	0.8	30	1	Training	2.4760	2.4494	0.0266	0.0157
Sucrose	20	10	0.8	30	1	Training	3.0052	2.9838	0.0214	0.0126
Sucrose	10.5	20	0.8	30	1	Training	2.9615	2.9672	-0.0057	0.0033
Sucrose	10.5	30	1.1	30	1	Training	3.0395	3.0092	0.0303	0.0179
Sucrose	10.5	30	0.8	30	0	Validation	3.0659	3.0629	0.0030	0.0017
Sucrose	10.5	30	0.8	60	1	Validation	3.0706	3.0382	0.0324	0.0191
Sucrose	10.5	30	0.8	30	2	Validation	3.0780	3.0576	0.0205	0.0121
Sucrose	10.5	30	0.8	2	1	Training	3.0718	3.0471	0.0247	0.0146
Sucrose	10.5	30	0.5	30	1	Validation	3.0980	3.1072	-0.0092	0.0054
Sucrose	20	30	0.8	30	1	Training	3.1595	3.1452	0.0142	0.0084
Sucrose	1	30	0.8	30	1	Training	2.7123	2.7369	-0.0247	0.0146
Sucrose	10.5	20	0.8	30	1	Validation	2.9615	2.9554	0.0061	0.0036
Maltose	10.5	20	1.1	30	2	Training	2.9247	2.9512	-0.0266	0.0157
Maltose	10.5	20	1.1	2	1	Training	2.9230	2.9352	-0.0123	0.0072
Maltose	10.5	20	1.1	30	0	Training	2.9164	2.9309	-0.0146	0.0086
Maltose	10.5	20	1.1	60	1	Training	2.9160	2.9247	-0.0087	0.0051
Maltose	10.5	20	0.8	30	1	Training	2.9623	2.9721	-0.0098	0.0058
Maltose	10.5	20	0.8	2	0	Training	2.9596	2.9440	0.0156	0.0092
Maltose	10.5	20	0.8	60	2	Training	2.9621	2.9546	0.0075	0.0044
Maltose	10.5	20	0.8	2	2	Validation	2.9619	2.9550	0.0069	0.0041
Maltose	10.5	20	0.8	60	0	Training	2.9557	2.9480	0.0077	0.0046
Maltose	10.5	20	0.8	30	1	Training	2.9623	2.9534	0.0089	0.0052
Maltose	10.5	20	0.5	60	1	Training	2.9965	3.0162	-0.0197	0.0117
Maltose	10.5	20	0.5	2	1	Validation	2.9922	3.0044	-0.0122	0.0072

Maltose	10.5	20	0.5	30	2	Validation	2.9958	3.0046	-0.0087	0.0052
Maltose	10.5	20	0.5	30	0	Training	2.9953	2.9955	-0.0002	0.0001
Maltose	1	20	1.1	30	1	Validation	2.5015	2.5024	-0.0009	0.0005
Maltose	1	20	0.8	60	1	Training	2.5210	2.5182	0.0028	0.0017
Maltose	1	20	0.8	2	1	Training	2.5204	2.5242	-0.0039	0.0023
Maltose	1	20	0.8	30	0	Training	2.5224	2.5281	-0.0057	0.0033
Maltose	1	20	0.8	30	2	Training	2.5201	2.5323	-0.0122	0.0072
Maltose	1	20	0.5	30	1	Training	2.5456	2.5625	-0.0168	0.0099
Maltose	10.5	20	0.8	30	1	Training	2.9623	2.9608	0.0015	0.0009
Maltose	20	20	1.1	30	1	Training	3.0794	3.0710	0.0084	0.0050
Maltose	20	20	0.8	2	1	Training	3.1070	3.1042	0.0029	0.0017
Maltose	20	20	0.8	60	1	Training	3.1022	3.1181	-0.0158	0.0093
Maltose	20	20	0.8	30	0	Training	3.1031	3.1283	-0.0252	0.0149
Maltose	20	20	0.8	30	2	Training	3.1079	3.1206	-0.0127	0.0075
Maltose	20	20	0.5	30	1	Validation	3.1259	3.1775	-0.0515	0.0304
Maltose	10.5	20	0.8	30	1	Training	2.9623	2.9505	0.0118	0.0069
Maltose	10.5	10	1.1	30	1	Training	2.7563	2.7683	-0.0120	0.0071
Maltose	10.5	10	0.8	2	1	Training	2.7971	2.7993	-0.0022	0.0013
Maltose	10.5	10	0.8	60	1	Training	2.7978	2.8023	-0.0045	0.0027
Maltose	10.5	10	0.8	30	2	Validation	2.7981	2.7979	0.0002	0.0001
Maltose	10.5	10	0.8	30	0	Validation	2.7991	2.7966	0.0025	0.0015
Maltose	10.5	10	0.5	30	1	Validation	2.8413	2.8507	-0.0094	0.0055
Maltose	1	10	0.8	30	1	Training	2.4631	2.4456	0.0175	0.0103
Maltose	20	10	0.8	30	1	Training	3.0109	2.9870	0.0239	0.0141
Maltose	10.5	20	0.8	30	1	Validation	2.9623	2.9690	-0.0067	0.0039
Maltose	10.5	30	1.1	30	1	Training	3.0435	3.0102	0.0332	0.0196
Maltose	10.5	30	0.8	30	0	Validation	3.0664	3.0596	0.0068	0.0040
Maltose	10.5	30	0.8	60	1	Validation	3.0681	3.0432	0.0249	0.0147
Maltose	10.5	30	0.8	30	2	Training	3.0715	3.0606	0.0109	0.0064
Maltose	10.5	30	0.8	2	1	Training	3.0684	3.0503	0.0181	0.0107
Maltose	10.5	30	0.5	30	1	Validation	3.0890	3.1091	-0.0201	0.0119
Maltose	20	30	0.8	30	1	Training	3.1575	3.1459	0.0116	0.0069

Maltose	1	30	0.8	30	1	Training	2.6656	2.7326	-0.0669	0.0395
Maltose	10.5	20	0.8	30	1	Training	2.9623	2.9578	0.0045	0.0027
Raffinose	10.5	20	1.1	30	2	Training	2.9051	2.9473	-0.0422	0.0249
Raffinose	10.5	20	1.1	2	1	Validation	2.8920	2.9330	-0.0411	0.0243
Raffinose	10.5	20	1.1	30	0	Training	2.8799	2.9298	-0.0499	0.0295
Raffinose	10.5	20	1.1	60	1	Training	2.8890	2.9214	-0.0323	0.0191
Raffinose	10.5	20	0.8	30	1	Validation	2.9492	2.9716	-0.0224	0.0132
Raffinose	10.5	20	0.8	2	0	Training	2.9335	2.9440	-0.0105	0.0062
Raffinose	10.5	20	0.8	60	2	Validation	2.9605	2.9511	0.0094	0.0055
Raffinose	10.5	20	0.8	2	2	Validation	2.9515	2.9550	-0.0035	0.0021
Raffinose	10.5	20	0.8	60	0	Training	2.9359	2.9549	-0.0190	0.0112
Raffinose	10.5	20	0.8	30	1	Training	2.9492	2.9530	-0.0038	0.0023
Raffinose	10.5	20	0.5	60	1	Validation	3.0019	3.0165	-0.0147	0.0087
Raffinose	10.5	20	0.5	2	1	Training	2.9869	3.0055	-0.0185	0.0109
Raffinose	10.5	20	0.5	30	2	Training	3.0051	3.0042	0.0009	0.0005
Raffinose	10.5	20	0.5	30	0	Training	2.9878	2.9971	-0.0092	0.0054
Raffinose	1	20	1.1	30	1	Training	2.5543	2.5040	0.0503	0.0297
Raffinose	1	20	0.8	60	1	Training	2.5782	2.5217	0.0565	0.0333
Raffinose	1	20	0.8	2	1	Training	2.5748	2.5290	0.0458	0.0270
Raffinose	1	20	0.8	30	0	Training	2.5795	2.5296	0.0499	0.0295
Raffinose	1	20	0.8	30	2	Training	2.5759	2.5328	0.0431	0.0254
Raffinose	1	20	0.5	30	1	Training	2.6034	2.5633	0.0401	0.0237
Raffinose	10.5	20	0.8	30	1	Training	2.9492	2.9605	-0.0114	0.0067
Raffinose	20	20	1.1	30	1	Validation	3.1110	3.0699	0.0411	0.0242
Raffinose	20	20	0.8	2	1	Training	3.1452	3.1049	0.0403	0.0238
Raffinose	20	20	0.8	60	1	Training	3.1456	3.1186	0.0270	0.0159
Raffinose	20	20	0.8	30	0	Validation	3.1371	3.1296	0.0075	0.0044
Raffinose	20	20	0.8	30	2	Training	3.1562	3.1229	0.0333	0.0197
Raffinose	20	20	0.5	30	1	Validation	3.1748	3.1745	0.0004	0.0002
Raffinose	10.5	20	0.8	30	1	Training	2.9492	2.9504	-0.0012	0.0007
Raffinose	10.5	10	1.1	30	1	Training	2.7210	2.7641	-0.0431	0.0254
Raffinose	10.5	10	0.8	2	1	Training	2.7671	2.7988	-0.0317	0.0187

Raffinose	10.5	10	0.8	60	1	Training	2.7738	2.8009	-0.0271	0.0160
Raffinose	10.5	10	0.8	30	2	Training	2.7766	2.7956	-0.0190	0.0112
Raffinose	10.5	10	0.8	30	0	Training	2.7682	2.7973	-0.0291	0.0172
Raffinose	10.5	10	0.5	30	1	Training	2.8267	2.8500	-0.0232	0.0137
Raffinose	1	10	0.8	30	1	Training	2.4918	2.4450	0.0468	0.0276
Raffinose	20	10	0.8	30	1	Training	3.0462	2.9877	0.0586	0.0346
Raffinose	10.5	20	0.8	30	1	Training	2.9492	2.9673	-0.0182	0.0107
Raffinose	10.5	30	1.1	30	1	Training	3.0207	3.0117	0.0090	0.0053
Raffinose	10.5	30	0.8	30	0	Training	3.0492	3.0556	-0.0064	0.0038
Raffinose	10.5	30	0.8	60	1	Training	3.0626	3.0441	0.0184	0.0109
Raffinose	10.5	30	0.8	30	2	Training	3.0741	3.0607	0.0133	0.0079
Raffinose	10.5	30	0.8	2	1	Training	3.0581	3.0481	0.0100	0.0059
Raffinose	10.5	30	0.5	30	1	Training	3.0967	3.1078	-0.0111	0.0065
Raffinose	20	30	0.8	30	1	Training	3.1914	3.1477	0.0437	0.0258
Raffinose	1	30	0.8	30	1	Validation	2.7082	2.7295	-0.0213	0.0126
Raffinose	10.5	20	0.8	30	1	Training	2.9492	2.9560	-0.0068	0.0040
N-Ac D glucosa-mine	10.5	20	1.1	30	2	Test	2.9337	2.9755	-0.0418	0.0247
N-Ac D glucosa-mine	10.5	20	1.1	2	1	Test	2.9315	2.9600	-0.0285	0.0168
N-Ac D glucosa-mine	10.5	20	1.1	30	0	Test	2.9236	2.9596	-0.0360	0.0212
N-Ac D glucosa-mine	10.5	20	1.1	60	1	Test	2.9236	2.9513	-0.0278	0.0164
N-Ac D glucosa-mine	10.5	20	0.8	30	1	Test	2.9717	2.9904	-0.0187	0.0111
N-Ac D glucosa-mine	10.5	20	0.8	2	0	Test	2.9680	2.9751	-0.0071	0.0042
N-Ac D glucosa-mine	10.5	20	0.8	60	0	Test	2.9641	2.9789	-0.0148	0.0087
N-Ac D glucosa-mine	10.5	20	0.8	30	1	Test	2.9717	2.9814	-0.0097	0.0057

N-Ac D glucosamine	10.5	20	0.5	60	1	Test	3.0057	3.0391	-0.0333	0.0197
N-Ac D glucosamine	10.5	20	0.5	2	1	Test	3.0017	3.0308	-0.0291	0.0172
N-Ac D glucosamine	10.5	20	0.5	30	2	Test	3.0059	3.0331	-0.0272	0.0161
N-Ac D glucosamine	10.5	20	0.5	30	0	Test	3.0041	3.0246	-0.0205	0.0121
N-Ac D glucosamine	1	20	1.1	30	1	Test	2.5316	2.5386	-0.0070	0.0041
N-Ac D glucosamine	1	20	0.8	60	1	Test	2.5541	2.5568	-0.0027	0.0016
N-Ac D glucosamine	1	20	0.8	2	1	Test	2.5561	2.5659	-0.0098	0.0058
N-Ac D glucosamine	1	20	0.8	30	0	Test	2.5589	2.5667	-0.0078	0.0046
N-Ac D glucosamine	1	20	0.8	30	2	Test	2.5532	2.5672	-0.0139	0.0082
N-Ac D glucosamine	1	20	0.5	30	1	Test	2.5844	2.5948	-0.0104	0.0061
N-Ac D glucosamine	10.5	20	0.8	30	1	Test	2.9717	2.9882	-0.0165	0.0097
N-Ac D glucosamine	20	20	1.1	30	1	Test	3.0899	3.1020	-0.0121	0.0072
N-Ac D glucosamine	20	20	0.8	2	1	Test	3.1146	3.1354	-0.0208	0.0123
N-Ac D glucosamine	20	20	0.8	60	1	Test	3.1111	3.1462	-0.0350	0.0207
N-Ac D glucosamine	20	20	0.8	30	0	Test	3.1112	3.1536	-0.0424	0.0251
N-Ac D glucosamine	20	20	0.8	30	2	Test	3.1161	3.1555	-0.0394	0.0233

N-Ac D glucosamine	20	20	0.5	30	1	Test	3.1319	3.2051	-0.0732	0.0432
N-Ac D glucosamine	10.5	20	0.8	30	1	Test	2.9717	2.9800	-0.0083	0.0049
N-Ac D glucosamine	10.5	10	1.1	30	1	Test	2.7586	2.7893	-0.0307	0.0181
N-Ac D glucosamine	10.5	10	0.8	2	1	Test	2.8060	2.8263	-0.0203	0.0120
N-Ac D glucosamine	10.5	10	0.8	60	1	Test	2.8029	2.8295	-0.0267	0.0157
N-Ac D glucosamine	10.5	10	0.8	30	2	Test	2.8057	2.8257	-0.0200	0.0118
N-Ac D glucosamine	10.5	10	0.8	30	0	Test	2.8061	2.8249	-0.0188	0.0111
N-Ac D glucosamine	10.5	10	0.5	30	1	Test	2.8525	2.8778	-0.0253	0.0149
N-Ac D glucosamine	1	10	0.8	30	1	Test	2.4742	2.4787	-0.0045	0.0026
N-Ac D glucosamine	20	10	0.8	30	1	Test	3.0246	3.0151	0.0096	0.0056
N-Ac D glucosamine	10.5	20	0.8	30	1	Test	2.9717	2.9949	-0.0232	0.0137
N-Ac D glucosamine	10.5	30	1.1	30	1	Test	3.0463	3.0454	0.0009	0.0006
N-Ac D glucosamine	10.5	30	0.8	30	0	Test	3.0683	3.0840	-0.0157	0.0093
N-Ac D glucosamine	10.5	30	0.8	60	1	Test	3.0711	3.0745	-0.0033	0.0020
N-Ac D glucosamine	10.5	30	0.8	30	2	Test	3.0752	3.0877	-0.0125	0.0074
N-Ac D glucosamine	10.5	30	0.8	2	1	Test	3.0711	3.0819	-0.0109	0.0064

N-Ac D glucosa-mine	10.5	30	0.5	30	1	Test	3.0921	3.1401	-0.0480	0.0283
N-Ac D glucosa-mine	20	30	0.8	30	1	Test	3.1586	3.1782	-0.0197	0.0116
N-Ac D glucosa-mine	1	30	0.8	30	1	Test	2.7134	2.7688	-0.0553	0.0327
N-Ac D glucosa-mine	10.5	20	0.8	30	1	Test	2.9717	2.9825	-0.0108	0.0064
N-Ac D-mannosa-mine	10.5	20	1.1	30	2	Training	2.9337	2.9579	-0.0242	0.0143
N-Ac D-mannosa-mine	10.5	20	1.1	2	1	Training	2.9315	2.9488	-0.0173	0.0102
N-Ac D-mannosa-mine	10.5	20	1.1	30	0	Training	2.9236	2.9468	-0.0232	0.0137
N-Ac D-mannosa-mine	10.5	20	1.1	60	1	Training	2.9236	2.8209	0.1027	0.0606
N-Ac D-mannosa-mine	10.5	20	0.8	30	1	Training	2.9717	2.9716	0.0001	0.0000
N-Ac D-mannosa-mine	10.5	20	0.8	2	0	Training	2.9680	2.9601	0.0079	0.0047
N-Ac D-mannosa-mine	10.5	20	0.8	60	2	Training	2.9715	2.9821	-0.0106	0.0062
N-Ac D-mannosa-mine	10.5	20	0.8	2	2	Training	2.9721	2.9823	-0.0102	0.0060
N-Ac D-mannosa-mine	10.5	20	0.8	60	0	Training	2.9641	2.9678	-0.0037	0.0022
N-Ac D-mannosa-mine	10.5	20	0.8	30	1	Validation	2.9717	2.9679	0.0038	0.0023
N-Ac D-mannosa-mine	10.5	20	0.5	60	1	Validation	3.0057	3.0244	-0.0187	0.0110
N-Ac D-mannosa-mine	10.5	20	0.5	2	1	Training	3.0017	3.0162	-0.0145	0.0085

N-Ac D-mannosa-mine	10.5	20	0.5	30	2	Validation	3.0059	3.0185	-0.0126	0.0074
N-Ac D-mannosa-mine	10.5	20	0.5	30	0	Training	3.0041	3.0092	-0.0051	0.0030
N-Ac D-mannosa-mine	1	20	1.1	30	1	Training	2.5316	2.5246	0.0070	0.0042
N-Ac D-mannosa-mine	1	20	0.8	60	1	Validation	2.5541	2.5423	0.0118	0.0070
N-Ac D-mannosa-mine	1	20	0.8	2	1	Training	2.5561	2.5491	0.0070	0.0041
N-Ac D-mannosa-mine	1	20	0.8	30	0	Training	2.5589	2.5496	0.0093	0.0055
N-Ac D-mannosa-mine	1	20	0.8	30	2	Training	2.5532	2.5545	-0.0012	0.0007
N-Ac D-mannosa-mine	1	20	0.5	30	1	Training	2.5844	2.5755	0.0089	0.0052
N-Ac D-mannosa-mine	10.5	20	0.8	30	1	Validation	2.9717	2.9719	-0.0002	0.0001
N-Ac D-mannosa-mine	20	20	1.1	30	1	Training	3.0899	3.0889	0.0010	0.0006
N-Ac D-mannosa-mine	20	20	0.8	2	1	Training	3.1146	3.1204	-0.0058	0.0034
N-Ac D-mannosa-mine	20	20	0.8	60	1	Training	3.1111	3.1329	-0.0217	0.0128
N-Ac D-mannosa-mine	20	20	0.8	30	0	Training	3.1112	3.1422	-0.0310	0.0183
N-Ac D-mannosa-mine	20	20	0.8	30	2	Training	3.1161	3.1396	-0.0235	0.0138
N-Ac D-mannosa-mine	20	20	0.5	30	1	Training	3.1319	3.1900	-0.0581	0.0343
N-Ac D-mannosa-mine	10.5	20	0.8	30	1	Training	2.9717	2.9648	0.0069	0.0041

N-Ac D-mannosa-mine	10.5	10	1.1	30	1	Validation	2.7586	2.7804	-0.0218	0.0128
N-Ac D-mannosa-mine	10.5	10	0.8	2	1	Training	2.8060	2.8142	-0.0082	0.0048
N-Ac D-mannosa-mine	10.5	10	0.8	60	1	Training	2.8029	2.8137	-0.0108	0.0064
N-Ac D-mannosa-mine	10.5	10	0.8	30	2	Training	2.8057	2.8106	-0.0050	0.0029
N-Ac D-mannosa-mine	10.5	10	0.8	30	0	Training	2.8061	2.8104	-0.0044	0.0026
N-Ac D-mannosa-mine	10.5	10	0.5	30	1	Training	2.8525	2.8636	-0.0111	0.0066
N-Ac D-mannosa-mine	1	10	0.8	30	1	Validation	2.4742	2.4656	0.0086	0.0051
N-Ac D-mannosa-mine	20	10	0.8	30	1	Training	3.0246	2.9982	0.0265	0.0156
N-Ac D-mannosa-mine	10.5	20	0.8	30	1	Training	2.9717	2.9799	-0.0082	0.0048
N-Ac D-mannosa-mine	10.5	30	1.1	30	1	Training	3.0463	3.0302	0.0161	0.0095
N-Ac D-mannosa-mine	10.5	30	0.8	30	0	Training	3.0683	3.0731	-0.0048	0.0028
N-Ac D-mannosa-mine	10.5	30	0.8	60	1	Training	3.0711	3.0586	0.0126	0.0074
N-Ac D-mannosa-mine	10.5	30	0.8	30	2	Validation	3.0752	3.0757	-0.0005	0.0003
N-Ac D-mannosa-mine	10.5	30	0.8	2	1	Training	3.0711	3.0704	0.0006	0.0004
N-Ac D-mannosa-mine	10.5	30	0.5	30	1	Validation	3.0921	3.1244	-0.0322	0.0190
N-Ac D-mannosa-mine	20	30	0.8	30	1	Training	3.1586	3.1642	-0.0056	0.0033

N-Ac D-mannosa-mine	1	30	0.8	30	1	Training	2.7134	2.7460	-0.0326	0.0192
N-Ac D-mannosa-mine	10.5	20	0.8	30	1	Training	2.9717	2.9682	0.0035	0.0020

Filter constant: 0 – none; 1 – low; 2 – high
Residuals – the difference between experimentally obtained and values calculated by network
Error – the overall error on each case

4.4 HPLC-CAD analysis of bisphosphonate drugs by means of mixed-mode chromatography

1. Introduction

Since the 1960s, bisphosphonate drugs have been used in the treatment of diseases related to the bone mineral metabolism such as osteoporosis as well as for others such as Paget's disease [1, 2]. Their mechanism of action is based upon impairing osteoclast activity and survival [3-5].

In general, bisphosphonates (BPs) can be divided into two groups. The first group are the so-called "simple BPs" which do not contain a nitrogen atom in the side chain (Figure 1). These substances cause osteoclast apoptosis through the accumulation of toxic ATP metabolites [4]. The second group has been developed more recently and is represented by substances containing a nitrogen atom in the side chain (Figure 2). The potency of these *N*-containing BPs is 1 to 4 orders of magnitude higher [4, 6]. Their mechanism of action involves inhibition of the mevalonate pathway which results in the accumulation of a toxic isoprenoid metabolite that is detrimental to the osteoclasts [4].

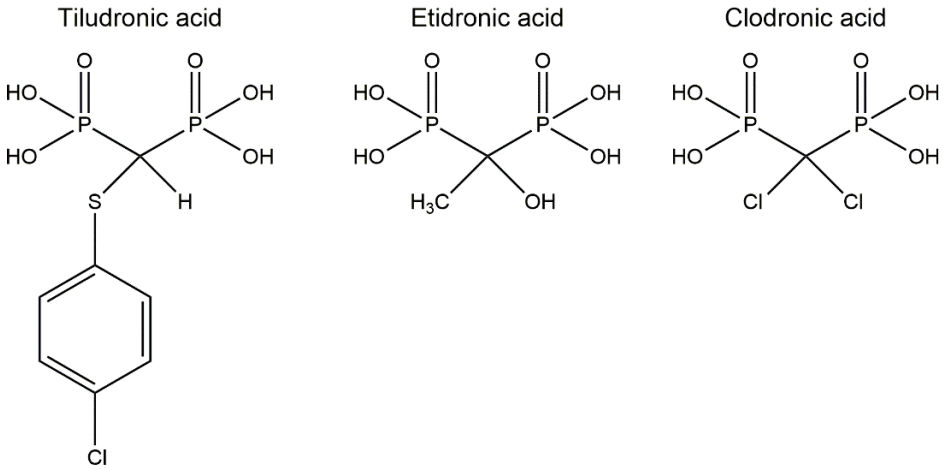

Figure 1: Chemical structures of the "simple bisphosphonates".

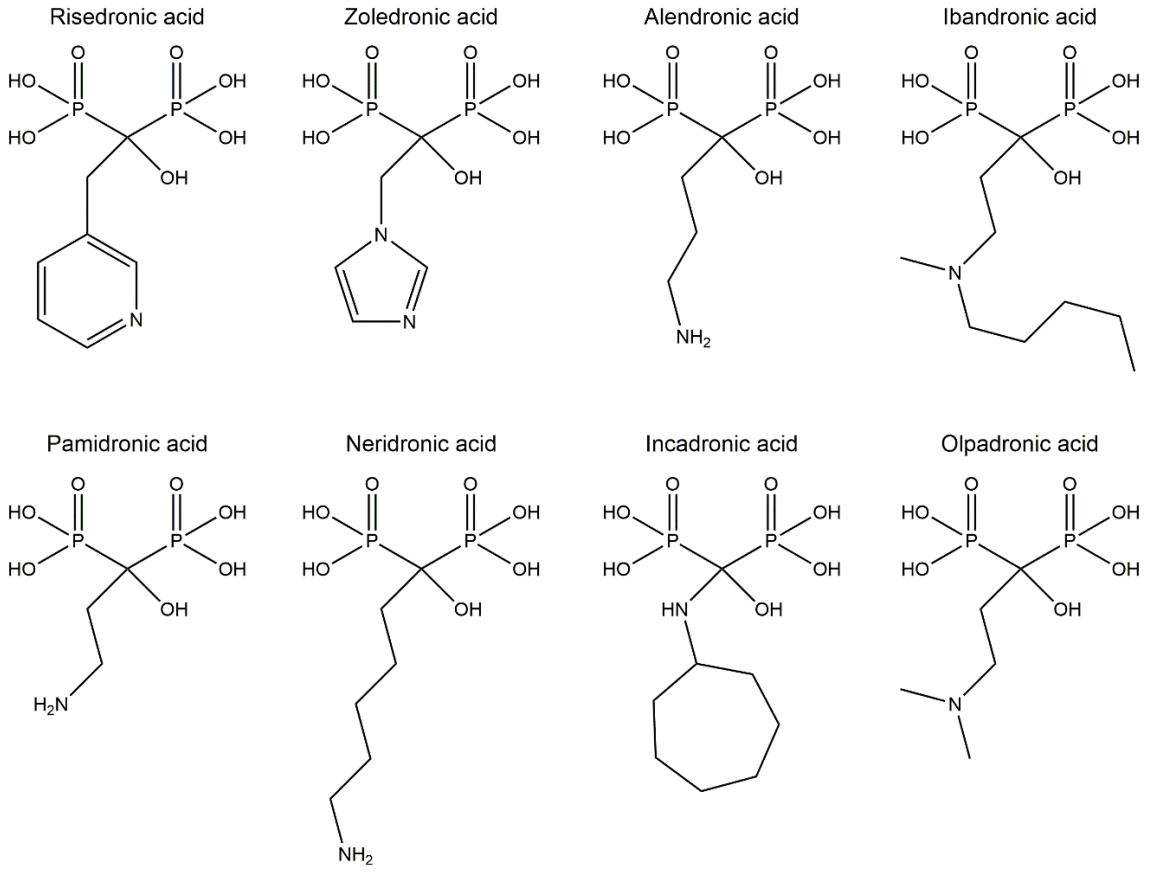

Figure 2: Chemical structures of the *N*-containing bisphosphonates.

BPs represent a challenging analytical group since they usually do not possess a chromophore which makes them unsuitable for classic liquid chromatography (LC) analysis or capillary electrophoresis (CE) coupled to UV detectors. Furthermore, the polar and ionized nature of the compounds represents a chromatographic challenge itself. Because they are polar and non-volatile, the direct application of gas chromatography (GC) is not possible. As comprehensively reviewed by Zacharis and Tzanavaras in 2008 [6], there are several derivatization procedures available to overcome these issues. Reversed-phase LC can be possible after fluorenylmethyl chloroformate (FMOC) [7-9] or fluorescamine [10, 11] derivatization, whereas ion-pairing chromatography methods can be used either with derivatization procedures [12, 13] or directly, employing tetrabutylammonium salts and UV detection for the BPs with aromatic side chains [14, 15]. A chromatographic approach avoiding the RP mechanism is the application of ion-exchange columns, more specifically such ones having an anion-exchange mechanism in order to interact with the deprotonated phosphonates. These techniques can employ rather universal detection principles such as conductivity [16] or refractive index detection [17]; however these detection principles lack sensitivity and robustness [18, 19]. Although GC [20] and CE [21] can

be applied after appropriate derivatization or complexation procedures, HPLC has some practical advantages over these techniques such as easier instrumentation, superior robustness, as well as a more established acceptance and presence in compendial quality control [22]. Additionally, derivatization procedures can be prone to errors, very tedious and time-consuming, and derivatization reactions can be incomplete or yield unwanted side products and thus difficult to validate [23]. Hence, it is desirable to avoid such highly reactive sample pretreatments and instead resort to the universal detection principles as presented in chapter 1.2. and 1.3. of this work. Amongst these, the most promising approach is the CAD due to its simple operation, superior sensitivity and robustness in comparison to the other aerosol-based detectors whilst being cheaper than mass spectrometry in terms of instrumentation, consumables, and maintenance.

In order to achieve compatibility with the aerosol-based universal detection principle for the analysis of ionic compounds, one needs to either rely on using volatile ion-pairing reagents or mixed-mode chromatography columns which have already been highlighted in chapter 1.4. as a chromatographic approach capable of achieving an adequate retention for polar compounds. The absence of ion-pairing reagents leads to an improved sensitivity of the method because of a lowered background noise; and, of note, compliance with modern laboratory practices due to the avoidance of using toxic substances such as the volatile ion-pairing reagents.

Applications for the analysis of BPs by means of aerosol-detectors have already been published in the literature: Xie and colleagues [24] simultaneously analysed four BPs by means of an RPIP method coupled to ELSD, using *n*-amylamine as an ion-pairing reagent. The same reagent has also been used for the specific analyses of alendronate [25] and incadronate [26]. Liu and coworkers [2] employed an anion-exchange and reversed phase mixed-mode column coupled to a CAD to monitor the phosphate and phosphite content in etidronate. Using the same column chemistry, Wahl and Holzgrabe [27] established a method capable of profiling the impurity pattern of ibandronate by means of mixed-mode HPLC-CAD. This method could also be applied to the determination of phosphate and phosphite in clodronate and etidronate.

The studies of the BPs described here had three challenges and goals:

1) Upon method transfer in other laboratories, the ibandronate impurity profiling of Wahl and Holzgrabe [27] failed to achieve the originally reported sensitivity. The cause of this and the hypothesis of a strong adsorption of the ionic compounds onto the stationary phase was investigated.
2) Almeling and Holzgrabe [28] published on the occurrence of “spike peaks” with ELSD, when a high sample load is applied. Taking the BPs as challenging application, their occurrence in the newest generation of ELS detectors was examined.
3) The impurity profile of pamidronate disodium is currently compendially assessed by means of two analytical methods, namely a refractive index IC method and a TLC procedure. Hence, developing a mixed-mode CAD method for the impurity profiling, assessing all compendial impurities in one chromatographic run, and possible application to other BPs was intended.

2. Experimental

2.1 Apparatus

2.1.1. HPLC-Corona CAD system

The experiments were performed on an Agilent 1100 modular chromatographic system (Waldbronn, Germany) equipped with an online degasser, a binary pump and a thermostatted column compartment connected to an ESA Corona CAD (Dionex Softron/ThermoFisher, Germering, Germany) operated at a filter setting of “none”, an output range of 100 pA, and a nitrogen gas pressure of 35.0 ± 0.1 psi supplied by an ESA nitrogen generator connected to the in-house compressed air system. Modules were controlled and data was processed using the Agilent ChemStation® Rev.B.03.02 software.

2.1.2. HPLC-ELSD system

The ELSD experiments were performed on an Agilent 1100 modular chromatographic system (Waldbronn, Germany) equipped with an online degasser, a binary pump and a thermostatted column compartment connected to a Sedere® Sedex100 ELS detector (Olivet, France) supplied with nitrogen from an ESA nitrogen generator (DionexSoftron/ThermoFisher, Germering, Germany) connected to the in-house compressed air system. The instruments were controlled and runs were processed using the Agilent ChemStation Rev.B.03.02 software.

2.1.3. HPLC-Vanquish H CAD system

The experiments on the 2015 introduced Vanquish CAD were performed on a ThermoFisher Scientific® Vanquish Flex UHPLC modular system equipped with a binary pump, a thermostatted autosampler, a thermostatted column compartment with active pre-heater, a VWD, and Vanquish Horizon CAD. This instrument was controlled and runs were processed using the Chromeleon Data System 7.2.6 Software (all ThermoFisher Scientific, Germering, Germany).

2.2. Chemicals and reagents

All chemicals and reagents were at least of analytical grade and obtained from Sigma-Aldrich (Schnelldorf, Germany) and VWR (Darmstadt, Germany). The

bisphosphonate drugs were obtained from the EDQM (Strasbourg, France). Ultra-pure water was supplied by a Merck Milli-Q system (Merck Millipore, Darmstadt).

3. Results and discussion

3.1. Adsorption and secondary interactions of ionic species on mixed-mode columns

The impurity profiling of ibandronate sodium by means of mixed-mode chromatography CAD as reported by Wahl and Holzgrabe [27] employs a reversed phase and strong anion-exchange column and a gradient elution using water, acetonitrile and TFA in order to separate ibandronate from the impurities listed in pharmacopoeias. Reports from other laboratories showed that the necessary sensitivity could not be achieved using the method. The phosphonate moieties in the BP drugs have pK_a values of 1.35, 2.87, 7.03, and 11.3 [29], hence under any given applicable chromatographic condition within the pH range of common RP and mixed-mode columns (generally about pH 2-8), the vast majority will be present as anions. Since BPs are known to be able to form complexes with metal cations [12, 30], they also might strongly interact with cations in stationary phases or capillaries, leading to a loss of analyte before a saturation is achieved.

The Ph.Eur. monograph for zoledronic acid describes an RPIP method with a preconditioning procedure that requires the test solution to be injected 15 consecutive times before the first analysis [31]. This implies the presence of such saturation effects and their relevance with regard to compendial purity analytics. Since a stationary phase used for RPIP becomes irreversibly modified by the ionic species of the ion-pairing reagent present in the mobile phase, the requirement of a saturation with the analyte of interest should behave similar in mixed-mode chromatography.

This behavior was studied by using the same system as in the original publication, operated with a shorter mixed-mode RP-SAX column and modified gradient times in accordance with the method of Wahl and Holzgrabe [27]. The chromatographic conditions were as follows: SIELC Coresep® SB (50 x 4.6 mm i.d.; 2.7 µm particle size; 100 Å), mobile phase A: water; mobile phase B: 15% v/v MeCN with 15 mM TFA; flow rate: 1.2 mL/min; gradient: 0-0.5 min 30 % B; 0.5-2 min 30-100% B; 2-6 min 100% B; 6-8 min 100-30% B; 8-10 min 30% B.

It was found that when the column was equilibrated with the mobile phase directly after storage and the first API injections were made, the sensitivity was also low in our lab. To saturate the column with the charged analyte, injection cycles of highly concentrated “saturation injections” made from the method’s test solution (20 mg/mL) and subsequent injections of low-concentrated ibandronate were performed. Blank injections were done in between to avoid carry-over effects. In order to saturate the column with the analyte, highly concentrated solutions were injected. The success of this preconditioning is reflected in an increasing sensitivity and a decreasing difference between analysis results of consecutive injection cycles, eventually leading to constant and reliable values. Figure 3 shows chromatograms of 1 µg of ibandronate sodium on column with one cycle of a highly concentrated “saturation injection” between each signal trace and Figure 4 depicts the peak area as a function of number of injections.

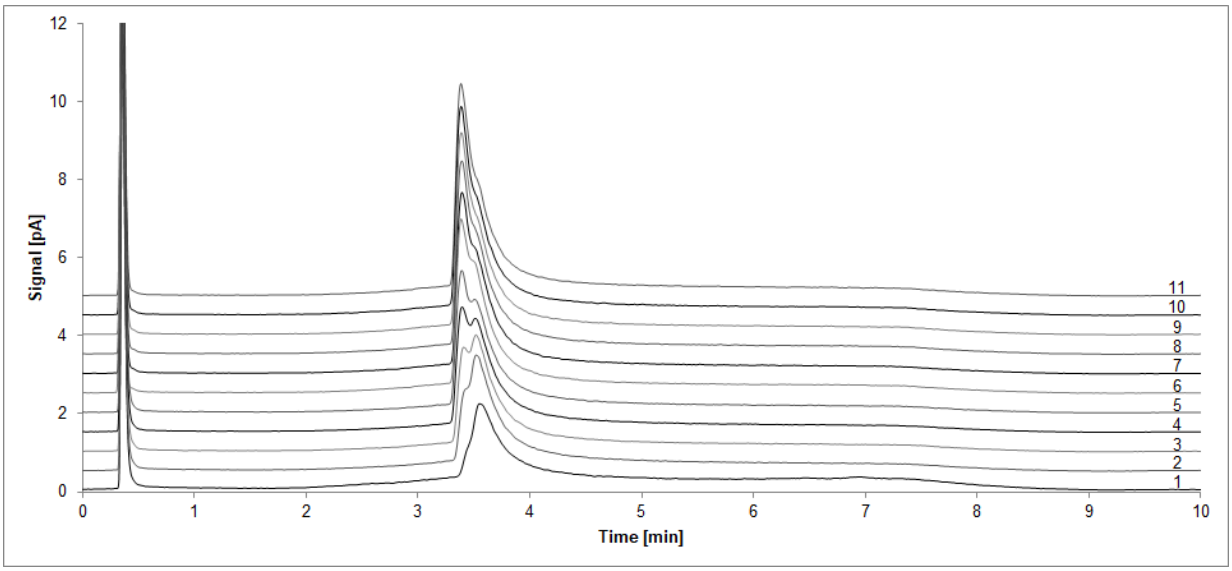

Figure 3: 1 µg on column of ibandronate sodium. In order to saturate the column, 1 injection of 200 µg on column alongside blank injections to avoid carry over was done between each cycle. [32]

As presented in this overlay of chromatograms, more than ten injections of the highly concentrated ibandronate solution were necessary to obtain reproducible results for the peak area. The relative standard deviation of the peak areas obtained in the sequences 8 to 11 was 2.1%, functioning as another indicator of approaching a saturated state.

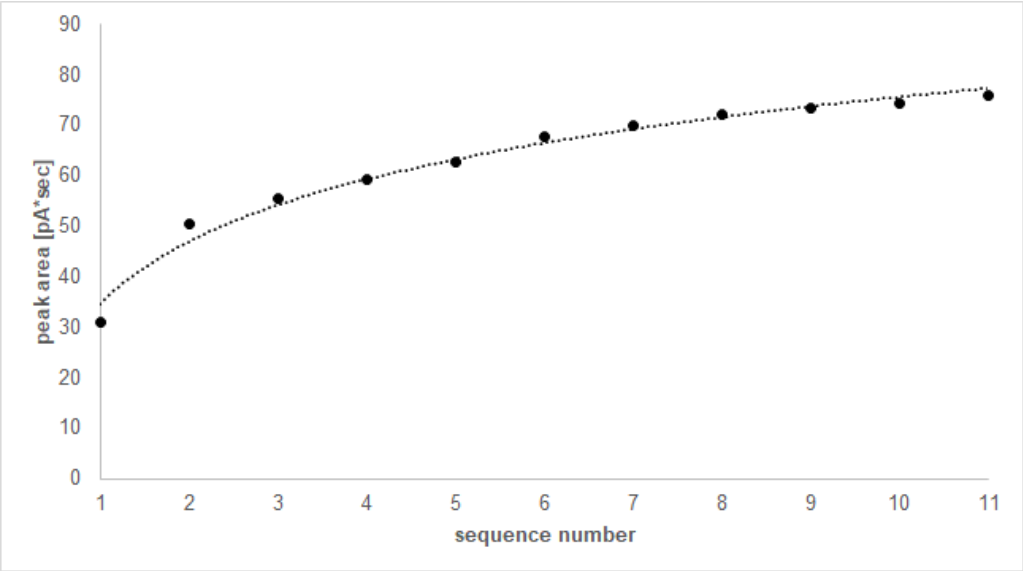

Figure 4: peak area as a function of performed injection cycles [32]

Other results indicate that not only the column but also steel capillaries and other wettable surfaces within the system may also be partially responsible for the observed behaviour, however, more investigation on this aspect is required. This consideration should be kept in mind and examined specifically during method development for ionic compounds in mixed-mode LC or even RPIP separations. During method development, the system and the column will most likely enter a saturated state due to the high amounts of experiments being performed with the test substance. However, during the validation procedure new columns and/or washed and stored columns should be used and examined with regard to the presence of this behaviour. If this phenomenon is problematic for the measurements, preconditioning steps as in the monograph of zoledronic acid [31] can represent appropriate countermeasures and should be considered and investigated.

3.2. On the occurrence of “spike peaks” in the current generation ELSD

As presented by Almeling and Holzgrabe [28], the ELSD suffers from drawbacks when it comes to the analysis of highly concentrated solutions for impurity profiling, although it represents a comparably cheaper alternative for the use of aerosol-based universal detection,. The authors found randomly occurring “spike peaks” in the chromatograms when a high sample load is present. Although this phenomenon was affected by the detector settings (such as gas flow rate or evaporation temperature), it was identified as a major drawback of this detection principle because parameters that lead to high sensitivity also lead to a high presence of these random spikes.

As elaborated in chapter 1.2., there have been some advances in the operation of the ELSD such as the introduction of an automated adjustment of the “gain” setting which eliminates the small dynamic range as a drawback of this detector. However, the occurence of these “spike peaks” can be regarded as a major issue for the purity assessment of pharmaceutical drugs and products because they can lead to severe misinterpretation and loss of specificity.

The chromatographic conditions for the experiments were adopted from the impurity profiling mixed-mode CAD method for ibandronate sodium published by Wahl and Holzgrabe [27]. The chromatographic conditions were as follows: SIELC Coresep® SB (150 x 4.6 mm i.d.; 2.7 µm; 100 Å), mobile phase A: water; mobile phase B: 15% v/v MeCN with 15 mM TFA; flow rate: 1.2 mL/min; gradient: 0-3 min 30% B; 3-10 min 30-100% B; 10-30 min 100% B; 30-32 min 100-30% B; 32-36 min 30% B. ELSD settings: filter 1s, evaporation temperature 80°C, nebulizer pressure 3.5 bar, 2 Hz sampling rate, Gain dynamic.

As presented in Figure 5, analysis was conducted six consecutive times without any injections in between, simulating an n=6 intraday precision experiment. In referral to the preceding section 3.1., the column was sufficiently saturated with analyte. Every chromatogram contains different random “spike peaks”, thus a robust and proper assessment of the impurity profile of the batch is not possible with the ELSD. Of note, none of these random spiked have yet been observed in analyses using the CAD.

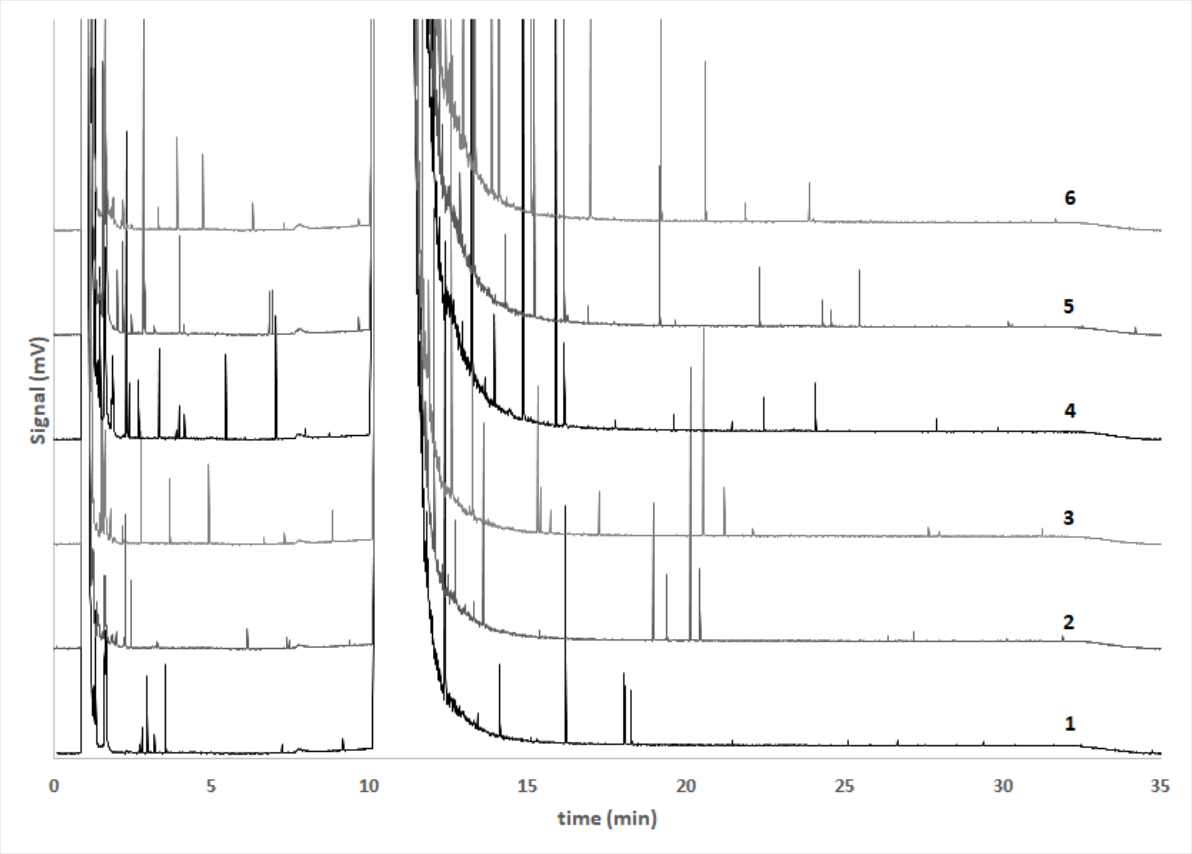

Figure 5: Six consecutive injections of the same spiked ibandronate sample solution analysed by means of HPLC-ELSD. For chromatographic conditions see section 3.2. [32]

The appearance of these random spikes was not only restricted to the application of this method, but also present in flow injection analyses of e.g. sulfanilamide (data not shown). This is in accordance with further reports on the occurrence of these random spike peaks made by Ilko et. al. [33] and Fontes and colleagues [34] in more recent publications and represents an issue that does not seem to be resolved by the manufacturer yet. The latter authors have specifically identified the nebulizer and its mode as the main culprit of this behaviour.

3.3. Impurity profiling of pamidronate disodium by means of mixed-mode HPLC-CAD

The compendially monographed substance pamidronate disodium pentahydrate is a BP drug derived from β-alanine. Hence, its impurity profile consists of phosphate and phosphite - as it is to be expected for every BP - and β-alanine. Previously reported mixed-mode approaches coupled to aerosol-detection were not applicable for the determination of phosphate and phosphite in pamidronate, let alone for β-alanine. However, mixed-mode chromatography coupled to CAD is an elegant way to avoid the

use of toxic and expensive ion-pairing reagents and enable the detection of all compounds present in the impurity profile at a glance.

In order to assess the full impurity profile of pamidronate, the Ph.Eur. employs a semi-quantitative TLC procedure with ninhydrin detection to determine β-alanine at a level of 0.5%. For the quantification of phosphate and phosphite, a second method using ion exchange chromatography and refractive index detection is described. However, the method suffers from poor selectivity due to the tailing of the pamidronate signal, likely co-eluting with the phosphate. This is accompanied by the general drawbacks of refractive index detection that were presented before such as the incompatibility with gradient elution (chapter 1.2.).

Pamidronate belongs to the group of *N*-containing BPs shown in Figure 2, therefore it possesses a basic moiety in the side chain. The majority of the amine will be almost fully protonated at any given pH value within the range of usual LC columns. Many mixed-mode columns have a narrow pH range from about 2 to about 5 which is suitable for their operation. The fact that pamidronate will be present as a zwitterionic substance during the chromatography can be a useful property in order to achieve a separation from phosphate. Mixed-mode columns with ternary stationary phases and complex retention mechanisms represent an opportunity to obtain an increased retention for the zwitterion. A Sielc® Obelisc N column was chosen as a suitable candidate because it originates from the same manufacturer as the columns used in methods by Wahl [27] and Liu [2] and enhances the retention for cationic and zwitterionic substances through the incorporation of a third retention mechanism. The Obelisc N column possesses embedded cation-exchange groups, which are connected to anion-exchange groups via a hydrophilic linker. The column therefore additionally allows for interactions of cationic structures by means of separations in normal phase, HILIC, and ion exchange modes. The terminal anion-exchange sites allow for sufficient retention of phosphate and phosphite. The method’s intended purpose is the impurity profiling rather than the assay of the pamidronate content. Therefore, deteriorated peak shapes for the main substance’s peak are acceptable for this purpose.

Initial method development was performed using the Agilent system connected to the Corona CAD as presented in section 2.1.1.

The initial approach was using the HILIC separation mode in an ammonium acetate buffered water and acetonitrile mixture applying various concentrations, pH values and

gradients ranging from 90% to 30% of organic content. However, because pamidronate is monographed and commercially available as its disodium salt, sodium ions will always be present in every sample. This is of no concern when only anion-exchange mechanisms contribute to the chromatography, but this ternary stationary phase offers cation-exchange sites which retain sodium. The high amounts of sodium were found to result in large and tailing peaks that interfered with other signals, thus affecting the specificity of the method. It was therefore necessary to decrease the retention of phosphate and phosphite while also increasing the retention for sodium at the same time.

Optimizing the elution order was achieved by solely using TFA as an additive to the mobile phase. TFA competes with phosphate and phosphite at the anion-exchange moieties and can thus block their availability by ion-pair formation on the surface of the column material. This leads to a decreased retention of these two ions, achieving a reasonable separation from sodium. Additionally, the amount of TFA, the starting conditions, the initial isocratic hold and the steepness of the gradient were then optimized in order to achieve a separation between β-alanine and the remaining substances. This was accomplished by applying a gradient increasing the ionic strength along with a decrease of organic content. The final method had the following chromatographic conditions: mobile phase A was 0.1% TFA dissolved in ultrapure water and mobile phase B was acetonitrile. The flow rate was set to 1.3 mL/min and the column was thermostatted at 25°C. The gradient program was set to: 0-5 min 80% B, 5–9 min 80–30% B, 9-15 min 30% B followed by a reequilibration step of 15-17 min 80-30% B and 17-23 min 30% B.

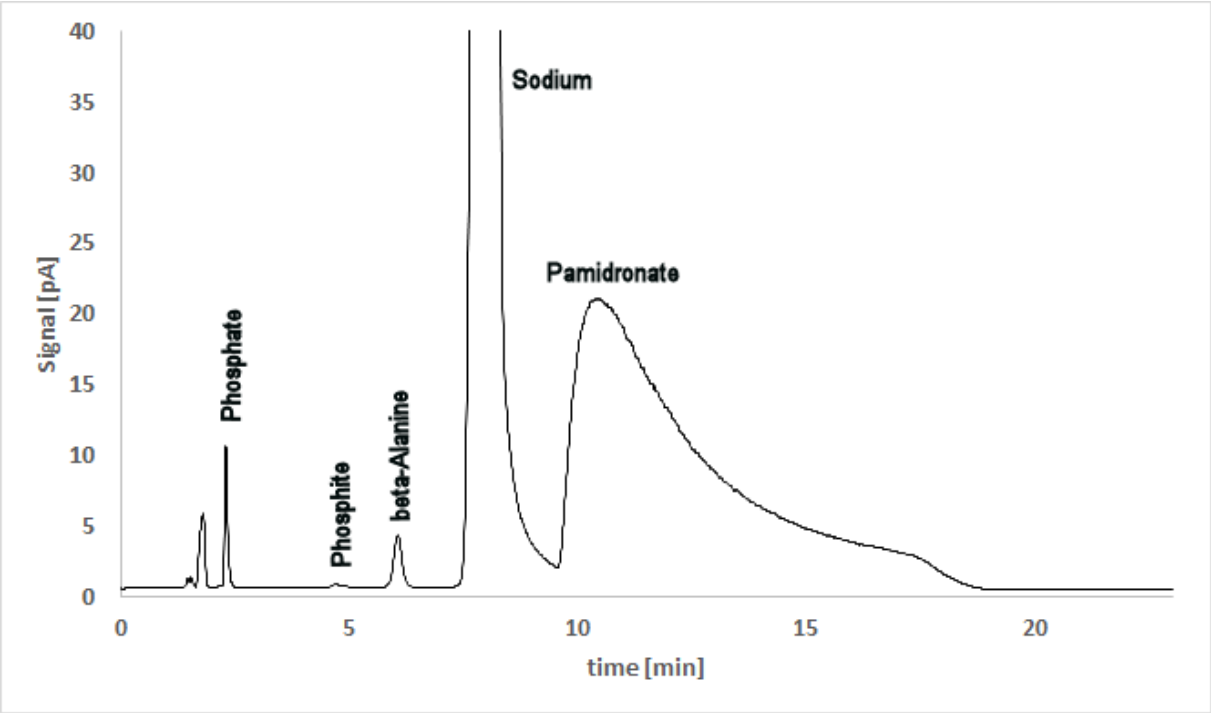

Figure 6: Chromatogram of a 10 mg/mL pamidronate disodium solution spiked with 0.1% of each impurity run on the Agilent system with Corona CAD.

As shown in Figure 6, the method was found to be able to separate all impurities of pamidronate from each other in a test solution spiked with 0.1% of each impurity. The irregular peak shape of the pamidronate peak is acceptable for the purpose of impurity profiling. With a sample concentration of 10 mg/mL, the next challenge was to achieve acceptable values for the limits of quantification (LOQ). The LOQ of a method intended for the impurity profiling should be below the reporting threshold, which usually is described by an impurity content of 0.05% (m/m) in a pharmaceutical substance's monograph [35].

The CAD of the older generation failed to achieve the necessary sensitivity for phosphite, but changing chromatographic conditions, such as increasing the amount of organic modifier or decreasing any mobile phase additive was not possible. Such changes would lead to an improved sensitivity, but upon changing those parameters, the separation was impaired. An alternative to adjusting chromatographic conditions in order to benefit the sensitivity is finetuning instrument settings of the detector. As discussed in chapters 1.3., 3 and 4.2., these features are exclusive to newer generations of the CAD. Hence, the method was optimized by means of CAD parameter optimization on a ThermoFisher Scientific® Vanquish Flex UHPLC modular system as described in section 2.1.3.

As elaborated before, the evaporation temperature is the most crucial parameter when it comes to optimizing the signal-to-noise ratios. Therefore, an increase of the evaporation temperature was chosen as the first step of optimization. The desired result could be obtained with an increase of the evaporation temperature of the CAD to a value of 50 °C. For all monographed impurities of pamidronate LOQ values below 0.05% were achieved. A representative chromatogram of the newly developed and CAD optimized mixed-mode method for pamidronate disodium spiked with all its specified impurities at a concentration level of 0.1% is shown in Figure 7.

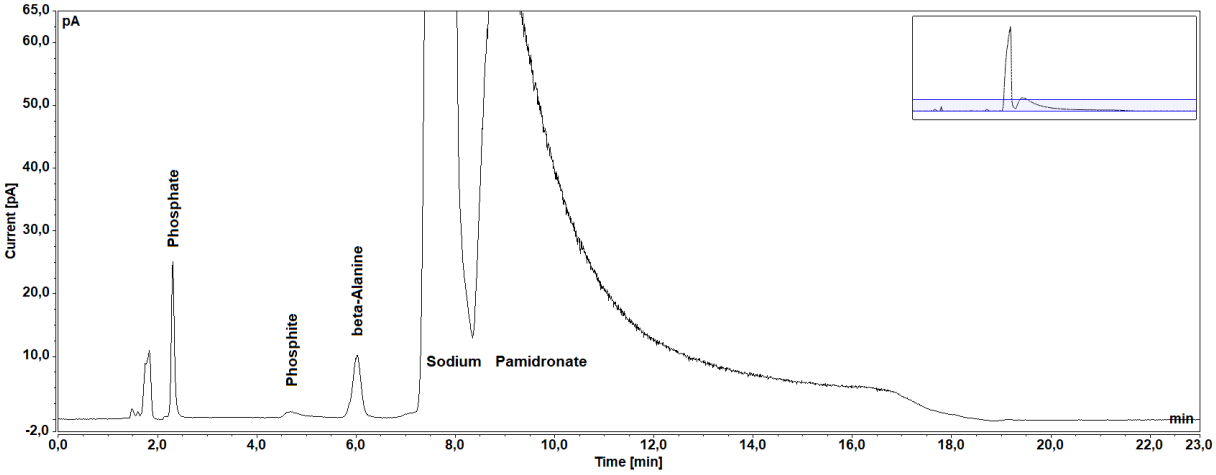

Figure 7: Impurity profiling of pamidronate disodium by means of the newly developed method with optimized CAD settings. For chromatographic conditions see section 3.3.

The next step was to evaluate whether this method is suitable for the analysis of other BPs and their impurity profiling. More specifically, it was intended to apply this method for the determination of phosphate and phosphite of as many BPs as possible. Ibandronate, risedronate, clodronate, alendronate, and etidronate were evaluated as possible candidates for the application. For ibandronate sodium, the method was not applicable due to an interference of the ibandronate signal with phosphite.

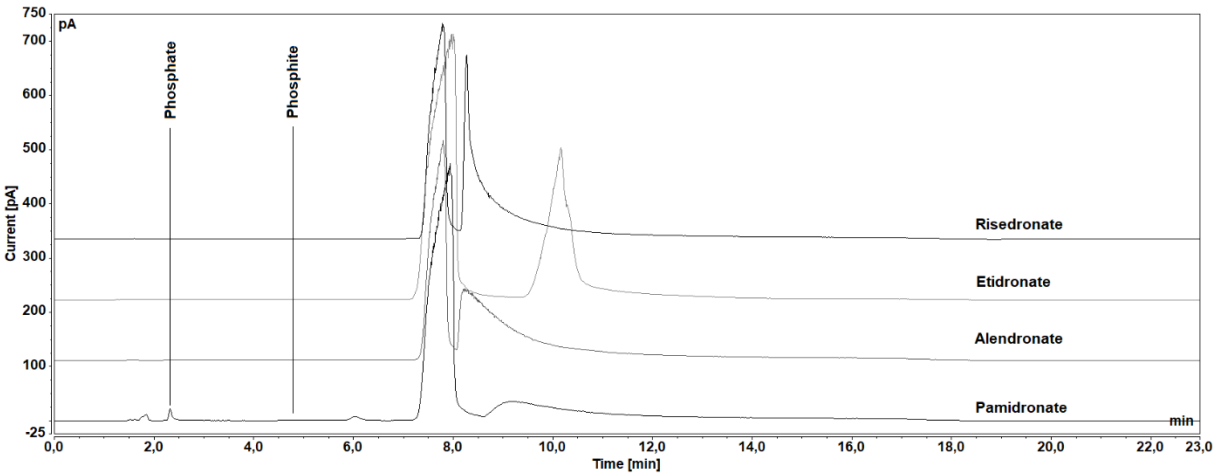

Figure 8: Overlay of the application of the optimized method to the analysis of phosphate and phosphite in alendronate, etidronate, risedronate and pamidronate.

As it is evident from Figure 8, the method is readily applicable to the quantification of phosphate and phosphite in alendronate, etidronate, risedronate, and pamidronate. In order to be able to quantify these two ions in clodronate, the isocratic step at 30% B needs to be prolonged for another 15 min to elute the main substance, leading to a total run time of 38 min including the reequilibration procedure. The method is yet to be validated according to the ICH guidelines.

3. Conclusions

It was shown that ionic substances can require careful column preconditioning or saturation procedures when mixed-mode chromatography is applied. Strong interactions and adsorptions can lead to improper results and impaired sensitivity during initial analyses on fresh columns. During method development and validation for the analysis of ionic species, trial experiments examining the behaviour of new or previously washed and stored columns should be performed.

With the utilization of high sample load in ELSD, it is known that random “spike peaks” can occur. This is a huge disadvantage of this detector and represents a challenge in purity analysis because instrument settings enhancing the sensitivity readily promote the formation of these “spike peaks”. This phenomenon was confirmed to be present in the 2016 introduced generation of Sedex100 detectors as well.

Last, a new method capable of performing compendial quality control of pamidronate disodium was developed. The mixed-mode HPLC-CAD method is able to quantify all specified impurities of pamidronate in one chromatographic run. This represents an improvement over the current approach of the Ph.Eur. monograph which requires the

application of two separate tests, namely ion chromatography with refractive index detection and a semi-quantitative TLC procedure applying ninhydrin derivatization. Furthermore, it could be demonstrated that the method is feasible for being applied to four other bisphosphonates in order to assess phosphate and phosphite.

Acknowledgements

Dr. Christiane Theiss is gratefully acknowledged for accompanying the first two projects of this chapter with practical and theoretical expertise. Thanks are due to ERC GmbH (Hohenbrunn, Germany) and ThermoFisher Scientific (Germering, Germany) for supplying our group with the required instrumentation.

Conflict of interest

The ThermoFisher Scientific Vanquish system was made available within a cooperative relationship. The Sedere Sedex100 ELSD was made available for trial experiments.

References

1. Widler L, Jaeggi KA, Glatt M, Müller K, Bachmann R, Bisping M et al. Highly potent geminal bisphosphonates. From pamidronate disodium (Aredia) to zoledronic acid (Zometa). J Med Chem. 2002;45:3721-38.

2. Liu X-K, Fang JB, Cauchon N, Zhou P. Direct stability-indicating method development and validation for analysis of etidronate disodium using a mixed-mode column and charged aerosol detector. J Pharm Biomed Anal. 2008;46:639-44.

3. Fleisch H. The role of bisphosphonates in breast cancer: Development of bisphosphonates. Breast Cancer Res. 2001;4:30.

4. Rogers MJ, Crockett JC, Coxon FP, Mönkkönen J. Biochemical and molecular mechanisms of action of bisphosphonates. Bone. 2011;49:34-41.

5. Rogers MJ, Gordon S, Benford H, Coxon F, Luckman S, Monkkonen J et al. Cellular and molecular mechanisms of action of bisphosphonates. Cancer. 2000;88:2961-78.

6. Zacharis CK, Tzanavaras PD. Determination of bisphosphonate active pharmaceutical ingredients in pharmaceuticals and biological material: a review of analytical methods. J Pharm Biomed Anal. 2008;48:483-96.

7. De Marco JD, Biffar SE, Reed DG, Brooks MA. The determination of 4-amino-1-hydroxybutane-1, 1-diphosphonic acid monosodium salt trihydrate in pharmaceutical dosage forms by high-performance liquid chromatography. J Pharm Biomed Anal. 1989;7:1719-27.

8. Yun M-H, Kwon K-i. High-performance liquid chromatography method for determining alendronate sodium in human plasma by detecting fluorescence: application to a pharmacokinetic study in humans. J Pharm Biomed Anal. 2006;40:168-72.

9. Ptáček P, Klíma J, Macek J. Determination of alendronate in human urine as 9-fluorenylmethyl derivative by high-performance liquid chromatography. J Chromatogr B. 2002;767:111-6.

10. Wong JA, Renton KW, Crocker JF, O'Regan PA, Acott PD. Determination of pamidronate in human whole blood and urine by reversed-phase HPLC with fluorescence detection. Biomed Chromatogr. 2004;18:98-101.

11. Flesch G, Tominaga N, Degen P. Improved determination of the bisphosphonate pamidronate disodium in plasma and urine by pre-column derivatization with fluorescamine, high-performance liquid chromatography and fluorescence detection. J Chromatogr B. 1991;568:261-6.

12. Sparidans RW, den Hartigh J, Ramp-Koopmanschap WM, Langebroek RH, Vermeij P. The determination of pamidronate in pharmaceutical preparations by ion-pair liquid chromatography after derivatization with phenylisothiocyanate. J Pharm Biomed Anal. 1997;16:491-7.

13. Al Deeb SK, Hamdan II, Al Najjar SM. Spectroscopic and HPLC methods for the determination of alendronate in tablets and urine. Talanta. 2004;64:695-702.

14. Rao BM, Srinivasu M, Rani CP, Kumar PR, Chandrasekhar K, Veerender M. A validated stability indicating ion-pair RP-LC method for zoledronic acid. J Pharm Biomed Anal. 2005;39:781-90.

15. Kyriakides D, Panderi I. Development and validation of a reversed-phase ion-pair high-performance liquid chromatographic method for the determination of risedronate in pharmaceutical preparations. Anal Chim Acta. 2007;584:153-9.

16. Tsai EW, Ip DP, Brooks MA. Determination of alendronate in pharmaceutical dosage formulations by ion chromatography with conductivity detection. J Chromatogr A. 1992;596:217-24.

17. Han Y-HR, Qin X-Z. Determination of alendronate sodium by ion chromatography with refractive index detection. J Chromatogr A. 1996;719:345-52.

18. Zhang K, Kurita K, Venkatramani C, Russell D. Seeking universal detectors for analytical characterizations. J Pharm Biomed Anal. 2019;162:192-204.

19. Vervoort N, Daemen D, Török G. Performance evaluation of evaporative light scattering detection and charged aerosol detection in reversed phase liquid chromatography. J Chromatogr A. 2008;1189:92-100.

20. Muntoni E, Canaparo R, Della Pepa C, Serpe L, Casale F, Barbera S et al. Determination of disodium clodronate in human plasma and urine using gas-chromatography–nitrogen-phosphorous detections: validation and application in pharmacokinetic study. J Chromatogr B. 2004;799:133-9.

21. Tsai EW, Singh MM, Lu HH, Ip DP, Brooks MA. Application of capillary electrophoresis to pharmaceutical analysis: Determination of alendronate in dosage forms. J Chromatogr A. 1992;626:245-50.

22. Görög S. The sacred cow: the questionable role of assay methods in characterising the quality of bulk pharmaceuticals. J Pharm Biomed Anal. 2005;36:931-7.

23. Wahl O, Holzgrabe U. Amino acid analysis for pharmacopoeial purposes. Talanta. 2016;154:150-63.

24. Xie Z, Jiang Y, Zhang D-q. Simple analysis of four bisphosphonates simultaneously by reverse phase liquid chromatography using n-amylamine as volatile ion-pairing agent. J Chromatogr A. 2006;1104:173-8.

25. Jiang Y, Xie Z, Zhang D-q. Separation of Alendronate and Its Related Substances by Ion-Pair Reverse Phase Chromatography with Evaporative Light-Scattering Detector. J Anal Sci. 2006;22:137.

26. Zhao J, Jiang Y. Determination of Incadronate Disodium and Its Related Substances by HPLC-ELSD. Chinese J Pharm. 2007;38:509.

27. Wahl O, Holzgrabe U. Impurity profiling of ibandronate sodium by HPLC–CAD. J Pharm Biomed Anal. 2015;114:254-64.

28. Almeling S, Holzgrabe U. Use of evaporative light scattering detection for the quality control of drug substances: Influence of different liquid chromatographic and evaporative light scattering detector parameters on the appearance of spike peaks. J Chromatogr A. 2010;1217:2163-70.

29. DeRuiter J, Clark R. Bisphosphonates: Calcium antiresorptive agents. Endocr Mod. 2002:1-7.

30. Kosonen JP. Determination of disodium clodronate in bulk material and pharmaceuticals by ion chromatography with post-column derivatization. J Pharm Biomed Anal. 1992;10:881-7.

31. EDQM, Strasbourg, France., Monograph No. 2743 - Zoledronic acid monohydrate. European Pharmacopoeia Online 9.8.. Available from: http://online6.edqm.eu/ep908/

32. Schilling K, Theiss C. unpublished data. 2017.

33. Ilko D, Neugebauer RC, Brossard S, Almeling S, Türck M, Holzgrabe U. Impurity Control in Topiramate with High Performance Liquid Chromatography: Validation and Comparison of the Performance of Evaporative Light Scattering Detection and Charged Aerosol Detection. Charged Aerosol Detection for Liquid Chromatography and Related Separation Techniques. John Wiley & Sons; Hoboken, 2017.

34. Fontes PR, Ribeiro JAdA, Costa PP, Damaso MC, Gonzalez WdA, dos Santos CMC et al. Development and validation of a HILIC-UPLC-ELSD method based on optimized chromatographic and detection parameters for the quantification of polyols from bioconversion processes. Anal Methods. 2016;8:2048-57.

35. ICH Guideline Q3B (R2). Impurities in new drug products. 2006.

5 Final Discussion

The projects of this thesis aimed to elaborate the suitability of liquid chromatography for quality control of challenging and polar as well as weakly or non-chromophore active pharmaceutical ingredients and excipients. In order to achieve a liquid chromatographic separation for polar compounds without the need of derivatization procedures, non-classical methods of analysis were applied. These were ion-pairing reversed phase and mixed-mode chromatography methods yielding sufficient retention even for ionized substances were investigated. For the analysis of non- and weakly chromophore compounds, low wavelength UV detection and the utilization of aerosol-based universal detection principles were chosen. They are applicable to all molecules which are sufficiently non-volatile. Amongst these principles, the CAD stands out favorably due to its high sensitivity, robustness, and almost universality of its response [1, 2]. Therefore, the CAD was selected as the detector of choice.

5.1 Reversed phase ion-pairing chromatography

The separation of polar and ionized structures is almost impossible by means of reversed phase liquid chromatography. A suitable alternative is found in the use of ion-pairing reagents on common RP columns. With regard to the detection principle employed, special considerations need to be made. If the substance is detectable by UV, any mobile phase additives must not interfere at the detection wavelength. This can limit the choices of possible ion-pairing reagents severely, making method development challenging. If the substance is to be assessed by means of MS or one of the aerosol-based universal detectors, the ion-pairing reagent needs to be sufficiently volatile. Further restrictions with regard to the mobile phase additives need to be kept in mind, such as the incompatibility of e.g. TFA and ammonia which are individually volatile but form nonvolatile salts when combined.

A successful application of an RPIP method combined with low wavelength UV detection was shown during the analysis of L-asparagine monohydrate. To refrain from any interference with the detection wavelength of 210 nm, which would lead to an impaired sensitivity, sodium octanesulfonate was employed as ion-pairing reagent. The pH value of the buffer and the concomitant ionization state of the analyte are of paramount importance for obtaining satisfying peak shape and retention. When multiple retention mechanisms are present, peaks naturally tend to form irregular

shapes and can react unpredictably to changes in the eluent system. This is minimized when the analyte itself is present in a defined ionization state, leading to reproducible retention and analysis.

However, potentially impaired sensitivity, sometimes costly and toxic ion-pairing reagents, as well as long equilibration times accompanied by irreversible modification of the stationary phase have to be considered as drawbacks of this chromatographic approach [3].

5.2 Mixed-mode chromatography

An elegant way to avoid the use of ion-pairing reagents is employing stationary phases that combine multiple retention mechanisms in one single column. The possibilities of combining different stationary phase modifications seem endless, ranging from RP with one additional ion-exchange moiety to HILIC methods having two additional ionic groups. These ion-exchange sites can be modified chemically, leading to various different pK_a values, thus having an ionization state depending on the present pH value and adding a further layer of complexity to these columns. Such a ternary mixed-mode column possessing anion- and cation-exchange properties as well as a hydrophilic linker was successfully applied for the impurity profiling of the bisphosphonate drug pamidronate disodium by means of HPLC-CAD. The developed method was furthermore capable of monitoring the phosphate and phosphite content in four other drug substances of the bisphosphonate group.

A column with a dual retention mechanism, namely RP and anion-exchange properties, was utilized for investigating the relevance of column preconditioning procedures and saturation effects of ionic analytes on such columns. Ibandronate sodium was used as a model analyte and found to yield unreliable results unless the column was fully saturated with the analyte. Such countermeasures avoiding retention shift and loss of analyte can be employed by performing multiple injections of highly concentrated solutions of the respective compound during the equilibration procedure.

Especially for the application with aerosol-based universal detectors and MS, it is beneficial to avoid using ion-pairing reagents. This leads to a significantly decreased background noise and therefore a higher sensitivity. However, mixed-mode columns have their own set of drawbacks which comprise of a shorter lifetime and a higher commercial price than common RP columns. Furthermore, columns with the same

declared stationary phase chemistry but which are from different manufacturers are not necessarily interchangeable and method development tends to be less systematic and more of a “trial and error” approach due to the complexity and contribution of multiple retention mechanisms [4].

5.3 Charged Aerosol Detection

CAD represents a suitable option for the determination of non- and semi-volatile compounds that lack a suitable chromophore for their assessment. Due to having identical mobile phase requirements, all developed methods are directly transferrable to identification purposes using LC/MS. Although CAD does not allow such identification procedures, it offers a comparably cheaper instrument for quantification purposes. The review of analytical methods incorporating the use of this detector highlighted the benefit of its nearly universal response for physicochemically similar compounds under constant conditions. Approaches for (semi-)quantitative assessments of herbal extracts and substances of pharmaceutical interest were presented.

The CAD is known to have a non-linear signal output and response. Therefore, a design of experiment approach and quantitative structure property relationship modeling was applied using sugar and sugar-related molecules. It could be shown that artificial neural networks are capable of leading to predictive models describing the CAD response for a physicochemically related compound under conditions within the design space. This proof-of-concept can be the foundation for further research, eventually leading to larger libraries of structures and eluent conditions, elaborating more in-depth knowledge on the response of the CAD in dependency of physicochemical properties of the analyte, mobile phase conditions, and more recently added instrument parameters.

Recent generations of the CAD allow for more alterations of instrument parameters such as evaporation temperature and power function value which can lead to an increased linear range alongside an improved sensitivity and selectivity. These factors have been extensively studied for the excipient polysorbate 80 and its fatty acid profile, highlighting the evaporation temperature as the most influential setting and presenting general considerations for the use of the PFV. Because the volatility of fatty acids strongly varies based on their chain length, the behavior of semi-volatile analytes could

be studied as well. Transferring methods from older detector generations to modern systems can be a blessing and a curse at the same time: a direct transfer using the default conditions for both instruments might lead to different results. However, the possibility of adjusting and optimizing the instrument settings on the new generation of CAD results in more sensitive and linear methods. A successful approach for the transfer to modern generation systems and subsequent optimization in order to obtain an improved sensitivity was also shown with the polysorbate studies.

Once again using ibandronate sodium as a model substance, a comparison of the CAD to its main competitor ELSD was undertaken. High sample loads are typical in impurity profiling and the ELSD was described to suffer from randomly occurring “spike peaks” under these circumstances [5-7]. Although one former drawback, the rather small dynamic range, was resolved with the new generation of ELSD, the random “spike peaks” still remained an unresolved issue during our investigations, making an impurity profiling of drugs impossible.

5.4 Conclusion

Taken together, the literature overview of CAD applications manifested its increasing acceptance and use for the quality control of pharmaceutical substances, botanical extracts and excipients. A superior sensitivity and robustness over the ELSD, the absence of the random spikes, and sometimes even an on-par sensitivity with MS [8] highlight the role of the CAD amongst other universal detection approaches. Hyphenated techniques using UV-CAD or UV-CAD/MS are powerful tools for an almost comprehensive analysis within one single run. However, mobile phases need to be sufficiently volatile for such applications and the destructiveness of the CAD’s operating principle means that it needs to be the last detector when coupled in-line. For a convenient combination of CAD and MS, flow-splitting devices are available [9].

Due to the sensitivity benefits concomitant with the absence of ion-pairing reagents, mixed-mode chromatography was evaluated as a powerful separation technique when coupled to CAD. Although the complexity and the high costs of the stationary phases leads to a challenging and possibly long-winded “trial and error” method development, these drawbacks need to be compared to using ion-pairing reagents. Such reagents can also be costly and toxic, while method development in RPIP is not necessarily simpler than in mixed-mode chromatography. Hence, both chromatographic

techniques can represent proper solutions for challenging analytes and have a justifiable place in analytical chemistry. By using either one of these two techniques, one can refrain from applying tedious and error-prone derivatization procedures.

The modern CADs allow for alterations of instrument settings that significantly increase performance, most importantly sensitivity and linearity, of the method. For a GMP environment it has to be noted that the data transformation by means of the PFV can lead to error propagation. Because these features are fairly new, transferability studies and ranges of allowed changes to these settings as well as the definition of appropriate system suitability criteria should be subject to further research. This could help to set a defined space for the use of such instrument settings in compendial or other validated routine applications, although the existence of only one single manufacturer of the instrument hinders its acceptance by the regulatory authorities. As presented exemplarily for pamidronate disodium, the application of e.g. an elevated evaporation temperature can be necessary to obtain LOQs in accordance with the ICH guidelines and compendial monographs, emphasizing the relevance of further research with regard to these instrument settings.

References

1. Hutchinson JP, Li J, Farrell W, Groeber E, Szucs R, Dicinoski G, Haddad PR. Universal response model for a corona charged aerosol detector. J Chromatogr A. 2010;1217:7418-27.

2. Zhang K, Kurita K, Venkatramani C, Russell D. Seeking universal detectors for analytical characterizations. J Pharm Biomed Anal. 2019,162:192-204.

3. Wahl O, Holzgrabe U. Impurity profiling of ibandronate sodium by HPLC–CAD. J Pharm Biomed Anal. 2015;114:254-64.

4. Zhang K, Liu X. Mixed-mode chromatography in pharmaceutical and biopharmaceutical applications. J Pharm Biomed Anal. 2016;128:73-88.

5. Ilko D, Neugebauer RC, Brossard S, Almeling S, Türck M, Holzgrabe U. Impurity Control in Topiramate with High Performance Liquid Chromatography: Validation and Comparison of the Performance of Evaporative Light Scattering Detection and Charged Aerosol Detection. Charged Aerosol Detection for Liquid Chromatography and Related Separation Techniques. John Wiley & Sons, Hoboken; 2017.

6. Almeling S, Holzgrabe U. Use of evaporative light scattering detection for the quality control of drug substances: Influence of different liquid chromatographic and evaporative light scattering detector parameters on the appearance of spike peaks. J Chromatogr A. 2010;1217:2163-70.

7. Fontes PR, Ribeiro JAdA, Costa PP, Damaso MC, Gonzalez WdA, dos Santos CMC et al. Development and validation of a HILIC-UPLC-ELSD method based on optimized chromatographic and detection parameters for the quantification of polyols from bioconversion processes. Analytical Methods. 2016;8(9):2048-57.

8. Zhou Q, Chen M, Zhu L, Tang H. Determination of perfluorinated carboxylic acids in water using liquid chromatography coupled to a corona-charged aerosol detector. Talanta. 2015;136:35-41.

9. Poplawska M, Blazewicz A, Bukowinska K, Fijalek Z. Application of high-performance liquid chromatography with charged aerosol detection for universal quantitation of undeclared phosphodiesterase-5 inhibitors in herbal dietary supplements. Journal of pharmaceutical and biomedical analysis. 2013;84:232-43.

6 Summary

Liquid chromatography has become the gold standard for modern quality control and purity analytics since its establishment in the 1930s. However, some analytical questions remain very challenging even today. Several molecules and impurities do not possess a suitable chromophore for the application of UV detection or cannot be retained well on regular RP columns. Possible solutions are found in derivatization procedures, but they are time-consuming and can be prone to errors. In order to detect non-chromophore molecules underivatized, the concept of aerosol-based universal detection was established with the introduction of the evaporative light scattering detector (ELSD) in the 1970s and the charged aerosol detector (CAD) followed in 2002. These two challenging fields – polar and non-chromophore molecules – are tackled in this thesis.

An overview of applications of the CAD in the literature and a comparison to its aerosol-based competitors and MS is presented, emphasizing on its high sensitivity and robustness. Parameters and techniques to overcome the drawbacks of CAD, such as the use of gradient compensation or adjusted evaporation temperatures are discussed. A consideration of aspects and drawbacks of data transformation such as the integrated power function value (PFV) in the GMP environment is performed.

A method for the fatty acid analysis in polysorbate 80 that was developed on HPLC-CAD was transferred to UHPLC-CAD. Time and eluent savings of over 75% and 40%, respectively, as well as ways to determine the optimal CAD parameters resulted from this investigation. The evaporation temperature was determined as the most crucial setting, which has to be adjusted with care. Optimal signal-to-noise ratios are found at a compromise between maintaining analyte signal and reducing background noise. The incorporation of semi-volatile short chain fatty acids enabled the observation of differences based on volatility of the analyte. E.g. for semi-volatiles, an improved linearity by means of adjusting the PFV is achieved at values below 1.0 instead of at elevated PFVs.

Using sugars and sugar-related antibiotics, a proof-of-concept was given that artificial neural networks can describe correlations between the structure and physicochemical properties of molecules and their response in CAD. Quantitative structure-property relationships obtained by design of experiment approaches were able to predict the

response of unseen substances and yielded insights on the response generation of the detector, which heavily relies on the formed surface area of the dried particle. Further work can substantiate upon these findings, eventually building a library of diverse eluent compositions, analytes and settings.

In order to cope with a chromatographically challenging substances, the application of ion-pairing reversed phase chromatography coupled to low wavelength UV detection has been shown as a possible approach for the amino acid L-asparagine. A method capable of compendial purity analysis in one single HPLC approach, thus making the utilization of the semi-quantitative TLC-ninhydrin analysis obsolete, resulted from this. One cyclic dipeptide impurity (diketoasparagine) that was formerly not assessed, could be identified in several batches and added to the monograph of the Ph.Eur.

Studying ibandronate sodium with CAD and ELSD, it was found that randomly occurring spike peaks represent a major flaw of the ELSD when high sample load is present. The research with this non-chromophore bisphosphonate drug furthermore shed light on possible drawbacks of mixed-mode chromatography methods and ways to overcome these issues. Due to strong adsorption of the analyte onto the column, over ten injections of the highly concentrated test solution were found to be necessary to ensure reproducible peak areas. Preconditioning steps should thus be evaluated for mixed-mode approaches during method development and validation.

Last, using a ternary mixed-mode stationary phase coupled to CAD, a method for the impurity profiling of pamidronate disodium, also applicable to the assessment of phosphate and phosphite in four other bisphosphonate drugs, has been developed. This represents a major advantage over the Ph.Eur. impurity profiling of pamidronate, which requires two different methods, one of which is only a semi-quantitative TLC approach.

7 Zusammenfassung

Flüssigchromatographische Untersuchungen sind seit deren Einführung in den 1930er Jahren zum Goldstandard für die moderne Qualitätskontrolle und Reinheitsanalytik geworden. Allerdings sind auch noch heutzutage einige Fragestellungen sehr herausfordernd. Viele Moleküle und Verunreinigungen besitzen keinen geeigneten Chromophor, das die Anwendung klassischer UV-Detektion ermöglicht, oder erfahren auf gewöhnlichen Umkehrphasen keine ausreichende Retention. Lösungsansätze in Form von Derivatisierungsverfahren sind zeitaufwändig und fehleranfällig. Um underivatisierte Moleküle ohne geeignetes Chromophor zu analysieren, wurde das Prinzip der auf Aerosolen basierenden universellen Detektion mit dem „Evaporative Light Scattering Detector (ELSD)“ in den 1970er Jahren entwickelt und 2002 folgte der „Charged Aerosol Detector (CAD)“. Diese zwei Felder - polare und nicht-chromophore Analyte - werden in der vorliegenden Dissertation bearbeitet.

Eine Literaturübersicht und -analyse von Applikationen des CAD, sowie ein Vergleich zu seinen auf Aerosoltechnik basierenden Konkurrenten und der Massenspektroskopie wird dargestellt; besonders die hohe Sensitivität und Robustheit werden ersichtlich. Geräteeinstellungen und Techniken, mit denen sich Nachteile des CAD ausgleichen lassen, werden erläutert und diskutiert. Hierbei werden beispielsweise die Gradientenkompensation oder die Veränderung der Verdampfungstemperatur diskutiert. Ein Überblick über Möglichkeiten und Nachteile der Datentransformation des CAD Signals mittels des eingebauten „Power Function Values (PFV)“ im GMP Umfeld wird gegeben.

Ein Methodentransfer der Analytik von Fettsäuren in Polysorbat 80 von HPLC-CAD zu UHPLC-CAD wurde durchgeführt. Chemikalien- und Zeitersparnisse jenseits von 40 bzw. 75%, sowie Herangehensweisen für die Optimierung der CAD-Einstellungen resultierten hieraus. Die Verdampfungstemperatur ist der wichtigste Parameter des Detektors und sollte stets feinjustiert werden. Die höchste Sensitivität findet sich für einen Kompromiss aus verringertem Rauschen und auch erhaltenem Analytsignal. Durch die Analyse von semi-flüchtigen Fettsäuren konnten Unterschiede, die auf der Flüchtigkeit von Substanzen basieren, erarbeitet werden. Für semi-flüchtige Stoffe ist die Linearisierung mittels PFV bespielsweise bei Werten unter 1.0 erfolgreich, wohingegen für nicht-flüchtige Analyte Werte jenseits von 1.0 optimal sind.

Für Zucker und zuckerverwandte Antibiotika konnte ein konzeptioneller Beweis erbracht werden, dass künstliche neuronale Netzwerke Korrelationen zwischen den physikochemischen Eigenschaften der Moleküle und deren Signal im CAD herstellen können. Ein solches Netzwerk wurde mittels Methoden des experimentellen Designs erstellt. Die CAD-Detektorantwort, die stark von der Oberfläche der Partikel abhängt, konnte auf diese Weise für Substanzen innerhalb des Experimentalraumes vorhergesagt werden. Hierauf aufbauend kann eine Bibliothek aus Analyten, Fließmitteln und Detektorparametern erarbeitet werden, um weiteres Detailwissen über den CAD zu erhalten.

Die Aminosäure L-Asparagin stellt eine chromatographische Herausforderung dar. Es wurde eine Ionenpaar-Umkehrphasen-Methode mit UV-Detektion bei 210 nm als erfolgreicher Ansatz gezeigt. Die arzneibuchkonforme Bestimmung des Verunreinigungsprofils ist mit dieser Methode in einem Lauf möglich, wodurch die Nutzung der halbquantitativen Dünnschichtchromatographie obsolet wird. Weiterhin konnte ein cyclisches Dipeptid (Diketoasparagin), welches zuvor nicht im Verunreinigungsprofil gelistet war, in einigen Batches gefunden und so der Monographie des Ph.Eur. hinzugefügt werden.

Bei der Untersuchung von Natrium-Ibandronat mit dem CAD und dem ELSD konnte gezeigt werden, dass zufällig auftretende „spike peaks“ bei hohen Probenkonzentrationen ein enormes analytisches Problem des ELSD darstellen. Weiterhin wurde mit der Analyse der nicht-chromophoren Bisphosphonaten ein Problem von „mixed-mode“ Chromatographie aufgedeckt. Durch die starke Adsorption des Analyten auf der Säule waren über zehn Injektionen der konzentrierten Testlösung notwendig, um reproduzierbare Peakflächen zu erhalten. Derartige Sättigungs- und Vorkonditionierungsprozesse sollten für „mixed-mode“ Chromatographie während der Entwicklung und Validierung untersucht werden.

Zuletzt wurde eine ternäre „mixed-mode“ stationäre Phase gekoppelt mit CAD verwendet, um das Verunreinigungsprofil von Pamidronat-Dinatrium zu analysieren. Diese entwickelte Methode konnte auch für die Bestimmung von Phosphat und Phosphit in vier anderen Bisphosphonaten genutzt werden. Erneut ergibt sich ein Vorteil gegenüber der Arzneibuchmethode für Pamidronat, welche zwei verschiedene Methoden - eine davon nur eine halbquantitative Dünnschichtchromatographie - nutzt.

8 Appendix

8.1 List of Publications

Review article

Schilling, K.; Holzgrabe, U. *Recent applications of the Charged Aerosol Detector for liquid chromatography [manuscript accepted at Journal of Chromatography A, **2020**].*

Research papers

- Schilling, K.; Amstalden, M.C.; Meinel, L.; Holzgrabe, U. *Impurity Profiling of L-asparagine monohydrate by Ion Pair Chromatography Applying Low Wavelength UV Detection,* J Pharm Biomed Anal **2016**, 131, 202-207.
- Schilling, K.; Pawellek, R.; Lovejoy, K.; Muellner, T.; Holzgrabe, U. *Influence of charged aerosol detector instrument settings on the ultra-high-performance liquid chromatography analysis of fatty acids in polysorbate 80,* J Chromatogr A **2018**, 1576, 58-66.
- Schilling, K.; Krmar, J.; Maljuric, N.; Pawellek, R.; Protic, A.; Holzgrabe, U. *Quantitative Structure – Property Relationship modeling of polar analytes lacking UV chromophores to Charged Aerosol Detector Response,* Anal Bioanal Chem **2019**, 411/13, 2945-2959.
- Güntzel, P.; Schilling, K.; Hanio, S.; Schollmayer, C.; Wiest, J.; Meinel, L.; Holzgrabe, U. *Organic Acids in Nature: Ionic Liquids and their supramolecular behavior [manuscript in preparation]*
- Pawellek, R.; Schilling, K.; Holzgrabe, U. *Impurity profiling of L-aspartic acid and glycine using high-performance liquid chromatography coupled with simultaneous charged aerosol and ultraviolet detection [revised manuscript submitted to the Journal of Pharmaceutical and Biomedical Analysis]*

Other publications

- Schilling, K.; Pawellek, R.; Wahl, O.; Holzgrabe, U. *HPLC-CAD impurity profiling of carbocisteine using SCX RP mixed-mode chromatography* Application note for the Thermo Scientific™ Vanquish™ Charged Aerosol Detector, URL: https://assets.thermofisher.com/TFS-Assets/CMD/Application-Notes/an-72706-hplc-cad-impurity-carbocisteine-an72706-EN.pdf

8.2 Documentation of authorship

This section contains a list of the individual contribution for each author to the publications reprinted in this thesis. Unpublished manuscripts are handled accordingly.

M1	**Schilling, K.; Holzgrabe, U.** Recent applications of the Charged Aerosol Detector for liquid chromatography [accepted manuscript at Journal of Chromatography A 2020].		
Author		**1**	**2**
Concept development, manuscript planning		x	x
Literature analysis and interpretation		x	
Manuscript writing		x	
Correction of manuscript		x	x
Supervision of Klaus Schilling			x

P1	**Schilling, K.; Amstalden, M.C.; Meinel, L.; Holzgrabe, U.** Impurity Profiling of L-asparagine monohydrate by Ion Pair Chromatography Applying Low Wavelength UV Detection, J Pharm Biomed Anal 2016, 131, 202-207.				
Author		**1**	**2**	**3**	**4**
Study design		x			x
Experimental work: HPLC		x			
Experimental work: peptide synthesis			x		
Data analysis and interpretation		x	x		
Manuscript planning		x			x
Manuscript writing		x	x		
Correction of manuscript		x	x	x	x
Supervision of Klaus Schilling					x

P2	**Schilling, K.; Pawellek, R.; Lovejoy, K.; Muellner, T.; Holzgrabe, U.** Influence of charged aerosol detector instrument settings on the ultra-high-performance liquid chromatography analysis of fatty acids in polysorbate 80, J Chromatogr A 2018, 1576, 58-66					
Author		**1**	**2**	**3**	**4**	**5**
Study design		x	x	x	x	x
Experimental work		x	x			
Data analysis and interpretation		x	x	x	x	x
Manuscript planning		x	x	x	x	x
Manuscript writing		x	x	x	x	
Correction of manuscript		x	x	x	x	x
Supervision of Klaus Schilling						x

P3	**Schilling, K.; Krmar, J.; Maljuric, N.; Pawellek, R.; Protic, A.; Holzgrabe, U.** Quantitative Structure – Property Relationship modeling of polar analytes lacking UV chromophores to Charged Aerosol Detector Response, Anal Bioanal Chem 2019, 411/13, 2945-2959.

Author	**1**	**2**	**3**	**4**	**5**	**6**
Study design	x	x	x	x	x	x
Experimental work : HPLC	x					
Experimental work : data modeling		x	x		x	
Data analysis and interpretation	x	x	x	x	x	
Manuscript planning	x	x	x		x	x
Manuscript writing	x	x	x		x	x
Correction of manuscript	x	x	x	x	x	x
Supervision of Klaus Schilling						x

Erklärung zu den Eigenanteilen des Doktoranden sowie der weiteren Doktoranden als Koautoren an Publikationen und Zweitpublikationsrechten bei einer kumulativen Dissertation.

Für alle in dieser kumulativen Dissertation verwendeten Manuskripte liegen die notwendigen Genehmigungen der Verlage (‚reprint permission') für die Zweitpublikation vor, außer das betreffende Kapitel ist noch gar nicht publiziert. Dieser Umstand wird einerseits durch die genaue Angabe der Literaturstelle der Erstpublikation auf der ersten Seite des betreffenden Kapitels deutlich gemacht oder die bisherige Nichtveröffentlichung durch den Vermerk „unpublished" oder „nicht veröffentlicht" gekennzeichnet.

Die Mitautoren_innen der in dieser kumulativen Dissertation verwendeten Manuskripte sind sowohl über die Nutzung als auch über die oben angegebenen Eigenanteile informiert.

Die Beiträge der Mitautoren_innen an den Publikationen sind in den vorausgehenden Tabellen aufgeführt.

Prof. Dr. Ulrike Holzgrabe _____ _____

Ort, Datum Unterschrift

Klaus Schilling _____ _____

Ort, Datum Unterschrift

8.3 Conference Contributions

- Schilling, K.; Pawellek, R.; Lovejoy, K.; Muellner, T.; Holzgrabe, U.

UHPLC-CAD analysis of fatty acids in polysorbate 80: Influence of CAD parameters

DPhG Annual meeting, **2018**, Hamburg